



Terms and Conditions of Use of Digitised Theses from Trinity College Library Dublin

Copyright statement

All material supplied by Trinity College Library is protected by copyright (under the Copyright and Related Rights Act, 2000 as amended) and other relevant Intellectual Property Rights. By accessing and using a Digitised Thesis from Trinity College Library you acknowledge that all Intellectual Property Rights in any Works supplied are the sole and exclusive property of the copyright and/or other IPR holder. Specific copyright holders may not be explicitly identified. Use of materials from other sources within a thesis should not be construed as a claim over them.

A non-exclusive, non-transferable licence is hereby granted to those using or reproducing, in whole or in part, the material for valid purposes, providing the copyright owners are acknowledged using the normal conventions. Where specific permission to use material is required, this is identified and such permission must be sought from the copyright holder or agency cited.

Liability statement

By using a Digitised Thesis, I accept that Trinity College Dublin bears no legal responsibility for the accuracy, legality or comprehensiveness of materials contained within the thesis, and that Trinity College Dublin accepts no liability for indirect, consequential, or incidental, damages or losses arising from use of the thesis for whatever reason. Information located in a thesis may be subject to specific use constraints, details of which may not be explicitly described. It is the responsibility of potential and actual users to be aware of such constraints and to abide by them. By making use of material from a digitised thesis, you accept these copyright and disclaimer provisions. Where it is brought to the attention of Trinity College Library that there may be a breach of copyright or other restraint, it is the policy to withdraw or take down access to a thesis while the issue is being resolved.

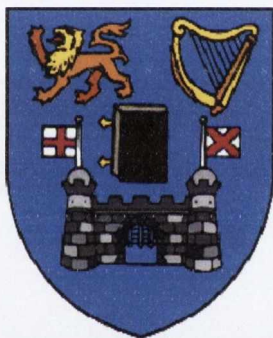
Access Agreement

By using a Digitised Thesis from Trinity College Library you are bound by the following Terms & Conditions. Please read them carefully.

I have read and I understand the following statement: All material supplied via a Digitised Thesis from Trinity College Library is protected by copyright and other intellectual property rights, and duplication or sale of all or part of any of a thesis is not permitted, except that material may be duplicated by you for your research use or for educational purposes in electronic or print form providing the copyright owners are acknowledged using the normal conventions. You must obtain permission for any other use. Electronic or print copies may not be offered, whether for sale or otherwise to anyone. This copy has been supplied on the understanding that it is copyright material and that no quotation from the thesis may be published without proper acknowledgement.

Ferrocene Containing Polyaromatic Hydrocarbons and the Formation of a Discotic Nitrogen-Heterosuperbenzene

Dilwyn John Roberts



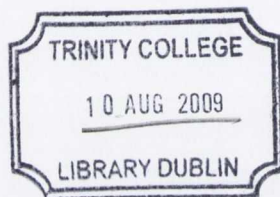
University of Dublin, Trinity College

**A Thesis Submitted to the University of Dublin for the Degree of Doctor of
Philosophy**

School of Chemistry

Trinity College Dublin

2009



THOS
8858

Declaration

This thesis has not been submitted as an exercise for a degree at this or any other university. Except where acknowledgement is given, all work is original and was carried out by the author. I agree that the library may lend or copy this thesis upon request.

Dilv



Education is the great engine of personal development. It is through education that a daughter of a peasant can become a doctor, that the son of a mineworker can become the head of the mine, that a child of farmworkers can become the president of a great nation.

It is what we make out of what we have, not what we are given, that separates one person from another.

Nelson Rolihlahla Mandela, 1994

Er Cof am taid, John P.G,
- gorffwyswch mewn hedd

Summary

Chapter 1 describes the synthesis and characterisation of a series of novel ferrocene containing polyphenylene compounds. These consist of polyphenylene molecules containing one, two, four and six ferrocene moieties. Also described is the formation of the first hexa-*peri*-benzocoronene (HBC) supporting a fully conjugated ferrocene moiety. UV-vis spectroscopy results indicate that the cyclopentadienyl rings of the ferrocenyl units tilt to differing degrees and this has consequences for subsequent cyclodehydrogenation attempts. The HBC supporting a fully conjugated ferrocene moiety undergoes an anodic shift in its redox potential when compared to ferrocene signifying the electron-withdrawing nature of the HBC.

Chapter 2 details the synthesis of four novel fluoranthene-based compounds that also support ferrocenyl moieties. Attempts to exploit intermolecular cyclodehydrogenation of these compounds are described as well as their photophysical and electrochemical properties. The molecular structures of all four compounds were confirmed by single crystal X-ray crystallographic analysis.

Chapter 3 introduces the newest member to the N-heterosuperbenzene (N-HSB) family, a tetra substituted dodecyl derivative. Its synthesis and complete characterisation is discussed. Through TGA and DSC analysis this compound was shown to be thermally very stable. It has been shown to be discotic over the entire temperature range studied (-30 - +300 °C) and is the first heteroatom containing HBC with a quantifiable charge carrying mobility, as determined by pulse-radiolysis time-resolved microwave conductivity technique (PR-TRMC). Absorption and emission spectroscopy showed that the docecyl substituted N-HSB self-associates in solution even at very low concentrations.

Chapter 4 gives a full account of the experimental details of the work undertaken.

Acknowledgements

First of all I would like to sincerely thank my supervisor, Prof. Sylvia Draper for all her help, guidance, support and encouragement since I arrived in Ireland. I must also thank Dr. Ferdinand Grozema for all his help in measuring the one-dimensional charge carrying properties at TU Delft in the Netherlands. Dr. John O'Brien, thank you very much for all your support and enthusiastic NMR analysis. Also thanks to Dr. Manuel Reuther for the NMR analysis, Dr. Martin Feeney for running all my mass spectrometry samples as well as Dr. Chris Fitches and Dr. Sunil Varghese for the X-ray crystallography.

I would also like to take this opportunity to thank all the Draper group members past and present. Original members; Angelica, Cecile, Chris, Dan, Fran, Gareth, Guillaume, Pablo and Roberto, thanks a million for all your help and the amazing welcome you gave me when I first arrived in Ireland. The newer members; Colin, Buddhie, Deanne, Ania, Belen, Carols, Lorraine, Amy, Gearoid and Tash thanks again for all your support you have been excellent people to work with.

Thanks also to the amazing friends I have been so fortunate to make outside the group; Ger, Con, Gar, Ian, Johnny, Joe and the many others, thanks a million for one of the best periods of my life.

Buaswn nawr yn hoffi diolch yn fawr iawn i fy nheulu, yn enwedig mam a dad am yr holl gymorth dwi wedi ei dderbyn dros yr holl flynyddoedd yn enwedig ers dwi wedi bod yn Iwerddon. Dilolch yn fawr am y holl gefnogaeth a cariad dwi wedi ei dderbyn, buaswn byth wedi medru llwyddo heb chi y tu ol i mi. Diolch hefyd i fy annwyl chwaer Catrin am bob dim.

Finally I would like to thank Trinity College and IRCSET for their financial support.

Table of Contents

Abbreviations and Symbols.....	i
List of Tables.....	iv
List of Schemes	v
List of Figures	vii
Chapter 1: Ferrocenyl Susbstituted Fused and Un-Fused Polyphenylenes	1
1.1. Introduction	3
1.1.1. Superbenzene	3
1.1.2. Cyclodehydrogenation	6
1.1.3. N-HSB Introduction	8
1.1.4. Ferrocenyl Containing PAHs	11
1.1.5. Synthesis of Ferrocene Containing Polyphenylene Compounds	12
1.1.6. Synthesis by Forming PAHs and Coupling	13
1.2. Synthesis and Characterisation.....	18
1.2.1. Synthesis of hexa- <i>tert</i> -butyl-hexa-peri-hexabenzocoronene (3)	18
1.2.2. Ferrocenyl Containing Polyphenylene Compounds.....	19
1.2.3. Mono-ferrocenyl Containing Polyphenylenes	19
1.2.4. Di-ferrocenyl Containing Polyphenylenes	22
1.2.4.1. Synthesis and Characterisation of 1,2-bis(4-phenylferrocene)ethane-1,2-dione (13)	22
1.2.4.2. Synthesis and Characterisation of 2,5-bis-(3,5-dimethoxy-phenyl)-3,4-bis-(4-phenylferrocene)- cyclopenta-2,4-dienone (15)	24
1.2.4.3. Synthesis of dipyrimidyl acetylene (18).....	25
1.2.4.4. Synthesis and Characterisation of Polyphenylene 19	26
1.2.5. Tetra-ferrocenyl Containing Polyphenylenes.....	28
1.2.5.1. Synthesis and Characterisation bis(4-ferrocenylphenyl)acetylene (24)	28
1.2.5.2. Synthesis and Characterisation of Polyphenylene 25	31
1.2.5.3. Synthesis and Characterisation of 2,3,4,5-tetra-(4-ferrocenyl-phenyl)cyclopenta-2,4-dienone (29)	32
1.2.5.4. Synthesis and Characterisation of Polyphenylene 30	35
1.2.6. Hexa-ferrocenyl Containing Polyphenylene	37
1.2.6.1. Synthesis and Characterisation of (4-ferrocenylphenyl)benzene (31)	37
1.2.7. Cyclodehydrogenation of Ferrocenyl Polyphenylenes	40
1.2.8. Synthesis of ferrocenyl-HBC	40
1.2.8.1. Synthesis and Characterisation of iodo-polyphenylene (37).....	40
1.2.8.2. Cyclodehydrogenation and Characterisation of iodo-HBC (38).	43
1.2.8.3. Synthesis of ferrocenyl-HBC	45
1.2.8.4. NMR Characterisation of ferrocenyl-HBC	47
1.2.8.5. NMR Concentration Dependence of Ferrocenyl-HBC (41)	49
1.2.9. Spectral Comparisons of Derivatives.....	51
1.2.10. UV-visible Absorption Spectroscopy.....	52
1.2.11. Electrochemistry.....	57

1.3.	Summary.....	60
1.4.	Future Work.....	62
Chapter 2: Ferrocenyl Fluoranthenes		67
2.1.	Introduction.....	69
2.1.1.	Fluoranthene	69
2.1.2.	Cyclodehydrogenation of Fluoranthenes	70
2.1.3.	Synthetic Methodology.....	71
2.2.	Synthesis and Characterisation.....	73
2.2.1.	Synthesis and Characterisation of the mono-ferrocenyl Containing Fluoranthene 43	73
2.2.2.	Synthesis of the di-ferrocenyl Containing Fluoranthene (52)	75
2.2.2.1.	Cyclopentadienone Synthesis	75
2.2.2.2.	Di-ferrocenyl Acetylene Synthesis	76
2.2.2.3.	Diels-Alder [2+4]-cycloaddition	77
2.2.2.4.	Characterisation of the di-ferrocenyl Containing Fluoranthene (52).....	78
2.2.3.	Synthesis of the di-fluoranthene ferrocenyl 54	79
2.2.3.1.	Characterisation of the mono-fluoranthene Containing byproduct 53	80
2.2.3.2.	Characterisation of the di-fluoranthene Containing Compound 54	83
2.2.4.	Proton NMR Comparisons	85
2.2.5.	Cyclodehydrogenation of the Fluoranthene based Compounds	86
2.2.6.	Spectral Comparisons of Derivatives	86
2.2.7.	UV-visible Absorption Spectroscopy	87
2.2.8.	X-Ray Crystallographic Analysis	93
2.2.9.	Electrochemistry	99
2.3.	Summary	102
2.4.	Future Work.....	104
Chapter 3: Synthesis of the Long-Chain Tetra-Dodecyl Nitrogen-Heterosuperbenzene		109
3.1.	Introduction.....	111
3.1.1.	Discotic Liquid Crystals	111
3.1.2.	Nematic Phases.....	111
3.1.3.	Columnar and Lamellar Phases	112
3.1.4.	Discotic Conducting Materials	114
3.1.5.	HBC Discotic Materials.....	115
3.1.6.	N-doped HBCs.....	118
3.2.	Results and Discussion	121
3.2.1.	Synthesis of hexa(4-dodecylphenyl)benzene (60).....	121
3.2.2.	Synthesis of 1, 2-dipyrimidyl-3, 4, 5, 6-tetra(4-dodecyl-phenyl)benzene (67)	122
3.2.2.1.	NMR Spectroscopic Characterisation of 67	125
3.2.2.2.	UV-vis Absorption Spectroscopy of 67	127
3.2.3.	Synthesis and Characterisation of tetra - <i>peri</i> -(dodecyl-benzo)-di- <i>peri</i> -(pyrimidino)-coronene (68)	129
3.2.4.	Solubility	131
3.2.5.	Thermal Stability	131

3.2.6.	Differential Scanning Calorimetry (DSC).....	132
3.2.7.	Photophysical Properties of 68	134
3.2.7.1.	UV-vis Absorption Spectroscopy	134
3.2.7.2.	Electronic Transitions within 68	136
3.2.7.3.	Emission Spectroscopy-Comparison of 68 with 60	139
3.2.7.4.	General Characteristics	140
3.2.8.	Absorption and Fluorescence Properties of the Protonated form of 68 ..	142
3.2.9.	Absorption and Fluorescence Properties of an Exciplex of 68	146
3.2.10.	Quantum Yield	148
3.2.11.	Self-association of 68 in Solution	151
3.2.12.	Ruthenium(II) Complex of 68	154
3.2.13.	One Dimensional Charge Carrier Mobility in 68	158
3.2.13.1.	Introduction	158
3.2.13.2.	Sample Preparation and the Sample Cell	158
3.2.13.3.	Formation of Mobile Charge Carriers	159
3.2.13.4.	Charge Carrier Mobility Results for 68	160
3.3.	Summary	163
3.4.	Future Work	166
Chapter 4:	Experimental	171
4.1.	General Methods	173
4.2.	Experimental Procedures.....	175
References.....		230
Annex.....		236

Abbreviations and Symbols

1-D	One-dimensional
2-D	Two-dimensional
Å	angstrom
aq.	aqueous
Ar	aromatic
bpy	2,2'-bipyridine
br	broad
COSY	Correlation Spectroscopy
CV	cyclic voltammetry
d	doublet
DCM	dichloromethane
dd	doublet of doublets
DEPT	Distortionless Enhancement by Polarization Transfer
DIBAL	diisobutylaluminiumhydride
DMF	dimethylformamide
DMPD	1,4-Dimethylpiperazine-2,3-dione
DMSO	dimethylsulfoxide
dppp	1,3-bis(diphenylphosphino)propane
δ	chemical shift (ppm)
ESI-MS	Electrospray Mass Spectrometry
Et	ethyl
Fc	ferrocenyl
g	gram
h	hour
HBC	hexa- <i>peri</i> -benzocoronene
HMBC	Heteronuclear Multiple Bond Correlation
HMQC	Heteronuclear Multiple Quantum Correlation
HOMO	Highest Occupied Molecular Orbital
HSQC	Heteronuclear Single Quantum Correlation
Hz	hertz
IC	Intersystem Crossing
IR	infrared

J	coupling constant (Hz)
λ	wavelength
LC	Ligand Centred
LCD	Liquid Crystal Displays
LF	Ligand Field
LUMO	Lowest Unoccupied Molecular Orbital
m	multiplet
MALDI-TOF	Matrix Assisted Laser Desorption Ionization- Time of Flight
MC	Metal Centred
Me	methyl
mg	milligram
MHz	megahertz
MLCT	Metal to Ligand Charge Transfer
mmol	millimol
mL	millilitre
m.p.	melting point
MS	mass spectrometry
m/z	mass to charge ratio
N-HSB	nitrogen-heterosuperbenzene
NLO	non-linear optics
NMR	nuclear magnetic resonance
NOE	nuclear Overhauser effect
ns	nanosecond
v	stretching frequency
PAH	polyaromatic hydrocarbon
ppm	parts per million
PR-TRMC	pulse-radiolysis time-resolved microwave conductivity
RT	room temperature
s	singlet
sat.	saturated
$\Sigma\mu_{1D}$	one dimensional charge carrier mobility
t	triplet
tert	tertiary
TLC	thin layer chromatography

TMS	trimethylsilyl-
TOCSY	Total Correlation Spectroscopy
TOF	Time-of-flight
quat	quaternary
UV/vis	ultra violet/visible
vs.	versus

List of Tables

Table 1: ^1H NMR spectral data and assignments for compounds 8 and 9 .	21
Table 2: Assignment of the ^{13}C signals for compound 30 by HMBC experiment.	37
Table 3: Spectroscopic data for complexes 8 , 9 , 19 , 25 , 30 , 31 and 41 .	52
Table 4: The UV-vis data for ferrocene, PAH-3 and the ferrocenyl compounds 8 , 9 , 19 , 25 , 30 , 31 and 41 .	53
Table 5: Electrochemical data for complexes 8 , 9 , 19 , 25 , 30 , 31 and 41 .	58
Table 6: NMR and mass spectrometry data for complexes 43 , 52 , 53 and 54 .	86
Table 7: The UV-vis data for ferrocene and compounds 43 , 52 , 53 and 54 .	88
Table 8: The cyclopentadienyl ring tilt angles in compounds 43 , 52 , 53 and 54 .	97
Table 9: Electrochemical data for complexes 43 , 52 , 53 and 54 .	100
Table 10: The intra-columnar charge mobilities ($\Sigma\mu_{\text{ID}}$) determined for a given macrocyclic core.	115
Table 11: Phase transition temperatures and structural assignments of three alkylated HBC compounds.	116
Table 12: Assignment of ^{13}C NMR signals for 67 .	127
Table 13: The molar extinction coefficients for the absorption maxima at each wavelength of 60 and 68 , both in toluene.	136
Table 14: The lowest energy absorption, highest energy emission wavelength and Stokes' shift for 68 in toluene.	141
Table 15: Fluorescence data for N-HSB and 68 .	150
Table 16: The bands in the absorption spectrum of 70 and $[\text{Ru}(\text{bpy})_2(\text{N-HSB})]^{2+}$.	156
Table 17: Maximum one dimensional mobilities, $\Sigma\mu_{\text{ID}}$, determined for the discotic (D_h) and crystalline (K) phases for a range of alkyl substituted HBCs. ¹⁴¹	167
Table 18: Crystal data and structure refinement for 43 .	236
Table 19: Bond lengths (\AA) for 43 .	237
Table 20: Angles ($^\circ$) for 43 .	237
Table 21: Crystal data and structure refinement for 52 .	239
Table 22: Bond lengths (\AA) for 52 .	240
Table 23: Angles ($^\circ$) for 52 .	241
Table 24: Crystal data and structure refinement for 53 .	245
Table 25: Bond lengths (\AA) for 53 .	246
Table 26: Angles ($^\circ$) for 53 .	247
Table 27: Crystal data and structure refinement for 54 .	250
Table 28: Bond lengths (\AA) for 54 .	251
Table 29: Angles ($^\circ$) for 54 .	252

List of Schemes

Scheme 1: Polymerization of benzene.	4
Scheme 2: Synthesis of a soluble HBC.	5
Scheme 3: Two possible routes to synthesising symmetric polyphenylenes.	6
Scheme 4: The two proposed mechanisms for dehydrogenation.	7
Scheme 5: Proposed mechanism for the cyclodehydrogenation of all-carbon polyphenylene molecules via the Scholl reaction.	8
Scheme 6: The synthesis of N- $\frac{1}{2}$ HSB and N-HSB.	10
Scheme 7: Retrosynthetic analysis on how to synthesise non-symmetrical polyphenylene compounds.	12
Scheme 8: Reaction of halogen containing HBCs. ⁹	14
Scheme 9: An example of Sonogashira coupling with halogens directly attached to a HBC platform.	14
Scheme 10: The synthesis of chromium tricarbonyl containing HBCs.	15
Scheme 11: Total synthesis of HBC 3	18
Scheme 12: Synthesis of 1, 1'-iodoferrocene (4).	19
Scheme 13: Synthesis of phenylalkynyl-trimethylstannane, (6).	20
Scheme 14: Synthesis of compound 7	20
Scheme 15: Synthesis of compounds 8 and 9	21
Scheme 16: The total synthesis of compound 15	23
Scheme 17: The synthesis of dipyrimidine acetylene 18	26
Scheme 18: The synthesis of polyphenylene 19	26
Scheme 19: The total synthesis of acetylene 24	29
Scheme 20: Diels-Alder [2+4]-cycloaddition reaction yielding polyphenylene 25	31
Scheme 21: The total synthesis of compound 29	33
Scheme 22: The synthesis of the N-doped tetra-ferrocenyl polyphenylene 30	35
Scheme 23: Cyclotrimerisation of 24 yielding 31	38
Scheme 24: The synthesis of tetraphenylcyclopentadienone 35	41
Scheme 25: The synthesis of 36	42
Scheme 26: Synthesis of iodo-HBC 38	44
Scheme 27: The synthesis of ethynylferrocene (40).	46
Scheme 28: The synthesis of 41 via Sonogashira coupling	47
Scheme 29: Possible synthetic route towards a PAH with two different halogens that could lead to differential coupling reactions.	63
Scheme 30: Possible synthesis of a new “push-and-pull” molecule.	64
Scheme 31: The synthesis of two perylene based chromophores via cyclodehydrogenation from a simple fluoranthene derivative.	70
Scheme 32: Synthetic route towards fluoranthene based compounds with differing R groups.	71
Scheme 33: The synthesis of 43	73
Scheme 34: Synthesis of cyclopentadienone 46	76
Scheme 35: The synthesis of diferrocenylacetylene (51).	77
Scheme 36: Synthesis of compound 52	78
Scheme 37: The synthesis of 53 and 54	80
Scheme 38: Possible synthetic routes towards nitro analogues of compounds 43 and 52 , with enhanced “push-and-pull” characteristics.	105
Scheme 39: Possible synthetic route towards a halogenated fully cyclised PAH, based on the fluoranthene sub-unit.	106
Scheme 40: The synthetic route toward 58	121

Scheme 41: The cyclotrimerisation of 58 yielding 59	122
Scheme 42: The synthesis of HBC 60	122
Scheme 43: The two possible routes for the synthesis of diketone 63	123
Scheme 44: Synthetic pathway for the synthesis of the cyclopentadienone, 66	124
Scheme 45: The synthesis of N-doped, dodecyl substituted polyphenylene 67	124
Scheme 47: The synthesis of the ruthenium(II) complex 70	154
Scheme 48: Two possible N-doped systems which could be synthesised employing the route utilised in the synthesis of 68	168

List of Figures

Figure 1: Some examples of polycyclic aromatic hydrocarbons (PAHs).	3
Figure 2: Two members of the “superbenzene” family.	4
Figure 3: The N-heterosuperbenzene (N-HSB) family to date.	9
Figure 4: Examples of metallocene containing polyphenylenes.	13
Figure 5: Two mono-ferrocenyl containing polyphenylene compounds synthesised by Mc. Glinchey et al. ^{27, 28}	13
Figure 6: The structures of the only two molecules to date where a ferrocene moiety is attached to a PAH platform.	16
Figure 7: The ¹ H NMR spectrum of the 1,2-diaryl-1,2-diketone 13	24
Figure 8: The ¹ H NMR spectrum of 15	25
Figure 9: The ¹ H NMR spectra of the aromatic and ferrocenyl region of 19	27
Figure 10: The ¹³ C NMR and ¹ H NMR spectra of 24	30
Figure 11: ¹ H NMR spectrum of 25	32
Figure 12: ¹ H NMR spectrum of 28	34
Figure 13: ¹ H NMR spectrum of 29	35
Figure 14: The ¹ H NMR of 30	36
Figure 15: The ¹ H NMR and the ¹³ C NMR spectra of 31	39
Figure 16: The ¹ H NMR spectrum for 37	43
Figure 17: The aromatic and aliphatic regions of the ¹ H NMR spectrum for 38	45
Figure 18: The ¹ H NMR spectrum of 41	48
Figure 19: The ¹³ C DEPT spectrum of 41	48
Figure 20: The concentration dependence of the ¹ H NMR aromatic signals of compound 41	50
Figure 21: Plot showing the concentration dependence on the chemical shifts of the aromatic protons in compound 41	51
Figure 22: The UV-vis absorption spectra of the ferrocenyl complexes, (i) 8 , (ii) 9 , (iii) 19 , (iv) 25 , (v) 30 (vi) 31 and (vii) ferrocene for comparison.	54
Figure 23: The UV-vis absorption spectra of, (i) 3 , (ii) 38 , (iii) 40 and (iv) 41	56
Figure 24: Cyclic voltammetric (i) ferrocene and (ii) 41	59
Figure 25: The synthesis of a fluoranthene derivative that represents 60 % of an aromatic analogue of C ₆₀	69
Figure 27: The ¹ H spectrum of 43	74
Figure 28: The ¹ H NMR spectrum of 52	79
Figure 29: The ¹ H NMR spectrum of 53	82
Figure 30: The ¹ H NMR spectrum 54	84
Figure 31: (a) ¹ H NMR spectrum of 43 with the ferrocenyl region magnified, (b) schematic representation of 43	87
Figure 32: The UV-vis absorption spectra of (i) 43 , (ii) 52 , (iii) 53 and (iv) 54	88
Figure 33: The UV-vis absorption spectra of the ferrocenyl region for the fluoranthene complexes, (i) 43 , (ii) 52 , (iii) 53 , (iv) 54 , (v) and ferrocene.	90
Figure 34: The UV-vis absorption spectra of the fluoranthene complexes, (i) 43 , (ii) 52 , (iii) 53 and (iv) 54	91
Figure 35: Structures and UV-vis data for two well studied fluoranthene based compounds	91
Figure 36: The UV-vis absorption spectra of 54	92
Figure 37: The X-ray crystal structures of (a) 43 and (b) 52	94
Figure 38: X-ray crystal structure of 52	95

Figure 39: The X-ray crystal structures of (a) 53 and (b) 54	96
Figure 40: The X-ray crystal structures of (a) 53 and (b) 54 , highlighting the CH... π interactions.....	98
Figure 41: Possible example of an extended PAH with conjugated ferrocenes.	106
Figure 42: Schematic representation of (a) nematic discotic, (b) chiral (helical) and (c) nematic columnar phase.	112
Figure 43: Schematic representation of (a) hexagonal columnar phase, (b) rectangular columnar phase, (c) columnar oblique phase, (d) columnar plastic phase, (e) helical phase and (f) columnar lamellar.	113
Figure 44: Macrocycles forming the cores of some discotic liquid crystals	114
Figure 45: Schematic representation of the formation of a hexagonal columnar mesophase formed by the staking of HBC cores with peripheral alkyl chains.	116
Figure 46: Structure of the first N-doped HBC, N-heterosuperbenzene (N-HSB). ..	118
Figure 47: The synchrotron molecular structure of N-HSB	119
Figure 48: Possible head-to-tail orientation within aggregates	120
Figure 49: (a) ^1H NMR and (b) ^{13}C NMR spectra of 67	126
Figure 50: The normalized absorption spectrum of 67	128
Figure 51: The ^1H NMR spectrum of 68	130
Figure 52: MALDI-TOF mass spectrum of 68	130
Figure 53: Thermogravimetric analysis of 68	132
Figure 54: The differential scanning calorimetry (DSC) trace for 68	
Figure 55: The normalized absorption spectra of (a) 60 and (b) 68	134
Figure 56: Absorption spectra of 68 in various solvents.....	138
Figure 57: Absorption and fluorescence spectra for (a) 60 and (b) 68	139
Figure 58: Jablonski energy level diagram	140
Figure 59: Overlay of the fluorescence spectra of 68 at different λ_{ex}	142
Figure 60: The absorbance spectra of 68 upon the addition of incremental amounts of trifluoroacetic acid	143
Figure 61: The fluorescence spectra of 68 upon the addition of incremental amount of trifluoroacetic acid	144
Figure 62: Normalized changes in fluorescence and absorption upon incremental addition of trifluoroacetic acid.....	145
Figure 63: Fluorescence spectra of 68 upon the incremental addition of aniline	147
Figure 64: The normalized changes in fluorescence of 68	148
Figure 65: Fluorescence of 68 at different concentrations..	150
Figure 66: Hypochromic effects on the three main absorption bands of 68	152
Figure 67: Models of association based on alignment of the transition dipoles of $\pi \rightarrow \pi^*$ bands and $n \rightarrow \pi^*$ bands.....	153
Figure 68: The ESI-mass spectrum of ruthenium complex 70	155
Figure 69: Representation of the tert-butyl analogue of 70 . ¹⁶	155
Figure 70: The absorption spectra of (i) $[\text{Ru}(\text{bpy})_3]^{2+}$, (ii) $[\text{Ru}(\text{bpy})_2(\text{N-HSB})]^{2+}$ and (iii) 70	156
Figure 71: The PR-TRMC waveguide cell.....	159
Figure 72: Schematic representation of the PR-TRMC set-up.....	160
Figure 73: The temperature dependence of the intra-columnar mobility of 68	161
Figure 74: Structure of the $-\text{C}_{10,8}$, swallow-tailed alkyl group. ¹⁴²	167

Chapter 1: Ferrocenyl Substituted Fused and Un-Fused Polyphenylenes

1.1. Introduction

1.1.1. Superbenzene

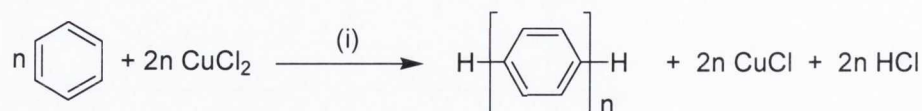
Polycyclic aromatic hydrocarbons (PAHs), which can formally be regarded as two-dimensional graphite sections, represent one of the most intensively investigated class of compound, alkyl substituted derivatives of these PAHs have been shown to form discotic liquid materials and have exiting conductive properties.¹ Indeed one of these compounds has been shown to have the highest ever recorded charge carrier mobility of any organic in the crystalline phase as well as in the liquid crystalline phase. Discotic liquid crystals will be discussed in more detail in chapter 3. Some examples of PAHs can be seen in Figure 1.



Figure 1: Some examples of polycyclic aromatic hydrocarbons (PAHs).

PAHs have regained much interest within the electronic industry, there has been a strategic shift towards what are termed as “soft” materials. These materials are organic molecules which are capable of the same function as more traditional inorganic semiconducting materials. Graphite with its network of π -electrons is still the best organic conductor since electrons are free to move within the sheets, in the delocalised π -orbitals formed from the unhybridised p-orbitals of the carbon atoms. By extension it is believed that PAHs will find extensive and valuable use in the area of molecular electronics^{1,2} and opto-electronics.^{3,4}

In the 1960s Kovacic *et al.* polymerized benzene and its derivatives to poly(*p*-phenylene) under mild reaction conditions using copper(II) chloride as an oxidant and aluminium(III) chloride as a Lewis acid in water, as shown in Scheme 1.^{5,6}



Scheme 1: Polymerization of benzene. (i) AlCl_3 , H_2O , 35°C , 30 min (60 %).

The reaction produced polymeric products unselectively, however it did demonstrate that multiple C-C bond formation was possible under mild conditions and it opened the way for creating highly selective oxidative dehydrogenation processes to convert oligophenylenes to PAHs.

Müllen *et al.* have developed a route to a series of pre-defined all-carbon framework PAHs, which are generally referred to as “superbenzenes”, by cyclodehydrogenating polyphenylene precursors. Two such molecules are shown in Figure 2, namely (a) hexa-*peri*-hexabenzocoronene (HBC) - superbenzene and (b) super naphthalene.⁷

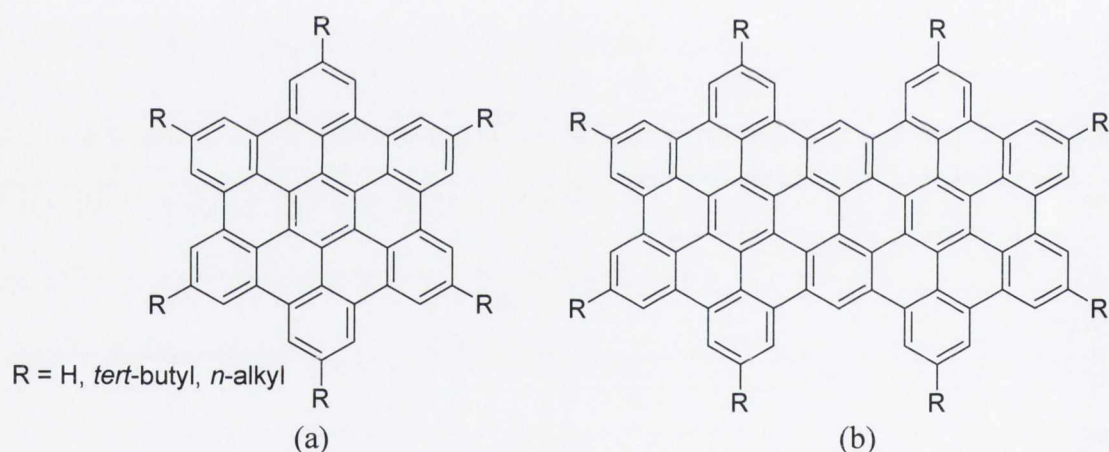


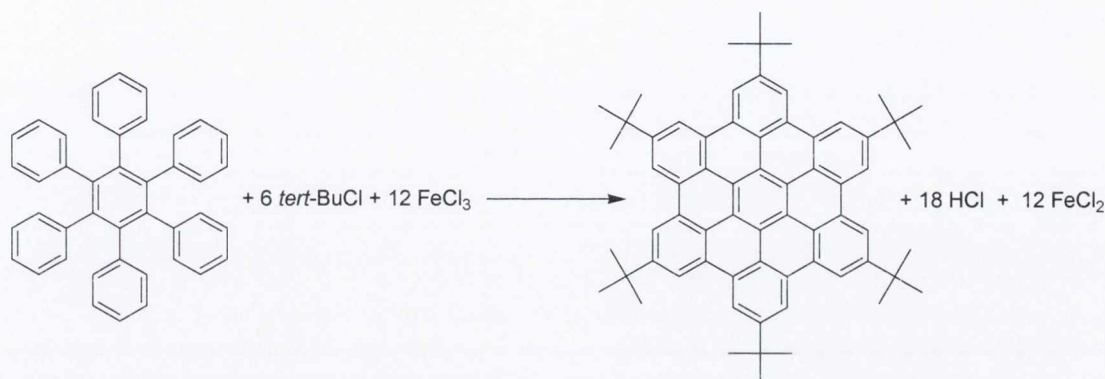
Figure 2: Two members of the “superbenzene” family.

These large PAHs often exhibit poor solubility, thus preventing their complete characterisation. However by changing the R groups from H to *tert*-butyl or long aliphatic chains this greatly increases solubility and aids an investigation of their properties.

Müllen *et al.* have shown that a wide variety of reagents can be used to cyclodehydrogenate polyphenylene systems. As well as the Kovacic conditions which employ copper(II) chloride/aluminium(III) chloride catalysts,³ copper(III) trifluoromethanesulfonate/aluminium(III) chloride,⁸ iron(III) chloride⁹ and

molybdenum(V) chloride¹⁰ have also been used. Such a range of reagents offers the opportunity to modify the products and yields of such reactions.

Rathore and Burn¹¹ developed a method to synthesise a soluble version of hexa-*peri*-hexabenzocoronene by introducing *tert*-butyl groups on the periphery. Their method was especially subtle since the *tert*-butyl groups were introduced during the cyclodehydrogenation step in one pot.

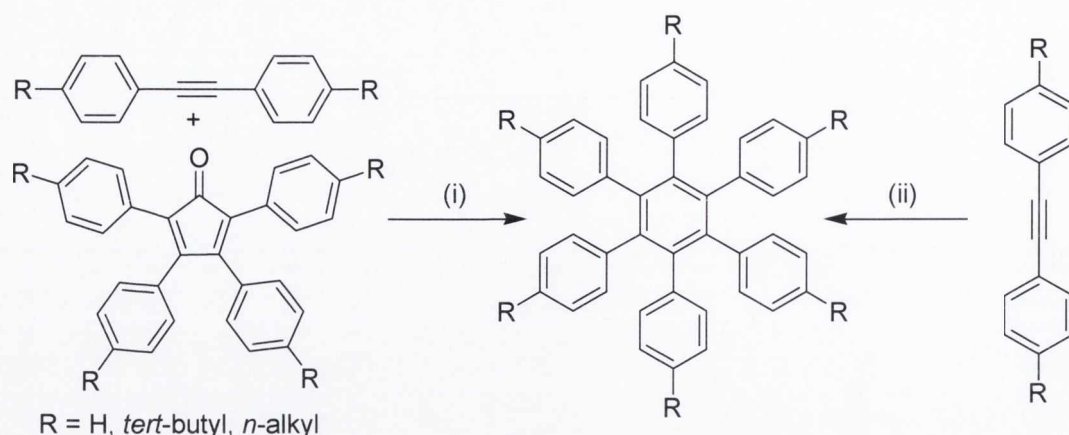


*Scheme 2: Synthesis of a soluble HBC by introducing the *tert*-butyl groups during the cyclodehydrogenation step.*

The limitation of this route is that it is appropriate only to totally symmetric PAHs. Obviously if groups other than *tert*-butyl are to be incorporated a new synthetic route was required.

One method to generate polyphenylenes involves the cyclotrimerisation of an acetylene using cobalt octacarbonyl as a catalyst in refluxing dioxane (Scheme 3). This method yields the desired polyphenylene compounds in excellent yields, usually over 90%, but produces only R₆ polyphenylenes i.e. again it is only good for the synthesis of very symmetric polyphenylene compounds.

A second method for polyphenylene formation involves a Diels-Alder reaction between acetylenes and suitably substituted tetraphenylcyclopentadienones in a [2 + 4]-cycloaddition reaction. During this reaction carbon monoxide is evolved, to produce the corresponding polyphenylene. Here different R groups can be introduced into either reagent giving rise to multiple substitution patterns.

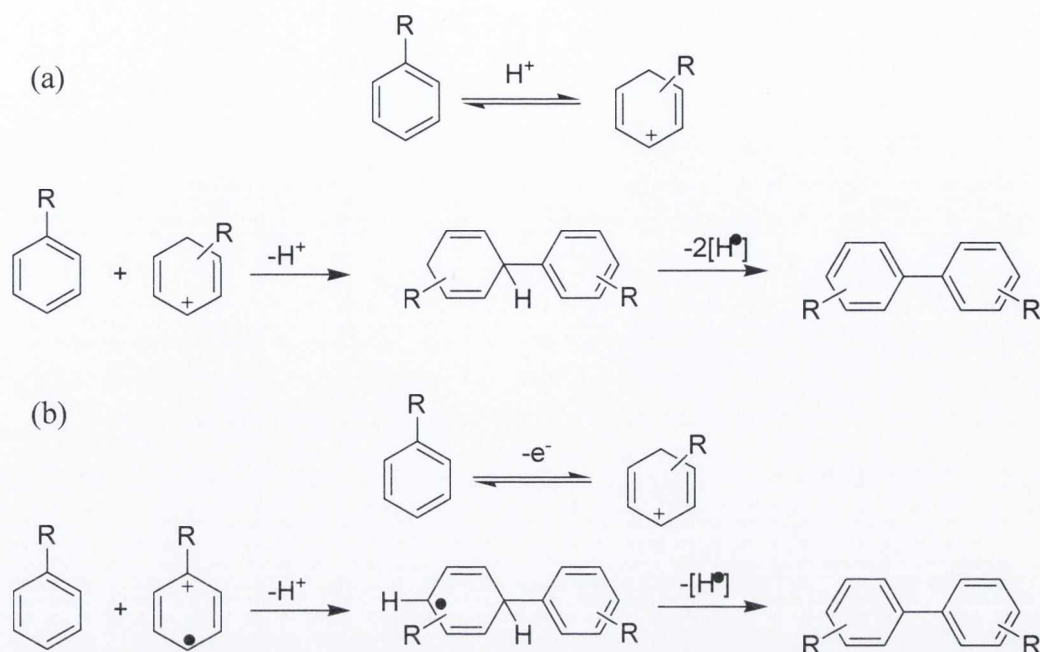


Scheme 3: Two possible routes to synthesising symmetric polyphenylene compounds, i.e. where all the R groups are the same, (i) via the Diels-Alder [2+4]-cycloaddition reaction, (ii) via cyclotrimerisation.

1.1.2. Cyclodehydrogenation

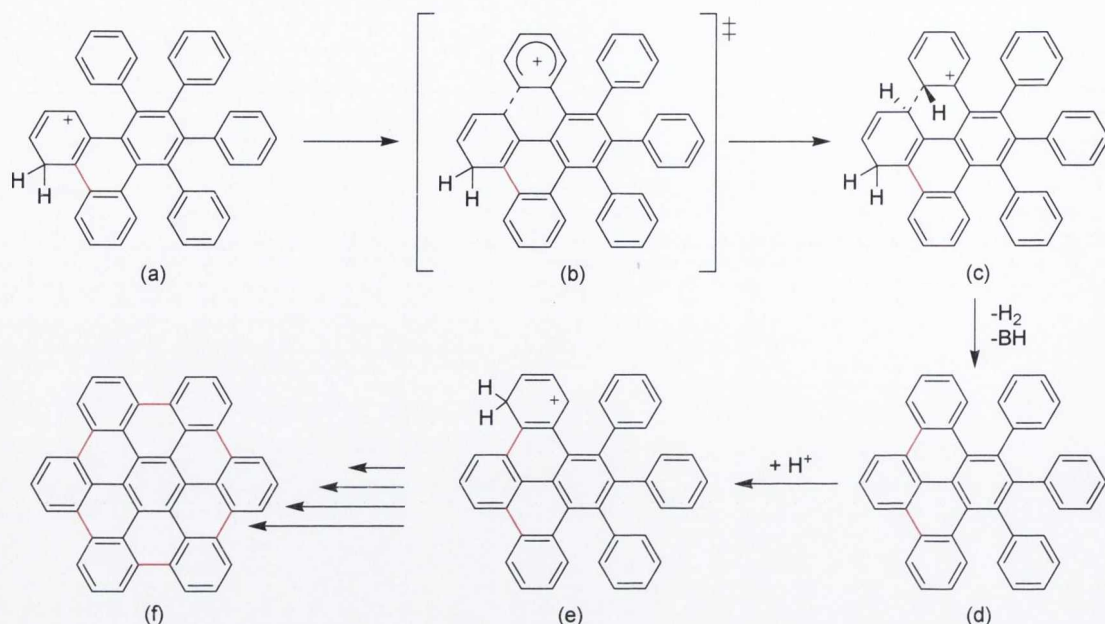
Whichever method is employed to generate the polyphenylene the key step in the synthesis of PAHs is cyclodehydrogenation whereby the polyphenylene is planarised. The results of this reaction is the elimination of two-aryl bound hydrogen atoms for each aryl-aryl C-C bond formed between a pair of adjacent phenyl rings on the precursor. Several suitable oxidant systems have been employed for these transformations however for the cyclodehydrogenation of alkyl substituted HBCs, the general catalyst of choice is iron(III) chloride which acts as a Lewis acid and oxidizing agent. The iron(III) chloride has to be added homogeneously to the uncyclised precursor so is dissolved in nitromethane and then added to the uncyclised precursor usually dissolved in dichloromethane.

The condensation of polyaromatic compounds by Lewis acid-catalysed oxidative cyclodehydrogenation is known as the Scholl reaction. Two possible reaction mechanisms have been proposed by both empirical and computational studies: (a) the arenium cation mechanism and (b) the radical cation mechanism, as shown in Scheme 4.



Scheme 4: The two proposed mechanisms for dehydrogenation, (a) via the arenium cation mechanism and (b) via the radical cation mechanism.¹²

A mechanistic study of the possible routes to cyclodehydrogenation of hexaphenylbenzene has been performed by King *et al.*¹² It is generally thought that the arenium cation mechanism¹⁰ is the most probable based on calculations of free energy values for C-C bond formation between adjacent phenyl rings around the hexaphenylbenzene which becomes increasingly exergonic as cyclodehydrogenation proceeds. Comparing the different mechanisms has revealed that the intermolecular Scholl reaction of hexaphenylbenzene most likely proceeds by protonation, electrophilic attack, deprotonation, and subsequent oxidation. Each C-C bond-forming step is consummated, restoring aromaticity before the next C-C bond-forming step begins. Aryl-aryl bonds are introduced along the pathway having least-strained, fully benzenoid intermediates, this pathway is contiguous, with the first C-C bond formation being the slowest. After formation of the first C-C bond between adjacent phenyl rings, newly planarised part of the molecule is protonated (a) in Scheme 5. This is followed by electrophilic attack of the arenium cation on the adjacent phenyl ring with (b) representing the transition state cation. Intermediate (c) is then deprotonated and the loss of H₂ restores aromaticity to compound (d). This process is repeated four more times to result in complete planarisation and formation of HBC (f). After the initial C-C bond formation, the other bonds are formed in a cascade-like manner.¹³



Scheme 5: Proposed mechanism for the cyclodehydrogenation of all-carbon polyphenylene molecules via the Scholl reaction.^{12,13}

Since the curve representing the decrease in energy for subsequent dehydrogenation steps is convex, the progress of the reaction is said to follow a slippery slope. Accordingly the Scholl reaction proceeds without the accumulation of partially-cyclised intermediates.

1.1.3. N-HSB Introduction

N-heterosuperbenzenes (N-HSBs) are a unique class of compounds synthesised by Draper *et al.*¹⁴ As with Müllens hexabenzocoronenes,¹⁵ these fused polyaromatic compounds exhibit an extraordinary degree of delocalisation. However, the inclusion of nitrogen donor atoms renders the HBC-type cores overall electron-accepting and confers on the new N-HSBs the dual advantage of ligand functionality and increased solubility. Such unusual characteristics offer the opportunity to study supramolecular effects such as π -stacking and to probe the electronic behaviour of the N-HSBs as ligands.

However the presence of the nitrogen atoms makes cyclodehydrogenation more problematic. As well as fully-cyclised N-HSB some partially cyclised intermediates have also been isolated during cyclodehydrogenation. One such intermediate is the

half-cyclised N- $^{1/2}$ HSB where the molecule is half planarised, leaving two phenyl rings which are free to rotate at the back of the ligand.

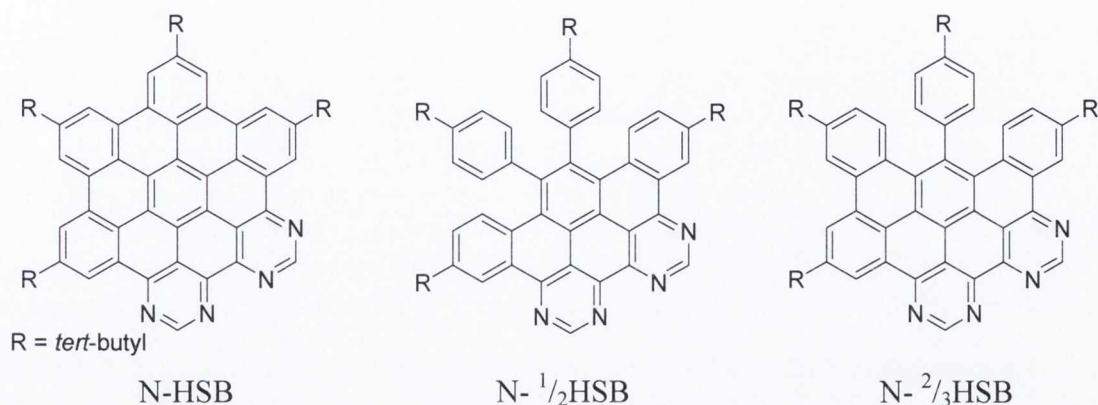


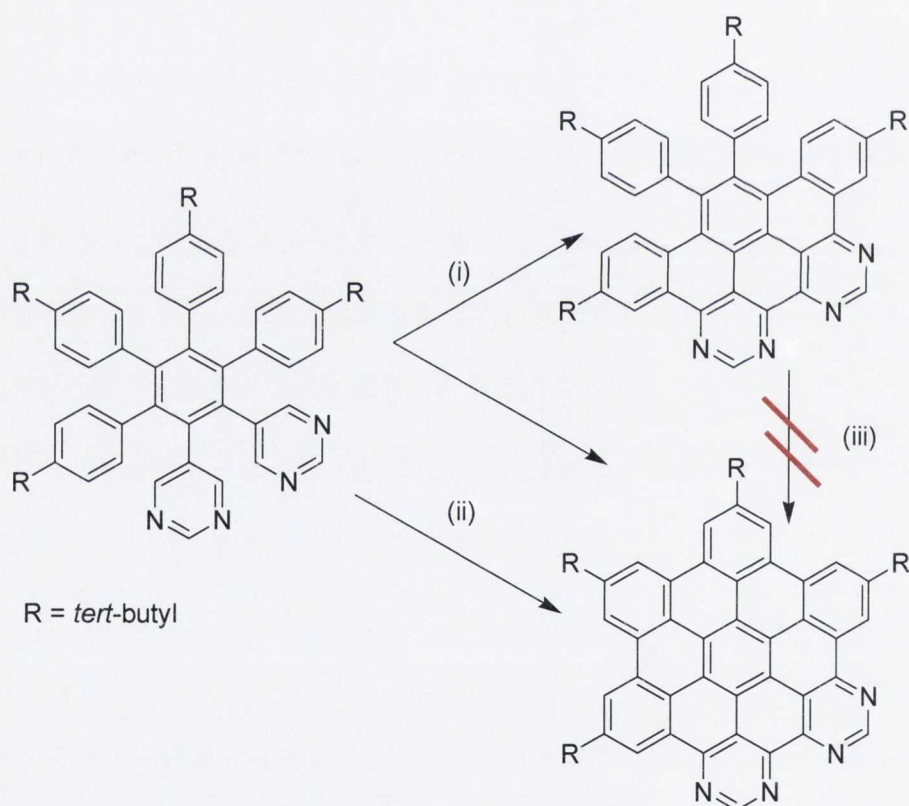
Figure 3: The *N*-heterosuperbenzene (*N*-HSB) family to date.

Other partially cyclised intermediates form the N-HSB family include the two-third cyclised product in which an additional aryl-aryl bond has been formed, leaving just one free phenyl ring which is not part of the extended aromatic platform.¹⁶ This is in contrast to what is observed in all-carbon HBCs, where no accumulation of partially-cyclised intermediates is observed. However it is thought that the arenium mechanism, as for the all-carbon analogues still applies even when heteroatoms are introduced to the system. Although it is thought to go *via* arenium mechanism the introduction of nitrogen heteroatoms onto the aromatic platform does affect the cascade effect of the Scholl reaction which leads to the isolated partially cyclised intermediates.^{12,13} It has been proposed that the initial step in the cyclodehydrogenation of N-doped polyphenylenes leading to the compounds shown in Figure 3 is most likely the protonation of the pyrimidine rings in preference to protonation of the other phenyl rings. The protonated or doubly protonated pyrimidine ring could act as an electrophile promoting the initial bond formation at the pyrimidine rings towards the formation of N- $^{1/2}$ HSB. Protonation of the phenyl rings on the aromatic portion of N- $^{1/2}$ HSB would be difficult since the basic nitrogen sites on the pyrimidine rings will be protonated and bear a positive charge. Alternatively if protonation of the phenyl substituents was possible, the nitrogen protonated PAH core would be a poor nucleophile, inhibiting electrophilic attack and thus inhibiting the formation of the aryl-aryl bonds required for complete cyclisation. This could explain why partially-cyclised products are isolated after the oxidative

cyclodehydrogenation to form N-HSB, while for all-carbon containing polyphenylene precursors no intermediates accumulate.^{12, 13}

The chelating substrate complicates the mechanistic analysis even further. It is worth noting that different cyclodehydrogenation reagents, iron(III) chloride or aluminium(III) chloride/copper(II) chloride give different product distributions.

Another interesting point in this reaction is that N-¹/₂HSB is not converted into N-HSB by treatment with aluminium(III) chloride/copper(II) chloride. This would suggest that N-¹/₂HSB is not an intermediate in the synthesis of N-HSB, and both compounds are synthesised independently of each other.



Scheme 6: The synthesis of N-¹/₂HSB and N-HSB. (i) FeCl₃, MeNO₂, DCM. (ii) AlCl₃/CuCl₂, CS₂. (iii) FeCl₃, MeNO₂, DCM or AlCl₃/CuCl₂, CS₂.

N-HSB¹⁷ and N-¹/₂HSB¹⁸ have been extensively studied, as have their corresponding ruthenium and osmium bi-bipyridyl complexes. The organic ligands themselves have interesting photophysical properties and are highly luminescent under UV irradiation.

1.1.4. Ferrocenyl Containing PAHs

Carbon-rich organometallic compounds represent a rapidly growing subfield at the interface of organic chemistry and organometallic chemistry. Carbon-rich ligands provide important properties, such as facile electron transfer to and from the metal surface, allowing these compounds to be used as molecular wires. As such, in recent years organometallic fragments assembled on substituted benzenes, polyaromatics and heteroaromatics, such as pyridines, have received immense interest as potential models for organometallic polymers¹⁹ and as targets for the study of electron-transfer processes.²⁰

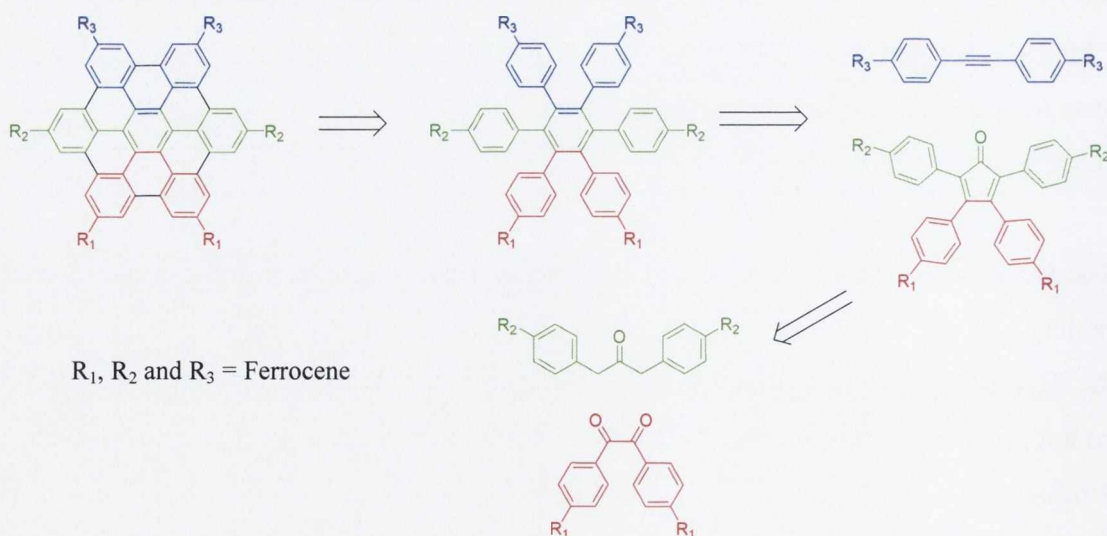
There is no doubt that ferrocene-based compounds represent one of the most important classes of compounds used in the design of ligands for use in organic synthesis.²¹ The ferrocenyl moiety is a robust organometallic electron-donor group which has been used in the preparation of new molecular materials exhibiting non-linear optical (NLO)²² and ferromagnetic properties.²³ There are several reasons for choosing the ferrocenyl group for such studies; amongst these are that it is a good electron donor and that it has well established substitution chemistry, allowing access to a wide variety of derivatives. The latter has been particularly important in the design and synthesis of new molecular materials with second order NLO properties. One of the most important features of such materials is the packing arrangement adopted in the solid state, as this can have major influences on the bulk properties of the molecular material. One example is in the formation of L-shaped molecules in which the ferrocenyl donor group is linked to a planar polyaromatic moiety. The spacing between the cyclopentadienyl rings is ~ 3.3 Å which is comparable to the spacing in π stacked structures.²³

The work described in the following chapter is concerned with linking the ferrocene moiety to large PAHs and N-doped PAHs. This was approached in two ways, firstly the ferrocene was introduced at an early synthetic stage, to generate ferrocene containing polyphenylenes for later cyclodehydrogenation. In such a scheme the ferrocene must withstand all subsequent steps without decomposition, specifically it must survive the harsh conditions associated with cyclodehydrogenation. The second approach involved synthesising a halogen containing PAH by which to introduce the

ferrocene group *via* a palladium catalysed coupling reaction. These new compounds we anticipated to show attractive NLO behaviour and potentially act as molecular redox switches.

1.1.5. Synthesis of Ferrocene Containing Polyphenylene Compounds

The synthetic strategy that has been adopted for the formation of the polyphenylene systems in this work, is based on the Diels-Alder reaction in which acetylenes are reacted thermally with suitably substituted tetraphenylcyclopentadienones in a [2+4]-cycloaddition reaction. During this process carbon monoxide is evolved, to produce the corresponding hexaphenylbenzene. The main objective of this work was to synthesise the precursors to the polyphenylene shown in Scheme 7. At the outset of this work the di-ferrocenyl containing 1,3-diaryl-2-propanone (shown in green), the di-ferrocenyl 1,2-diaryl-1,2-diketone (shown in red) and di-ferrocenyl acetylene (shown in blue) were unknown. Through the generation of these three ferrocenyl containing precursors in combination with non-ferrocene containing analogues polyphenylenes containing, one, two, four and six ferrocene units could be prepared. Therefore a wide range of ferrocene containing polyphenylenes were synthesised and heteroatoms were incorporated into these polyphenylene systems. Nitrogen atoms were introduced in order to investigate possible coordination capabilities were cyclodehydrogenation successful and methoxy groups were incorporated in the hope that they would increase the solubility of the polyphenylenes and since they have been shown to aid cyclodehydrogenation.^{23, 24}



Scheme 7: Retrosynthetic analysis on how to synthesise non-symmetrical polyphenylene compounds.

Many metallocene-containing polyphenylenes can be found in the literature, such as $(C_5Ph_5)Fe(CO)(HC=O)PR_3$,²⁴ $(C_6Ph_6)Cr(CO)_3$,²⁵ and $[C_7Ph_6FcH]^+[SbCl_6]^-$,²⁶ shown in Figure 4.

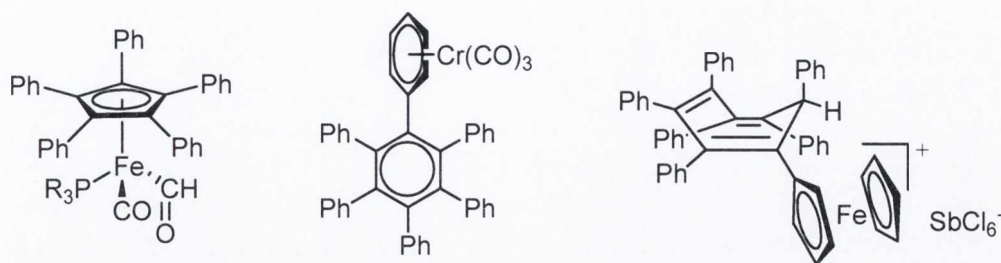


Figure 4: Examples of metallocene containing polyphenylenes synthesised to date.

Mc. Glinchey *et al* have synthesised many ferrocenyl containing polyphenylene compounds containing one ferrocene moiety as model systems in micromachines and nanotechnology (Figure 5).^{26, 27}

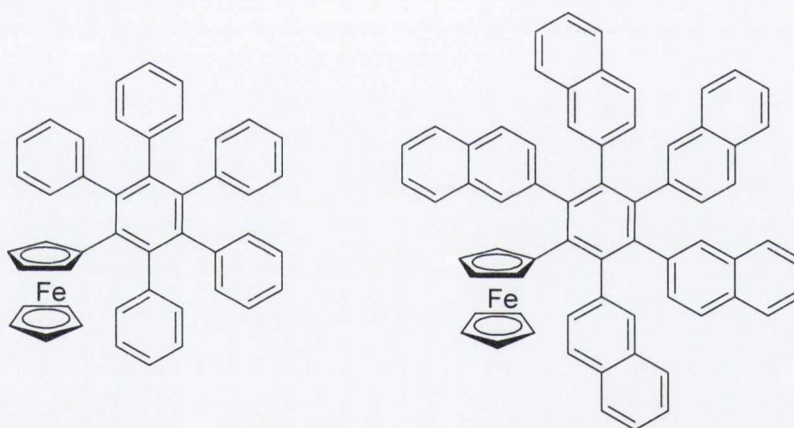
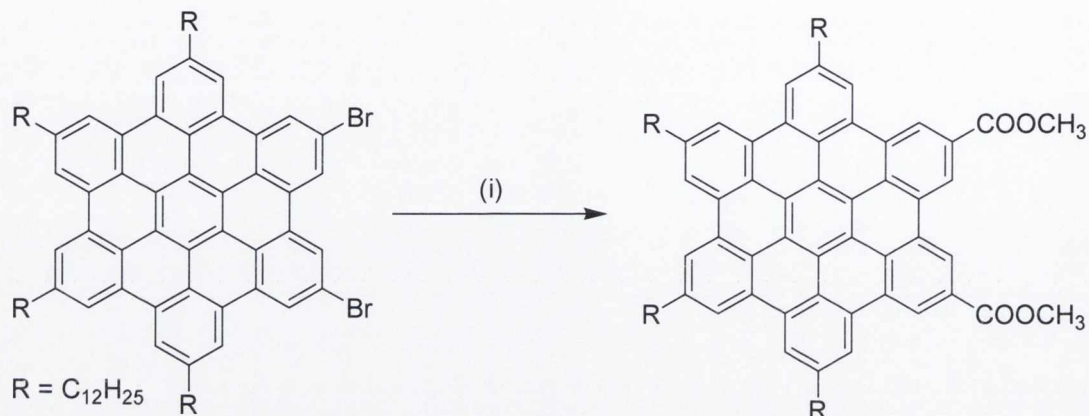


Figure 5: Two mono-ferrocenyl containing polyphenylene compounds synthesised by Mc. Glinchey *et al*.^{27, 28}

1.1.6. Synthesis by Forming PAHs and Coupling

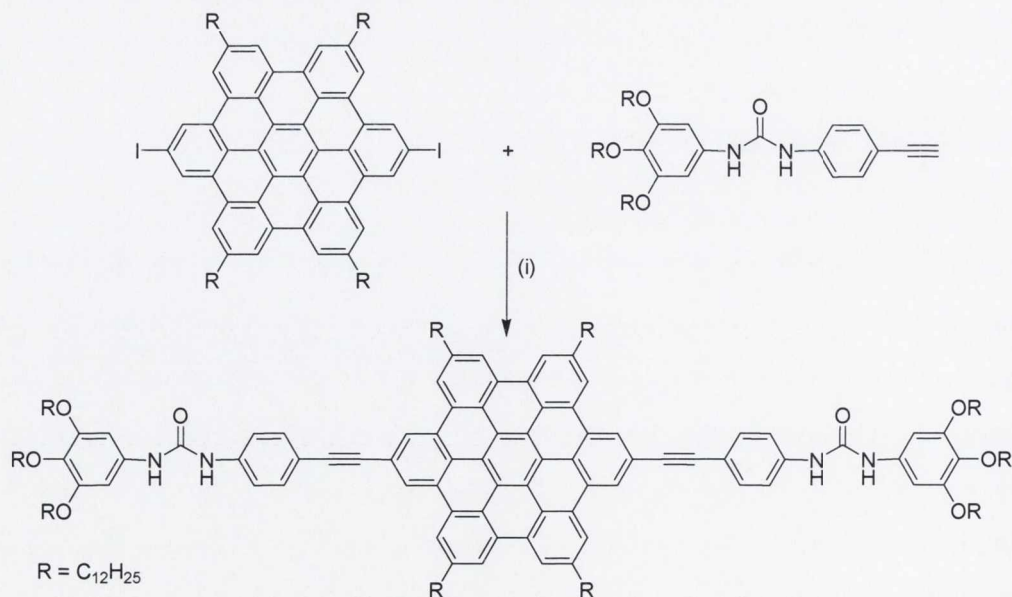
One avenue to synthesising PAHs with ferrocene on the periphery would be to synthesise a halogenated PAH platform and the careful synthetic replacement of the halogen with ferrocene e.g. by a lithiation reaction. However halogenated PAHs on lithiation and subsequent quenching generally form all-carbon PAHs in yields of up to 80 %, i.e. the lithiated species is simply protonated even in the presence of an electrophile. This is due to the fact that upon removal of the halogen the negative charge created is stabilised by the large π system of the PAH and upon quenching is simply protonated.

However palladium mediated couplings are an alternative. Scheme 8 shows the formation of a PAH containing two methyl esters, which was synthesised in a palladium catalysed carbonylation reaction with carbon monoxide and methanol under high pressure in 62 % yield.²⁸



Scheme 8: Reaction of halogen containing HBCs. (i) CO, methanol, $[\text{Pd}(\text{PPh}_3)_2\text{Cl}_2]$, PPh_3 , triethylamine, THF, 100 °C, 5 days (62 %).²⁸

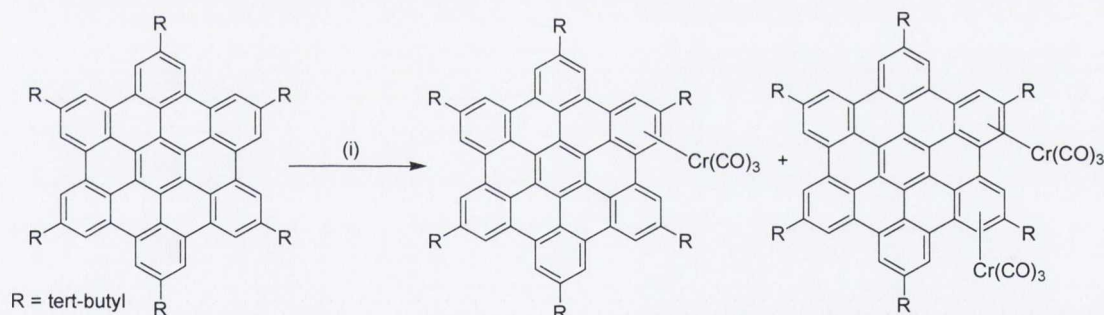
Halogen containing PAHs have also been shown to undergo Sonogashira coupling reactions which would be more suited to introducing ferrocene groups since a number of ferrocene acetylenes are known in the literature. In Scheme 9 is shown one example where a di-iodo PAH undergoes a Hagihara-Sonogashira reaction in a 13 % yield. The low yield is thought to be due to the difficulty of the work-up, which was a consequence of strong intermolecular hydrogen bonds.²⁹



Scheme 9: An example of Sonogashira coupling with halogens directly attached to a HBC platform. (i) $[\text{Pd}(\text{PPh}_3)_4]$, CuI , triethylamine, THF, 50 °C, 4 days (13 %).²⁹

Therefore as has been shown there are two possible routes to achieving the end goal of introducing the ferrocene moiety onto the periphery of a PAH system, both of which will be explored and discussed.

Although there has been great interest in these types of molecules very little research has been carried out into compounds with a ferrocene donor linked to a planar PAH moiety. PAHs have a number of attributes which could make them useful as linking groups in donor-acceptor organometallic systems. They are planar, relatively rigid with a fixed geometry and have various isomeric positions through which organometallic moieties can be bound. Their highly delocalised π -systems with small HOMO-LUMO energy separations and low vacant π^* -orbitals are likely to facilitate electronic communication between donors and acceptors. Although large polycyclic materials incorporating over 200 carbon atoms have been characterised, very few of these systems include an organometallic moiety. The only known examples are Bunz's cobalt containing ethynylated cyclobutadienes,³⁰⁻³² and the incorporation of tricarbonyl chromium into a HBC system (Scheme 10).³³



Scheme 10: The synthesis of chromium tricarbonyl containing HBCs.
 (i) Tricarbonyl(naphthalene)chromium, dioxane, THF, reflux, 3 h (20 % and 25 % respectively).

There are two compounds reported^{23,34} where ferrocene is attached to a PAH, one is attached to a PAH made up of four fused benzene rings whereas the other is composed of eight benzene rings (Figure 6), still some way off the thirteen fused benzene rings found in HBC.

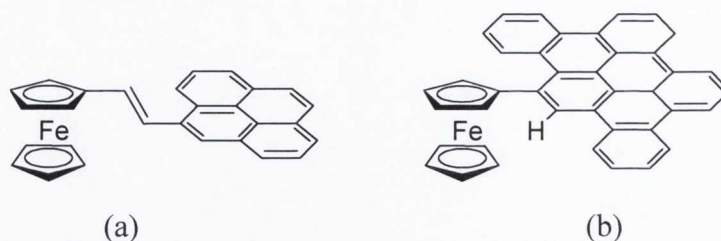


Figure 6: The structures of the only two molecules to date where a ferrocene moiety is attached to a PAH platform, (a) 1,2-ferrocenyl-pyrenyl-ethane and (b) tetra-peri-benzo-ferrocenyl-coronene.

The novel, L-shaped 1,2-ferrocenyl-pyrenyl-ethene shown as (a) in Figure 6, which links a ferrocene donor group to a planar PAH moiety, was synthesised in 1998 and has fascinating solid state electrical conductivity properties.²³ The other example shown as (b) was synthesised within the group in 2003.³⁴ It has shown interesting photophysical properties but it is unclear if there is any communication between the ferrocene and the PAH since there is free rotation around the ferrocene-PAH bond. Therefore for these compounds to be of real use and to be studied in detail we ideally need to extend the size of the PAH system and to include a form of conjugated bridge between the ferrocene and PAH to ensure communication between the donor and acceptor.

Relevant to our long term goal of preparing ferrocene intercalated graphitic sheets, and in continuation of our interest in the study of PAHs, the following chapter describes the synthesis, characterisation, electronic and redox properties of a series of novel ferrocene containing polyphenylene compounds. The ferrocene moiety will be incorporated into the polyphenylene systems by synthesising the di-ferrocenyl 1,3-diaryl-2-propanone, the di-ferrocenyl 1,2-diaryl-1,2-diketone as well as the di-ferrocenyl acetylene all of which are novel. Therefore with these three building blocks a series of ferrocene containing polyphenylene compounds will be synthesised with varying numbers of ferrocene units, some will have nitrogen atoms introduced and some will have methoxy groups incorporated in to them in order to increase the solubility of the Diels-Alder [2+4]-cycloaddition product and to aid cyclodehydrogenation.^{35, 36} The attempted cyclodehydrogenation of these compounds will be discussed.

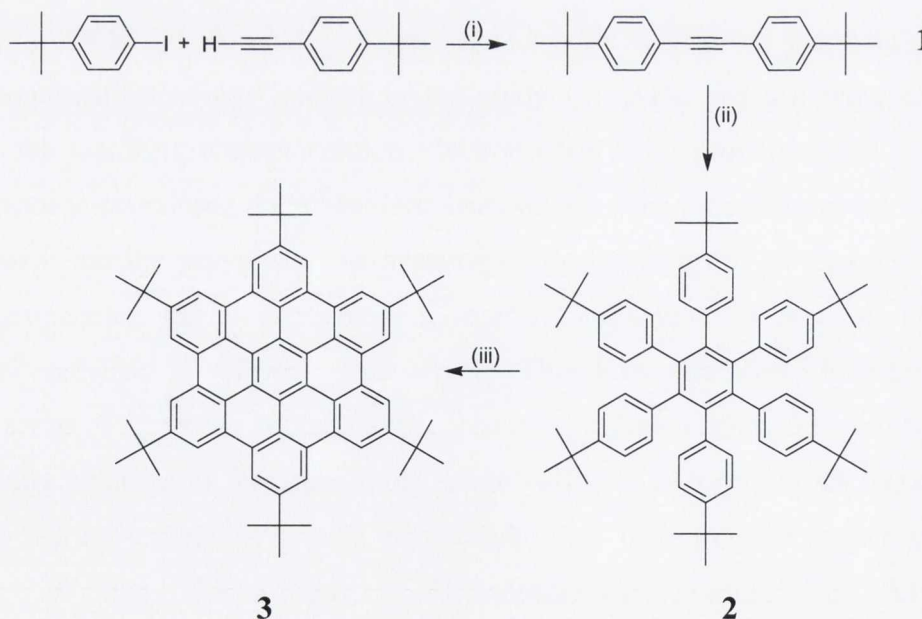
Also reported herein is the successful synthesis of the ferrocenyl containing PAH derivative (**41**) and its comprehensive characterisation including electrochemical data, which to date is the largest PAH supporting a ferrocene moiety reported.

1.2. Synthesis and Characterisation

1.2.1. Synthesis of hexa-*tert*-butyl-hexa-*peri*-hexabenzocoronene (**3**)

In order to check the synthetic conditions for the cyclodehydrogenation reaction and to have a point of reference for the characterisation of any novel compounds synthesised, the alkyl-substituted HBC **3** was synthesised. Before the cyclodehydrogenation could be attempted and optimised a series of precursors had to be synthesised in a logical manner. Acetylene **1** was synthesised *via* the Sonogashira coupling reaction between 4-*tert*-butyl-iodobenzene and 4-*tert*-butylphenylacetylene in 78 % yield. The un-cyclised polyphenylene **2** was synthesised by cyclotrimerisation with a catalytic amount of $\text{Co}_2(\text{CO})_8$ in refluxing dioxane giving compound **2** in 18 % yield.

It was found that **2** upon cyclodehydrogenation using FeCl_3 does indeed yield **3**, in 62 % yield with no apparent destruction or damage to the *tert*-butyl groups provided that a flow of argon through the reaction mixture is maintained throughout the course of the reaction.



Scheme 11: Total synthesis of HBC 3. (i) $\text{Pd}(\text{PPh}_3)_2\text{Cl}_2$, CuI , piperidine, RT, 24 h (78 %), (ii) $\text{Co}_2(\text{CO})_8$, dioxane, reflux, 20 h (18 %), (iii) FeCl_3 , CH_3NO_2 , CH_2Cl_2 , RT, 18 h (62 %).

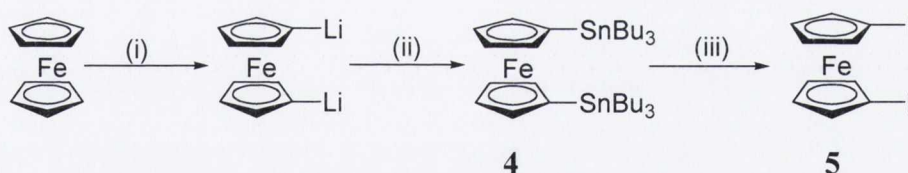
1.2.2. Ferrocenyl Containing Polyphenylene Compounds

Most of the compounds synthesised are orange/red in colour, crystalline, air-stable solids, soluble in most chlorinated and aromatic solvents. The orange/red colour is characteristic of ferrocene-containing compounds and is due to absorption in the λ 440 nm region caused by the MLCT.

In particular ferrocenyl compounds have proven themselves to be useful building blocks. Less common are synthetic and electrochemical investigations of sterically hindered ferrocenes, although these have applications as molecular machines. In our case such compounds were formed from ferrocenylacetylenes or ferrocenyl cyclopentadienones and their subsequent Diels Alder cycloaddition.

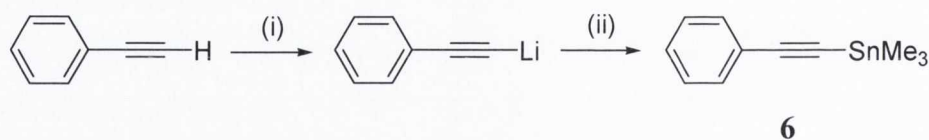
1.2.3. Mono-ferrocenyl Containing Polyphenylenes

A common starting place for a lot of ferrocene chemistry is mono- or di-iodo ferrocene due to its well understood coupling chemistry. In this vain 1, 1'-iodoferrocene was synthesised by the di-lithiation of ferrocene, followed by reaction with two equivalents of tributyltinchloride to yield 1,1'-(tri-*n*-butylstannyl)ferrocene (**4**) in 67 % yield. Subsequent reaction with iodine gave **5** in 76 % yield (Scheme 12).



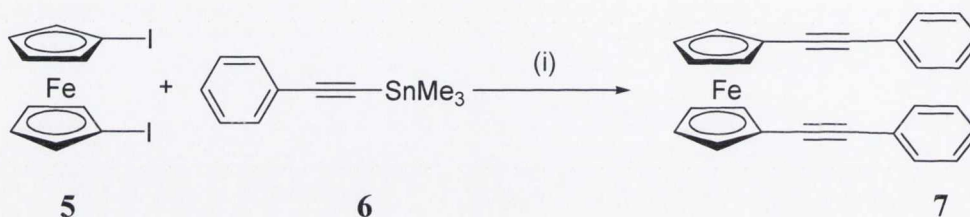
*Scheme 12: Synthesis of 1, 1'-iodoferrocene (**4**), from ferrocene. (i) *n*-BuLi, TMEDA, hexane, RT, 18 h, (ii) tributyltinchloride, Et₂O, 0 °C→RT, 6 h (67%). (iii) I₂, CH₂Cl₂, RT, 18 h (76 %).*

In order to incorporate an acetylene unit onto the ferrocene, phenylalkynyl-trimethylstannane (**6**) was synthesised by the lithiation of phenylacetylene followed by reaction with trimethyltinchloride, **6** was synthesised in 68 % yield (Scheme 13).



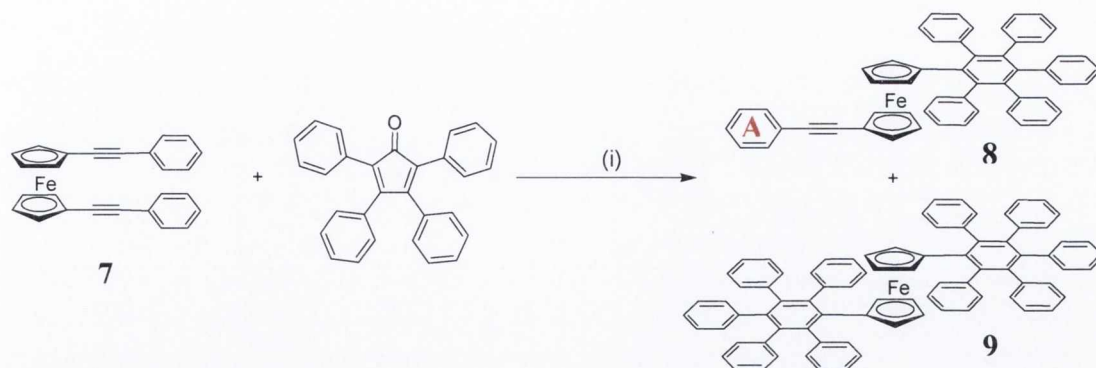
Scheme 13: Synthesis of phenylalkynyl-trimethylstannane, (6). (i) $n\text{-BuLi}$, THF, $-78\text{ }^{\circ}\text{C}$, 20 min, (ii) trimethyltin chloride, RT, 1 h (68 %).

5 and **6** had undergone Stille coupling using tetrakis(triphenylphosphine)palladium as a catalyst. The di-coupling was shown to be successful with **7** synthesised in 50 % yield (Scheme 14).



Scheme 14: Synthesis of compound 7, via a double Stille coupling. (i) $\text{Pd}(\text{PPh}_3)_4$, THF, $75\text{ }^{\circ}\text{C}$, 20 h (50 %).

The next logical step was the double [4+2] cycloaddition of tetraphenylcyclopentadienone with **7** (Scheme 15). Usually within our group and in the literature it is stated that Diels-Alder reactions of this type take place best in refluxing benzophenone ($330\text{ }^{\circ}\text{C}$), however at these temperatures ferrocene readily decomposes, therefore **7** was reacted with 2.2 equivalents of tetraphenylcyclopentadienone in a benzophenone melt and the temperature was raised slowly, while the disappearance of the starting material was monitored by TLC. The optimum temperature that was found to give reaction in a good yield but not cause decomposition of **7** was $175\text{ }^{\circ}\text{C}$. After 2 days at this temperature no **7** was evident in the reaction mixture and two new orange products were observed by TLC. After separation, the two new compounds were found to be **8** and **9** respectively.



Scheme 15: Synthesis of compounds **8** and **9** via the Diels-Alder [2+4]-cycloaddition reaction. (i) benzophenone, 175 °C, 2 d, (**8** 44 %), (**9** 18 %).

Table 1 shows the proton assignments for compounds **8** and **9**.

Compound	Chemical shift (ppm)	Multiplicity	Integration	Assignment
8	7.45-7.44	m	2	<i>ortho</i> phenyl protons (ring A)
	7.38-7.36	m	3	<i>meta</i> and <i>para</i> phenyl protons (ring A)
	7.19-7.07	m	10	<i>ortho</i> phenyl protons
	6.83-6.79	m	15	<i>meta</i> and <i>para</i> phenyl protons
	4.11	t, $^3J_{\text{HH}} = 1.8 \text{ Hz}$	2	Cp protons
	3.94	t, $^3J_{\text{HH}} = 1.8 \text{ Hz}$	2	Cp protons
	3.78	t, $^3J_{\text{HH}} = 1.8 \text{ Hz}$	2	Cp protons
	3.68	t, $^3J_{\text{HH}} = 1.8 \text{ Hz}$	2	Cp protons
9	7.00	m	20	<i>ortho</i> phenyl protons
	6.78	m	30	<i>meta</i> and <i>para</i> phenyl protons
	3.43	br s	4	Cp protons
	3.19	br s	4	Cp protons

Table 1: ^1H NMR spectral data and assignments for the mono-ferrocenyl polyphenylene compounds **8** and **9**.

One interesting feature of the proton NMR spectrum of **8** is that the protons on the substituted cyclopentadienyl rings appear as four distinct triplets, since all four pairs of cyclopentadienyl protons are non-equivalent and there is free rotation about the ferrocene axis. In the ^1H NMR spectrum of **9** two cyclopentadienyl signals are observed as expected, but in this case the signals are unresolved and broadened. This is a result of the large polyphenyl systems on both cyclopentadienyl rings of which hinder free rotation about the ferrocene axis.

Although for simplicity the phenyl rings of **8** and **9** are represented as being planar in Scheme 15 in reality work done by Mc.Glinchey *et al.*²⁴ as well as other members of the group show that they will be propeller-like. The result is that in the case of **9** there is little or no chance that the bulky polyphenyl groups can rotate about the ferrocene hence the signals appear as broad singlets.

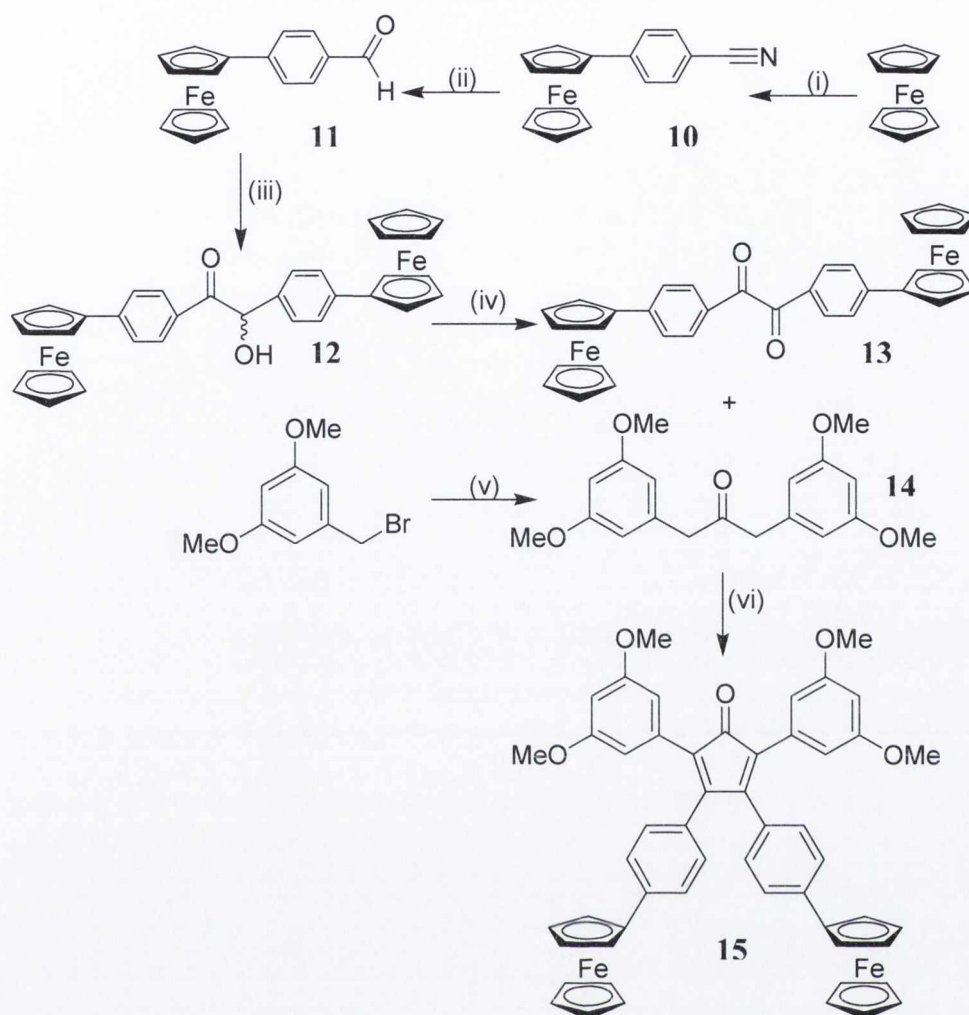
Attempts to cyclodehydrogenate **8** and **9** proved unsuccessful. Two methods were employed, CuCl_2 and AlCl_3 in CS_2 as well as FeCl_3 in MeNO_2 , both of which yielded un-characteriseable black material.

After this initial disappointment a number of polyphenylene systems containing more than one ferrocene groups were synthesised. As well as ferrocene, groups such as *tert*-butyl, methoxy groups and heteroatoms were also incorporated into these ferrocene containing polyphenylene systems in order to investigate if these groups would aid characterisation and cyclodehydrogenation.

1.2.4. Di-ferrocenyl Containing Polyphenylenes

1.2.4.1. Synthesis and Characterisation of 1,2-bis(4-phenylferrocene)ethane-1,2-dione (**13**)

In order to incorporate two ferrocene moieties into the polyphenylene systems a diketone containing two ferrocene units was synthesised. The novel 1,2-diaryl-1,2-diketone **13**, shown in Scheme 16 was synthesised in 4 steps from ferrocene. The first step in this synthesis involved a diazotization reaction between ferrocene and 4-aminobenzonitrile³⁷ and yielded **10** in 35 % yield, which was then converted to **11** in almost quantitative yield by reaction with DIBAL in toluene. Both these compounds were known in the literature, however the keto-alcohol **12** was novel and was synthesised *via* the benzoin condensation between two molecules of **11** in 59 % yield. This was then oxidized using manganese dioxide in chloroform to yield **13** in 88 % yield.



*Scheme 16: The total synthesis of compound **15**, starting from ferrocene. (i) $\text{H}_2\text{SO}_4/\text{H}_2\text{O}$, sodium nitrite, 4-aminobenzonitrile, HCl , Cu powder, 24 h (35 %). (ii) DIBAL, toluene, RT, 6 h (91 %). (iii) NaCN , water/ethanol, reflux 1 h (59 %). (iv) MnO_2 , CHCl_3 , reflux, 24 h (88 %). (v) $\text{Ca}(\text{OH})_2$, $\text{Bu}_4\text{N}(\text{HSO}_4)$, $\text{Fe}(\text{CO})_5$, $\text{CH}_2\text{Cl}_2/\text{H}_2\text{O}$, 5.5 h (65 %). (vi) KOH , EtOH , reflux, 3 h (64 %).*

Novel compounds **12** and **13** were both fully characterised by ^1H , ^{13}C NMR spectroscopy and mass spectrometry. The ^1H NMR spectrum of **13** can be seen in Figure 7, and shows the characteristic AA'XX' splitting pattern for the two aromatic protons (H6 and H7) at δ 7.93 and 7.57 ppm with a coupling constant of 8.5 Hz. Also shown in Figure 7 are the substituted ferrocenyl cyclopentadienyl protons (H2 and H3) at δ 4.77 and 4.47 ppm as well as the ten unsubstituted cyclopentadienyl ferrocene protons (H1) at δ 4.07 ppm.

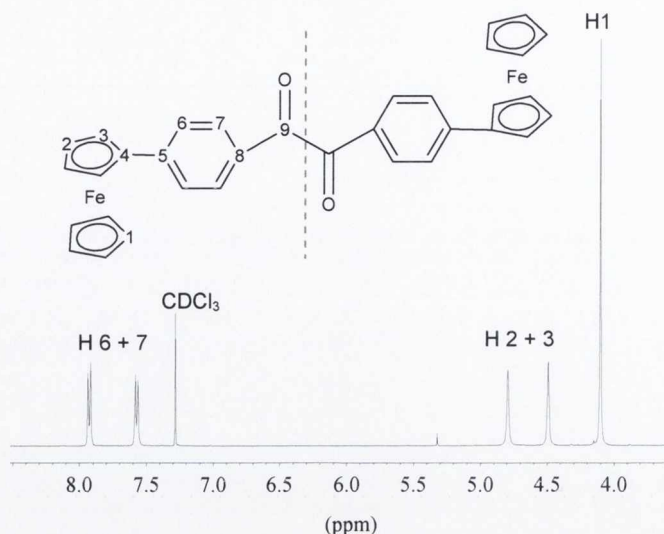


Figure 7: The ^1H NMR spectrum of the 1,2-diaryl-1,2-diketone **13** (CDCl_3 , RT, 400 MHz).

1.2.4.2. Synthesis and Characterisation of 2,5-bis-(3,5-dimethoxyphenyl)-3,4-bis-(4-phenylferrocene)-cyclopenta-2,4-dienone (**15**)

The methoxy-substituted 1,3-diaryl-2-propanone **14** (shown in Scheme 16) was prepared in 65 % yield from 3,5-dimethoxybenzyl bromide using iron pentacarbonyl in a biphasic system. The two-fold Knoevenagel condensation between **13** and **14** in an ethanolic potassium hydroxide solution yielded the tetraarylcyclopentadienone **15** in 64 % yield. Compound **15** was fully characterised by ^1H and ^{13}C NMR spectroscopy and mass spectrometry. The ^1H NMR spectrum is shown in Figure 8.

The ^1H NMR spectrum of **15** (Figure 8) is greatly simplified by the C_2 axis of symmetry that runs through the molecule. The doublets corresponding to the two aromatic protons on phenyl ring **A** are clearly visible with a $^3J_{\text{HH}}$ coupling of 8.5 Hz. The aromatic protons on phenyl ring **B** are also very distinctive; they appear as a doublet (δ 6.51 ppm) and a triplet (δ 6.39 ppm) with an integral ratio of 4:2, corresponding to H12 and H14 respectively. The coupling constant between these signals is only 2.0 Hz as it represents $^4J_{\text{HH}}$ coupling. In the ferrocenyl region we see the characteristic signals due to the ferrocene moiety and the methoxy protons. At δ 4.64 and δ 4.34 ppm the characteristic ferrocenyl *pseudo*-triplets can be seen due to H2 and H3, both integrating to 4. The remaining ferrocenyl protons corresponding to the unsubstituted cyclopentadienyl ring (H1) can be seen at δ 4.01 ppm with an

integration of 10. Finally the methoxy protons with an integration of 12 appear at δ 3.66 ppm as a singlet.

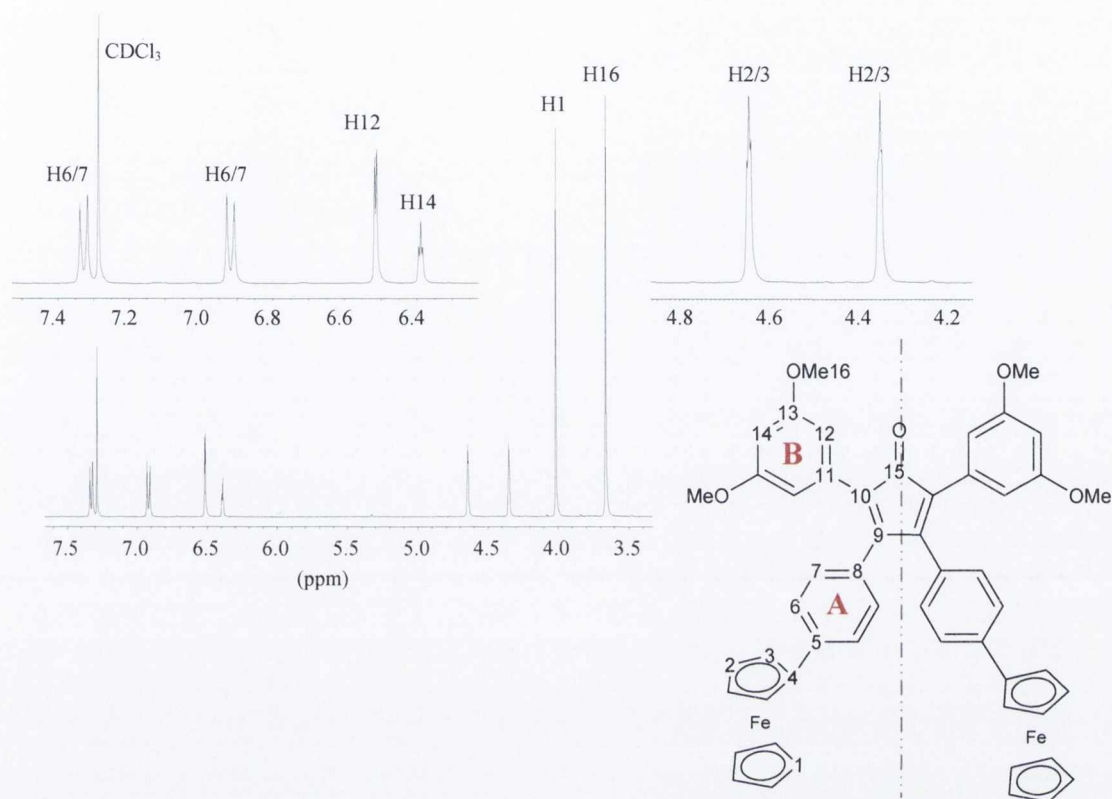
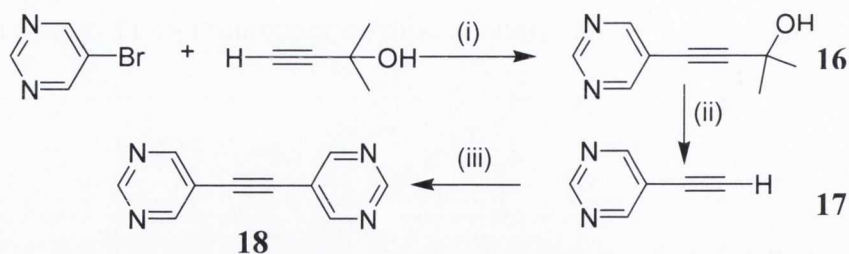


Figure 8: The ^1H NMR spectrum of **15** with the aromatic and ferrocenyl region magnified for clarity (CDCl_3 , RT, 400 MHz).

1.2.4.3. Synthesis of dipyrimidyl acetylene (**18**)

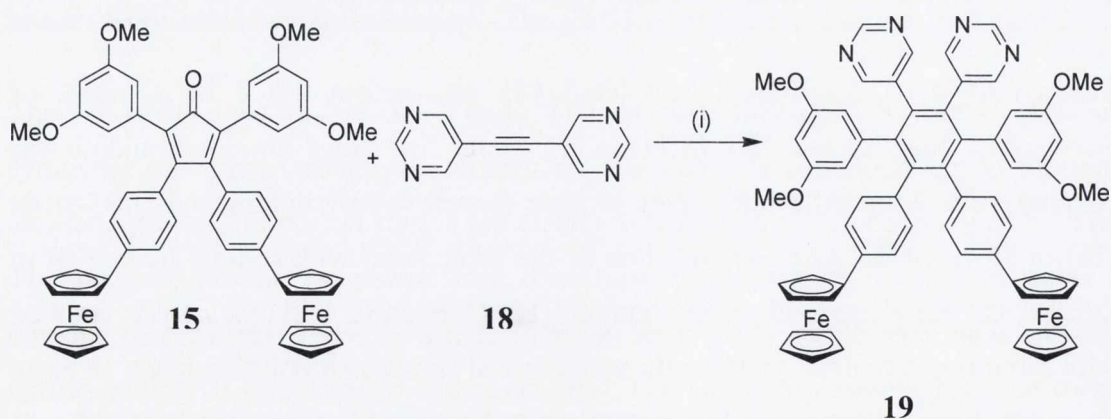
The synthesis of dipyrimidyl acetylene (**18**) was accomplished by a series of Sonogashira coupling reactions (Scheme 17). In the first step 5-bromopyrimidine was coupled with 2-methyl-3-butyn-2-ol to give 2-methyl-4-pyrimidin-5-yl-but-3-yn-ol (**16**) in 59 % yield. After deprotection of the triple bond with sodium hydroxide in toluene, the acetylene 5-ethynylpyrimidine (**17**) (formed in 43 % yield) was coupled with 5-bromopyrimidine, yielding the symmetrical substituted building block **18** as an air-stable, light yellow crystalline compound in 37 % yield. Compounds **16**, **17**, and **18** were characterised by ^1H and ^{13}C NMR spectroscopy and corresponded to the reported literature values.



*Scheme 17: The synthesis of dipyrimidine acetylene **18**. (i) $\text{Pd}(\text{PPh}_3)_2\text{Cl}_2$, CuI , Et_2NH , RT, 3 h (59 %). (ii) NaOH , toluene, reflux, 2 h (43 %). (iii) $\text{Pd}(\text{PPh}_3)_2\text{Cl}_2$, CuI , Et_3N , DMF, 55 °C, 90 min (37 %).*

1.2.4.4. Synthesis and Characterisation of Polyphenylene **19**

Central to the work was the introduction of heteroatoms into a polyphenylene precursor, introduction of methoxy groups to hopefully aid cyclodehydrogenation and finally to introduce ferrocene groups to further increase the solubility of these systems. Polyphenylene **19**, was synthesised in 58 % yield, in a stepwise manner via the Diels-Alder [2+4]-cycloaddition reaction between **15** and **18** (Scheme 18). The careful choice of starting materials and the established stereochemistry of the [2+4]-cycloaddition reaction meant that the system was chemioselective, ensuring the *ortho*-arrangement of the pyrimidine subunits on the generated benzene core of **19**. Careful consideration when synthesising the precursors to **19** has also allowed the introduction of four methoxy groups and two ferrocene moieties into the system for the reasons outlined earlier.



*Scheme 18: The synthesis of polyphenylene **19**, via the Diels-Alder [2+4]-cycloaddition. (i) benzophenone, 200 °C, 18 h (58 %).*

The full ^1H NMR spectrum of **19** can be seen in Figure 9, the presence of a C_2 axis of symmetry greatly simplifies the assignment of this spectrum. The two most downfield signals with an integral ratio of 2:4, respectively can be readily assigned as

the protons of the pyrimidine ring. The most downfield proton at δ 8.86 ppm can be assigned to H18, located between the two electron-withdrawing nitrogen atoms. The other proton of the pyrimidine ring H17 can be seen at δ 8.33 ppm. The characteristic AA'XX' splitting pattern for the two aromatic protons (H6 and H7) at δ 7.05 and 6.80 ppm, with a coupling constant of 8.0 Hz is also observed. At δ 6.05 ppm there is a singlet which has been assigned as the overlapping signals of H12 and H14, usually these appear as a doublet and a triplet respectively with small coupling constants since they are $^4J_{HH}$ couplings, but in this case they appear as one overlapping signal. Protons of the substituted ferrocenyl cyclopentadienyl rings (H2 and H3) at δ 4.55 and 4.26 ppm as well as the ten unsubstituted cyclopentadienyl ferrocene protons (H1) at δ 3.89 ppm are also observed. There is one further singlet at δ 3.52 ppm which is attributed to the twelve protons of the four equivalent methoxy groups (H19).

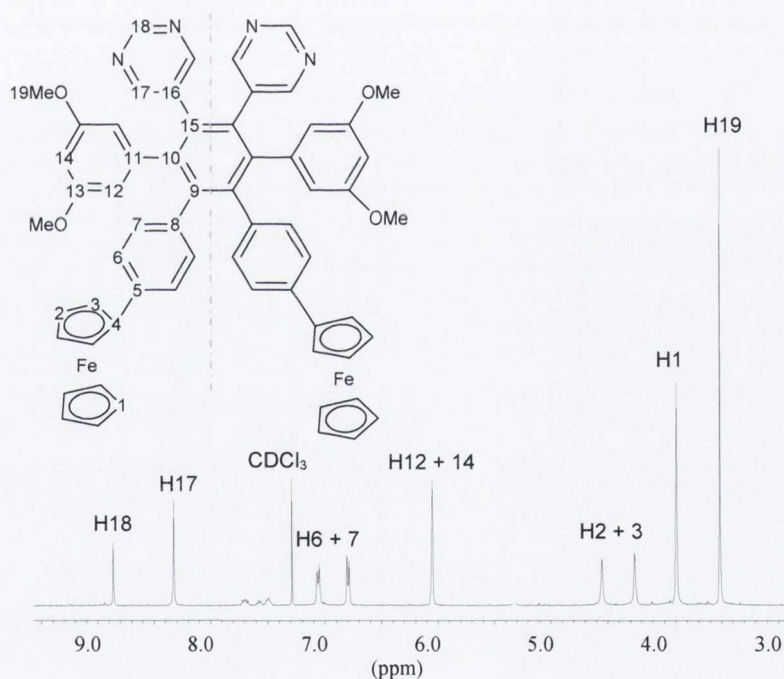


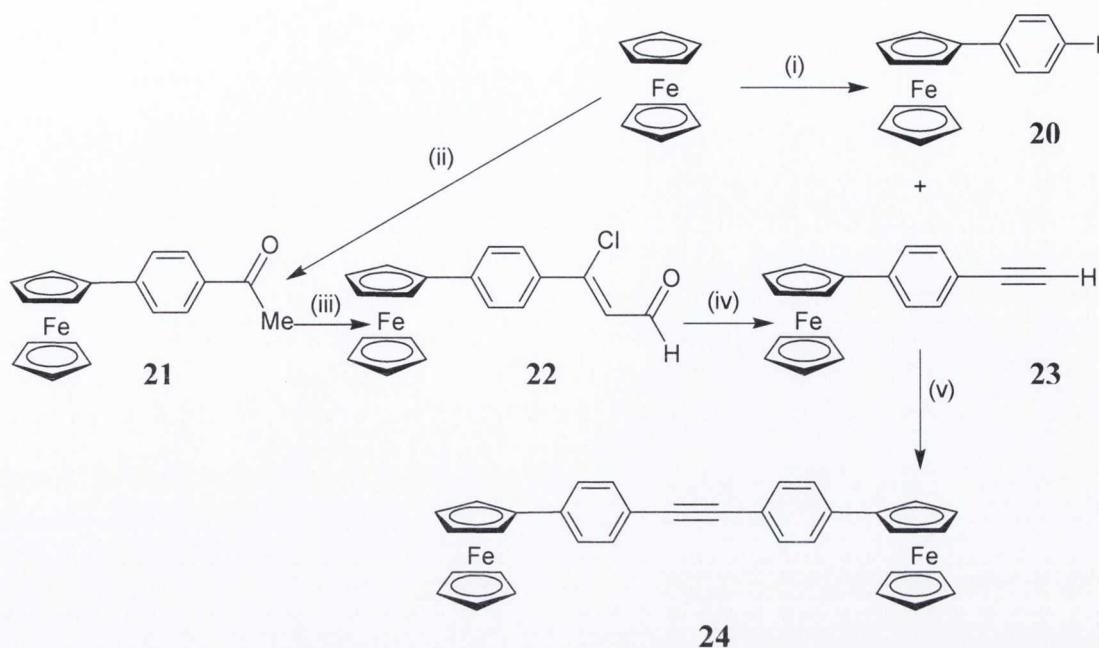
Figure 9: The ^1H NMR spectra of the aromatic and ferrocenyl region of **19** (CDCl_3 , RT, 600 MHz).

1.2.5. Tetra-ferrocenyl Containing Polyphenylenes

1.2.5.1. Synthesis and Characterisation bis(4-ferrocenylphenyl)acetylene (**24**)

In order to try and incorporate four ferrocene moieties into the polyphenylene system an acetylene containing two ferrocene moieties was successfully synthesised. It is worth noting that this acetylene was novel but during the course of my PhD another group published independently a different method for synthesising this compound.³⁸ Before the desired acetylene could be synthesised a number of precursors had to be synthesised. First of all 4-iodophenylferrocene (**20**) was synthesised by diazotization in 33 % yield. Then 4-ethynylphenylferrocene (**23**) was synthesised in a modified version of the Rosenblum method.³⁹ This involved first synthesising 4-acetylphenylferrocene (**21**) by diazotization followed by treatment with an excess of phosphorous oxychloride and DMF to yield α -chloro- β -formyl-p-ferrocenylstyrene (**22**). This was then carefully purified and heated in a basic aqueous solution and transformed into **23** in 93 % yield.

Acetylene **24** was synthesised by the Sonogashira coupling between **20** and **23** in 94 % yield as a bright orange microcrystalline solid. It is worth noting that $\text{Pd}(\text{PPh}_3)_4$ was used as a catalyst in the Sonogashira coupling so as to halt the synthesis of the homocoupled di-acetylene which proved to be inseparable from the product **24** by column chromatography and *via* selective recrystallisation. When $\text{Pd}(\text{PPh}_3)_2\text{Cl}_2$ was used a roughly one-to-one mixture of **24** and the undesired di-acetylene (formed by the homocoupling of two molecules of **23**) was formed because copper(I) iodide is used as a co-catalyst.



*Scheme 19: The total synthesis of acetylene **24** from ferrocene. (i) $\text{H}_2\text{SO}_4/\text{H}_2\text{O}$, sodium nitrite, 4-iodoaniline, HCl , Cu powder, 24 h (33 %). (ii) $\text{H}_2\text{SO}_4/\text{H}_2\text{O}$, sodium nitrite, 4-aminoacetophenone, HCl , Cu powder, 25 h (34 %). (iii) POCl_3 , DMF, $0^\circ\text{C} \rightarrow 15 \text{ min}$, $\text{RT} \rightarrow 5.5 \text{ h}$ (50 %). (iv) dioxane, aq. NaOH , reflux, 5 min (93 %). (v) $\text{Pd}(\text{PPh}_3)_4$, $\text{Et}_2\text{NH}/\text{DMF}$ (2/1), 55°C , 2 d (94 %).*

The ^1H and ^{13}C NMR spectra of **24** can be seen in Figure 10, along with assignments which correspond to the data published independently from this work.³⁸

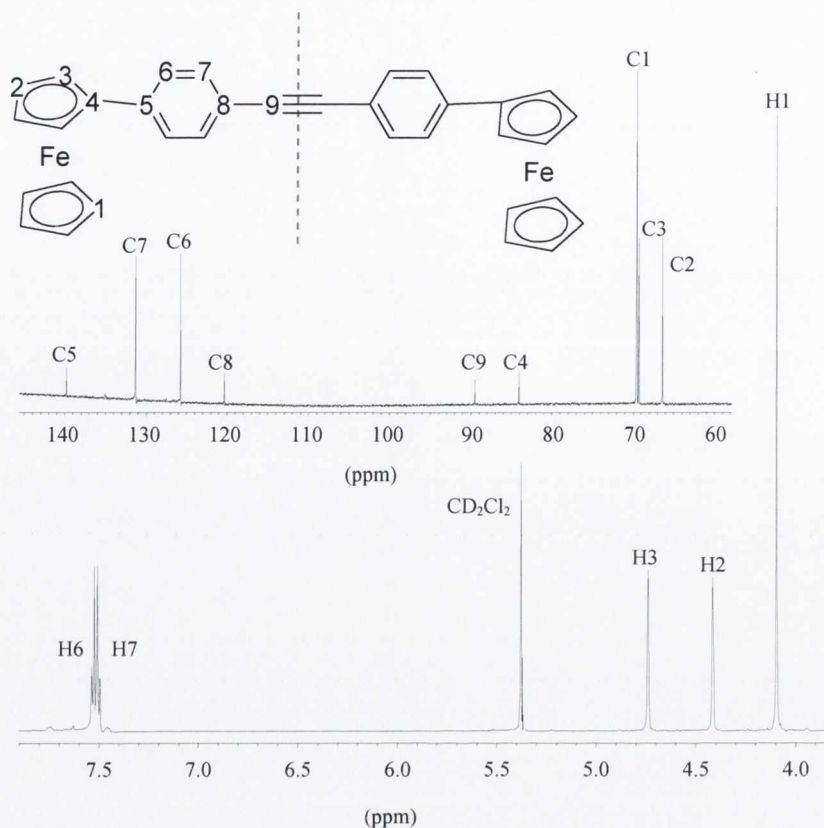
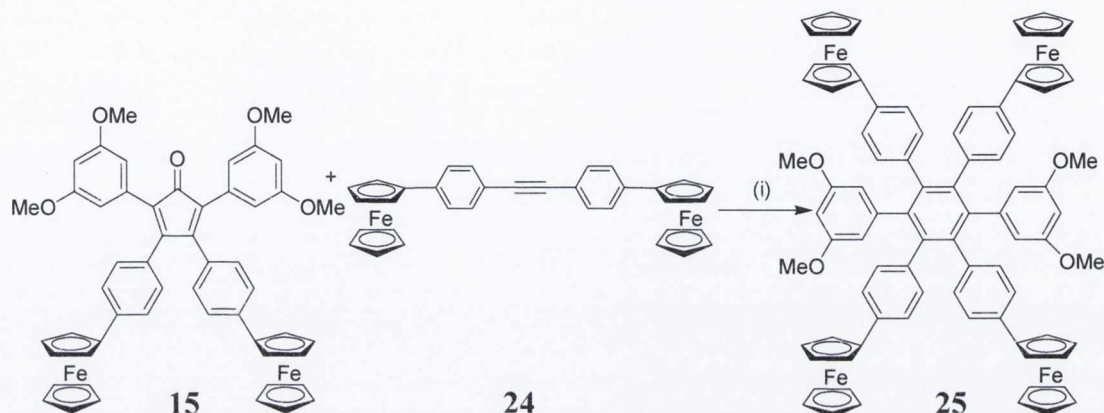


Figure 10: The ^{13}C NMR (150 MHz) and ^1H NMR (600 MHz) spectra of the aromatic and ferrocenyl region of acetylene **24** (CD_2Cl_2 , RT).

The assignment of both the ^1H and ^{13}C NMR spectra were achieved through a series of HMBC, ^{13}C - ^1H COSY and NOE experiments. The quaternary ferrocenyl carbon (C4) was easily identified from the long range coupling between it and the two ferrocenyl protons of the substituted cyclopentadienyl ring (H2 and H3). However the key to full assignment was the HMBC experiment which showed that the proton at δ 7.52 ppm had a three bond interaction with carbon atoms at δ 84.0 ppm (known to be C4) and δ 120.3 ppm which can be concluded to be C8, thus making the proton at δ 7.52 ppm, H6. The alkyne carbon atom (C9) was shown to have a long range interaction with the proton at δ 7.49 ppm, known to be H7, which in turn had a long range interaction with C5 at δ 140.6 ppm. The signal due to H3 was shown to be at δ 4.73 ppm from an NOE interaction with H6, thus all the remaining signals could be easily assigned by elimination and from the ^{13}C - ^1H COSY experiment.

1.2.5.2. Synthesis and Characterisation of Polyphenylene 25

The tetra-ferrocenyl polyphenylene **25** was synthesised by the Diels-Alder [2+4]-cycloaddition reaction between **15** and **24** at 190 °C in a benzophenone melt. The yield for this reaction (18 %) was very poor in comparison to other reactions of this type mentioned thus far.



Scheme 20: Diels-Alder [2+4]-cycloaddition reaction yielding polyphenylene **25**.
(i) benzophenone, 190°C, 18 h (18%).

In Figure 11 the full proton NMR spectrum of **25** can be seen and is simplified by the presence of a C_2 axis of symmetry. The characteristic AA'XX' splitting pattern for the two aromatic protons (H6 and H7) at δ 7.06 and 6.83 ppm, with a coupling constant of 8.0 Hz is clearly observed. At δ 6.14 ppm the doublet corresponding to H12 can be seen which is coupled *via* a $^4J_{HH}$ coupling to the H14 triplet at δ 6.02 ppm, with a coupling constant of 2.0 Hz. Protons of the substituted ferrocenyl cyclopentadienyl rings (H2 and H3) at δ 4.54 and 4.23 ppm as well as the ten unsubstituted cyclopentadienyl ferrocene protons (H1) at δ 3.91 ppm are also observed. There is one further singlet at δ 3.48 ppm which is attributed to the twelve protons of the four equivalent methoxy groups (H15).

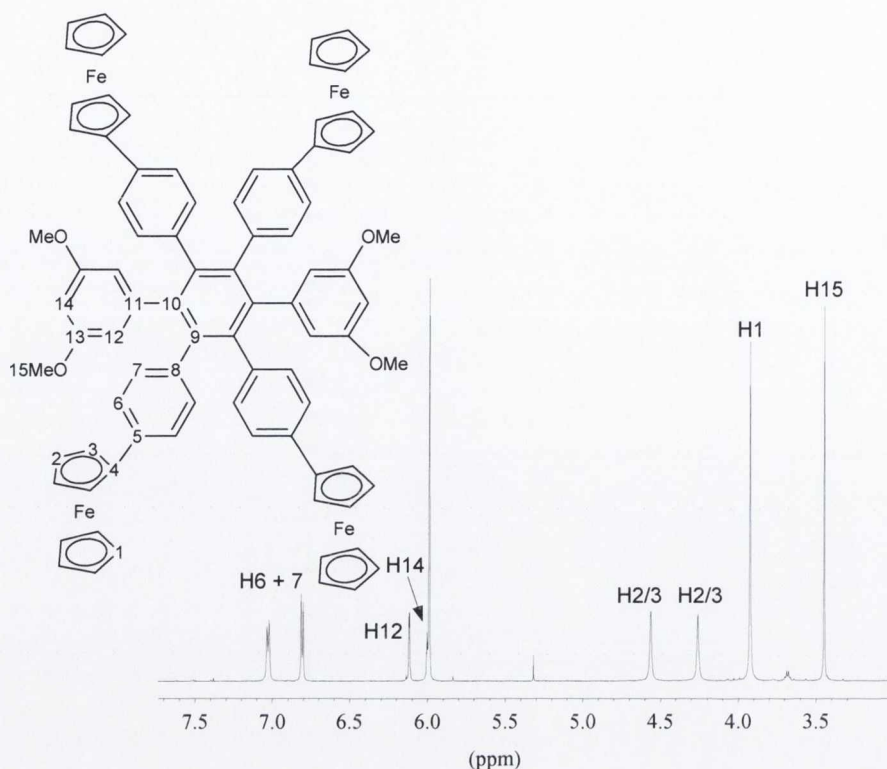
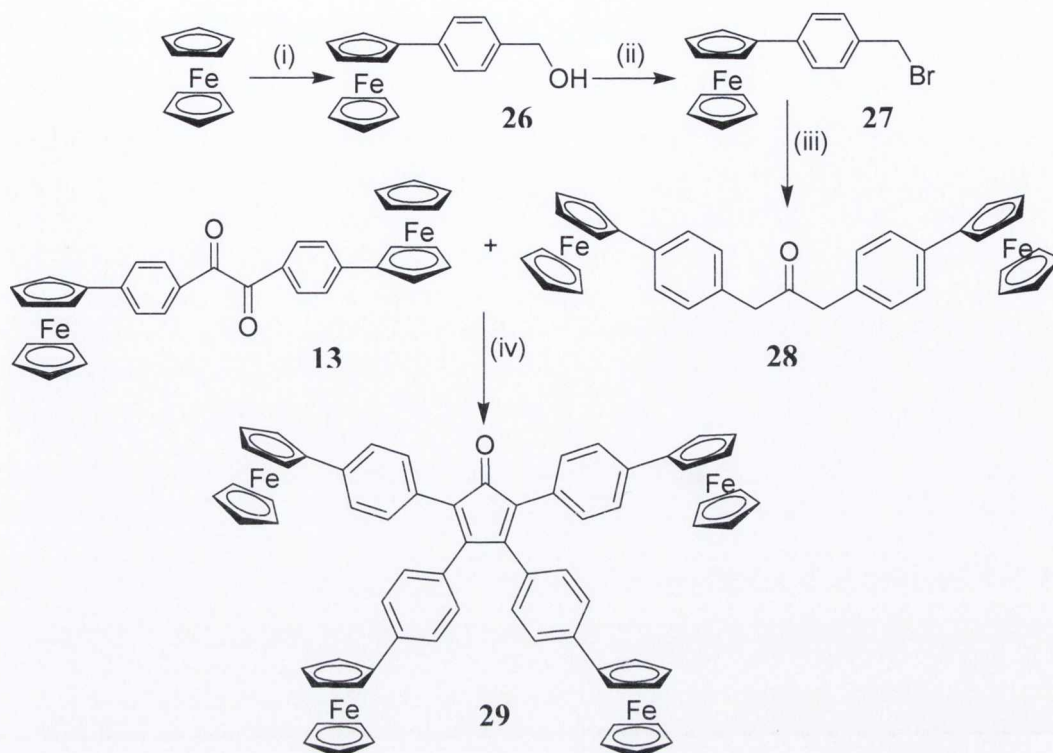


Figure 11: ^1H NMR spectrum of the aromatic and ferrocenyl region of polyphenylene **25**. ($\text{C}_2\text{D}_2\text{Cl}_4$, 60°C , 400 MHz).

1.2.5.3. Synthesis and Characterisation of 2,3,4,5-tetra-(4-ferrocenyl-phenyl)cyclopenta-2,4-dienone (**29**)

In order to complete the series of these ferrocene containing polyphenylene systems with both nitrogen atoms and methoxy groups it was decided to synthesise the novel tetra-ferrocenyl containing cyclopentadienone **29**. This was synthesised in eight steps (including the four steps required to synthesise **13**, discussed earlier) as shown in Scheme 21.



*Scheme 21: The total synthesis of compound **29** starting from ferrocene (i) H_2SO_4/H_2O , sodium nitrite, 4-aminobenzylalcohol, HCl , Cu powder, 24 h (31 %). (ii) PBr_3 , CH_2Cl_2 , $0^\circ C$, 30 min (94 %). (iii) $Ca(OH)_2$, $Bu_4N(HSO_4)$, $Fe(CO)_5$, CH_2Cl_2/H_2O , 6 h (58 %). (iv) KOH , $EtOH$, reflux, 18 h (63 %).*

The synthesis of **27** and the hydroxymethyl-substituted ferrocene **26** have been reported in the literature. The synthesis of **26** by Roth *et al.*⁴⁰ was achieved by the reduction of the corresponding ester. The treatment of this benzyl alcohol with PPh_3 and CBr_4 in diethylether yielded **27** in 46 % yield.⁴¹

The synthesis of **26** and **27** was improved by generating **26** from ferrocene. Therefore **26** was synthesised by diazotization in 31 % yield in one step as opposed to the two steps reported elsewhere. The bromination was done using phosphorous tribromide in dichloromethane and yielded **27** in quantitative yield.

The novel di-ferrocenyl containing 1,3-diaryl-2-propanone **28** was prepared from **27** using iron pentacarbonyl in a biphasic system in 58 % yield. The product was fully characterised by 1H and ^{13}C NMR spectroscopy as well as mass spectrometry.

The proton NMR spectrum of **28** can be seen in Figure 12, and it shows the expected number and types of signals. The most downfield signals are attributed to the aromatic protons H6 and H7 at δ 7.45 and 7.11 ppm yielding the characteristic AA'XX' splitting pattern, with a coupling constant of 8.0 Hz. Protons of the substituted ferrocenyl cyclopentadienyl rings (H2 and H3) at δ 4.65 and 4.34 ppm as well as the ten unsubstituted cyclopentadienyl ferrocene protons (H1) at δ 4.07 ppm are also observed. There is one further singlet at δ 3.75 ppm which is attributed to the benzylic proton H9. The full ^{13}C NMR spectrum can be seen in the experimental section and contains the characteristic downfield carbonyl carbon (C10) signal at δ 205.5 ppm as well as the expected number of aromatic, ferrocenyl and benzylic CHs and the expected number of quaternary carbons.

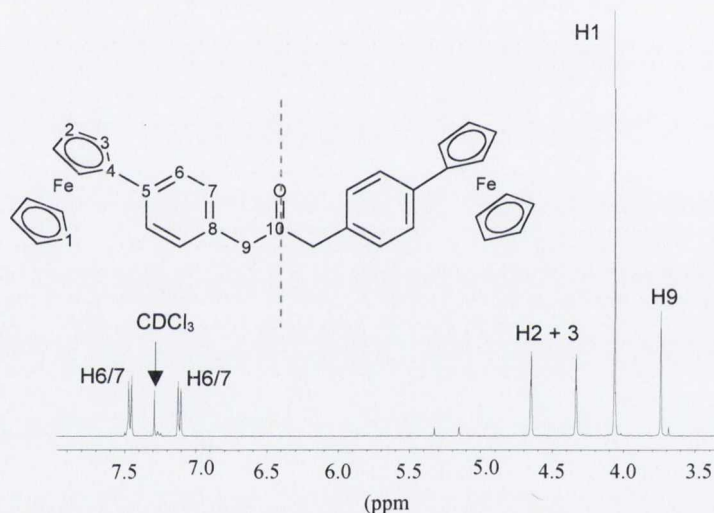


Figure 12: ^1H NMR spectrum of the aromatic and ferrocenyl region of the 1,3-diaryl-2-propanone **28** (CDCl_3 , RT, 400 MHz).

The two-fold Knoevenagel condensation between **28** and the di-ferrocenyl 1,2-diaryl-1,2-diketone **13** (Scheme 21) in an ethanolic potassium hydroxide solution yielded the tetra-ferrocenyl containing cyclopentadienone **29** as a purple solid in 63 % yield. Compound **29** was characterised by ^1H and ^{13}C NMR spectroscopy, and was found to be quite unstable as a solid and particularly unstable in solution.

The proton NMR spectrum of the tetraphenyl cyclopentadienone **29** can be seen in Figure 13. In the aromatic region two AA'XX' systems can be clearly observed attributed to the two different phenyl ring environments. A ^1H - ^1H COSY experiment made it was possible to assign which protons are coupled to each other in the two separate spin systems but not to determine which was which. The protons at δ 7.39

and 7.30 ppm are shown to make up one aromatic spin system whilst those at δ 7.34 and 6.94 ppm make up the other. In the ferrocenyl region, the four different sets of protons of the substituted ferrocenyl cyclopentadienyl rings can be seen clearly as four distinct *pseudo*-triplets at δ 4.67, 4.64, 4.35 and 4.33 ppm all with small coupling constants of 2.0 Hz. As well as these four ferrocenyl triplets, two singlets corresponding to the two different unsubstituted cyclopentadienyl ferrocene proton environments are observed at δ 4.05 and 4.04 ppm.

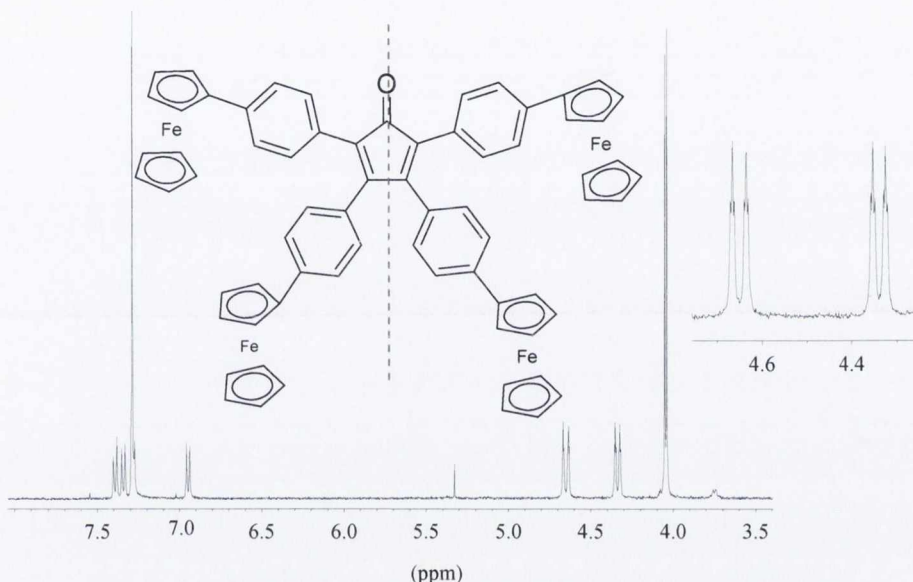
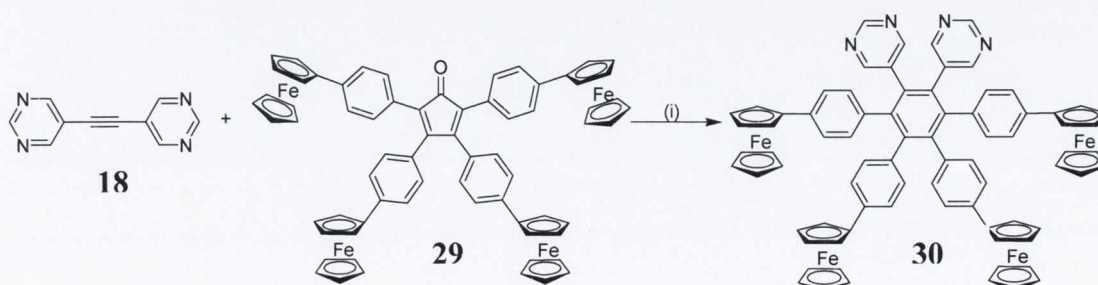


Figure 13: ^1H NMR spectrum of **29** (CDCl_3 , RT, 600 MHz).

1.2.5.4. Synthesis and Characterisation of Polyphenylene **30**

The N-doped tetra-ferrocenyl polyphenylene **30** was synthesised by the Diels-Alder [2+4]-cycloaddition reaction between **18** and **29** at 200 °C in a benzophenone melt. The desired product was purified by column chromatography as an orange crystalline solid in 54 % yield.



Scheme 22: The synthesis of the N-doped tetra-ferrocenyl polyphenylene **30**. (i) benzophenone, 200 °C, 18 h (54 %)

30 as can be seen in Figure 14 has a C_2 axis of symmetry. The two most downfield signals integrate 2:4, respectively, in the ^1H NMR spectrum and were assigned as the protons of the pyrimidine ring. The signal at δ 8.81 ppm is due to the resonance of H22, located between the two electron-withdrawing nitrogen atoms. The assignment of the other proton of the pyrimidine ring H21 to the signal at δ 8.32 ppm is key to the full assignment of the ^1H spectrum. The remaining aromatic signals are represented by four doublets. An NOE on H21 shows an interaction with a proton at δ 6.78 ppm which is thus identified as due to H12. This from the ^1H - ^1H COSY experiment is coupled to H13 at δ 7.07 ppm.

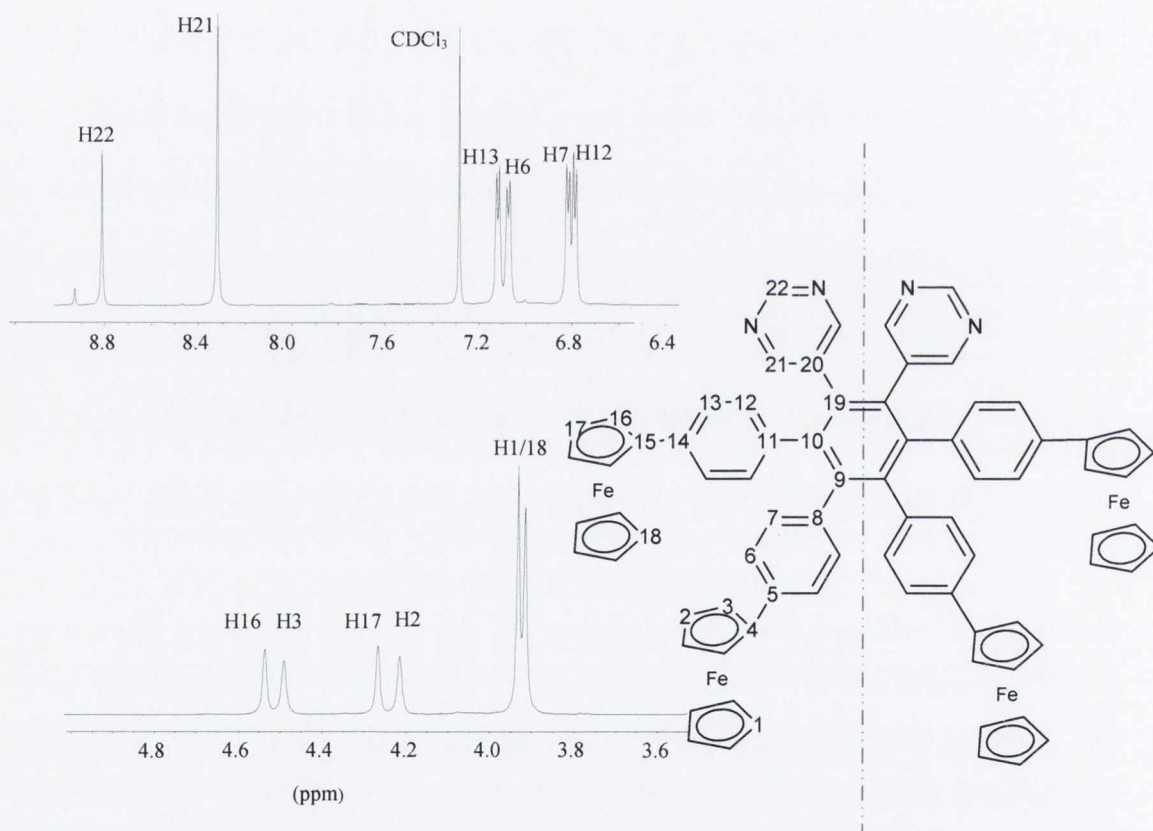


Figure 14: The ^1H NMR of **30** (CDCl_3 , RT, 600 MHz).

A long-range HMBC allowed all the other proton signals to be assigned along with their associated ^{13}C signals (Table 2).

^1H signal (ppm)	Carbon atom label ^{13}C NMR assignment	Long-range Coupling (HMBC) Data
4.21	C2	84.2 (C4)
4.26	C17	83.6 (C15)
4.48	C3	---
4.53	C16	---
6.78	C12	141.5 (C10), 137.5 (C14)
6.81	C7	136.7 (C5), 142.4 (C9)
7.07	C6	84.2 (C4), 136.9 (C8)
7.12	C13	83.6 (C15), 136.04(C11)
8.32	C21	133.1 (C19), 133.9 (C20)
8.81	C22	133.9 (C20)

Table 2: Assignment of the ^{13}C signals for compound **30** by HMBC experiment.

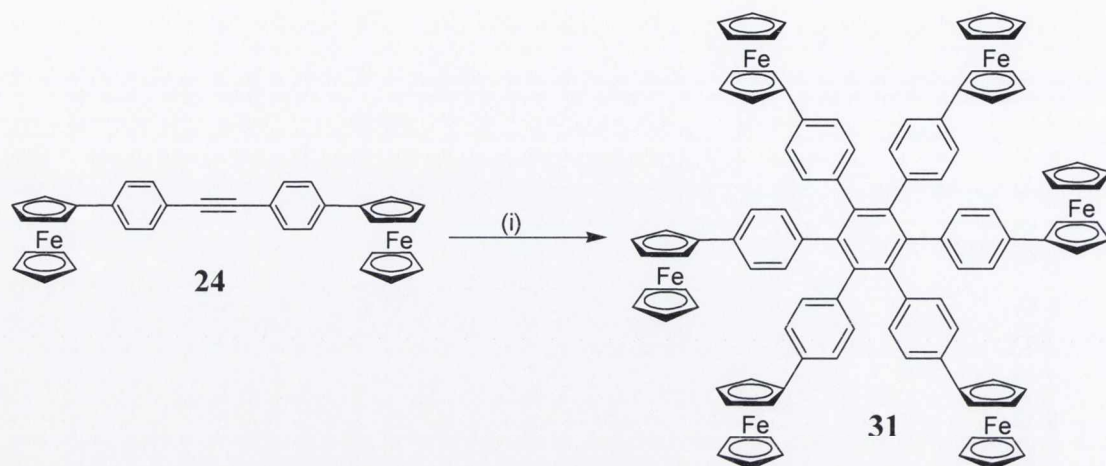
1.2.6. Hexa-ferrocenyl Containing Polyphenylene

1.2.6.1. Synthesis and Characterisation of hexa(4-ferrocenylphenyl)benzene (**31**)

With the two tetra-ferrocenyl polyphenylenes **25** and **30** synthesised the next logical step was to try and synthesise a hexa-ferrocenyl polyphenylene in order to complete a series of ferrocene containing polyphenylene compounds ranging from one to six ferrocene units. This could be done in one of two ways. Firstly the tetra-ferrocenyl cyclopentadienone (**29**) could be reacted in a Diels-Alder [2+4]-cycloaddition reaction with **24** yielding **31**. This was not done since in the synthesis of **25** it was seen that **24** does not yield Diels-Alder products in comparable yields to those obtained with non-ferrocene containing acetylenes.

A more efficient route toward the synthesis of **31** was *via* the cyclotrimerisation of **24**. When acetylene **24** was reacted with a catalytic amount of cobalt octacarbonyl in refluxing dioxane the hexa-ferrocenyl polyphenylene compound **31** was indeed synthesised in 25 % yield. As with the synthesis of **24**, **31** was also synthesised

independently and simultaneously by Rathore *et al.*³⁸ They did not report any attempted cyclodehydrogenation however.



*Scheme 23: Cyclotrimerisation of **24** yielding the hexa-ferrocenyl polyphenylene **31**.
(i) $\text{Co}_2(\text{CO})_8$, dioxane, reflux, 3 h (25 %).*

The ^1H and ^{13}C NMR spectra of compound **31** can be seen in Figure 15. The high degree of symmetry within the molecule yields only five signals in the proton spectrum. The most downfield signals are attributed to the aromatic protons H6 and H7 at δ 7.07 and 6.84 ppm yielding the characteristic AA'XX' splitting pattern, with a coupling constant of 8.0 Hz. Protons of the substituted ferrocenyl cyclopentadienyl rings (H2 and H3) at δ 4.51 and 4.20 ppm as well as the ten unsubstituted cyclopentadienyl ferrocene protons (H1) at δ 3.94 ppm are also observed.

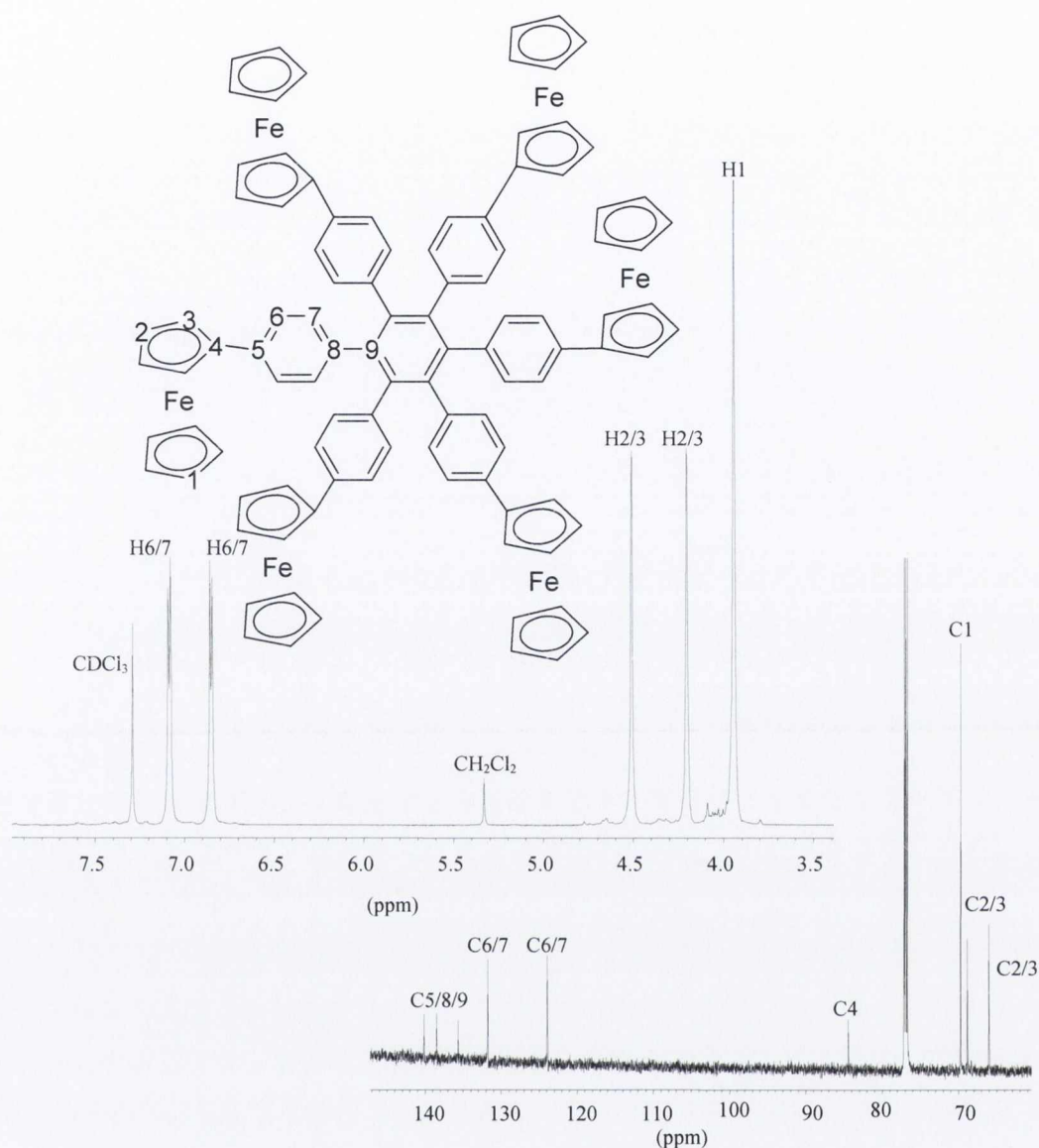


Figure 15: The ^1H NMR (600 MHz) and the ^{13}C NMR (150 MHz) spectra of the aromatic and ferrocenyl region of **31** (CDCl_3 , RT).

The quaternary aromatic carbons C5, C8 and C9 can be seen at δ 139.8, 138.1 and 135.3 ppm, and are the most downfield carbon signals in the ^{13}C NMR spectrum. The aromatic CHs C6 and C7 appear at δ 131.4 and 123.5 ppm. The quaternary ferrocenyl C4 is seen at δ 84.0 ppm at a very similar chemical shift to the quaternary ferrocenyl carbon in **24**. The main difference between the carbon spectra of **24** and **31** is the disappearance of the acetylene carbon signal at δ 89.5 present in **24** and the appearance of a new aromatic quaternary carbon, indicating that cyclotrimerisation has indeed occurred. These values concur with the values reported in the literature.³⁸

1.2.7. Cyclodehydrogenation of Ferrocenyl Polyphenylenes

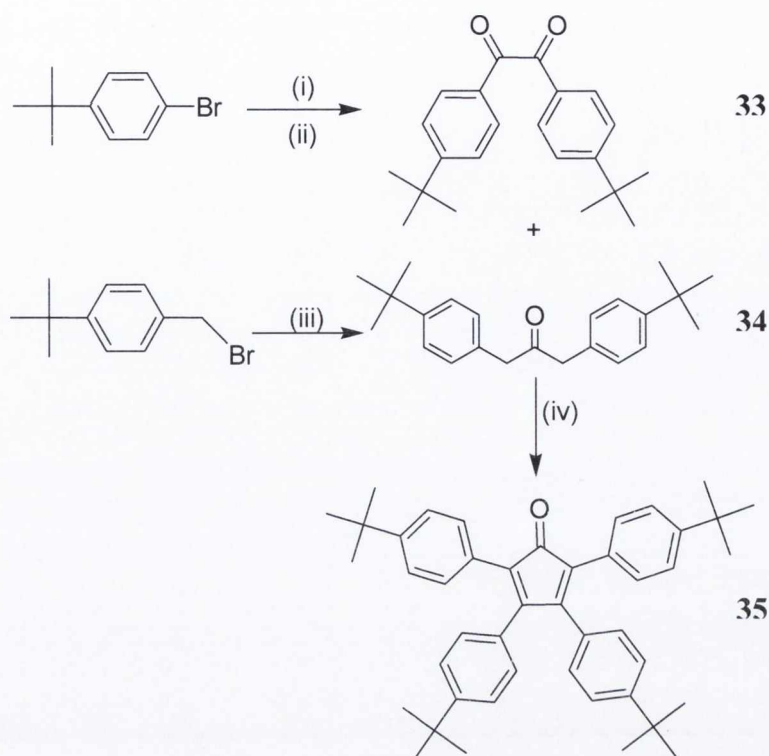
The attempted cyclodehydrogenation of compounds **3**, **8**, **9**, **19**, **25**, **30** and **31** proved unsuccessful. It was shown that after the attempted cyclodehydrogenation of **8** and **9** all that was recovered after work-up was un-characteriseable black material, and no starting material, most probable was that complete decomposition of **8** and **9** had taken place. However in the cases of compounds **19**, **25**, **30** and **31** no decomposition was observed and only starting material was recovered. This will be discussed fully in the discussion of the UV-vis spectra of these compounds in section 1.2.10.

1.2.8. Synthesis of ferrocenyl-HBC

1.2.8.1. Synthesis and Characterisation of iodo-polyphenylene (**37**)

Due to the unsuccessful cyclodehydrogenation of the ferrocene containing polyphenylenes **3**, **8**, **9**, **19**, **25**, **30** and **31** a change of tactic was required if a large PAH with ferrocene on the periphery was going to be synthesised. Müllen *et al.*^{28, 29} have shown that halogen atoms incorporated into PAH are labile enough to undergo palladium catalysed coupling reactions. It was decided to undertake the synthesis of iodo containing HBC which once cyclised should yield a site where the ferrocene moiety could be introduced.

The halogenated PAHs synthesised by Müllen *et al.* have been shown to be very insoluble, requiring a mixture of CS₂ and chloroform even for analysis by NMR spectroscopy. In order to avoid any future solubility problems after cyclodehydrogenation the *tert*-butyl substituted cyclopentadienone was synthesised as the diene for the Diels-Alder reaction with the iodo containing acetylene. The 1,2-diaryl-1,2-diketone synthesis by Muller-Westerhoff,⁴² and the synthesis of 1,3-diaryl-2-propanones, based on the synthesis of des Abbayes,⁴³⁻⁴⁵ permit the formation of alkyl-substituted cyclopentadienones (Scheme 24).



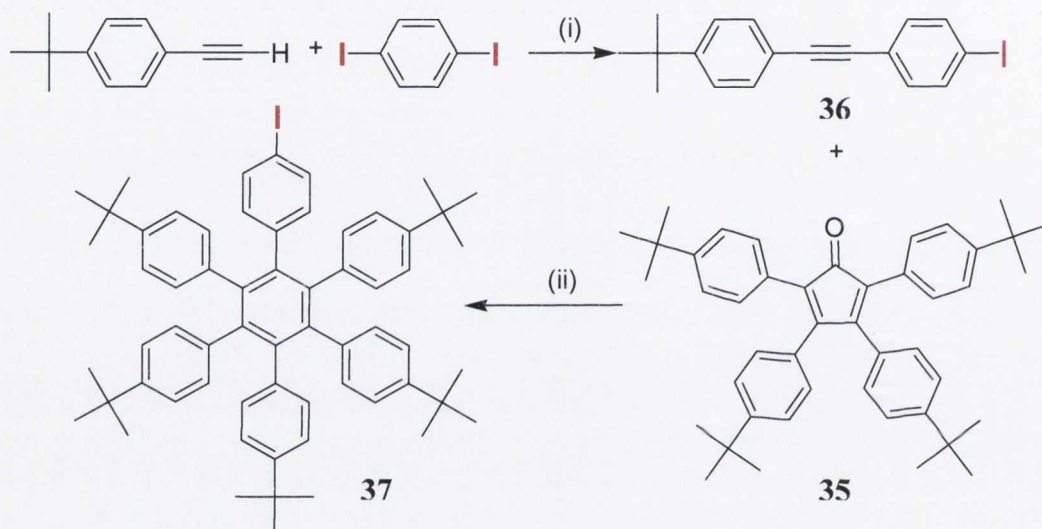
*Scheme 24: The synthesis of tert-butyl substituted tetraphenylcyclopentadienone **35**. (i) *n*-BuLi, THF, -78 °C, 90 min. (ii) DMPD (**32**), THF, -78 °C→RT, 4 h (45 %). (iii) Ca(OH)₂, Bu₄N(HSO₄), Fe(CO)₅, CH₂Cl₂/H₂O, 5 h (67 %). (iv) KOH, EtOH, 25 min (62 %).*

Treatment of 4-*tert*-butyl-bromobenzene with *n*-butyllithium at -78 °C, followed by addition of DMPD afforded the 1,2-diaryl-1,2-diketone, (**33**) in 45 % yield as a white crystalline solid. 4-*tert*-butyl-bromobenzylbromide was converted to the 1,3-diaryl-2-propanone (**34**), using iron pentacarbonyl in a biphasic system. The two-fold Knoevenagel condensation of **33** and **34** in refluxing ethanol with potassium hydroxide, yielded the cyclopentadienone building block **35** as a dark red/purple solid in 62 % yield.

Central to this work is the introduction of a halogen atom into a polyphenylene precursor. It made logical sense to introduce the halogen into the acetylene. The iron pentacarbonyl method for the synthesis of 1,3-diaryl-2-propanone is generally restricted to symmetric molecules although some work has been done on asymmetric 1,2-diaryl-2-propanones.⁴⁶ The same is true of the 1,2-diaryl-1,2-diketone synthesis, in that only symmetric diketones are synthesised *via* lithiation and reaction with

DMPD, however mixed diketones can be synthesised *via* a mixed benzoin condensation.²⁷

Therefore the halogen was incorporated into the acetylene in one step. 4-*tert*-butyl phenylacetylene was coupled with 1,4-diodobenzene in a Sonogashira coupling reaction which yielded **36** as a yellow-white crystalline solid in 65 % yield. The Diels-Alder [2 + 4]-cycloaddition reaction between **35** and **36** yielded **37** as a white crystalline solid in 63 % yield with the evolution of carbon monoxide.¹³



*Scheme 25: The synthesis of **36** via a Sonogashira coupling reaction, followed by Diels-Alder [2+ 4]-cycloaddition, yielding the polyphenylene **37**. (i) $\text{PdCl}_2(\text{PPh}_3)_2$, CuI , THF, diisopropylamine, RT, 18 h (65 %) (ii) diphenyl ether, 280 °C, 18 h (63 %).¹³*

Compound **37** contains a C_2 axis of symmetry. The ^1H NMR spectrum of **37** (Figure 16) consists of eight aromatic doublets some of which are overlapping, and full assignment of the ^1H NMR spectrum was more problematic as a result. The aromatic signals due to the iodo-phenyl group are the most distinguishable since H2 at δ 7.18 ppm is the most downfield signal and H3 at δ 6.60 ppm is the most upfield aromatic signal. The coupling constant between H2 and H3 is 8.0 Hz and they both integrate as expected for 2. The remaining signals integrate to 20 aromatic protons corresponding to H5-H10. H5, H7 and H9 i.e. the protons which are closest to the central phenyl ring are the most upfield in their respective spin systems whereas the protons H6, H8 and H10, which are at the periphery are the most downfield.¹³ The five *tert*-butyl groups represent a total of 45 protons and the C_2 symmetry should translate to three

non-equivalent proton environments for the *tert*-butyl protons. However in the ^1H spectrum of **37** there are just two singlets corresponding to the *tert*-butyl groups. A singlet at δ 1.15 ppm that integrates to 18 protons and a singlet at δ 1.12 ppm that integrates to 27 protons, due to the overlapping of the *tert*-butyl protons labelled H11 and H12.

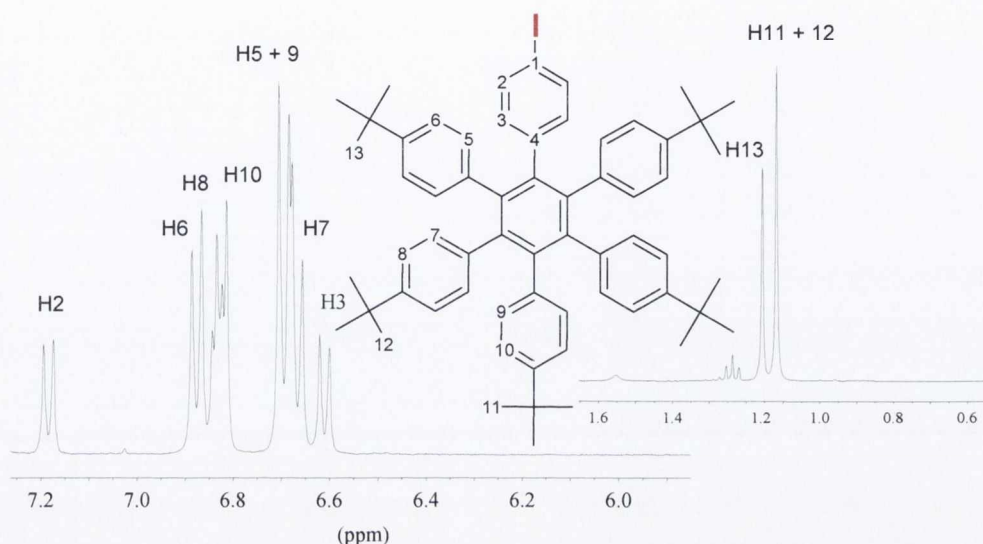


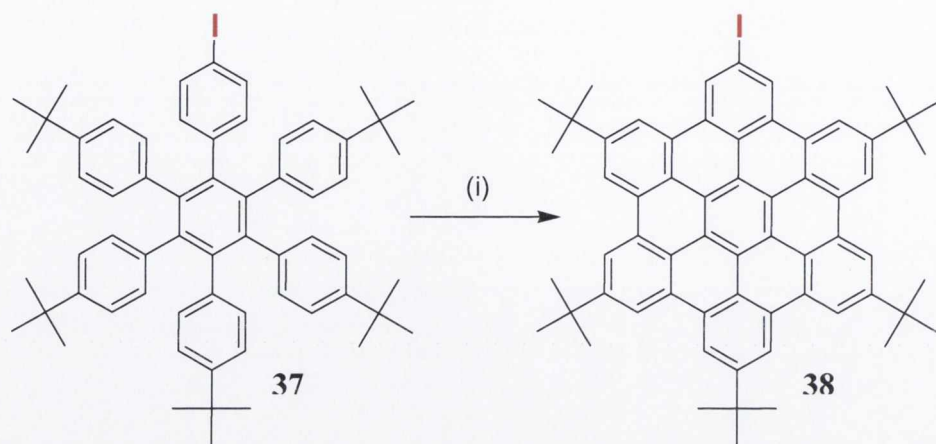
Figure 16: The ^1H NMR spectrum for **37**, with the aromatic region and the aliphatic region highlighted (CDCl_3 , RT, 600 MHz).

The carbon NMR spectrum of **37** shows the expected number of signals, 20 non-equivalent aromatic carbon atoms (eight aromatic CHs and twelve quaternary), in addition to the carbon signals of the *tert*-butyl groups. The most upfield signal was observed at δ 90.4 ppm corresponding to the quaternary signal at C1, adjacent to the iodine group.

1.2.8.2. Cyclodehydrogenation and Characterisation of iodo-HBC (**38**)

Subsequent cyclodehydrogenation of **37** with iron(III) chloride yielded the iodo-HBC **38**, as a yellow/orange solid in 85 % yield after purification by column chromatography on silica eluting with hexane:dichloromethane (4:1). The presence of five *tert*-butyl groups as well as the large iodine atom makes **38** readily soluble even

in hexane. The excellent yield reflects the Scholl mechanism since for all-carbon HBCs there is no accumulation of partially cyclised products.¹⁰



Scheme 26: Synthesis of iodo-HBC **38**. (i) FeCl_3 , CH_3NO_2 , CH_2Cl_2 , RT, 45 min (85 %).¹³

The ^1H NMR spectrum of **38** consists of six well defined singlets in the aromatic region due to the presence of a C_2 axis of symmetry in the molecule. Figure 17 shows that these signals are shifted downfield when compared to the aromatic protons in the uncyclised precursor **37**, due to the enhanced aromaticity and electron delocalisation of the HBC platform. As well as this, the signals due to the *tert*-butyl groups in **38** are better separated than they were in the uncyclised precursor **37**, appearing this time as three distinct singlets. These signals were assigned using long range ^1H - ^1H COSY experiments and NOE experiments. The *tert*-butyl group labelled H7 was readily assigned which then allowed for the assignment of H6 using an NOE experiment. A TOCSY (long-range ^1H - ^1H COSY) experiment then allowed observation of the long range interactions between protons on adjacent rings, and the full assignment of the aromatic protons as well as the *tert*-butyl protons.¹³

The carbon NMR spectrum of **38** shows the expected number of signals, 23 non-equivalent aromatic carbon atoms (6 aromatic CHs and 17 quaternary), in addition to the carbon signals of the *tert*-butyl groups.

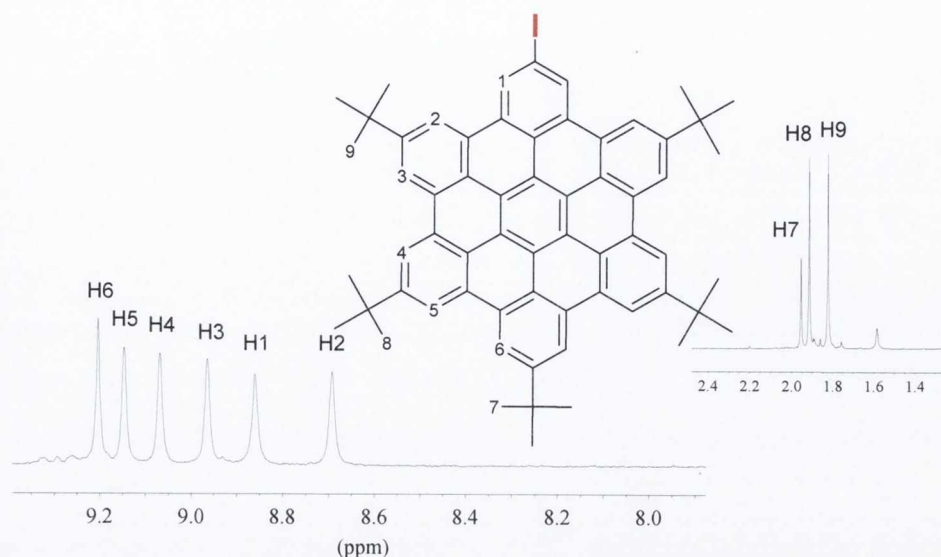


Figure 17: The aromatic and aliphatic regions of the ^1H NMR spectrum for **38**, (CDCl_3 , RT, 600 MHz).

1.2.8.3. Synthesis of ferrocenyl-HBC

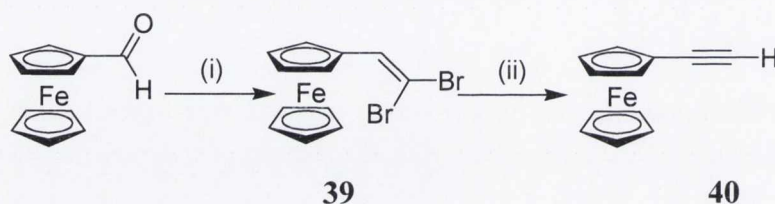
The iodo-HBC now synthesised provided an excellent platform to try and introduce the ferrocene moiety onto the periphery of the PAH. Many reactions could have been employed here such as Stille coupling or Suzuki coupling. However the ferrocene moiety is an electron donating group whereas the PAH with its extended delocalised π -system is electron accepting. For good electronic communication between the donating ferrocene and the electron accepting PAH there needs to be conjugation between the two groups.

Alkynes are reactive building blocks for organic and organometallic synthesis. There has been huge interest recently in ferrocenylacetylenes as they offer a wide range of potential application in NLO, catalysis, as models of charge transfer and in the synthesis of more complex molecules with well-defined magnetic and electronic properties.^{30, 47, 48}

So it was thought that ethylferrocene (**40**) would be an excellent candidate. Ferrocene itself could be introduced from ferroceneboronic acid to the PAH *via* a Suzuki type reaction but the ferrocene would be free to rotate around the ferrocenyl-PAH bond which would effect detrimentally the communication between the two

groups. Ethynylferrocene on the other hand has a triple bond which can act as an excellent electronic bridge between the ferrocene and the PAH.

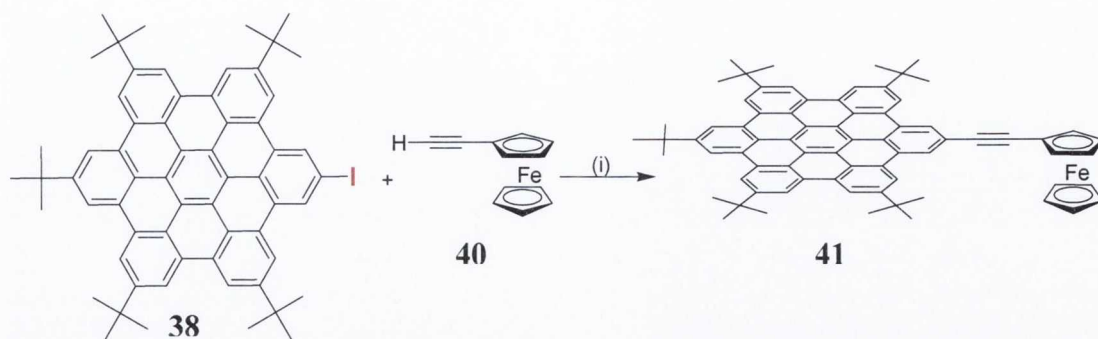
Since ethynylferrocene is a common starting material for more complicated molecules incorporating acetylene units, its synthesis has been widely investigated. It can be synthesised *via* the Rosenblum method,^{39, 49} which involves treating acetylferrocene with an excess of phosphorous oxychloride and DMF to give the (α -chloro, β -formyl)ferrocene which can then be converted to ethynylferrocene by heating in a basic aqueous solution. However it can also be synthesised as shown in Scheme 27.



Scheme 27: The synthesis of ethynylferrocene (40). (i) PPh_3 , CBr_4 , CH_2Cl_2 , $0\text{ }^{\circ}C$, 15 min (93 %). (ii) $n\text{-BuLi}$, THF, $-78\text{ }^{\circ}C \rightarrow RT$, 2 h (83 %).

The reaction of ferrocenecarboxaldehyde with triphenylphosphine and carbon tetrabromide in a Wittig type reaction, yielded the dibromoolefin (**39**) in almost quantitative yield, as a brown solid. Treatment of **39** with two equivalents of *n*-butyllithium in THF at $-78\text{ }^{\circ}C$, followed by recrystallisation from hexane yielded ethynylferrocene (**40**) as orange needles again in high yield (83 %).⁵⁰

HBCs have been shown to be very difficult to purify, not only because of their insolubility but because HBCs tend to streak on a column. More than one HBC present usually results in a inseparable mixture even if they contain very different peripheral functional groups.²⁸ Coupling between **38** and **40** needed to be quantitative. In the Sonogashira coupling of **38** and **40** $Pd(PPh_3)_4$ was employed as a catalyst as opposed to $Pd(PPh_3)_2Cl_2/CuI$ to avoid homocoupling previously observed in the synthesis of **24**. Secondly, the reaction was heated to $70\text{ }^{\circ}C$ for 18 hours, usually Sonogashira couplings on iodo-substrates are carried out at room temperature or below. Thirdly an excess of **40** was used.

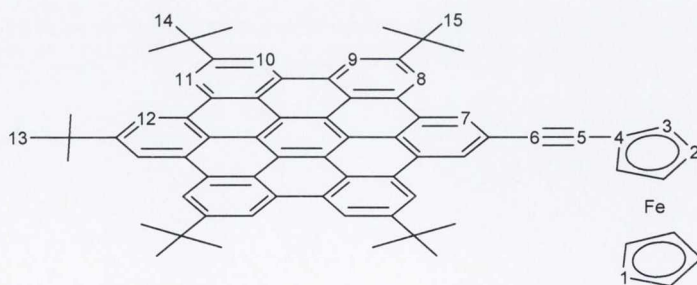


*Scheme 28: The synthesis of **41** via Sonogashira coupling. (i) $\text{Pd}(\text{PPh}_3)_4$, $\text{Et}_3\text{N}/\text{toluene}$ (1/2), 70°C , 18 h (77%).*

With all these precautions orange/red microcrystalline ferrocenyl-HBC **41** was successfully synthesised as the sole product in 77 %. It was purified by column chromatography and further purified by being extracted into chloroform and recrystallised from cold methanol.

1.2.8.4. NMR Characterisation of ferrocenyl-HBC

The ^1H NMR spectrum of **41** consists of six well-defined singlets in the aromatic region due a C_2 axis of symmetry rendering half the protons magnetically equivalent. The ferrocenyl region exhibits the expected three signals corresponding to the two non-equivalent proton environments of the substituted cyclopentadienyl ring and the one environment of the unsubstituted cyclopentadienyl ring. In the aliphatic region the three distinct methyl signals are clearly visible, integrating in the correct 1:2:2 ratio.



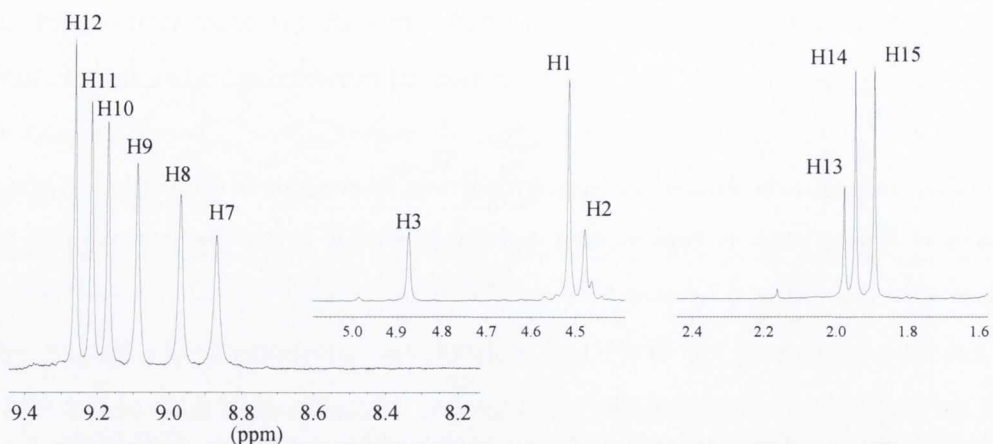


Figure 18: The ^1H NMR spectrum of **41** with the aromatic region, ferrocenyl region and the aliphatic region expanded (CDCl_3 , RT, 600 MHz).

The *tert*-butyl group labelled H13 at δ 1.98 ppm was easily assigned which then allowed for the assignment of H12 using an NOE experiment. A TOCSY (long-range ^1H - ^1H COSY) experiment then allowed observation of the long range interactions between protons on adjacent rings, and full assignment of the aromatic and *tert*-butyl protons.

The DEPT experiment in Figure 19 shows the aromatic CH signals of **41**. The full ^{13}C NMR spectrum shows the expected 18 quaternary carbon carbons as well as the acetylene and ferrocenyl carbon signals.

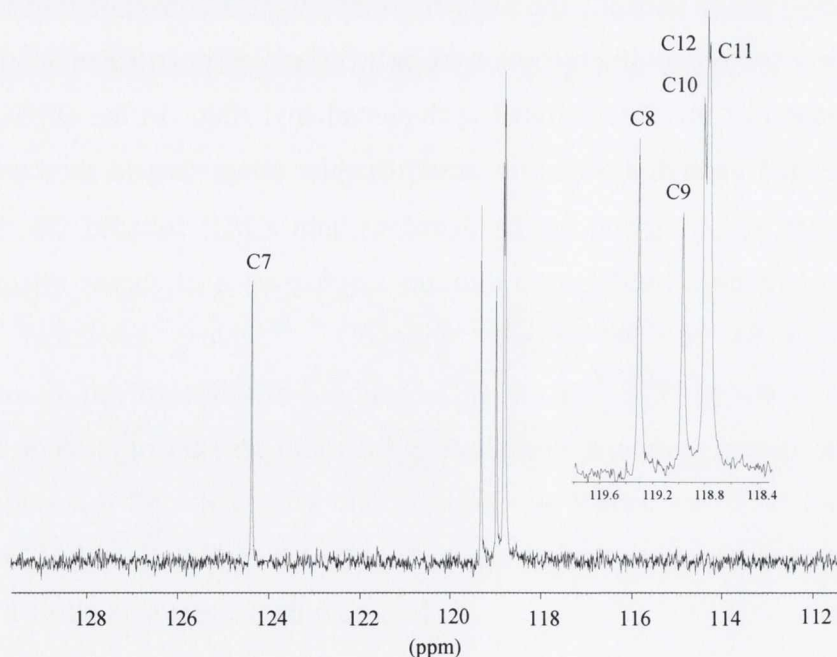


Figure 19: The ^{13}C DEPT spectrum of **41** showing the assignment of the aromatic CHs (CDCl_3 , RT, 600 MHz).

A HMBC experiment allowed all these signals to be assigned as well as confirming the assignments of the aromatic protons, discussed earlier. The ^{13}C NMR spectrum contains the two methyl carbon signals corresponding to the three *tert*-butyl groups with C13 and C14 overlapping. The ferrocenyl proton H3 at δ 4.85 ppm was readily assigned since it had a three bond interaction with C5 at δ 89.2, the other acetylene carbon at δ 87.4 ppm (C6) was shown to have a three bond interaction with H7 as expected. The quaternary ferrocenyl carbon (C4) at δ 91.5 ppm was assigned from its three bond interaction with H2 at δ 4.46 ppm.

1.2.8.5. NMR Concentration Dependence of Ferrocenyl-HBC (41)

It has been well-documented that aromatic groups prefer to associate in either an edge-to-edge or a face-to-face orientation.⁵¹ Face-to-face or π - π stacking interactions have been the subject of a number of investigations.⁵¹⁻⁵³ These studies have addressed the role of molecular geometry^{52, 53} and electrostatic factors in promoting aromatic association.⁵⁴⁻⁵⁷ Desiraju and Gavezzotti proposed that the packing of PAHs in solids is dictated by the molecular shape.^{52, 53} Their model does correlate the molecular shape and packing mode for a number of PAHs, but it does not take into consideration the electrostatic factors due to substituents, which are also known to be important.

Substituents strongly influence π - π stacking tendencies, though these effects cannot always be explained in terms of intuitive donor-acceptor concepts. This is illustrated by the surprisingly high association constant of complexes of 1, 3, 5-trinitrobenzene with aromatic substrates having strong electron withdrawing groups.⁵⁵ Donor-acceptor concepts also fail to explain why aromatic hydrocarbons associate strongly with aromatic fluorocarbons in a face-to-face orientation.

It is apparent from Figure 20 that the chemical shifts of the aromatic protons of **41** are very dependent on concentration, especially protons H7, H8 and H9, which are closest to the ferrocene moiety. At ambient temperature in chloroform the chemical shift for H7 varied greatly. At a concentration of $7.40 \text{ mmol dm}^{-3}$ H7 has a chemical shift of δ 8.90 ppm whereas at $0.06 \text{ mmol dm}^{-3}$ the same proton has a chemical shift of δ 9.19 ppm. This suggests that **41** self-associates in chloroform solutions.

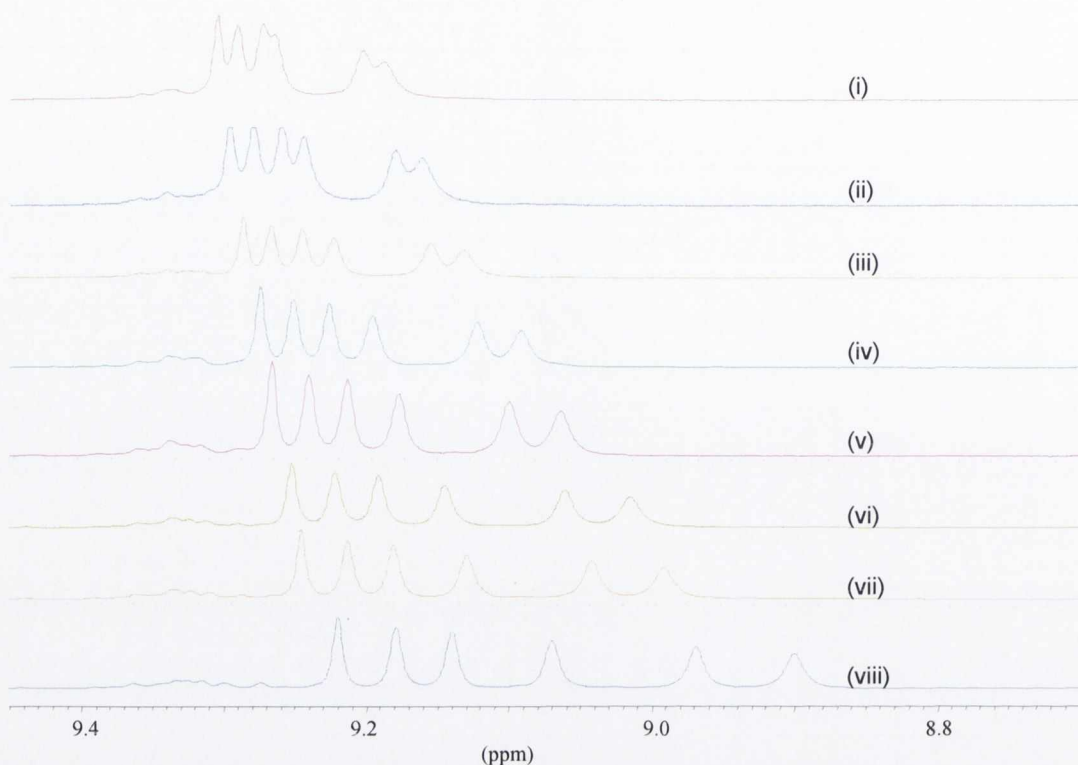


Figure 20: The concentration dependence of the ^1H NMR aromatic signals of compound **41** (CDCl_3 , RT, 600 MHz), (i) $0.06 \text{ mmol dm}^{-3}$, (ii) $0.12 \text{ mmol dm}^{-3}$, (iii) $0.23 \text{ mmol dm}^{-3}$, (iv) $0.46 \text{ mmol dm}^{-3}$, (v) $0.93 \text{ mmol dm}^{-3}$, (vi) $1.85 \text{ mmol dm}^{-3}$, (vii) $3.70 \text{ mmol dm}^{-3}$, (viii) $7.40 \text{ mmol dm}^{-3}$.

Figure 21 also demonstrates in a graphical manner how the chemical shifts of protons H7-H12 are dependent on concentration, and that the three protons of the HBC platform closest to the ferrocene moiety (H7-H9) are most affected. Although there are significant shifts in all the aromatic protons, the signals due to the *tert*-butyl groups and the ferrocenyl signals remained relatively unchanged.

It has been shown by Moore *et al.*⁵⁸ that acetylene groups can form π - π interactions with PAHs and macrocycles. The greatest overlap of π orbitals in the molecule will be in the region closest to the electron donating ferrocene since it is here that the π orbitals due to the PAH and the acetylene are to be found. The movement of the proton signals in the ^1H NMR would suggest that these are located in the region of greatest intermolecular overlap in the aggregated molecular system.

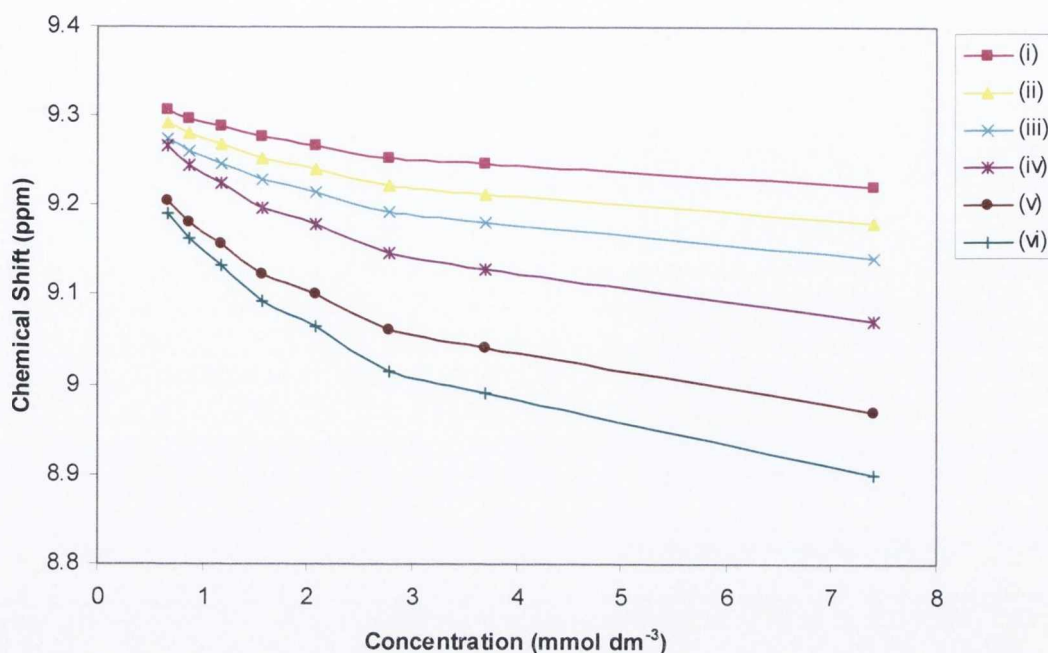


Figure 21: Plot showing the concentration dependence on the chemical shifts of the aromatic protons in compound **41**, (i) H12, (ii) H11, (iii) H10, (iv) H9, (v) H8, (vi) H7.

In order to understand the nature of this aggregation more fully an X-ray crystal structure is required since it would show how these molecules are stacking in the solid state. To date repeated attempts to grow crystals suitable for X-ray crystallographic analysis have proved unsuccessful.

1.2.9. Spectral Comparisons of Derivatives

Table 3 summarises the main spectroscopic data for the ferrocene containing polyphenylenes synthesised during the course of this work. In all cases, mass spectra were obtained by electro-spray ionisation (ESI) or MALDI-TOF spectrometry. Under these conditions a single peak corresponding to the $[M]^+$ ion was obtained for each complex except for **31**..

Compound	Mass Spectrum (m/z)	¹ H chemical shifts for ferrocene protons (ppm)	
		Unsubstituted Cp ring	<i>ortho</i> - and <i>meta</i> - protons of the substituted Cp ring
8	742.2297	---	3.68, 3.78, 3.94, 4.11,
9	1098.3873	---	3.19, 3.43
19	1026.2560	3.89	4.26, 4.55
25	1390.2739	3.91	4.23, 4.54
30	1274.2003	3.91, 3.92	4.21, 4.26, 4.48, 4.53
31	---*	3.94	4.20, 4.51
41	1010.4509	4.50	4.46, 4.85

Table 3: Spectroscopic data for complexes **8**, **9**, **19**, **25**, **30**, **31** and **41**, ---* accurate mass not obtained, complex not observed in ESI-MS nor MALDI-TOF MS.

All the *ortho*- and *meta*- protons of the substituted cyclopentadienyl rings should appear as *pseudo*-triplets, corresponding to the AA'BB' system, but some appear as singlets, due to broadening caused by steric constraints about the substituted cyclopentadienyl ring.

The table highlights the electron withdrawing effect of the fully cyclised PAH platform. It can be seen in Table 3 that the substituted cyclopentadienyl protons of **41** are the most downfield in the series at δ 4.46 and 4.85. This is due to the electron withdrawing effect of the PAH facilitated by the conjugated acetylene linker.

1.2.10. UV-visible Absorption Spectroscopy

It has been shown in past studies of the electronic absorption spectra of ferrocene and substituted ferrocenes that in ferrocene the metal centred d_{z^2} orbital is generally the HOMO, and the combination of the d_{xz} and d_{yz} is the LUMO.^{60, 61} The absorption around λ 440 nm in ferrocene is thus assigned as the $^1E_{1g} \leftarrow ^1A_{1g}$ ligand field (LF) transition and the higher energy band at around λ 325 nm as the $^1E_{2g} \leftarrow ^1A_{1g}$ LF transition. Substitution of the cyclopentadienyl ring with conjugated acceptor groups is generally followed by drastic changes in the absorption spectrum.^{59, 60} LF, otherwise known as “d-d” transitions, correspond to electronic transitions between the d-orbitals on the metal. Organometallics are highly covalent, so these metal centred d-orbitals actually have considerable ligand character and since they are involved in

metal-ligand bonding, the electronic transitions involving d-orbitals are sensitive to ligand binding.^{34, 61}

The electronic absorption spectra of the non-ferrocene containing PAH (**3**) and all the ferrocene containing compounds, **8**, **9**, **19**, **25**, **30**, **31** and **41** were recorded in toluene and the data is presented in Table 4. Excluding **41**, each of the ferrocenyl containing compounds displays two or three prominent absorption bands in the region λ 300-460 nm. Similar to other ferrocenyl compounds, they exhibit a weak low energy band attributable to the d-d transition arising from the ferrocene moiety. These broad, low energy features account for the orange to red colours of these compounds.

Compound	λ_{max} nm (ϵ , L mol ⁻¹ cm ⁻¹ x 10 ³)	
		Low energy d-d transition
Fc	326 (0.05)	441 (0.1)
3	330 (sh) (28.1), 344 (77.7), 362 (181.1), 391 (70.5)	---
8	358 (3.1)	460 (0.7)
9	300 (19.6), 359 (3.7)	464 (1.0)
19	354 (12.1)	436 (2.6)
25	350 (sh) (1.7)	445 (0.3)
30	355 (12.6)	445 (2.8)
31	353 (sh) (4.4)	445 (0.7)
41	334 (sh) (27.3), 350 (61.7), 366 (138.7), 396 (50.7), 414 (19.0)	ca. 440

Table 4: The UV-vis data for ferrocene, PAH-**3** and the ferrocenyl compounds **8**, **9**, **19**, **25**, **30**, **31** and **41**, all in toluene.

In Figure 22 the normalised UV-vis spectra of ferrocene, **8**, **9**, **19**, **25**, **30**, **31** and **41** are superimposed. In the ferrocene spectrum there is a very weak feature at around 440 nm. The ferrocene derivatives also display this typical ferrocenyl transition in the visible region, at about λ 450 nm, although as can be seen in Figure 22 the ferrocene transition varies in the range λ 436-464 nm.

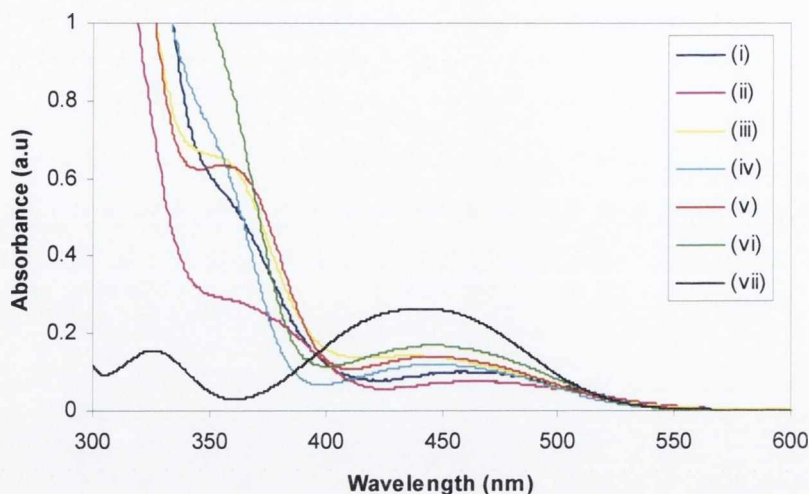


Figure 22: The UV-vis absorption spectra of the ferrocenyl complexes, (i) **8**, (ii) **9**, (iii) **19**, (iv) **25**, (v) **30** (vi) **31** and (vii) ferrocene for comparison, all recorded in toluene.

Attempts to cyclodehydrogenate **8** and **9** had proved unsuccessful, due most probably to their complete decomposition. It has been proposed that the mechanism for cyclodehydrogenation is an oxidative cationic mechanism under Lewis acid conditions. These conditions may prove problematic for some ferrocene-containing polyphenylenes. Investigations into the oxidation of substituted ferrocenes with air in acidic solutions have been carried out.^{34,62} It has been reported that the rate of the oxidation is influenced by the availability of a protonation site at the metal centre. Greater reactivity is accounted for by a specific, tilted conformation of the two cyclopentadienyl rings. The acidic and oxidative conditions of the cyclodehydrogenation reaction is likely to cause some decomposition of those ferrocene compounds with very tilted cyclopentadienyl rings.

It has been shown that the basicity of the iron atom in both **8** and **9** would be expected to be high because of the inclination of the cyclopentadienyl rings and thus protonation at the iron centre would be accelerated.⁶² In addition it has been shown in the literature and in work already done within the group³⁴ that there is a correlation between the degree of tilt of the ferrocene cyclopentadienyl rings (and thus the likelihood of cyclodehydrogenation) and the wavelength of the ferrocenyl absorption band, which is normally around $\lambda_{\text{max}} = 450$ nm. If the band appears at wavelengths greater than 450 nm then there is significant tilt between the cyclopentadienyl rings.

The ferrocenyl absorptions in **8** and **9** are at λ 460 nm and 464 nm respectively. This implies that the cyclopentadienyl rings are indeed significantly tilted and this could be the reason why under the conditions of cyclodehydrogenation acid attack at the metal centre results in decomposition. Single X-ray crystallography would provide valuable information to determine whether the postulate is valid, however attempts to grow crystals of **8** and **9**, using a range of solvents have been unsuccessful.

The cyclopentadienyl rings in compounds **19**, **25**, **30** and **31** appear to be less tilted since their d-d transitions occur at λ 436, 445, 445 and 445 nm respectively. No cyclodehydrogenation is observed but the compounds do not undergo decomposition. It is postulated that cyclodehydrogenation can follow either an arenium cation or radical cation mechanism. All the work done to date regarding cyclodehydrogenation on purely aromatic compounds, conclude that any radicals formed are on the phenyl rings leading to cyclodehydrogenation. With compounds **19**, **25**, **30** and **31** any radical formed could be located on one of the cyclopentadienyl rings of the ferrocene. Hence when the reaction is quenched by the addition of methanol the radical is protonated and the starting material is recovered.

When the ferrocene moiety is connected to a fully cyclised platform there is a dramatic change in the UV-vis spectra, a much more structured spectra is observed. In Figure 23 the normalized UV-vis spectra for compounds **3**, **38**, **40** and **41** have been superimposed.

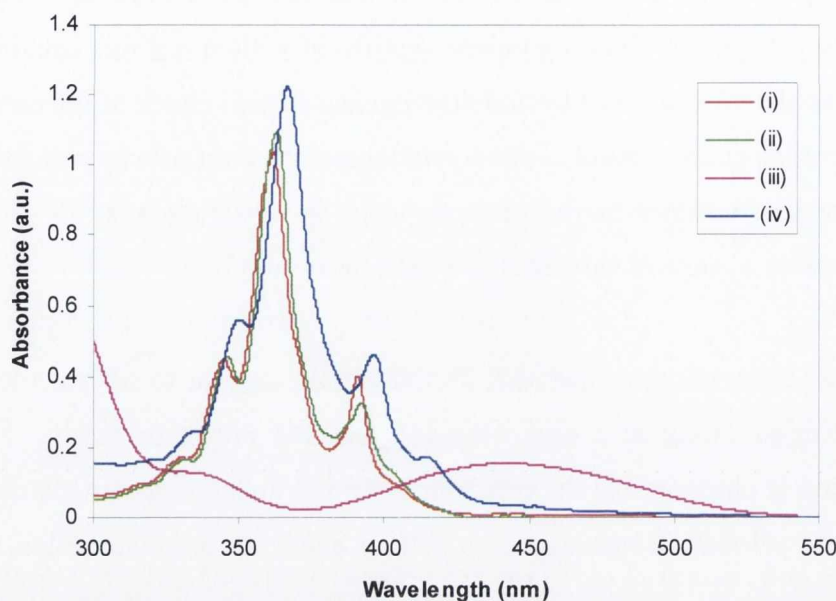


Figure 23: The UV-vis absorption spectra of, (i) **3**, (ii) **38**, (iii) **40** and (iv) **41**, all recorded in toluene.

The first thing to note from Figure 23, is how similar the spectra of **3** and **38** are, it seems that replacing one of the *tert*-butyl groups with an iodine has no effect on the photophysical properties of the PAH. The UV-vis spectrum of **41** is very different to all the other non-cyclised polyphenylene compounds, since it has four intense features in the region λ 350-450 nm. The broad signature of the ferrocene d-d transition has mostly vanished and instead only a small shoulder at around λ 440 nm occurs. In addition **41** is highly absorbing between 300 and 450 nm, in general the spectrum of **41** is dominated by $\pi \rightarrow \pi^*$ absorption bands with high absorption coefficients (Table 4), and is reminiscent of spectra obtained for PAH derivatives **3** and **38**.³⁴

The UV-vis spectra of **41** and **3** have an extremely similar shape and all the λ_{max} values are only slightly red-shifted in **41**. Both spectra shown three types of bands (α , β and p), which are typical of aromatic hydrocarbons. The β -band appears at λ 366 nm and corresponds to the electronic interaction between the benzoid rings of the PAH. A red-shift in these bands is a consequence of increasing the electronic interaction, for example by extending the π -system, which is what has happened in **41** since conjugation between the PAH platform and the ferrocene moiety *via* the acetylene linker has indeed extended the π -system. The p-bands appear at λ 396 nm

for **41**, which is a red shift of 5 nm compared to **3**, and this band involves the localization of the π -electrons in the excited state.

The extremely weak α -band at λ 405 nm for **3**, is assigned as the 0-0 transition, which is strictly forbidden in the D_{6h} symmetry, compound **41** on the other hand has a much more intense 0-0 transition (α -band) due to the further lifting of molecular symmetry to C_{2v} . Thus the red-shifted band at λ 414 nm is assigned to the 0-0, $^1(\pi, \pi^*)$ transition, with enhanced molar absorptivity when compared to **3**.³⁴

Therefore comparison of the spectral properties of **41** and **3** serves as further evidence that the ferrocene acetylene **40** was successfully coupled to the PAH platform.

1.2.11. Electrochemistry

Ferrocene/ferrocenium itself represents a strictly reversible one-electron redox couple.⁴⁷ In the case of some ferrocenium derivatives however, reversibility may be significantly lowered by the subsequent decomposition of the electrogenerated ferrocenium species. The ferrocene substituent may also be regarded as a redox active probe on a molecular level, since following the ferrocene/ferrocenium redox potentials offers a unique opportunity to detect alterations in the electronic structure of the ferrocene derived molecules, as well as in the nature of the metal- π -ligand bonding. This provides information about the changes of electron density distribution and HOMO energies in a series of related compounds.³⁴

Table 5 compares the electropotential of the $[Fc/Fc^+]$ redox couple in compounds **3**, **8**, **9**, **19**, **25**, **30**, **31** and **41** by cyclic voltammetry (CV), in dichloromethane (0.1 M (TBA)PF₆ as electrolyte). Under the applied experimental conditions, all the compounds studied exhibited a fully reversible one-electron oxidation attributable to the ferrocene/ferrocenium couple.

Compound	E° (V)
Fc	0.51
8	0.54
9	0.35
19	0.50
25	0.45
30	0.54
31	0.54
41	0.65

*Table 5: Electrochemical data for complexes **8**, **9**, **19**, **25**, **30**, **31** and **41**, measured against ferrocene. Supporting electrolyte: (TBA)PF₆ (0.1 M) in CH₂Cl₂; platinum working electrode, platinum wire auxiliary electrode, Ag/AgCl reference electrode, 100 mV s⁻¹ scan rate, measured for 1 mmol solutions.*

All potentials are quoted together with the [Fc/Fc⁺] couple, which had a potential 0.51 V vs the Ag/AgCl reference electrode used for this work. Although all the ferrocenyl compounds show a reversible one-electron oxidation, it is interesting to note that the redox potentials of the ferrocene units show a broad range of values, from 0.35 to 0.65 V, caused by altering the substituent on the ferrocene cyclopentadienyl ring.

As can be seen from Table 5, the redox potentials for compounds **8**, **19**, **25**, **30** and **31** all lie within the range E° 0.50 to 0.54 V, which is very similar to that for the ferrocene standard (0.51 V), which indicates that the ferrocene environments in these compounds have not been greatly altered.

However compounds **9** and **41** show deviations from these values, all be it in opposite directions. Compound **9** shows a significant cathodic shift (less positive shift) of 160 mV. The relatively low value for the ferrocene oxidation indicates that the ferrocenyl species is electron rich, and the ease in oxidation could be attributed to the electron donating ability of the two polyphenylene systems, stabilising the oxidised form with respect to ferrocene itself.

The cyclic voltammogram of **41** exhibits a redox potential of $E^{\circ} = 0.65$ V, which is an anodic shift (by 140 mV) as compared to ferrocene itself and is shown in Figure 24.

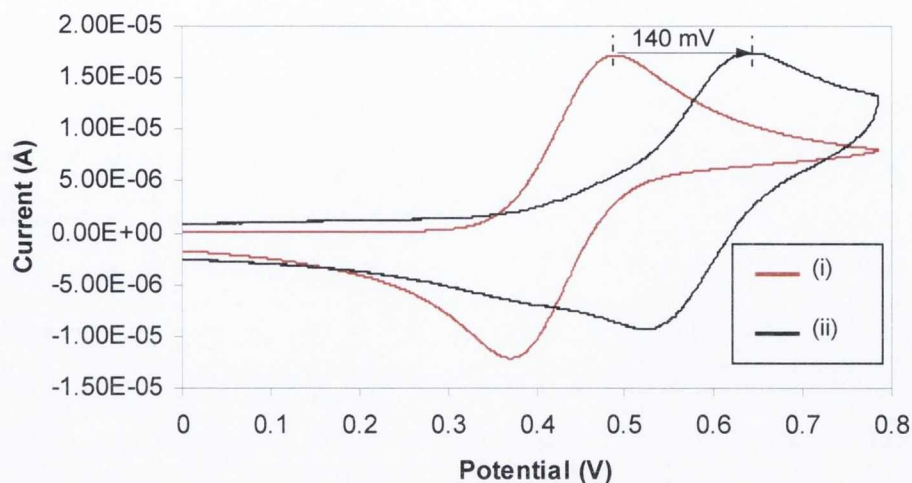


Figure 24: Cyclic voltammetric response of 1 mmol solution of, (i) ferrocene and (ii) **41**. Supporting electrolyte: (TBA)PF₆ (0.1 M) in CH₂Cl₂; platinum working electrode, platinum wire auxiliary electrode, Ag/AgCl reference electrode, 100 mV s⁻¹ scan rate.

This anodic shift is due to the electron-withdrawing effect of the fully cyclised polyaromatic substituent, which is bound to the ferrocene moiety *via* the acetylene linker. This makes the oxidation of the ferrocene unit in **41** thermodynamically more difficult than all the other compounds shown in Table 5. The loss of electron density from the ferrocenyl donor unit to the net electron-accepting polyaromatic moiety therefore gives an anodically shifted oxidation wave.³⁴

1.3. Summary

In this chapter it has been shown that by the careful modification of already known synthetic routes many ferrocenyl derivatives can be synthesised in excellent yields. All the compounds have been comprehensively characterised by ^1H , ^{13}C NMR, UV-vis spectroscopes and mass spectrometry. The electrochemistry of these ferrocenyl derivatives has also been investigated by cyclic voltammetry. Six novel ferrocenyl polyphenylene derivatives **8**, **9**, **19**, **25**, **30** and **31** were prepared and characterised as air-stable products. This work also led to the synthesis of **41** which is the largest PAH ever reported with a conjugated ferrocene moiety on its periphery. Although this work has shown that cyclodehydrogenation of polyphenylenes **8**, **9**, **19**, **25**, **30** and **31** was unsuccessful, it also details how it was possible to synthesise a halogenated PAH and then attach a ferrocene moiety *via* Sonogashira coupling. Having proven the formation of a model for an intercalated graphitic sheet, with a ferrocene moiety fully conjugated with a PAH platform this project may have wide-reaching applications for the future study and application of molecular materials.

The investigation of electrochemical and spectroscopic properties of these novel compounds helped to understand their chemical reactivity. There were many similarities in the absorption spectra of compounds **8**, **9**, **19**, **25**, **30** and **31**, but the main difference was shown to be in their ferrocenyl absorption. For **8** and **9** these were at λ 460 nm and 464 nm respectively, implying the presence of tilted cyclopentadienyl rings, which exposed the metal centre to accelerated protonation under the conditions of cyclodehydrogenation. Compounds **19**, **25**, **30** and **31** appear to have less tilted cyclopentadienyl rings since their d-d transitions occur at λ 436, 445, 445 and 445 nm respectively. No cyclodehydrogenation was observed for these compounds probably because the radical cation formed is located on one of the cyclopentadienyl rings of the ferrocene and simply protonated when the reaction is quenched.

In general the absorption spectra of **41** is dominated by $\pi \rightarrow \pi^*$ absorption bands, with high absorption coefficients, corresponding to the PAH platform. The UV-vis spectra of **41** and **3** are similar in shape and all the λ_{max} values are only slightly red-shifted for **41**. Both spectra show three types of bands (α , β and p), which are typical of PAHs.

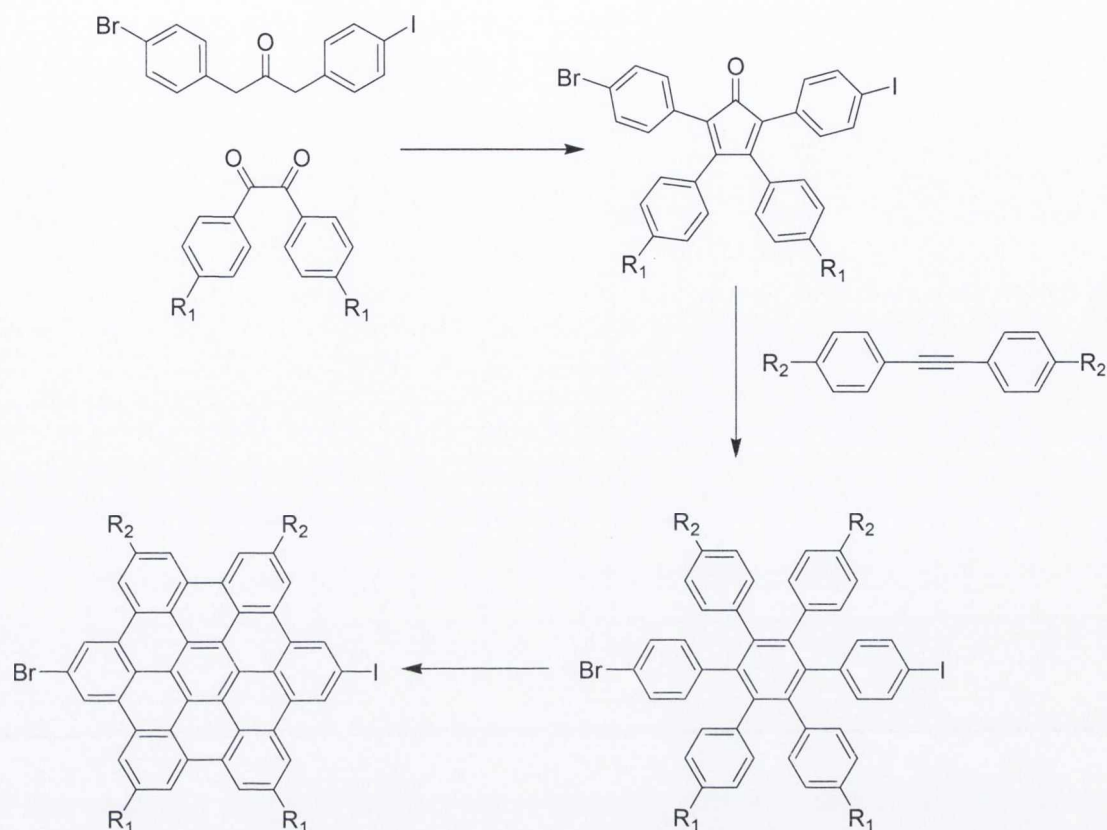
All the compounds exhibit the one-electron reversible oxidation wave associated with the ferrocene/ferrocenium couple. The E° value is influenced by the electronic effects of the substituent. The potential value for **41** is considerably more positive than all the other compounds due to the electron-withdrawing effect of the fully cyclised polyaromatic substituent, which is bound to the ferrocene moiety *via* the acetylene linker. This makes the oxidation of the ferrocene unit in **41** thermodynamically more difficult than all the other compounds.

1.4. Future Work

Although the cyclisation of ferrocenyl polyphenylenes proved unsuccessful, the methodology used to generate **41** could be used to synthesise a wide range of ferrocenyl containing PAH compounds.

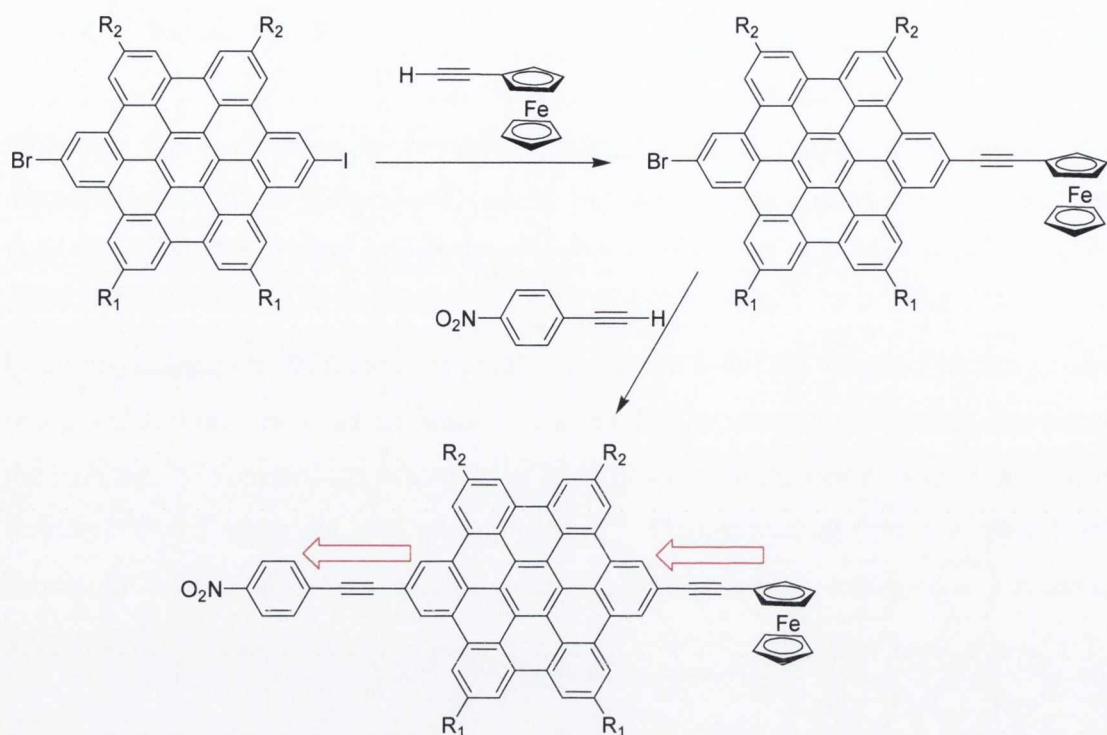
Conjugated organometallic systems that contain electronically coupled photo- and/or redox-active sites across an unsaturated organic bridge are of considerable interest at the moment.⁶³ Tremendous efforts have been devoted to the design and synthesis of ferrocene based materials with π -conjugation.⁶⁴ Compounds of this type have been shown to exhibit a variety of intriguing electronic optical, redox and structural properties.⁶⁵

The NLO properties of compound **41** have yet to be investigated but are underway in collaboration with Isabelle Ledoux at the Laboratoire de Photonique Quantique et Moléculaire at Cachan. If the NLO results for **41** prove to be promising there are other compounds that could be synthesised following the same synthetic methodology that could lead to even better NLO properties. One possible idea is shown in Scheme 29 where by a PAH is synthesised with two different halogens arranged in a *para* fashion which would be under total synthetic control. The key to the success of this proposed scheme is in the synthesis of the di-halogenated 1,3-diaryl-2-propanone. In all the work contained within this thesis all the 1,3-diaryl-2-propanones synthesised have been symmetric in nature following literature protocols.^{44, 45} However in work carried out by Hughes *et al.* it has been shown that unsymmetrical 1,3-diaryl-2-propanones can be synthesised in good yields by slightly modifying the established protocol.⁴⁶



Scheme 29: Possible synthetic route towards a PAH with two different halogens that could lead to differential coupling reactions.

With the synthesis of the di-halogenated PAH achieved this compound could then undergo selective differential coupling reactions. In this case for example ethynylferrocene could be coupled at the iodide position at room temperature (or below) ensuring that no coupling takes place at the bromide position. Then a nitro substituent could be coupled at the bromide position at slightly elevated temperatures. The difference in activity of the two halogens can be employed to allow differential coupling and lead to the synthesis of the compound shown in Scheme 30 with no by-products.



Scheme 30: Possible synthesis of a new “push-and-pull” molecule consisting of a ferrocene moiety fully conjugated with a nitro group through a fully cyclised PAH.

In general compounds with good NLO properties have been shown to contain donor (push) and acceptor (pull) moieties bridged by a π -conjugation system.⁵⁰ Therefore were the product shown in Scheme 30 to be synthesised it would be expected to have excellent NLO properties due to the pushing of electron density by the ferrocene moiety and the pulling of electron density by the nitro group. Obviously the acetylene linkers are essential to ensure conjugation between the ferrocene, PAH and nitro substituent.

Chapter 2: Ferrocenyl Fluoranthenes

2.1. Introduction

2.1.1. Fluoranthene

In the previous chapter a number of ferrocene containing polyphenylene compounds were discussed as well as one fully-cyclised PAH with a ferrocene moiety connected to the extended system *via* an acetylene linker (**41**). PAHs have a number of attributes which could make them useful as linking groups in donor-acceptor organometallic systems. They are planar, relatively rigid with a fixed geometry and their highly delocalised π -systems with small HOMO-LUMO energy separations and low energy vacant π^* -orbitals are likely to facilitate electronic communication.

Since the discovery of fullerenes, PAHs have regained considerable interest. However it is very difficult and problematic to synthesise fullerene subunits^{66, 67} and to produce larger and more complicated PAHs.⁶⁸⁻⁷⁰ The synthesis of fullerene subunits is especially difficult due to the inclusion within the extended structure of five membered rings. Nevertheless since the early 1990s,⁷¹ much attention has been directed toward bowl shaped hydrocarbons in which curved networks of trigonal carbon atoms map out the same patterns of five and six membered rings as those found on the surfaces of C_{60} and higher fullerenes.⁷² An example of this can be seen in Figure 25 where the $C_{36}H_{12}$ geodesic dome shown represents 60 % of C_{60} .⁷³

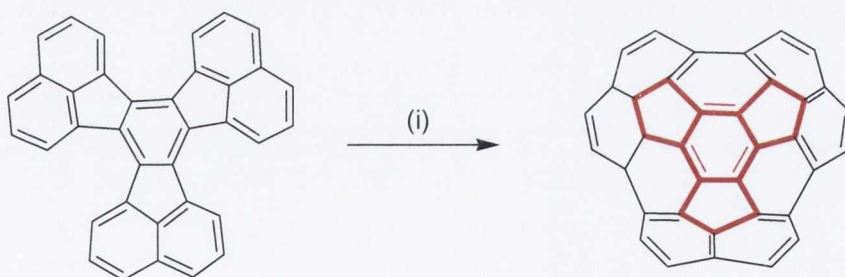


Figure 25: The synthesis of a cyclised fluoranthene derivative that represents 60 % of C_{60} . (i) Flash vacuum pyrolysis (FVP), 1200-1300 °C.⁷⁴

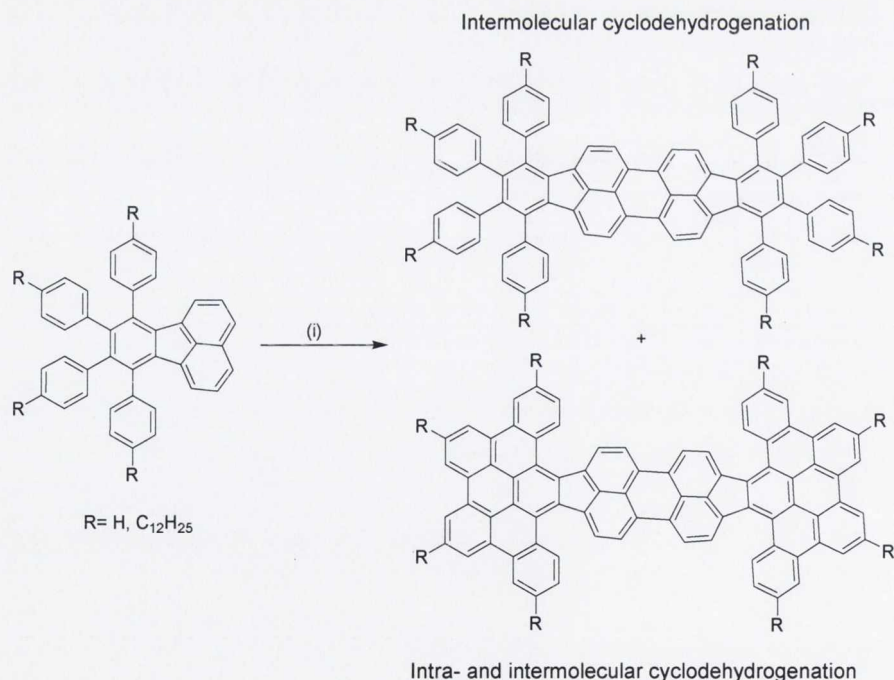
It is not however purely for the purpose of synthesising analogues of C_{60} that fluoranthenes have gained interest. There is considerable interest in the possible application of these compounds in the opto-electronics industry.⁷⁵ Fluoranthene based compounds have been shown to have interesting optical properties and it is

thought that the inclusion of ferrocene or multiple ferrocenes into these smaller delocalised systems could enhance their optical properties.

2.1.2. Cyclodehydrogenation of Fluoranthenes

The aim of this work is to incorporate the ferrocene moiety onto the periphery of a fluoranthene as a small PAH framework. Despite their remarkable potential for the synthesis of more complex structures, only a few aryl-substituted fluoranthenes have been reported,⁷ and to date the introduction of ferrocenyl groups into their framework is unknown.

Fluoranthenes are known to undergo intermolecular cyclodehydrogenation^{3, 77, 78} as well as intramolecular oxidative coupling⁷ which offer the possibility of extending to larger PAH platforms involving a perylene subunits, as shown in Scheme 31. Perylene chromophores are important in dye-stuff chemistry⁷⁶ due to their excellent thermal, chemical, and photochemical stability and they have also been applied in photovoltaic cells⁷⁷ and optical switches.⁷⁸

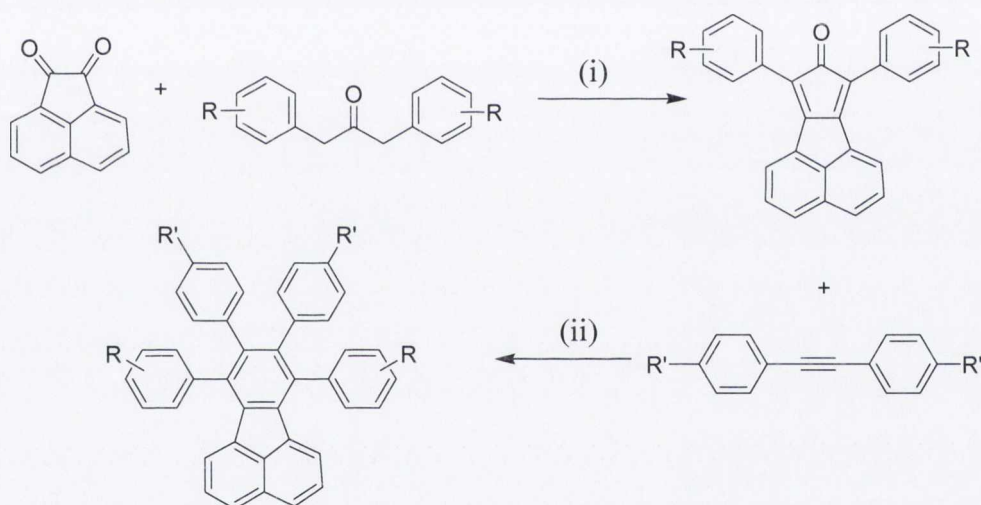


Scheme 31: The synthesis of two perylene based chromophores via cyclodehydrogenation from a simple fluoranthene derivative. (i) FeCl₃, CH₃NO₂, CH₂Cl₂, RT, 45 min.⁷

The inclusion of ferrocene moieties onto fluoranthene cores is therefore an attractive possibility due to the likelihood of favourable opto-electronic properties in the parent compounds as well as the potential for the synthesis of larger perylene units.

2.1.3. Synthetic Methodology

Fluoranthenes can be readily synthesised in the general manner as shown in Scheme 32. The fluoranthene-based cyclopentadienone can be synthesised *via* the two-fold Knoevenagel condensation between acenaphthenequinone and a substituted 1,3-diaryl-2-propanone. Subsequent Diels-Alder [2+4]-cycloaddition with a suitably substituted acetylene should yield the desired fluoranthene. This methodology allows the incorporation of differing R groups onto the fluoranthene.



Scheme 32: Synthetic route towards fluoranthene based compounds with differing R groups. (i) Two-fold Knoevenagel condensation, (ii) Diels-Alder [2+4]-cycloaddition.

The synthesis of ferrocenyl containing fluoranthenes, such as those shown in Figure 26, could lead *via* intermolecular cyclodehydrogenation to dimeric or even polymeric perylene based compounds.

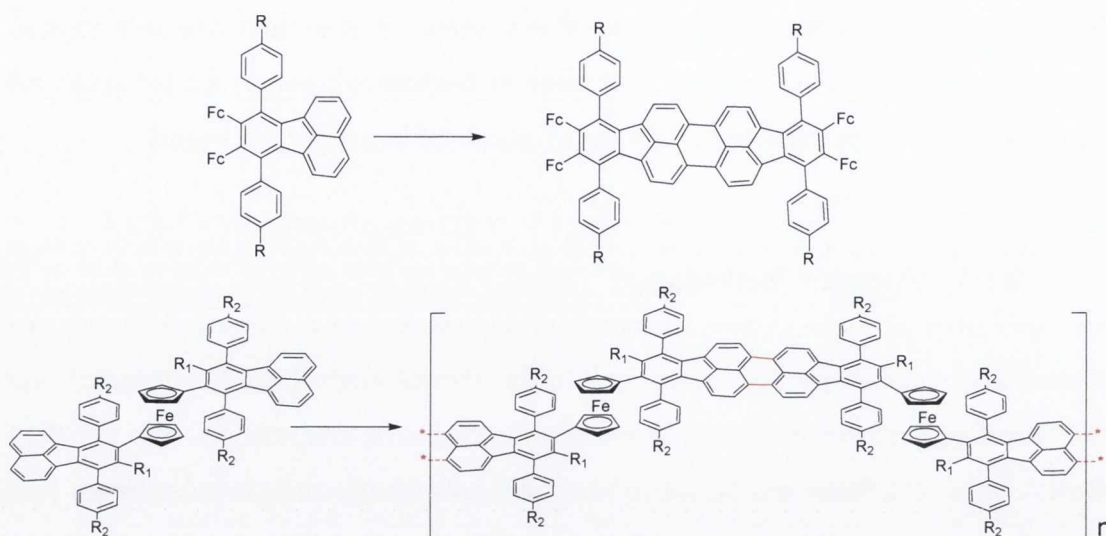


Figure 26: The possible synthesis of dimeric and polymeric perylene based compounds upon intermolecular cyclodehydrogenation of fluoranthene based precursors.

Relevant to our long term goal of preparing ferrocene intercalated graphitic sheets, and in continuation of our interest in the study of PAHs, this chapter describes the synthesis, characterisation, electronic and redox properties of a series of novel fluoranthene systems incorporating ferrocenyl moieties. The ferrocene moiety is introduced onto the fluoranthene system *via* ferrocenyl containing acetylenes (R' in Scheme 32). Methoxy groups shall also be introduced onto the other phenyl ring since they should increase the solubility of the Diels-Alder [2+4]-cycloaddition product and have been shown to aid cyclodehydrogenation.^{35, 36}

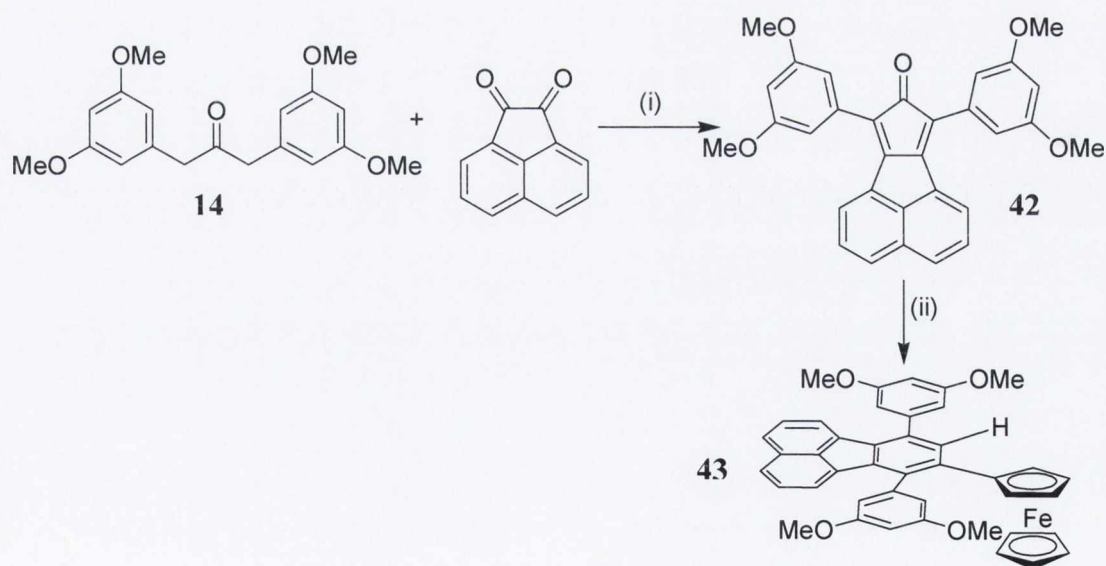
Also reported is the attempted cyclodehydrogenation of the novel compounds synthesised. Although unsuccessful with $FeCl_3$, there is still large potential for these types of compounds. An alternative synthetic route towards cyclised ferrocene containing fluoranthene/peryene based compounds will be suggested in the future work section.

2.2. Synthesis and Characterisation

2.2.1. Synthesis and Characterisation of the mono-ferrocenyl containing Fluoranthene **43**

The novel fluoranthene containing cyclopentadienone **42** was synthesised by the two-fold Knoevenagel condensation reaction between the commercially available diketone acenaphthenequinone and 1,3-diaryl-2-propanone **14** under basic methanolic conditions. Cyclopentadienone **42** was synthesised in 77 % yield and characterised by ^1H and ^{13}C NMR spectroscopy as well as mass spectrometry.

The ferrocene containing fluoranthene **43** was synthesised as a orange/red crystalline solid in 94 % yield by the Diels-Alder [2+4]-cycloaddition reaction between **42** and ethynylferrocene (**40**) at 200 °C in a benzophenone melt. **43** was characterised by ^1H and ^{13}C NMR spectroscopy, mass spectrometry and crystals suitable for single crystal X-ray diffraction were obtained.



*Scheme 33: The synthesis of **43**. (i) NaOH, CH₃OH, RT, 18 h (77 %). (ii) **40**, benzophenone, 200 °C, 18 h (94 %).*

The ^1H NMR spectrum of **43** can be seen in Figure 27. Proton H30 was easily assigned as the singlet at δ 7.81 ppm. An NOE experiment showed an interaction

between H30 and a proton at δ 6.90 ppm, which was assigned as H26, which also has a small $^4J_{\text{HH}}$ coupling with H28 (2.0 Hz). Another NOE experiment showed an interaction between H26 and a doublet at δ 7.45 ppm which was assigned as H21. The ^1H - ^1H COSY then allowed the assignment of H19 and H20 at δ 7.78 and δ 7.45 ppm respectively.

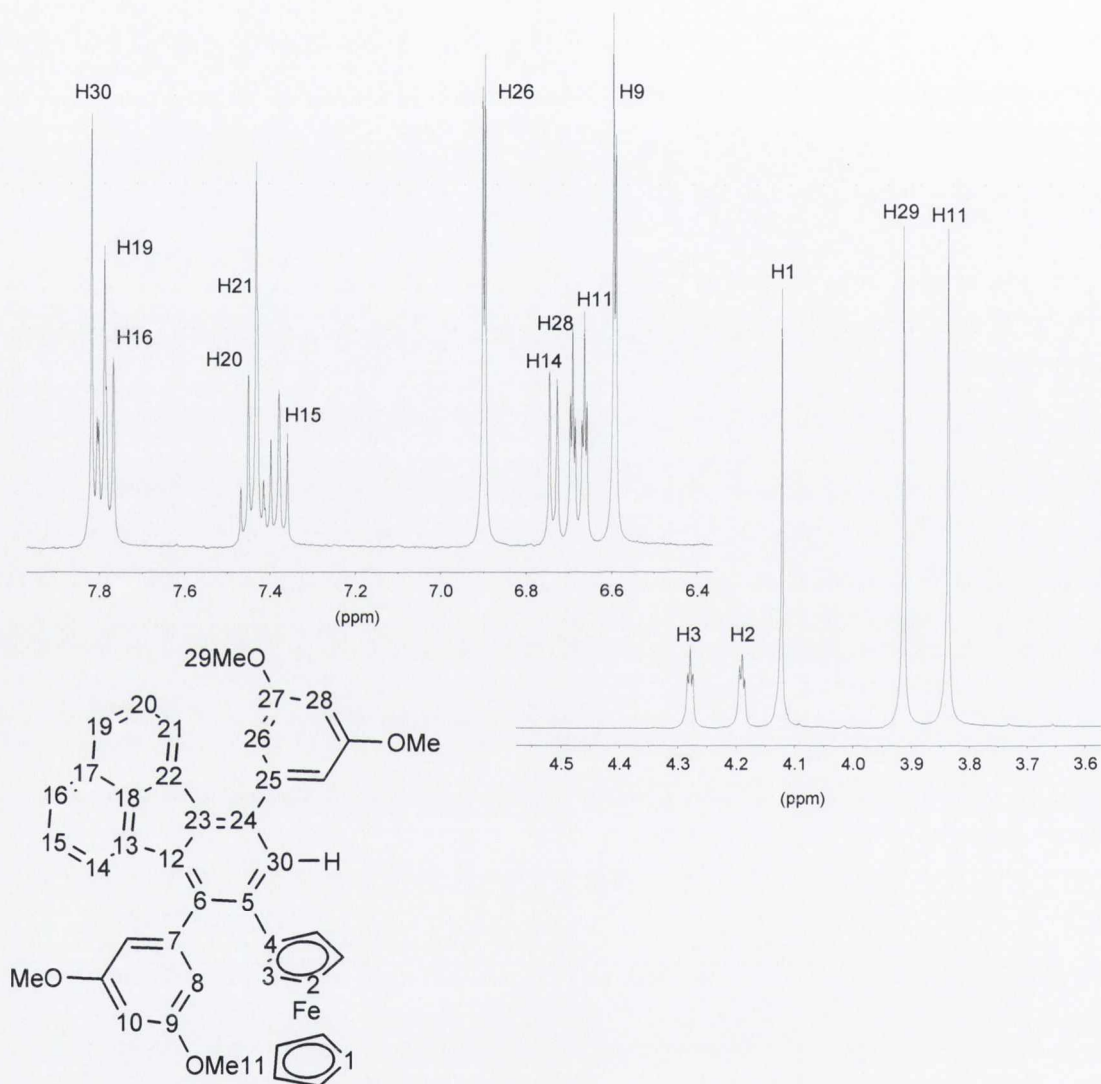


Figure 27: The ^1H spectrum of **43**, with the aromatic and ferrocenyl regions highlighted for clarity (CD_2Cl_2 , RT, 400 MHz).

The proton H14 was assigned as the doublet at δ 6.73 ppm from an NOE with H8 at δ 6.59 ppm which also has a small $^4J_{\text{HH}}$ coupling with H10 at δ 6.66 ppm (2.0 Hz). A ^1H - ^1H COSY experiment then yielded H15 and H16 at δ 7.38 and δ 7.76 ppm

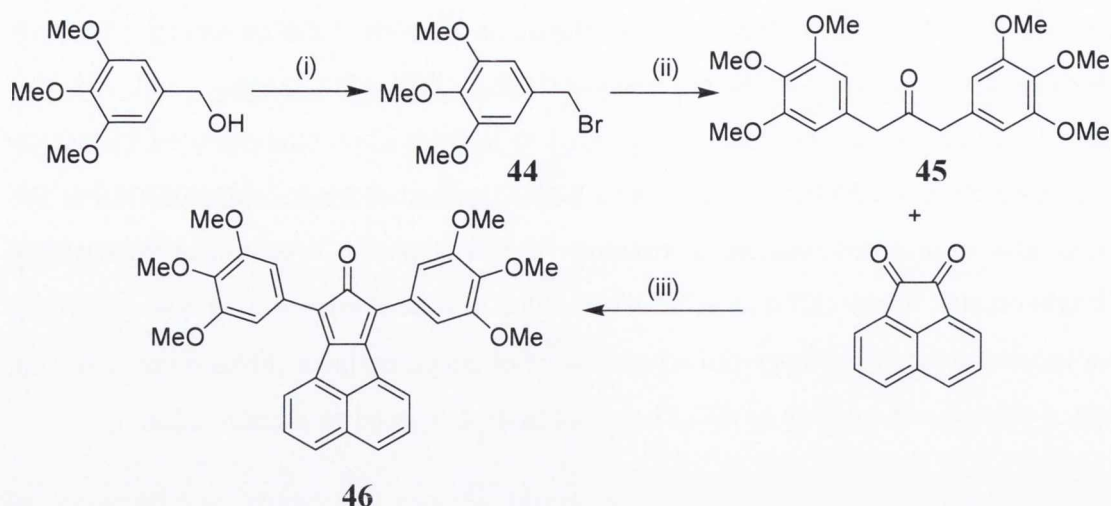
respectively. H2 and H3 were also distinguished from the NOE experiment on H30, which showed that H3 was the ferrocenyl *pseudo*-triplet at δ 4.28 ppm.

The accurate mass ESI-mass spectrum of **43** contained a single molecular ion at m/z 658.1816 in accord with the formation of $[\text{C}_{42}\text{H}_{34}\text{FeO}_4]^+$ (calculated 658.1806). Single-crystal X-ray diffraction of **43** enabled the determination of the solid-state molecular structure. Orange/red crystals were obtained by layer diffusion of methanol into a chloroform solution of **43**. The structure is discussed in section 2.2.8.

2.2.2. Synthesis of the di-ferrocenyl containing Fluoranthene (52)

2.2.2.1. Cyclopentadienone Synthesis

The novel methoxy containing 1,3-diaryl-2-propanone **45** was synthesised in two steps from the commercially available starting material 3,4,5-trimethoxybenzyl alcohol (Scheme 34). The first step involved bromination of the benzylic position and was done using phosphorous tribromide at -5 °C yielding **44** as an off-white solid in 88 % yield. **45** was prepared from **44** using iron pentacarbonyl in a biphasic system in 58 % yield. The novel cyclopentadienone **46** was synthesised by the two-fold Knoevenagel condensation reaction between acenaphthenequinone and **45** under basic methanolic conditions in 65 % yield. Compound **46** was characterised by ^1H and ^{13}C NMR spectroscopy.



*Scheme 34: Synthesis of the hexa-methoxy fluoranthene based cyclopentadienone **46**. (i) PBr_3 , CH_2Cl_2 , $-5\text{ }^\circ C$ (88 %). (ii) $Ca(OH)_2$, $Bu_4N(HSO_4)$, $Fe(CO)_5$, CH_2Cl_2/H_2O , 8 h (58 %). (iii) $NaOH$, CH_3OH , RT, 18 h (65 %).*

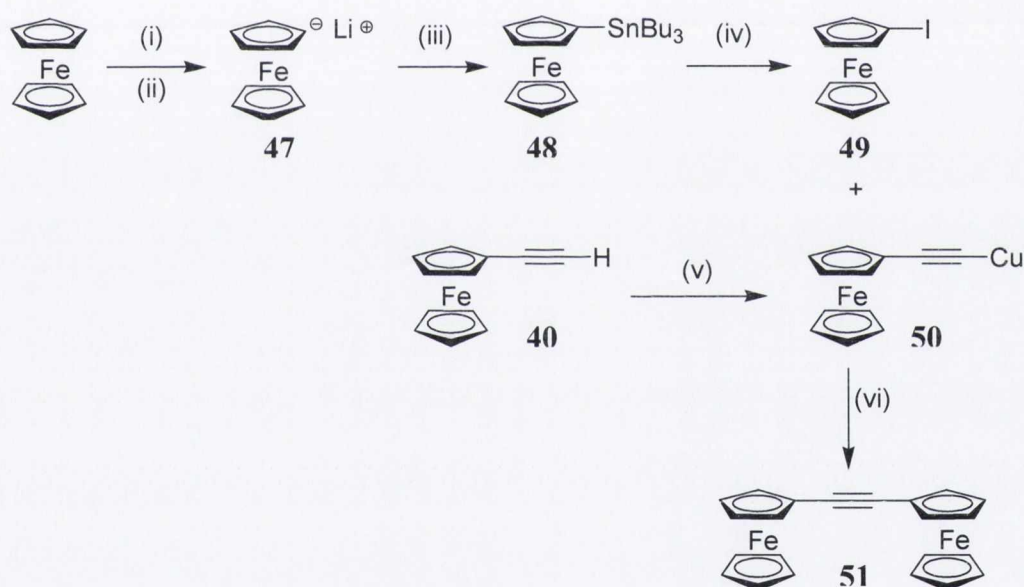
2.2.2.2. Di-ferrocenyl Acetylene Synthesis

Although the synthesis of **46** was relatively straight forward the synthesis of the di-ferrocenyl acetylene (**51**) was more problematic. The two constituent parts required for the successful synthesis of **51** were ethynylferrocene (**40**), the synthesis of which was discussed in the previous chapter, and iodoferrocene (**49**), which was synthesised using modified versions of different literature preparations (Scheme 35).^{79, 80} The first step involved the synthesis of lithioferrocene (**47**) which was achieved by the reaction of *tert*-butyllithium with ferrocene in tetrahydrofuran at $0\text{ }^\circ C$. The product was purified by removing any unreacted ferrocene through a series of schlenk filtrations using dry hexane. **47** was isolated in 54 % yield as a bright orange solid. Due to its pyrophoric nature, no characterisation was possible and it was stored under argon at $-30\text{ }^\circ C$.

Compound **47** underwent transmetallation with tributyltin chloride yielding **48** as a dark brown oil in 44 % yield. Compound **48** was readily converted into **49** (81 %) by reaction with iodine in dichloromethane at room temperature. Purification of these types of reactions have been shown to be difficult due to stannylated impurities in the product. A large amount of stannylated by-products could be seen in the 1H NMR spectrum of the product even after column chromatography on silica. In order to

overcome this problem the product was purified by column chromatography with 90 % silica and 10% KF,⁸¹ which held the stannylated by-products on the column and only allowed the desired product to elute.

Ethynylferrocene (**40**) was readily converted into the stable copper(I) salt (**50**) upon treatment with copper(I) iodide in an ethanolic ammonia solution. Iodoferrocene (**49**) underwent a Sonogashira type coupling reaction with **50** in refluxing pyridine and yielded **51** in a relatively poor yield (19 %) as an orange/red crystalline solid. Due to poor solubility **51** was characterised by its ESI-accurate mass spectrum which showed a single peak at m/z 394.0120 corresponding to $[M]^+$ C₂₂H₁₈Fe₂: (calculated 394.0107).

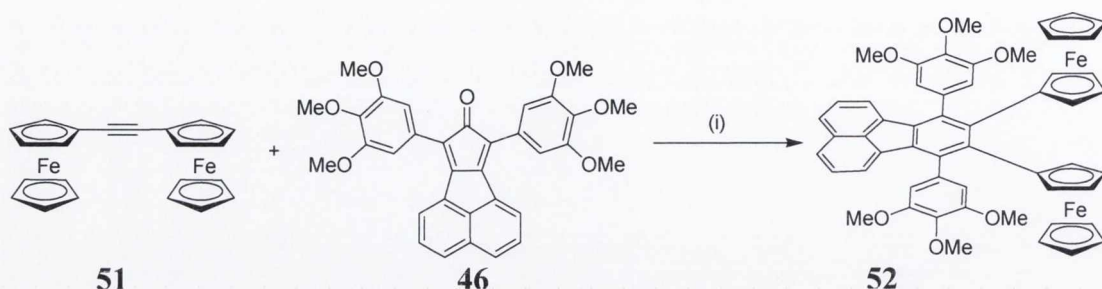


*Scheme 35: The synthesis of diferrocenylacetylene (**51**) from ferrocene. (i) *t*-BuLi, THF, 0 °C, 15 min, (ii) hexane, -78 °C (54 %). (iii) SnClBu₃, THF/hexane (1:1), 90 min (44 %), (iv) I₂, CH₂Cl₂, RT, 18 h (81 %), (v) CuI, aq. NH₃, EtOH, RT, 15 min (52 %), (vi) pyridine, reflux, 8 h (19 %).*

2.2.2.3. Diels-Alder [2+4]-cycloaddition

46 and the di-ferrocenyl acetylene **51** were heated in a benzophenone melt under argon for two days at 200 °C (Scheme 36). After cooling to room temperature and extraction into dichloromethane, **52** was purified using column chromatography to

afford a bright red crystalline air-stable solid in 38 % yield. ^1H and ^{13}C NMR spectroscopy, mass spectrometry and single crystal X-ray diffraction confirmed the formation of the di-ferrocenyl fluoranthene containing compound **52**.



*Scheme 36: Synthesis of compound **52** via a Diels-Alder [2+4]-cycloaddition reaction. (i) benzophenone, 200 °C, 48 h (38 %).*

2.2.2.4. Characterisation of the di-ferrocenyl containing Fluoranthene (**52**)

The accurate mass ESI-mass spectrum of **52** contained a single molecular ion at m/z 902.1957 consistent with the formation of $[\text{C}_{54}\text{H}_{46}\text{Fe}_2\text{O}_6]^+$ (calculated 902.1993). Single-crystal X-ray diffraction of **52** enabled the determination of the solid-state molecular structure. Red crystals were obtained by layer diffusion of methanol into a chloroform solution of **52**. The structure is discussed in section 2.2.8.

The symmetric nature of **52** can be seen clearly in its ^1H NMR spectrum (Figure 28), which is vastly simplified when compared to the ^1H NMR spectrum of **43** (Figure 27). Proton H8 can be easily assigned as the only aromatic singlet at δ 6.95 ppm, and an NOE experiment on this proton showed an interaction with a doublet at δ 6.40 ppm corresponding to H15. The ^1H - ^1H COSY experiments then yielded H16 and H17 at δ 7.33 and δ 7.73 ppm respectively. The protons of the substituted cyclopentadienyl ring (H2 and H3) could not be distinguished as one of their signals overlapped with that of H11.

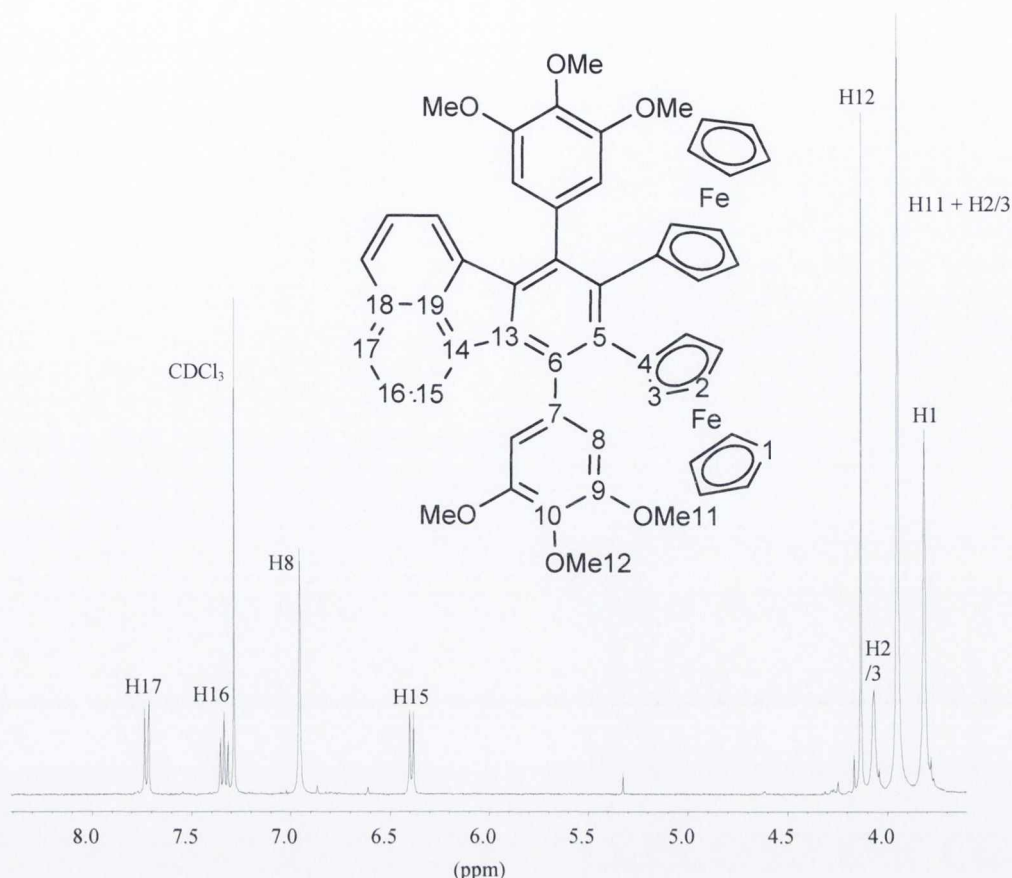


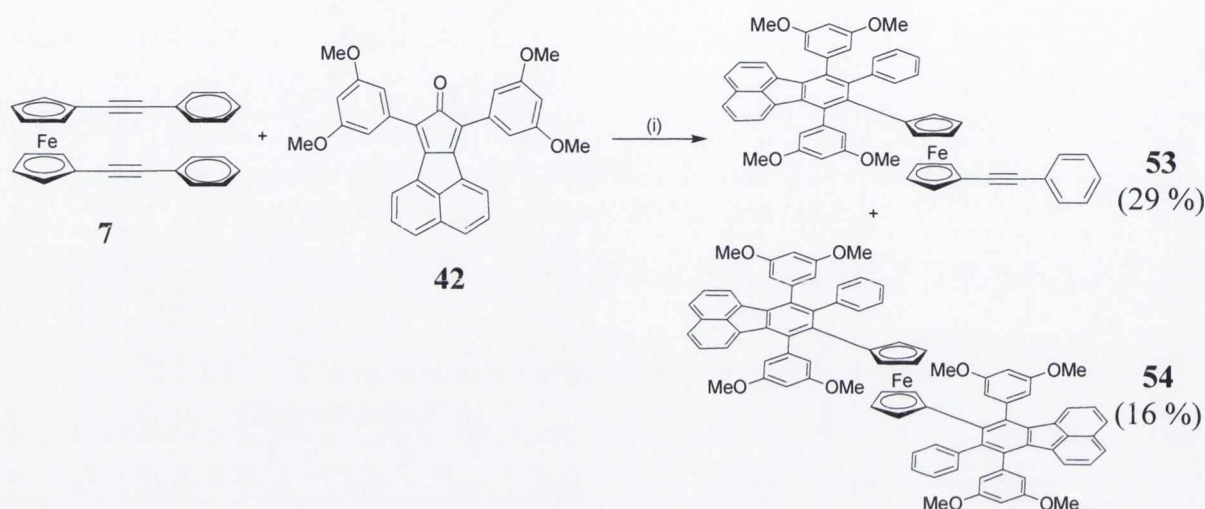
Figure 28: The ^1H NMR spectrum of the aromatic and ferrocenyl region for compound **52**, (CDCl_3 , RT, 400 MHz).

2.2.3. Synthesis of the di-fluoranthene ferrocenyl **54**

Although compounds **43** and **52** are substituted with different numbers of ferrocene moieties (one and two respectively) both only contain one fluoranthene platform. In order to see what effect having two fluoranthene moieties would have on the system, the synthesis of compound **54** was attempted. The synthesis of di-acetylene **7** was discussed in detail in chapter 1, while the synthesis of cyclopentadienone **42** has been discussed in section 2.2.1.

In order to synthesise compound **54**, just over two equivalents of the cyclopentadienone **42** and one equivalent of the di-acetylene **7** were heated in a benzophenone melt under argon for 24 hours at 200 °C (Scheme 37). After cooling to room temperature and extraction into dichloromethane, TLC analysis showed that two

new compounds had been synthesised. Separation of these two compounds was achieved through column chromatography. The first compound was eluted with a hexane/dichloromethane (2:1) mixture. Gradually increasing the amount of dichloromethane allowed elution of the second product. Characterisation of the first identified it as **53**, but the second product was the desired double Diels-Alder product **54**.



*Scheme 37: The synthesis of **53** via the mono Diels-Alder [2+4]-cycloaddition reaction and **54** via the double Diels-Alder [2+4]-cycloaddition reaction. (i) benzophenone, 200 °C, 24 h (**53** 29 %), (**54** 16 %).*

2.2.3.1. Characterisation of the mono-fluoranthene containing byproduct **53**

The mono-fluoranthene containing compound **53** was found to be an air-stable orange-red crystalline material. It was also found to be readily soluble in common chlorinated solvents and toluene. Compound **53** was fully characterised by ^1H and ^{13}C NMR spectroscopy and mass spectrometry as well as single crystal X-ray diffraction.

The accurate mass ESI-mass spectrum of **53** contained a single molecular ion at m/z 834.2421 in accord with the formation of $[\text{C}_{56}\text{H}_{42}\text{FeO}_4]^+$ (calculated 834.2432). Single crystal X-ray diffraction of **53** enabled the determination of the solid-state

molecular structure. Red needle-like crystals were obtained by layer diffusion of methanol into a chloroform solution of **53**. The structure is discussed in section 2.2.8.

The ^1H NMR spectrum of **53** can be seen in Figure 29, the assignment of both the ^1H and ^{13}C were achieved through a series of HMBC, ^{13}C - ^1H COSY, ^1H - ^1H COSY and NOE experiments. Due to the lack of symmetry within the molecule the full assignment of the ^1H NMR spectrum proved quite difficult. However, once the acetylene carbon atoms were identified in the ^{13}C spectrum this gave an opportunity to assign the ^1H NMR spectrum. The acetylene carbon signals at δ 87.8 and 86.8 ppm can be assigned to C5 or C6, however initially it was not possible to say which was which. This was overcome using the HMBC experiment, which showed that there was a long-range interaction between the acetylene carbon at δ 87.8 ppm and the ferrocene proton at δ 4.05 ppm and there was also a long-range interaction observed between the other acetylene carbon at δ 86.8 ppm with an aromatic proton at δ 7.14 ppm. This confirms that the acetylene carbon at δ 87.8 ppm is C6 which interacts with H8 on the ferrocene ring, which in turn interacts with the other ferrocenyl proton at H9 at δ 3.88 ppm. Thus the other acetylene carbon at δ 86.8 ppm corresponds to C5 which interacts with the *ortho*-proton on ring phenyl ring **D** shown as H3 at δ 7.14 ppm. The remaining protons of ring **D** were then easily assigned from the ^1H - ^1H COSY; H2 at δ 6.81 ppm (*meta*-proton) and H1 at δ 6.91 ppm (*para*-proton).

With ring **D** assigned the signals due to ring **A** could then be deduced as the large unresolved multiplet at δ 7.22 ppm which integrates for 5 aromatic protons. An NOE experiment on the multiplet revealed that the singlet at δ 3.68 ppm was due to the methoxy groups on ring **B**. This NOE also showed the doublet at δ 6.23 ppm to be H34 which in turn has a $^4J_{\text{HH}}$ interaction with the triplet at δ 6.35 ppm, corresponding to H36 with a small coupling constant of 2.0 Hz.

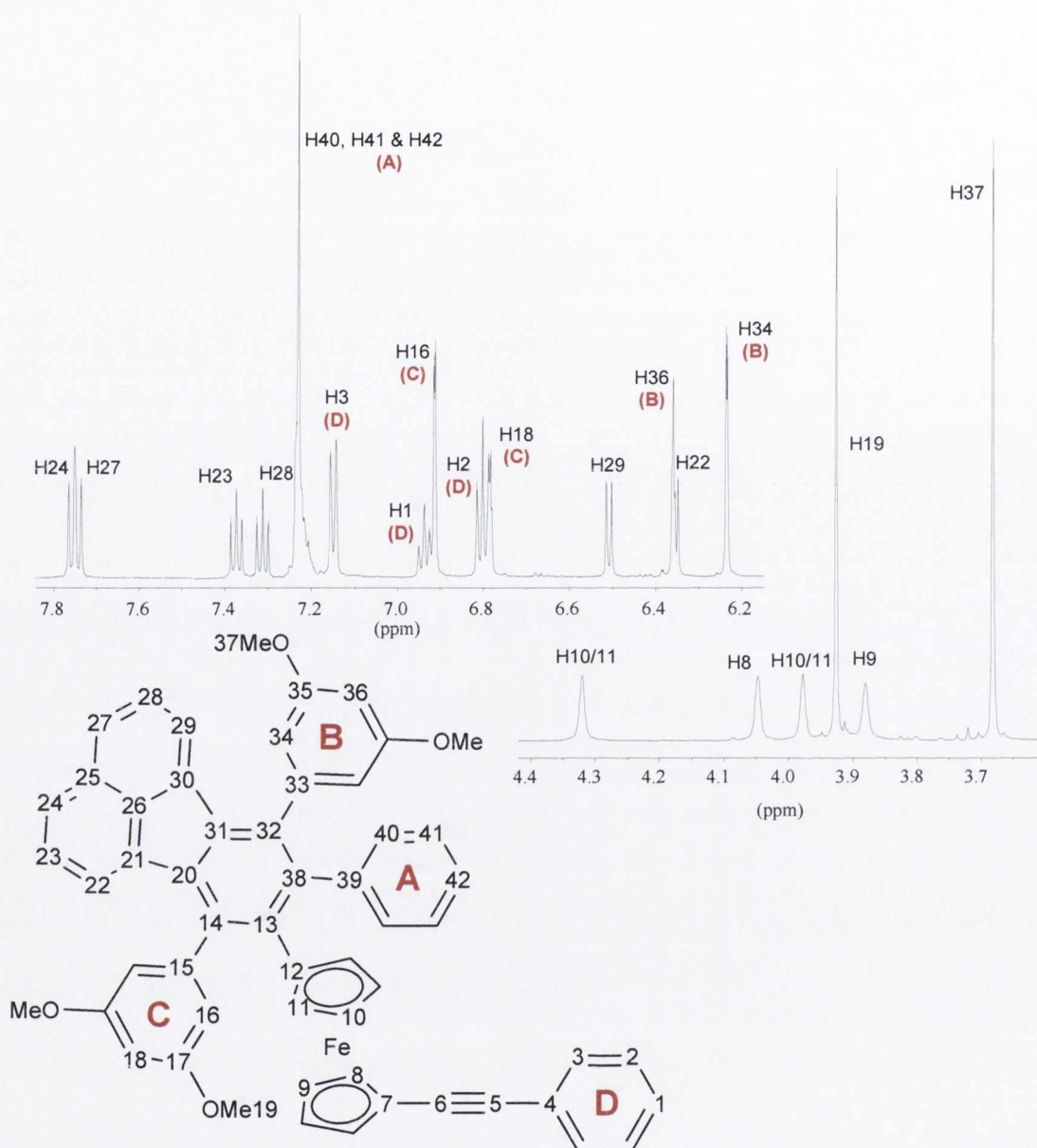


Figure 29: The ^1H NMR spectrum of the aromatic and ferrocenyl region for compound **53**, (CD_2Cl_2 , RT, 600 MHz).

With one of the methoxy groups assigned, by elimination the other methoxy signal at δ 3.93 ppm had to be H19 on ring C, which in turn has an NOE interaction with H16 at δ 6.91 ppm and H18 at δ 6.77 ppm. The doublet that is H16 has a $^4J_{\text{HH}}$ interaction with the triplet that is H18 with a small coupling constant of 2.0 Hz. The methoxy signal of H19 also showed an interaction in its NOE with H22 at δ 6.34 ppm which allowed the assignment of H23 and H24 at δ 7.37 and δ 7.76 ppm respectively through the ^1H - ^1H COSY experiment.

An NOE on H34 at δ 6.23 ppm yielded H29 at δ 6.51 ppm which *via* the ^1H - ^1H COSY allowed the assignment of the remaining fluoranthene protons H28 and H27 at δ 7.31 and δ 7.74 respectively ppm.

2.2.3.2. Characterisation of the di-fluoranthene containing Compound **54**

The di-fluoranthene containing compound **54** was found to be an air-stable red crystalline material. Although it was found to be soluble in common chlorinated solvents and toluene, it was significantly less soluble in these solvents compared to **53**. Compound **54** was fully characterised by ^1H and ^{13}C NMR spectroscopy and mass spectrometry as well as single crystal X-ray diffraction.

The accurate mass ESI-mass spectrum of **53** contained a single molecular ion at m/z 1282.4147 which is consistent with the formation of $[\text{C}_{86}\text{H}_{66}\text{FeO}_8]^+$ (calculated 1282.4107). Single-crystal X-ray diffraction of **53** enabled the determination of the solid-state molecular structure. Bright red needles were obtained by layer diffusion of methanol into a chloroform solution of **54**. The structure is discussed in section 2.2.8.

The ^1H NMR spectrum of **54** is shown in Figure 30, the assignment of both the ^1H and ^{13}C spectra was achieved through a series of HMBC, ^{13}C - ^1H COSY, ^1H - ^1H COSY and NOE experiments. The assignment of the protons of **54** was considerably easier than for **53** due to the higher degree of symmetry present.

Two methoxy signals H10 and H28 are observed at δ 3.59 and 3.70 ppm although on first inspection differentiating them was not possible. In order to overcome this, an NOE experiment was carried out on both signals. The methoxy signal at δ 3.59 ppm shows an interaction with the protons on ring **A**, thus confirming that this signal is H28. The protons on phenyl ring **A** can be readily assigned from their integration and multiplicity. The *ortho*-protons (H31) can be seen as a doublet equivalent to 4 protons at δ 6.96 ppm, the *meta*-protons (H32) are observed as a triplet equivalent to 4 protons at δ 7.05 ppm and the *para*-proton (H33) appears as a triplet equivalent to 2 protons at δ 7.08 ppm.

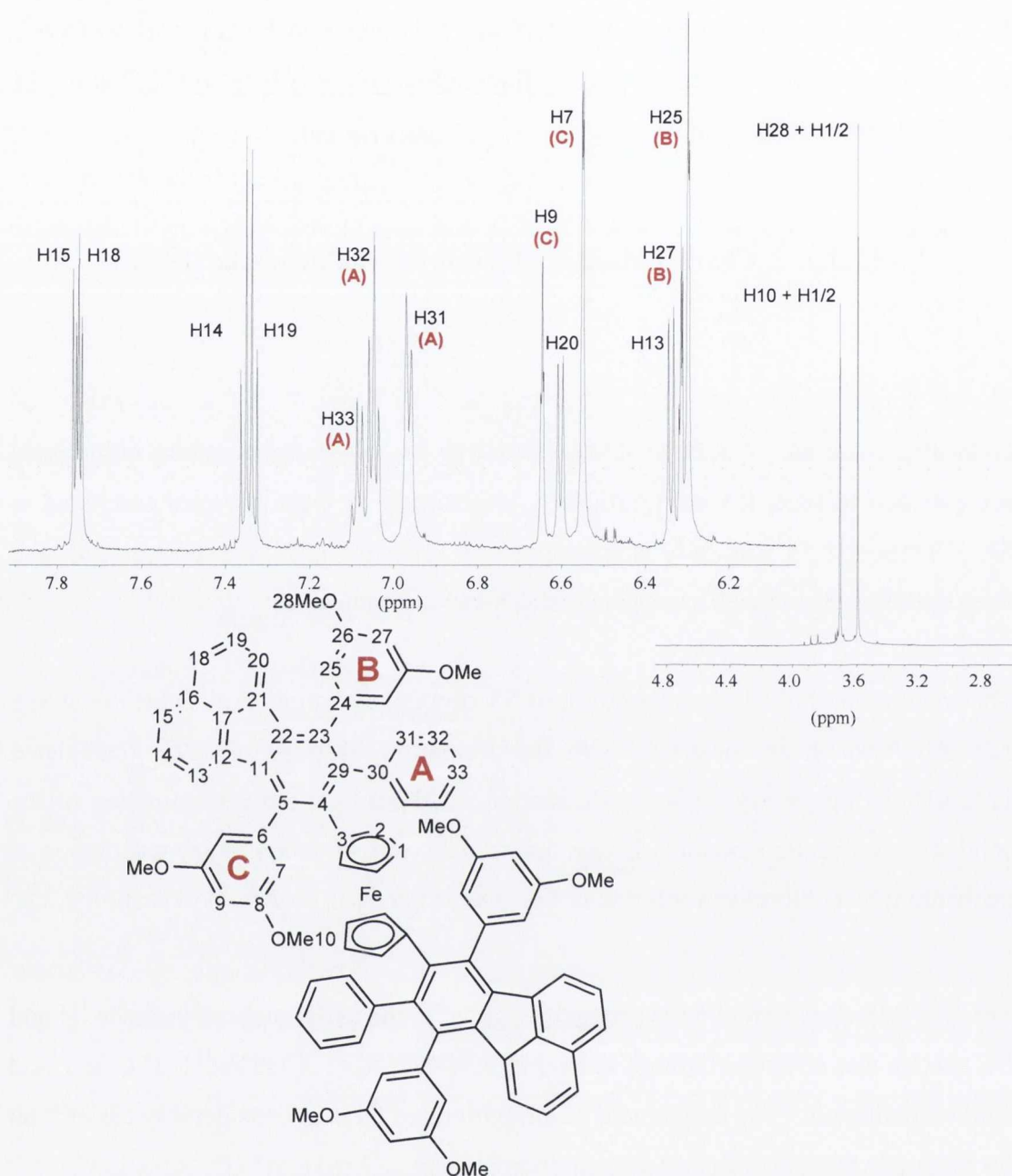


Figure 30: The ^1H NMR spectrum of the aromatic and ferrocenyl region of compound **54**, (CD_2Cl_2 , RT, 600 MHz).

The NOE of the H28 signal showed it to have interactions with three signals at δ 6.32, δ 6.30 and δ 6.60 ppm. The signal at δ 6.32 ppm is a triplet that is equivalent to 2 protons and has a very small coupling constant and thus can be assigned to H27. Proton H27 has a $^4J_{\text{HH}}$ interaction of 2.0 Hz with the doublet at δ 6.30 ppm which integrates as 4 protons, this can be assigned to H25.

The same NOE experiment also showed an interaction with the doublet at δ 6.60 ppm which integrates as 2 protons and is due to H20. Assignment of H20 in turn yielded H18 and H19 at δ 7.74 and δ 7.34 ppm respectively through the ^1H - ^1H COSY experiments.

With the methoxy signal H28 assigned, by elimination the other methoxy signal at δ 3.70 ppm could be assigned as H10. An NOE on H10 shows interactions with H7 and H9 at δ 6.55 and δ 6.65 ppm respectively. H7 appears as a doublet integrating to 4 which has a $^4J_{\text{HH}}$ interaction with the triplet H9 (which integrates to 2) with a small coupling constant of 2.0 Hz. An NOE on H7 revealed H13 to be responsible for the signal at δ 6.34 ppm which in turn *via* the ^1H - ^1H COSY experiments yielded H14 and H15 at δ 7.34 and δ 7.76 ppm respectively.

The two ferrocenyl signals H1 and H2 are overlapping with the two methoxy signals. Although it is not possible to say which ferrocene signal is under which methoxy signal from the integration it is clear that one ferrocene signal is under both methoxy signals since they both integrate for 16.

2.2.4. Proton NMR Comparisons

The ^1H NMR spectra of the fluoranthene compounds **43**, **52**, **53** and **54** show one very interesting common feature. In all four spectra there is a fluoranthene signal that has been shifted upfield when compared to all the other fluoranthene signals. It appears as a doublet at δ 6.73 ppm for **43** (H13), δ 6.40 ppm for **52** (H13), δ 6.34 ppm for **53** (H22) and δ 6.33 ppm for **54** (H13) and in all cases it is assigned as the fluoranthene proton that is closest to the ferrocene moiety. One possible reason for this shift is that the ferrocene moiety is such a large and bulky unit that it has the effect of pushing the phenyl group closest to it away from itself and thus closer to the fluoranthene proton labelled H13 (in **43**, **52** and **54**) or H22 (in **53**). Thus this proton is pushed closer to the electron cloud of the phenyl group causing a shielding effect and moving it to lower δ values.

2.2.5. Cyclodehydrogenation of the Fluoranthene based compounds

The attempted cyclodehydrogenation of compounds **43**, **52**, **53** and **54** proved unsuccessful. After the attempted cyclodehydrogenation with FeCl_3 of all four compounds, all that was recovered after work-up was un-characterisable black material, and no starting material, which suggested that complete decomposition had taken place.

2.2.6. Spectral Comparisons of Derivatives

Table 6 summarises the main spectroscopic data for the ferrocene containing fluoranthene compounds synthesised during the course of this work. In all cases, mass spectra were obtained by ESI (electro-spray ionisation) or MALDI-TOF spectrometry. Under these conditions a single peak corresponding to the $[\text{M}]^+$ ion was obtained for each complex.

Compound	Mass Spectrum (m/z)	¹ H chemical shifts for ferrocene protons (ppm)	
		Unsubstituted Cp ring	<i>ortho</i> - and <i>meta</i> - protons of the substituted Cp ring
43	658.1816	4.12	4.19, 4.28
52	902.1957	3.81	3.95, 4.07
53	834.2421	---	3.88, 3.93, 3.98, 4.05
54	1282.4147	---	3.59, 3.70

Table 6: NMR and mass spectrometry data for complexes **43**, **52**, **53** and **54**.

All the ^1H NMR spectroscopic signals of the *ortho*- and *meta*- protons of the substituted cyclopentadienyl rings should appear as *pseudo*-triplets, corresponding to the AA'BB' system. However some of them appear as singlets, due to broadening of the signals caused by steric constraints about the substituted cyclopentadienyl ring. One good example where the ferrocenyl *pseudo*-triplets are observed is in the ^1H NMR spectrum of **43**, which has been magnified in Figure 31.

In Figure 31 it is shown how the protons labelled α and α' are chemically equivalent but magnetically non-equivalent. If the α protons were magnetically equivalent they would simply appear as a doublet, being split by the β protons. Since they are

magnetically non-equivalent the characteristic *pseudo*-triplet is observed caused by the overlap of the doublet corresponding to α with the doublet corresponding to α' . The doublets do not overlap perfectly since they are magnetically non-equivalent and thus they appear at slightly different chemical shifts, although the difference is small. The same is also true for the β protons.

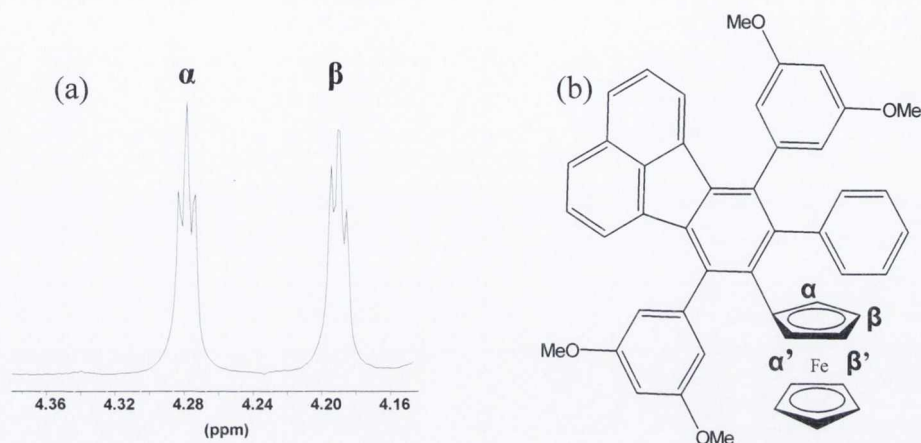


Figure 31: (a) ^1H NMR spectrum of **43** with the ferrocenyl region magnified, (b) schematic representation of **43**, highlighting the magnetic non-equivalence of the substituted cyclopentadienyl protons.

2.2.7. UV-visible Absorption Spectroscopy

The electronic absorption spectra of the ferrocene containing fluoranthene complexes **43**, **52**, **53** and **54** were recorded in acetonitrile and the data is presented in Table 7. Similar to the ferrocenyl containing compounds discussed in chapter 1, they exhibit a weak low energy band attributable to the d-d transition of the ferrocene moiety. These broad, low energy features account for the orange to red colours of these compounds.

Compound	λ_{max} nm (ϵ , L mol ⁻¹ cm ⁻¹ x 10 ³)	Low energy d-d transition
Fc	326 (0.5)	441 (0.5)
43	289 (21.0), 328 (11.4), 378(6.2)	479 (1.4)
52	299 (14.9), 335 (10.7), 380 (4.9)	474 (2.0)
53	289 (28.1), 332 (15.1), 359 (7.8)	482 (1.3)
54	289 (16.6), 332 (9.3), 359 (7.4), 378 (6.5)	490 (1.4)

Table 7: The UV-vis data for ferrocene and the ferrocenyl compounds **43**, **52**, **53** and **54**, in acetonitrile.

The UV-vis spectra of compounds **43**, **52**, **53** and **54** can be seen in Figure 32. However in order to discuss the main features of these spectra they have been divided into two regions: between λ 400 and 600 nm, which is dominated by ferrocenyl transitions (Figure 33) and between λ 200 and 400 nm which is dominated by fluoranthene transitions.

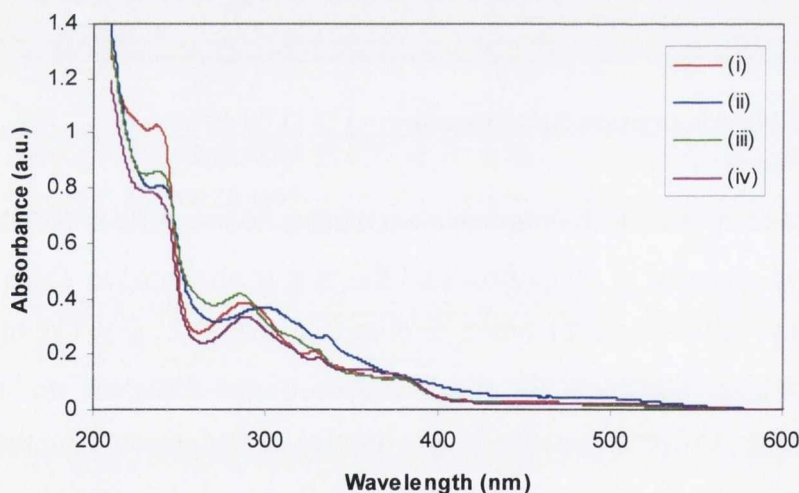


Figure 32: The UV-vis absorption spectra of the fluoranthene complexes, (i) **43**, (ii) **52**, (iii) **53** and (iv) **54**, recorded in acetonitrile.

Attempts to cyclodehydrogenate **43**, **52**, **53** and **54** proved unsuccessful, and starting material was not recovered which suggested that complete decomposition had taken place. It has been proposed that cyclodehydrogenation follows an oxidative cationic mechanism under Lewis acid conditions. The acidic and oxidative conditions of the

cyclodehydrogenation reaction is likely to cause some decomposition of those ferrocene compounds with very tilted cyclopentadienyl rings.

It has been shown that the basicity of the iron atom in **43**, **52**, **53** and **54** would be expected to be high because of the inclination of the cyclopentadienyl rings. Thus protonation at the iron centre would be accelerated,⁶² resulting in decomposition rather than cyclodehydrogenation. In addition it has been shown that there is a correlation between the degree of tilt of the ferrocene cyclopentadienyl rings (and thus the likelihood of cyclodehydrogenation) and the wavelength of the ferrocenyl absorption band which is normally around $\lambda_{\text{max}} = 450$ nm. If the band appears at wavelengths greater than 450 nm then there is significant tilt between the cyclopentadienyl rings.³⁴

The ferrocenyl absorptions of **43**, **52**, **53** and **54** are at λ 479, 474, 482 and 490 nm respectively. This implies that the cyclopentadienyl rings are indeed significantly tilted, even more so than the ferrocenyl compounds discussed in chapter 1. Compound **9**, in chapter 1 was one of the derivatives that decomposed upon cyclodehydrogenation and it also had the largest value for the ferrocenyl d-d transition at λ 464 nm, significantly longer than λ 450 nm. The d-d ferrocenyl transition in all four fluoranthene based compounds appear at a much longer wavelength than this, due to the increased steric bulk and hindrance caused by the fluoranthene unit in comparison to the polyphenylene platforms discussed in chapter 1.

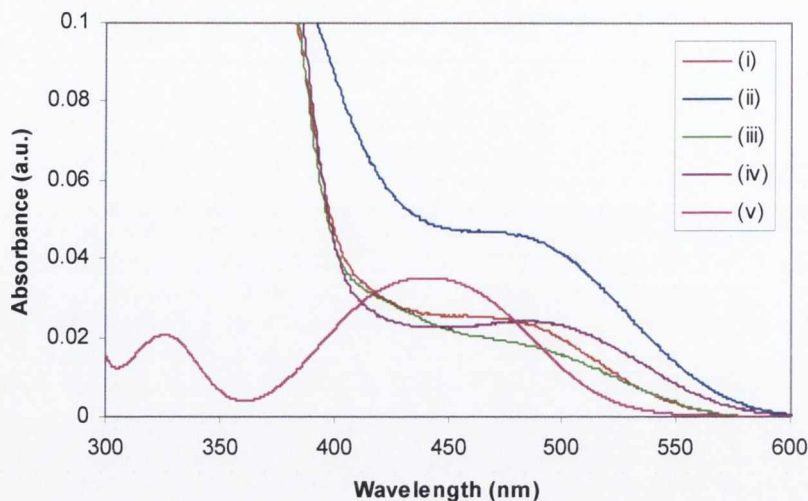


Figure 33: The UV-vis absorption spectra of the ferrocenyl region for the fluoranthene complexes, (i) **43**, (ii) **52**, (iii) **53**, (iv) **54**, (v) and ferrocene for comparison, in acetonitrile.

It was also no surprise that compound **54** displays the ferrocenyl transition at the longest wavelength, since the ferrocene moiety in **54** has a fluoranthene platform on each of its cyclopentadienyl rings and is thus going to be severely tilted. These results support the correlation between the degree of tilt in the ferrocene cyclopentadienyl rings and the wavelength of the ferrocenyl d-d absorption band.

The absorption spectra of compounds **43**, **52**, **53** and **54**, shown in Figure 34 were very similar in the region between λ 200 to 400 nm, which has been shown to be the region where the fluoranthene fragment absorbs. All four spectra show three main absorption bands, which concurs with spectra reported in the literature of other fluoranthene compounds. The region where $S_0 \rightarrow S_1$ transitions are observed is noted as S_1 in Figure 34, however this transition was not seen since they are very weak in these examples.

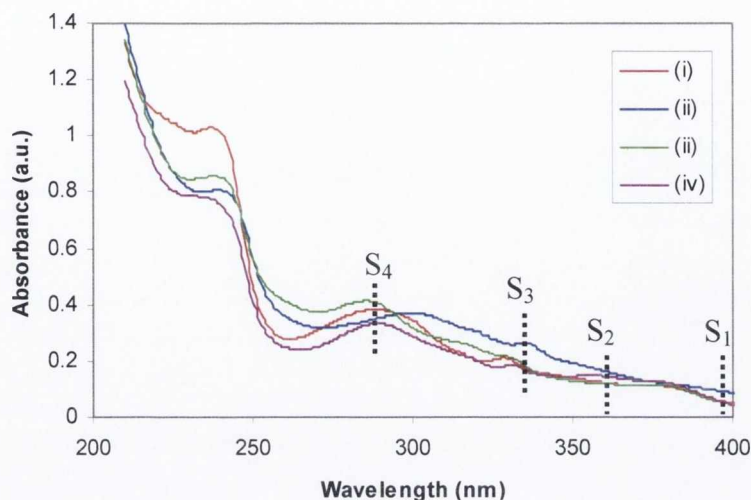


Figure 34: The UV-vis absorption spectra of the fluoranthene complexes, (i) **43**, (ii) **52**, (iii) **53** and (iv) **54**, in acetonitrile. The ferrocenyl region has been omitted for clarity.

Two well studied examples in the literature are shown in Figure 35, namely fluoranthene⁸² and benzo[k]fluoranthene.^{83, 84} These two compounds as well as compounds **43**, **52**, **53** and **54** show three main absorption bands at similar λ values.

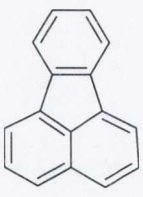
Compound		λ_{max} (nm)
 (a)	(a) in ethanol	290, 325, 360
	(b) in cyclohexane	295, 310, 360

Figure 35: Structures and UV-vis data for two well studied fluoranthene based compounds, (a) fluoranthene⁸² and (b) benzo[k]fluoranthene.^{83, 84}

Through computational analysis⁸⁵ and absorption spectra of fluoranthene recorded in the gas phase,⁸⁶ the three bands have been assigned as shown in Figure 34. Although the band system looks like one transition with vibrational spacing typical of a PAH, it actually represents a composite of at least three transitions $S_0 \rightarrow S_3$, $S_0 \rightarrow S_2$ and $S_0 \rightarrow S_1$,⁸⁴ but in some cases a fourth is observed $S_0 \rightarrow S_4$.⁸⁷

The absorption spectrum of fluoranthene in the gas phase shows the characteristic three bands but like in most cases the fourth band is absent. For fluoranthene in the gas phase the transitions to high energy states correspond to the strong absorption bands at λ 272, 277 and 282 nm. Recently these bands were assigned to vibrational levels of the $S_0 \rightarrow S_4$ absorption transition.⁸⁷ At lower energies, the absorption bands at λ 320 and 352 nm were assigned by Kolc *et al.*⁸⁸ to the $S_0 \rightarrow S_2$ and to the $S_0 \rightarrow S_3$ transitions, respectively. The $S_0 \rightarrow S_1$ transitions are not observed since they are very weak.

Compounds **43**, **52**, **53** and **54** all show these characteristics peaks as can be seen in Table 7 and Figure 34. However for comparison with fluoranthene the spectrum of **53** is shown in Figure 36, as the bands are resolved to a higher degree.

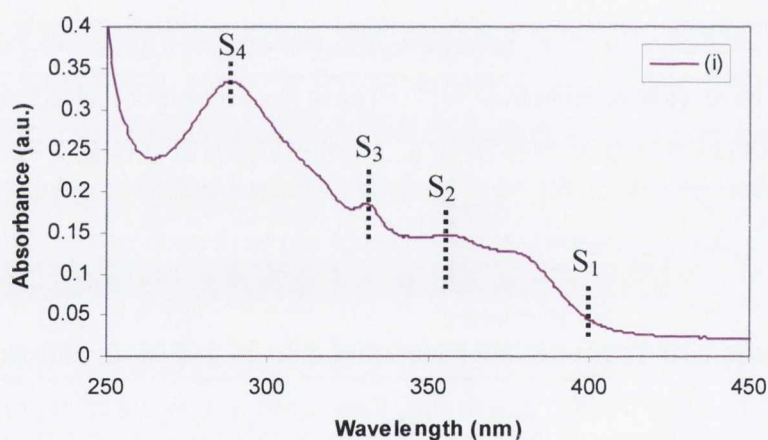


Figure 36: The UV-vis absorption spectra of (i) **54**, for comparison with the bands observed for fluoranthene by Wabyele *et al.*⁸⁶ Recorded in acetonitrile, the ferrocenyl region has been omitted for clarity.

The band at λ 289 nm corresponds to the $S_0 \rightarrow S_4$ transition, whereas at lower energies the absorption bands at λ 332 and 359 nm are assigned to the $S_0 \rightarrow S_3$ and to the $S_0 \rightarrow S_2$ transition, respectively. As with fluoranthene the $S_0 \rightarrow S_1$ is not seen since it is very weak.

2.2.8. X-Ray Crystallographic Analysis

Single-crystal X-ray diffraction studies of **43**, **52**, **53** and **54** were carried out to determine their solid-state molecular arrangements. Bright red crystals of all four compounds were obtained by the slow diffusion of methanol to a solution of the respective compounds in chloroform.

Figure 37 shows the X-ray crystal structures of compounds **43** and **52**. Compound **43** (Figure 37 (a)) crystallised in the monoclinic space group $P2_1/c$, with an R_1 of 14.54 %. The poor refinement was due to disorder in the unsubstituted cyclopentadienyl ring which could not be modelled. The molecular structure of **43** shown in Figure 37 (a), highlights the twisting of the ferrocene substituent and the phenyl rings with respect to the central fluoranthene plane. The ferrocene moiety is twisted by 45.8° from the central plane. The phenyl rings **A** and **B** are twisted by 81.5° and 82.2° respectively from the central fluoranthene plane.



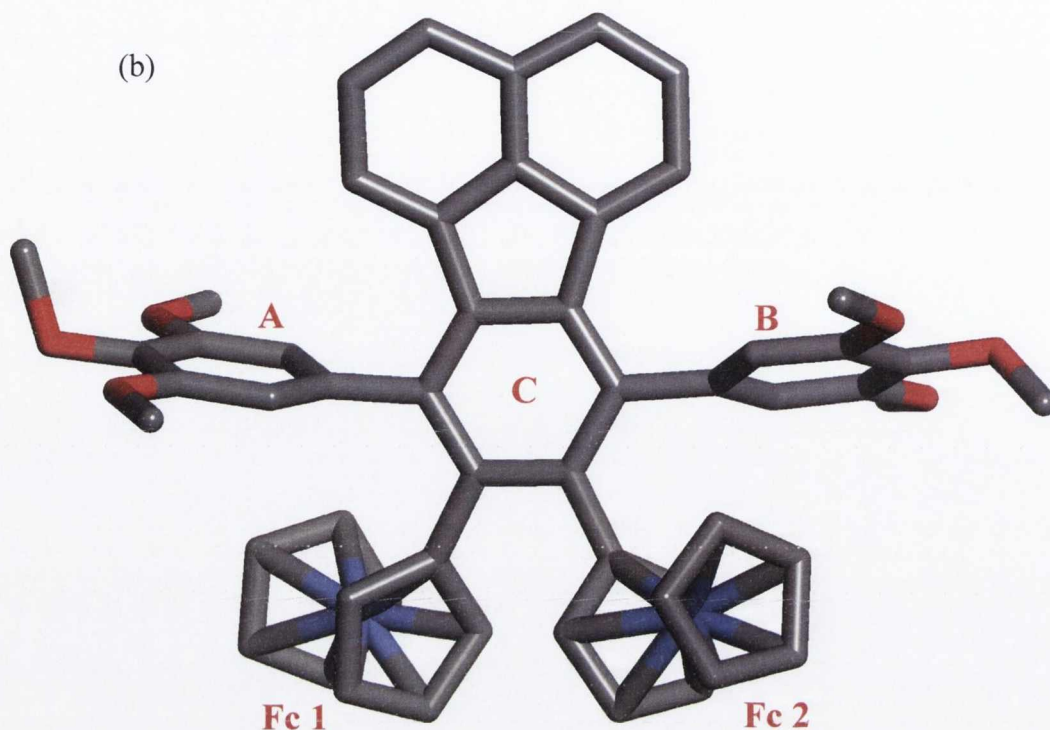


Figure 37: The X-ray crystal structures of (a) **43** and (b) **52**, protons and solvent molecules are omitted for clarity.

Compound **52** (Figure 37 (b)) crystallised in the triclinic space group P-1 with a R_1 of 7.42 %. The ferrocene groups **Fc 1** and **Fc 2** in **52** are also twisted from the fluoranthene plane by 9.2° and 8.8° respectively. As for **43** the phenyl rings in **52** are twisted in a propeller type arrangement from the fluoranthene plane. The phenyl rings **A** and **B** of **52** are twisted by 86.3° and 70.3° respectively with respect to the fluoranthene plane.

As can be seen in Figure 38, the presence of the two adjacent ferrocene groups in **52** leads to a large distortion from planarity in ring **C** of the fluoranthene core. In Figure 38 phenyl ring **A** and all of the protons have been omitted in order to show the extent of the distortion in ring **C** clearly. The two large ferrocene groups in such close proximity to each other induce a maximum deviation in ring **C** of 0.21 \AA when compared to the fluoranthene plane.

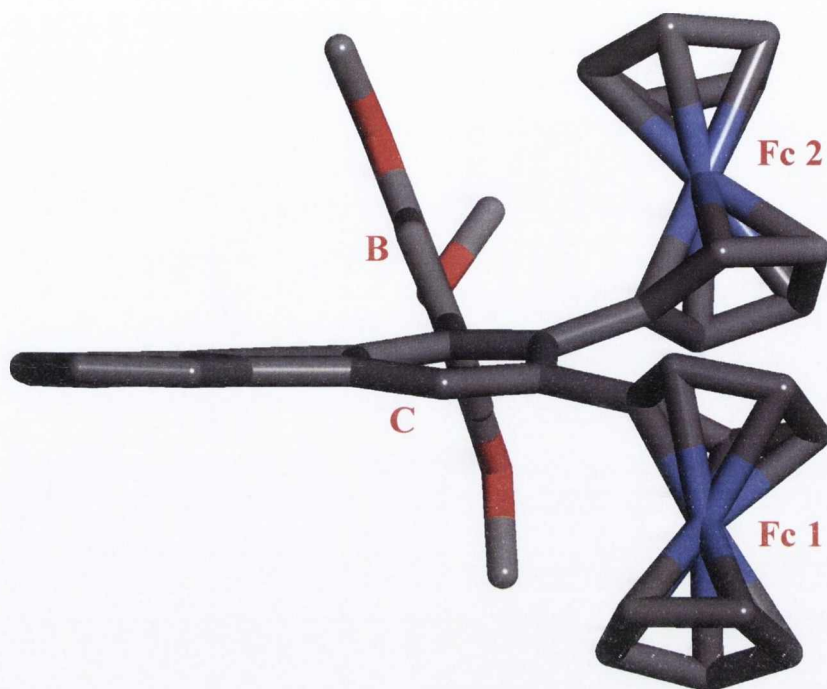


Figure 38: X-ray crystal structure of **52** with the methoxy groups and phenyl ring **A** omitted to highlight the distortion in phenyl ring **C**.

Figure 39 shows the X-ray crystal structures of compounds **53** and **54**. Compound **53** (Figure 39 (a)) crystallised in the monoclinic space group $P2_1/c$, with an R_1 of 4.62 %. The molecular structure of **53** shown in Figure 39 (a), highlights the twisting of the ferrocene and the phenyl rings **A**, **B** and **C** with respect to the central fluoranthene plane. The ferrocene moiety is twisted by 10.9° from the central plane. The phenyl rings **A**, **B**, and **C** are twisted by 84.9° , 85.0° and 83.1° respectively from the central fluoranthene plane again in a propeller type arrangement.

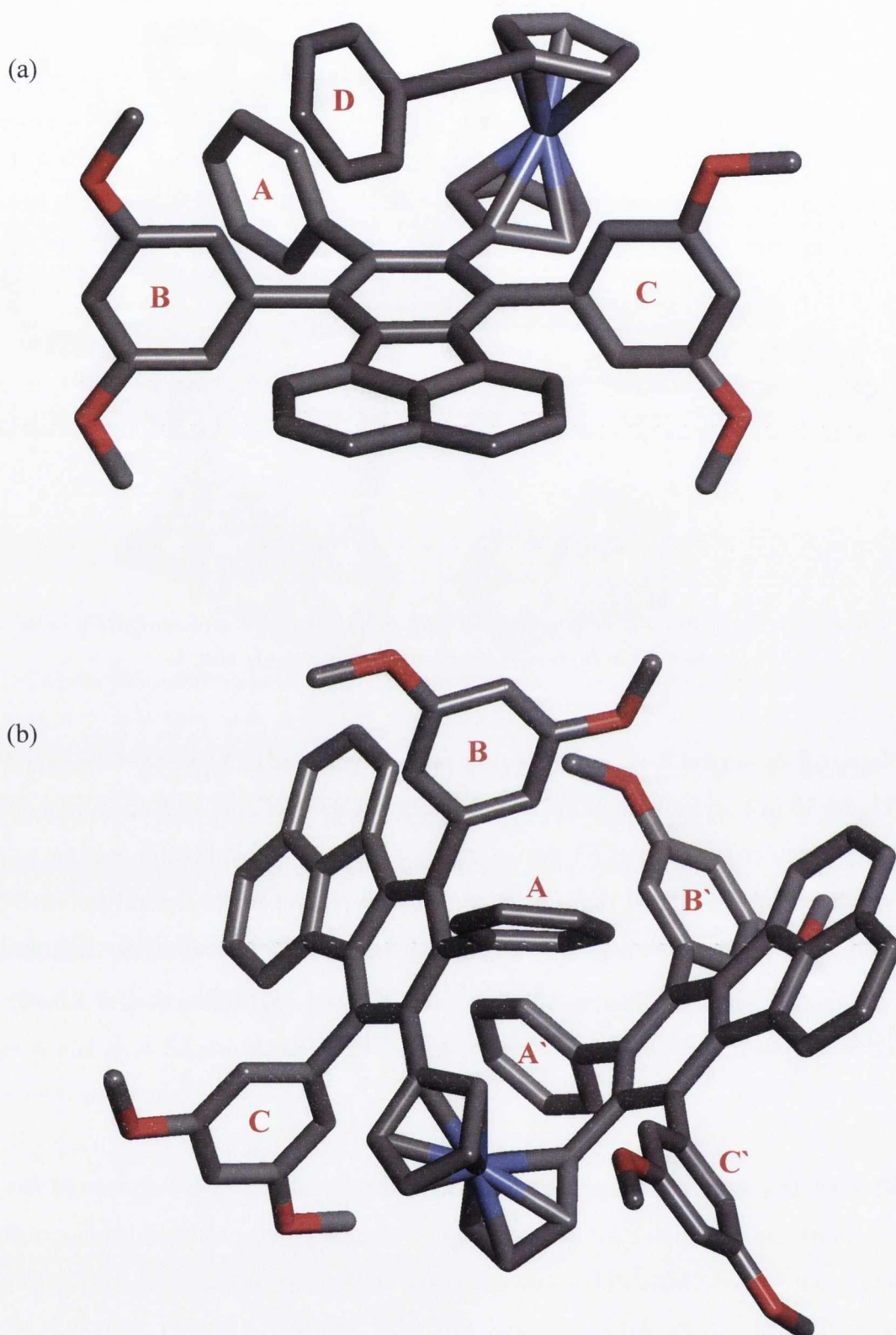


Figure 39: The X-ray crystal structures of (a) **53** and (b) **54**, protons and solvent molecules are omitted for clarity.

Compound **54** (Figure 39 (b)) crystallised in the monoclinic space group $P2_1/n$ with a R_1 of 11.67 %. Although in solution the two fluoranthene platforms are equivalent (as

observed in NMR experiments) in the solid state this is not the case. This is demonstrated in the different twisting angles of the phenyl rings from the fluoranthene planes. Phenyl rings **A**, **B** and **C** are twisted by 81.5 °, 72.4 ° and 88.4 ° respectively, whereas phenyl rings **A'**, **B'** and **C'** are twisted by 74.9 °, 83.2 ° and 84.3 ° respectively.

Table 8 compares the tilt angle of the cyclopentadienyl rings with the ferrocenyl transitions of compounds **43**, **52**, **53** and **54**. If the cyclopentadienyl rings are significantly tilted the basicity of the iron atom would be expected to be higher and thus protonation at the iron centre would be accelerated,⁶² preventing cyclodehydrogenation. In addition it has been shown that there is a correlation between the degree of tilt of the ferrocene cyclopentadienyl rings and the wavelength of the ferrocenyl absorption band which is normally around $\lambda_{\text{max}} = 450 \text{ nm}$.

Compound	Cyclopentadienyl ring tilt angle (°)	Low energy ferrocenyl d-d transition (nm)
43	7	479
52	9	474
53	4	482
54	2	490

Table 8: The cyclopentadienyl ring tilt angles in compounds **43**, **52**, **53** and **54**.

The ferrocenyl absorptions of compounds **43**, **52**, **53** and **54** are at λ 479, 474, 482 and 490 nm respectively, which implies that the cyclopentadienyl rings are indeed significantly tilted, which is proven by the tilt angles 7°, 9°, 4°, and 2° respectively (Table 8). It would be expected that **54**, with a ferrocenyl transition at λ 490 nm and its large bulky fluoranthene platforms on both cyclopentadienyl rings of the ferrocene moiety would have the largest tilt angle. As can be seen in Table 8 this is not the case. In fact **54** has the smallest tilt angle at 2°. This may be explained by considering the differences in solution and in the solid state of **54**.

There is a correlation between the degree of tilt of the ferrocene cyclopentadienyl rings and the wavelength of the ferrocenyl absorption band,⁶² and therefore in solution **54** is the most tilted due to the large bulky groups on both cyclopentadienyl rings of the ferrocene which is manifested by the ferrocenyl absorption appearing at λ 490

nm. However in the solid state compounds **53** and **54** show CH... π interactions which help keep the cyclopentadienyl rings reasonably parallel, as shown in Figure 40.

The hydrogen shown in Figure 40 (a) on ring **D** has two CH... π interactions, one with ring **F** (2.86 Å) and one with ring **E** (2.94 Å) of the fluoranthene platform.

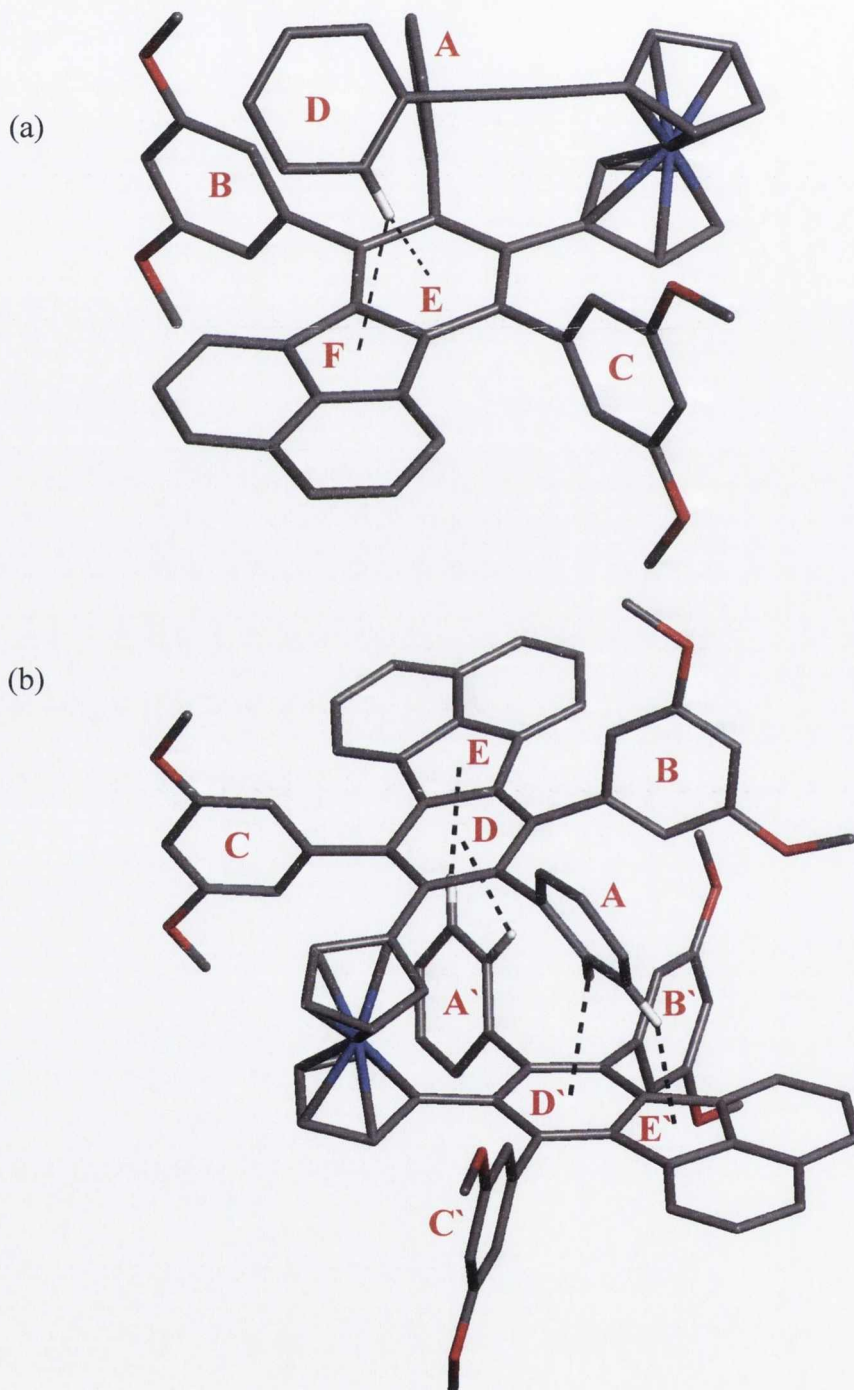


Figure 40: The X-ray crystal structures of (a) **53** and (b) **54**, highlighting the CH... π interactions. Only the hydrogens involved in the CH... π interactions are shown, other protons and solvent molecules are omitted for clarity.

In compound **54** there are four CH... π interactions which explains why the tilt angle is less than for **53** even though **54** has a bulky fluoranthene platform on each cyclopentadienyl ring. The *ortho* proton on phenyl ring **A** shown in Figure 40 (b) has a CH... π interaction with ring **D'** (2.81 Å) whereas the *meta* proton has a CH... π interaction with ring **E'** (3.10 Å) of the fluoranthene platform. This is also mirrored with phenyl ring **A'** where the *ortho* proton has a CH... π interaction with ring **D** (2.90 Å) and the *meta* proton has a CH... π interaction with ring **E** (3.0 Å) of the fluoranthene platform.

Therefore although in the solid state the cyclopentadienyl rings of **53** and **54** are not highly tilted, the UV-visible data implies that the tilt angles increase in solution, especially in the case of compound **54**. The small tilt angle in the solid state is a feature of the CH... π interactions, however in solution there is free rotation and these CH... π interactions are of reduced consequence. The crystallographic data for all four compounds are given in the Annex.

2.2.9. Electrochemistry

Ferrocene/ferrocenium itself represents a strictly reversible one-electron redox couple.⁴⁷ In the case of some ferrocenium derivatives however, reversibility may be significantly lowered by a subsequent decomposition of the electrogenerated ferrocenium species. The ferrocene substituent may also be regarded as a redox active probe on a molecular level, since following the ferrocene/ferrocenium redox potentials offers a unique opportunity to detect alterations in the electronic structure of the ferrocene derived molecules, as well as in the nature of the metal- π -ligand bonding. This provides information about the changes of electron density distribution and HOMO energies in a series of related compounds.³⁴

The following section compares the electrochemistry of compounds **43**, **52**, **53** and **54** by cyclic voltammetry (CV) in dichloromethane (0.1 M (TBA)PF₆ as electrolyte). Under the applied experimental conditions, all compounds studied exhibit a fully reversible one-electron oxidation attributable to the ferrocene/ferrocenium couple.

The relevant electrochemical data for the studied compounds, in dichloromethane, are shown in Table 9.

Compound	E° (V)
Fc	0.51
43	0.46
52	0.47
53	0.50
54	0.45

Table 9: Electrochemical data for complexes **43**, **52**, **53** and **54**, measured against ferrocene. Supporting electrolyte: (TBA)PF₆ (0.1 M) in CH₂Cl₂; platinum working electrode, platinum wire auxiliary electrode, Ag/AgCl reference electrode, 100 mV s⁻¹ scan rate, measured for 1 mmol solutions.

All potentials are quoted together with the [Fc/Fc⁺] couple, which had a potential of 0.51 V vs the Ag/AgCl reference electrode used for this work. Although all the ferrocenyl compounds show a reversible one-electron oxidation, it is noteworthy that the redox potentials of the ferrocene units for compounds **43**, **52**, **53** and **54** all lie within the range E° 0.45 to 0.50 V, which is very similar to that for the ferrocene standard (0.51 V), indicating that the ferrocene environments in these compounds have not been greatly altered by substitution with fluoranthene platforms.

Although all ferrocenyl compounds show reversible one-electron oxidation, it is interesting to note that the redox potentials of the ferrocene units do not show a broad range of values, as was the case with the ferrocenyl polyphenylene compounds in chapter 1. The ligand offers electron density to the iron atom, while the iron atom feeds electron density back to the ligand simultaneously. The net result of the two synergic interactions and the E° of the resulting Fc/Fc⁺ couple is therefore dependent on the substitution of the ligand. Since the fluoranthene moiety is common in all the compounds studied in this chapter it is intuitive that they all have similar redox potentials. In chapter 1 compound **41** showed an anodic shift (of 140 mV) as compared to ferrocene which was attributed to the electron-withdrawing effect of the fully cyclised polyaromatic substituent, which is bound to the ferrocene moiety *via* the acetylene linker. This makes the oxidation of the ferrocene unit in **41** thermodynamically more difficult than all the other compounds shown.

Compounds **43**, **52**, **53** and **54** on the other hand show a very slight cathodic shift compared to ferrocene, with **43**, **52** and **54** with the lowest redox potentials (0.46, 0.47 and 0.45 V) respectively. Compound **53** shows the highest redox potential of the four compounds under investigation in this chapter, at 0.50 V. This could be attributed to the conjugation that exists between the ferrocene moiety and the phenyl ring *via* the acetylene linker. The conjugation between the ferrocene and the phenyl group *via* the acetylene linker has a slight electron-withdrawing effect which makes the oxidation of the ferrocene unit in **53** thermodynamically more difficult than the other compounds shown in Table 9. This effect is only significant when comparing these four compounds, obviously the electron withdrawing effect in **53** is very slight compared to that exerted by the PAH in compound **41** which is reflected by the 150 mV difference in potential between the two compounds.³⁴

2.3. Summary

In this chapter it has been shown that by careful modification of known synthetic routes four novel ferrocene containing fluoranthene derivatives have been synthesised. All the compounds have been comprehensively characterised by ^1H and ^{13}C NMR spectroscopy, UV-vis spectroscopy and mass spectrometry. The redox chemistry of these ferrocenyl containing fluoranthene derivatives has also been investigated by cyclic voltammetry and the molecular structures of all four compounds **43**, **52**, **53** and **54** have been elucidated by single-crystal X-ray analysis.

Compounds **43**, **52**, **53** and **54** were all synthesised in good yields *via* the Diels-Alder [2+4]-cycloaddition reaction from appropriate starting materials. Also reported was the attempted cyclodehydrogenation of compounds **43**, **52**, **53** and **54**. Although unsuccessful, there is a large potential for these types of compounds and there are alternative synthetic routes that could be employed in order to synthesise extended PAH systems with ferrocene moieties on the periphery. These possible alternative synthetic routes will be discussed in the future work section.

UV-visible absorption studies provided evidence for why cyclodehydrogenation was unsuccessful. Compounds **43**, **52**, **53** and **54** were shown from their low energy ferrocenyl absorption wavelengths at λ 479, 474, 482 and 490 nm respectively, to contain very tilted cyclopentadienyl rings within the ferrocene moiety explaining why these four compounds decomposed during attempted cyclodehydrogenation reactions. Comparison of the X-ray data for compounds **43**, **52**, **53** and **54** supports this theory since their tilt angles are 7° , 9° , 4° and 2° respectively, which is in agreement with other ferrocenyl derivatives synthesised within the group.

The absorption spectra of the fluoranthene region for compounds **43**, **52**, **53** and **54** all show the characteristic three bands that are also observed in fluoranthene. In all four compounds the $S_0 \rightarrow S_4$, $S_0 \rightarrow S_3$ and $S_0 \rightarrow S_2$ transitions were assigned in complete agreement with the results obtained for fluoranthene in the gas phase by other groups.^{87, 88}

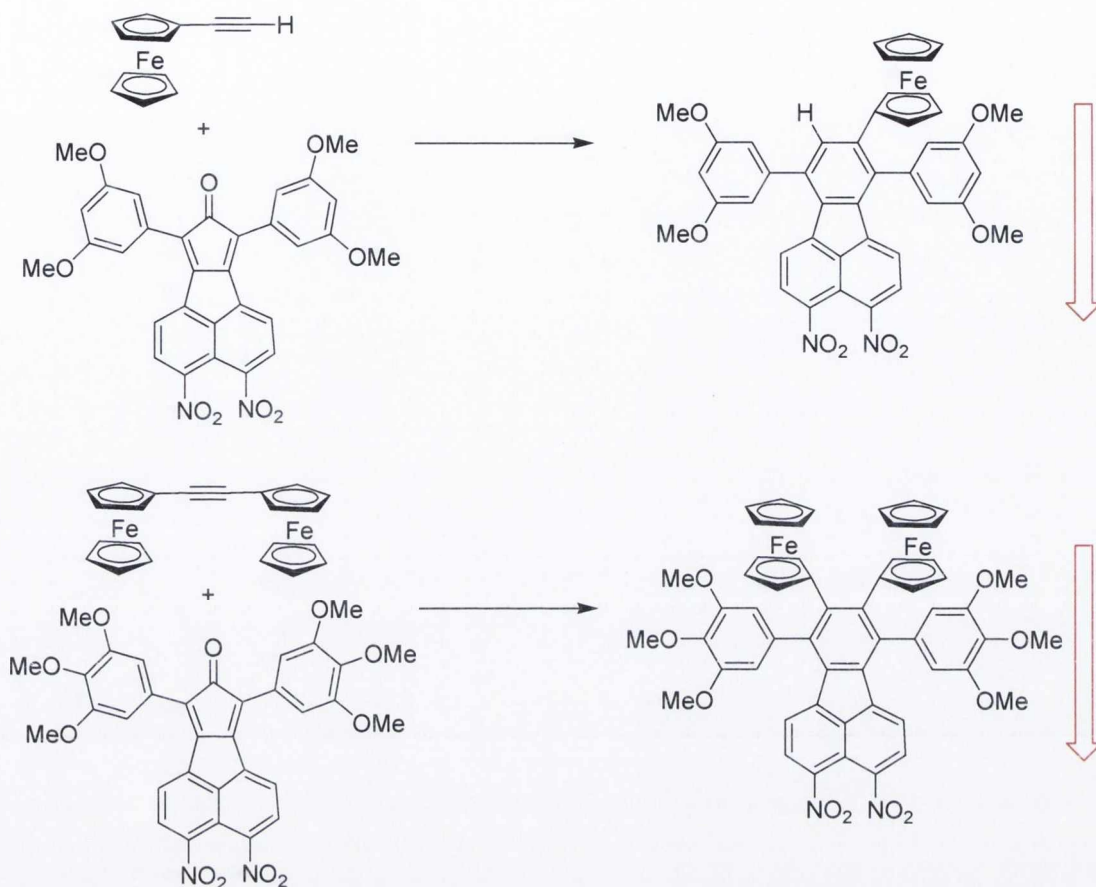
All of the compounds exhibited the one-electron reversible oxidation wave associated with the ferrocene/ferrocenium couple in electrochemical experiments. The E^0 value was influenced to a small degree by the electronic effects of the substituent. Compounds **43**, **52**, **53** and **54** all show a very slight cathodic shift when compared to ferrocene. Compound **53** showed the highest redox potential of the four compounds which could be attributed to the conjugation that exists between the ferrocene moiety and the phenyl ring *via* the acetylene linker. This conjugation has a slight electron-withdrawing effect which makes the oxidation of the ferrocene unit in **53** thermodynamically more difficult than for the other compounds.

2.4. Future Work

Within this chapter the synthesis of compounds **43**, **52**, **53** and **54** along with their thorough characterisation was reported. The unsuccessful attempts at cyclodehydrogenation was a disappointment, but after further studies on the compounds some of the uncyclised compounds could have some interesting NLO properties in their own right. Compounds **43**, **52** and **53** could have potential NLO properties, but **54** is unlikely to be a good candidate for NLO applications since it has a centre of symmetry and thus no dipole-moment which is essential if a compound is to have desirable NLO properties.

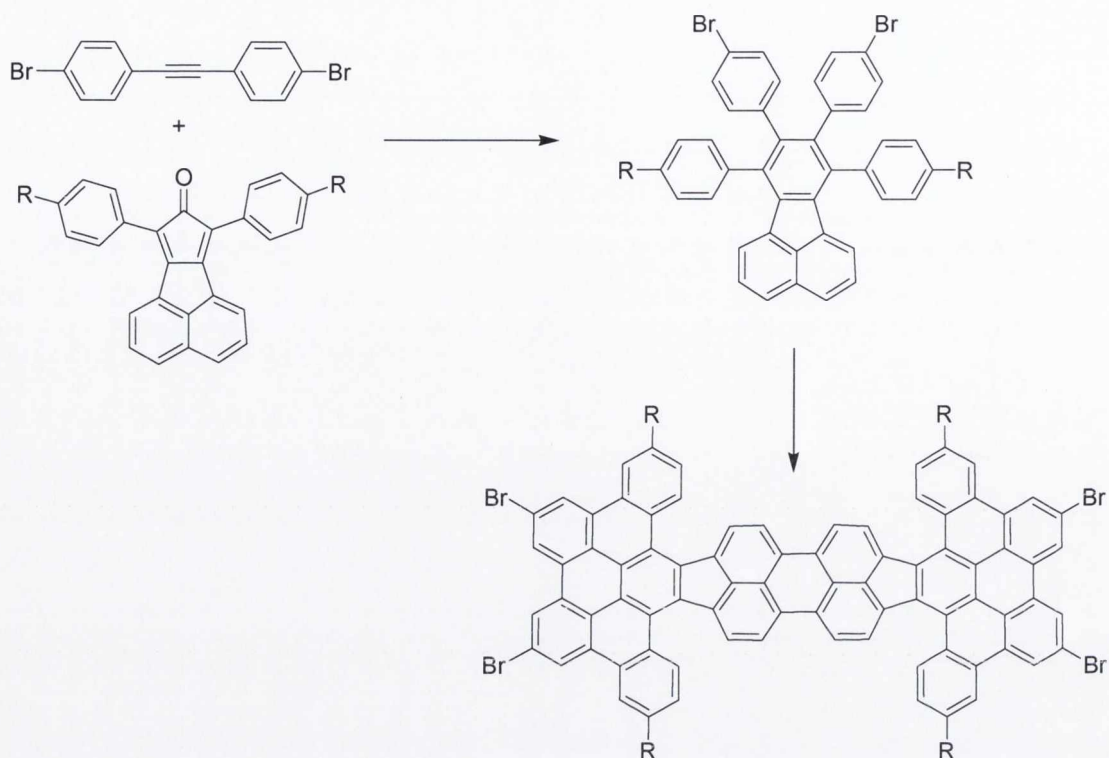
The NLO properties of compounds **43**, **52** and **53** have yet to be investigated but are underway in collaboration with Isabelle Ledoux at the Laboratoire de Photonique Quantique et Moléculaire at Cachan. These compounds are not considered to be as good candidates as compound **41** (in chapter 1) since there is limited conjugation between the ferrocene moiety and the fluoranthene platform. Conjugated organometallic systems that contain electronically coupled photo- and/or redox-active sites across an unsaturated organic bridge are of considerable interest at the moment. Although these compounds do not have an unsaturated organic bridge, as **41** does, they still possess an electron donating ferrocene moiety and a delocalised fluoranthene platform so would be expected to have some desirable NLO properties.

If the NLO results for **43** and **52** prove to be promising there are other compounds that could be synthesised following the same synthetic methodology that could lead to compounds with even better NLO properties. One possible idea is shown in Scheme 38, where by two nitro groups are inserted on the fluoranthene fragment early in the synthesis. The insertion of the nitro groups should lead to an increase in the “push-and-pull” characteristics within the molecule, thus yielding a larger dipole moment which in turn should give rise to enhanced NLO output.



Scheme 38: Possible synthetic routes towards nitro analogues of compounds **43** and **52**, with enhanced “push-and-pull” characteristics.

Although cyclodehydrogenation of the ferrocenyl containing fluoranthene compounds proved unsuccessful, the same methodology as employed in chapter 1 could be employed here. That is, to synthesise a halogenated fully cyclised PAH and then incorporate the bridged ferrocene moieties *via* a suitable coupling reaction. In Scheme 39 a possible route towards a fully cyclised halogenated PAH based on the intra- and inter-molecular cyclodehydrogenation of the fluoranthene sub-unit is shown. The synthesis of the dibromo-phenyl acetylene is well established and can be readily synthesised in one-pot,⁸⁹ yielding the fluoranthene based compound shown in Scheme 39. This then would be expected to undergo both intra- and inter-molecular cyclodehydrogenation since there are no ferrocenes present and all-carbon systems have been shown to cyclise fully. Halogens substituents as shown in chapter 1 and in work by Müllen *et al.* do not hinder the cyclisation step.^{28, 30}



Scheme 39: Possible synthetic route towards a halogenated fully cyclised PAH, based on the fluoranthene sub-unit.

With the fully cyclised halogenated system synthesised the bridged ferrocene moieties could then be inserted onto the periphery of the system *via* a four fold Sonogashira coupling reaction, similar to that undertaken in chapter 1, yielding the compound shown in Figure 41.

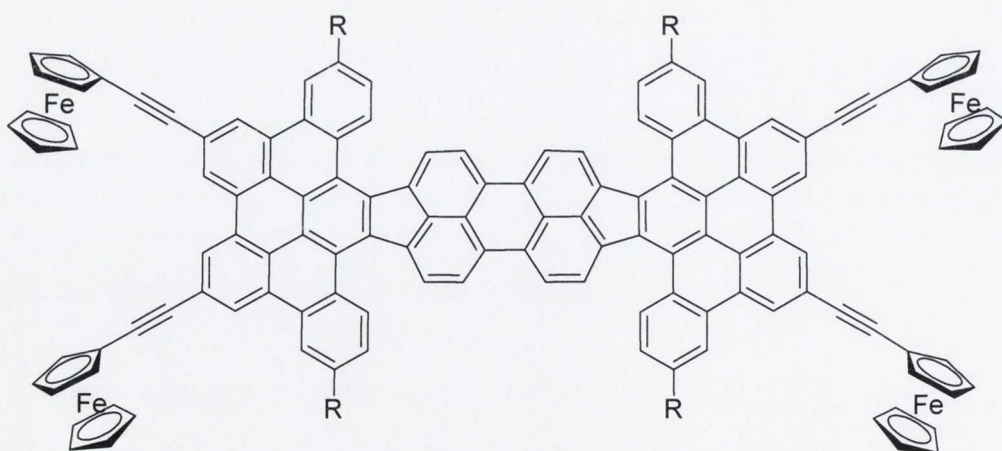


Figure 41: Possible example of an extended PAH with conjugated ferrocenes on its periphery.

The compound shown in Figure 41 would be expected to have interesting photophysical properties due to the size of the π -system and the fact that it has four ferrocenes fully conjugated to the PAH platform *via* the acetylene linkers. However it is not expected to have any NLO properties since the molecule has a centre of symmetry.

Chapter 3: Synthesis of the Long-Chain Tetra- Dodecyl Nitrogen-Heterosuperbenzene

3.1. Introduction

3.1.1. Discotic Liquid Crystals

The discovery of liquid crystals (LCs) in 1888 was a historic event and scientific milestone.⁹⁰ Liquid crystalline materials are divided into two categories, thermotropic and lyotropic. When a substance passes between the solid, liquid crystal and liquid state and *vice versa* as a function of temperature and in the absence of a solvent, the liquid crystalline phase are classified as thermotropic, while lyotropic phases form in the presence of a suitable solvent. As a result lyotropic mesophases, found abundantly in biological systems, are always mixtures, whereas thermotropic LCs can be a single component or a mixture.

Thermotropic liquid crystals can be distinguished with respect to the molecular shape of the constituent molecules. The majority of pure compounds exhibiting thermotropic mesophases have one distinctive feature in common: the rod-like shape of their molecules. The term “calamitic” has been used to describe liquid crystals of rod-shaped molecules, in order to distinguish them from discotic liquid crystals, which are composed of disk-like molecules. The hierarchical self-assembly of disc-shaped molecules leads to the formation of discotic liquid crystals. Most discotic liquid crystals exhibit only one type of mesophase but a few examples with polymorphism are also known. Discotic mesophases formed by disc-shaped molecules are primarily classified into three types: (1) nematic, (2) columnar and (3) lamellar.

3.1.2. Nematic Phases

The nematic phase of disc-shaped molecules can be sub-divided into three types, namely, (a) nematic discotic, (b) chiral nematic, and (c) nematic columnar, and all are presented in Figure 42.

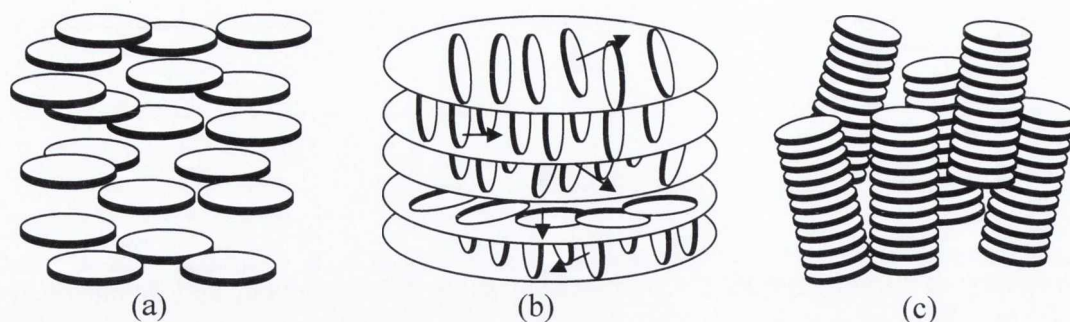


Figure 42: Schematic representation of (a) nematic discotic, (b) chiral (helical) and (c) nematic columnar phase.

In the nematic discotic phase the molecules stay more or less parallel to each other, having orientation order but no long range positional order (Figure 42 (a)). The helical structure of chiral discotic nematic phase can be seen in Figure 42 (b). The molecules have positional ordering in a layered structure with the molecules tilted by a finite angle with respect to the layer normal. Chiral discotic mesophases occur in mixtures of discotic nematic and mesophoric or non-mesomorphic chiral dopants, as well as in pure chiral discotic molecules.^{91, 92} The nematic columnar phase is characterised by a columnar stacking of molecules, however it is worth noting that they do not form two-dimensional lattice structures. They display a positional short range order and an orientational long range order as shown in Figure 42 (c).

3.1.3. Columnar and Lamellar Phases

In columnar mesophases, the molecules assemble themselves one on top of the other in columns which in contrast to nematic columnar phases, do have a two-dimensional lattice. As shown in Figure 43 columnar mesophases may be classified into five classes: (a) hexagonal columnar phase, (b) rectangular columnar, (c) columnar oblique phase, (d) columnar plastic phase (e) columnar helical phase, (f) lamellar phase.

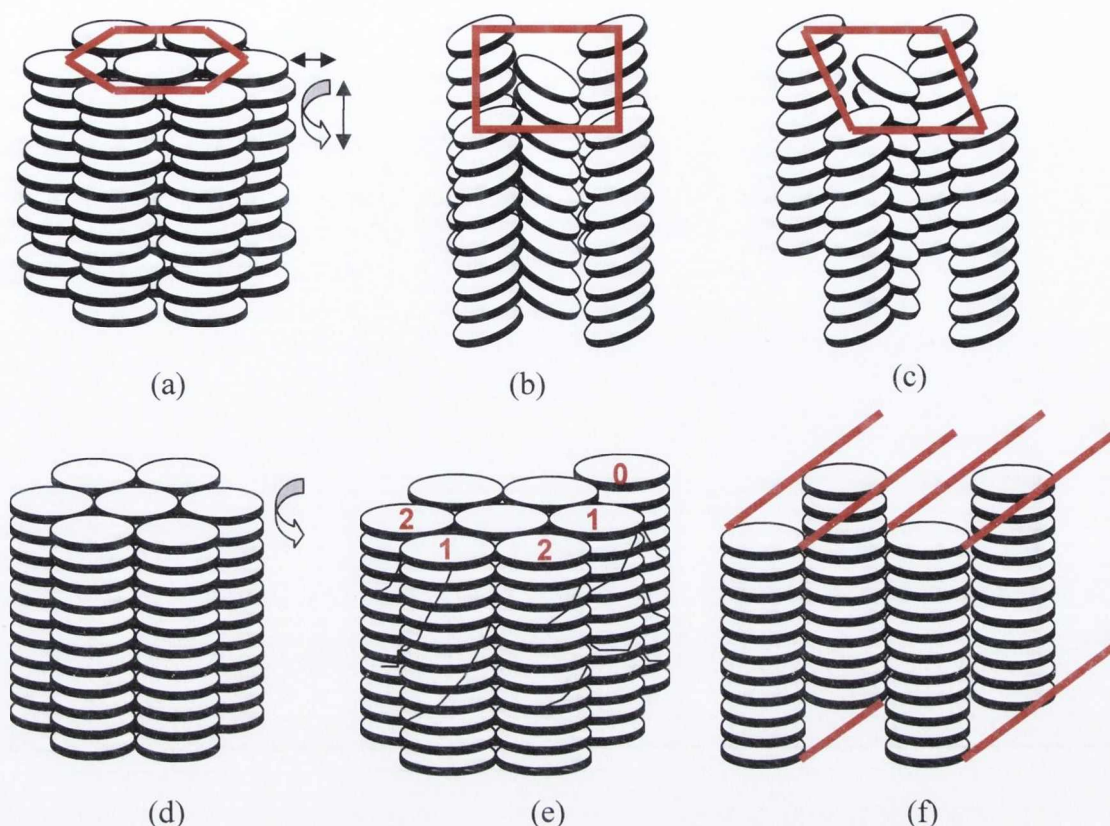


Figure 43: Schematic representation of (a) hexagonal columnar phase, (b) rectangular columnar phase, (c) columnar oblique phase, (d) columnar plastic phase, (e) helical phase and (f) columnar lamellar.

A columnar hexagonal phase is characterised by a hexagonal packing of the molecular columns. The columnar rectangular mesophase consists of the stacking of the aromatic cores of the molecules in columns and packed in a rectangular fashion. In the columnar oblique mesophase the columns are arranged with an oblique unit cell. The columnar plastic phase has been discovered only recently in discotic liquid crystals. The phase is characterised by three-dimensional crystal-like order in a hexagonal lattice, while the discs within the columns are able to rotate about the column axis. In the columnar plastic phase structural disorders such as non-parallel arrangements of the discs, longitudinal and lateral displacements and rotation around the columnar axis occur, although the motional freedom of the discs is restricted. The columnar helical phase has been demonstrated for hexahexylthiotriphenylene. The helical period is incommensurate, (that is the helical spacing is unlike that in neighbouring columns), with the intercolumnar spacing. As well as this it has been shown that a three-column superlattice develops, associated with both the helical phase and the vertical displacement of three columns.

A lamellar phase shown in Figure 43 (f) is a layered structure known to exist for mesophases of certain discotic compounds, e.g. bis(*p*-*n*-decylbenzoyl)methanato copper (II) and some perylene derivatives.

3.1.4. Discotic Conducting Materials

Over the past decade pulse-radiolysis time-resolved microwave conductivity technique (PR-TRMC) has been employed to measure the charge mobilities of a number of molecules which form columnar hexagonal mesophases (D_h) in which the macrocyclic cores are orthogonally stacked with respect to the columnar axis. The individual molecules differ in the nature of their central core and the type of peripherally substituted alkyl chains. Six different cores have been investigated by Warman *et al.*⁹³ and their structures are shown in Figure 44.

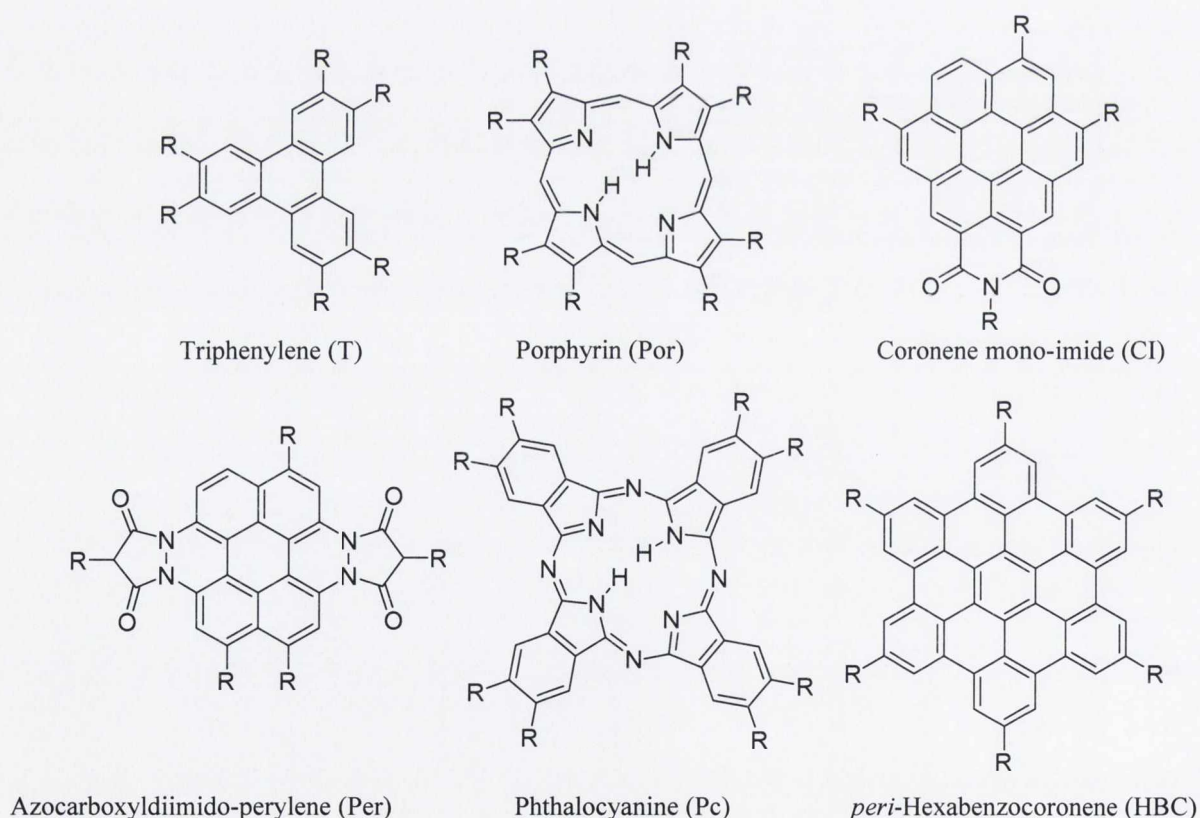


Figure 44: Macrocycles forming the cores of some studied discotic liquid crystals where *R* denotes mesogenic alkyl chains.⁹³

General information on the charge transport and mesomorphic properties corresponding to each core is given in Table 10.

Core	Core Size	Number of compounds	$\Sigma\mu_{1D}$ (cm ² V ⁻¹ s ⁻¹)		Average phase transition temperature (°C)	
			D _h phase	K phase	K→D _h	D _h →I
T	18	5	0.002-0.025	0.26	70	100
Por	24	5	0.060-0.081	0.27	96	135
CI	29	1	0.240	0.24	113	161
Per	34	3	0.150-0.210	0.24	53	>200
Pc	40	16	0.042-0.270	0.67	97	ca. 300
HBC	42	3	0.260-0.380	1.13	112	>400

Table 10: The intra-columnar charge mobilities ($\Sigma\mu_{1D}$) determined for a given macrocyclic core in a hexagonal columnar mesophase (D_h) and the crystalline solid phase (K) at temperatures just above and below K→D_h transition temperature, respectively. Also listed are the average phase transition temperatures for entering the liquid crystalline phase (K→D_h) and the isotropic liquid (D_h→I).⁹³

3.1.5. HBC Discotic Materials

As can be seen in Table 10, HBC based materials have the best charge carrying properties. They have been shown to form hexagonal columnar mesophases such as the one shown in Figure 45. They form these columnar arrangements due to intense π - π interactions between the polyaromatic cores. The core-core separation in a columnar mesophase is usually of the order 3.5 Å, so there is considerable overlap of π -orbitals. These π - π interactions are caused by intermolecular overlapping of p-orbitals in π -conjugated systems, so they become stronger as the number of π -electrons increase. The intercolumnar distance is usually 20-40 Å, depending on the lateral chain length of the long alkyl aliphatic chains that surround the core.^{94, 95} Therefore, the interactions between neighbouring molecules in the same column are stronger than the interactions between neighbouring molecules in different columns. Consequently the quasi-one-dimensional charge migration in these materials is expected and indeed observed.

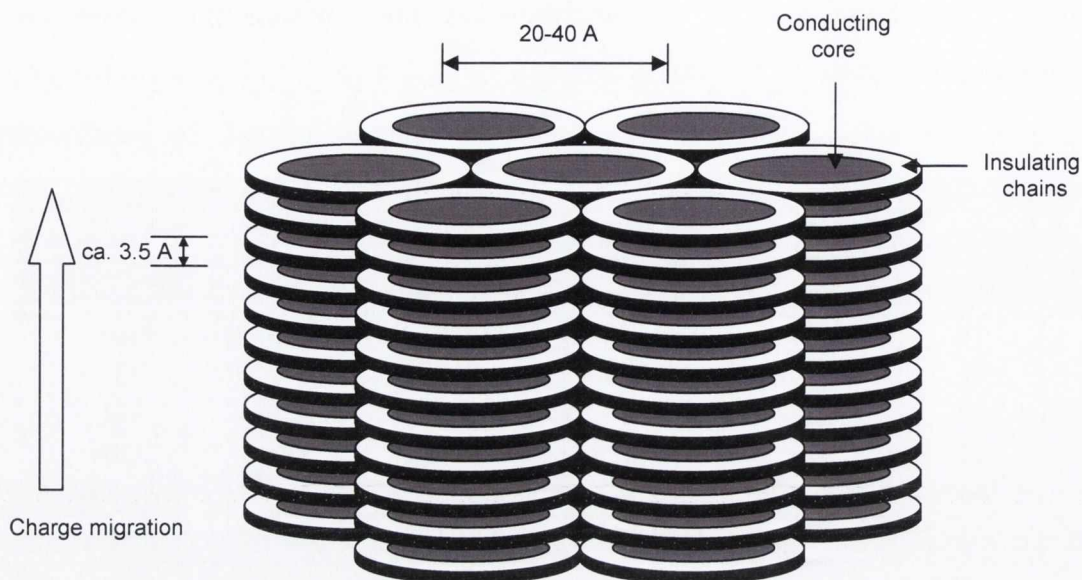


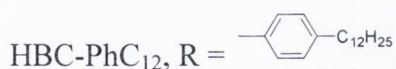
Figure 45: Schematic representation of the formation of a hexagonal columnar mesophase formed by the stacking of HBC cores with peripheral alkyl chains.

Although all-carbon HBCs have been shown to have excellent charge carrying properties, the charge mobility can vary greatly depending on the peripheral R groups incorporated onto the core. The R groups are essential in insulating the conducting cores from each other since they reduce inter-columnar conductivity losses and promote efficient intramolecular close-packing. Table 11 highlights three specific examples of all-carbon HBCs with desirable mesomorphic properties which illustrates the consequences of altering the length and shape of the peripheral R groups on charge mobility.

Ref.	Phase transition temperature (°C) [heating/cooling]	Assignment	Temperature (°C)	Phase	$\Sigma\mu_{1D}$ ($\text{cm}^2 \text{V}^{-1} \text{s}^{-1}$)
HBC-C ₁₂	42/[a]	K ₁ →K ₂	98	K ₂	0.96
	105/86	K ₂ ↔D _h	110	D _h	0.38
HBC-C ₁₄	52/[a]	K ₁ →K ₂	98	K ₂	1.13
	109/88	K ₂ ↔D _h	116	D _h	0.31
HBC-PhC ₁₂	18/0.6	D ₁ ↔D ₂	-78	D ₁	0.17
	83/72	D ₂ ↔D ₃	22	D ₂	0.22
			192	D ₃	0.46

[a] not determined.⁹⁶

Table 11: Phase transition temperatures and structural assignments of three alkylated HBC compounds as measured on a first heating and subsequent cooling run.



The mobility values for the liquid-crystalline phases of the above compounds are the highest found in discotic materials, and are well in excess of the value *ca.* $0.1 \text{ cm}^2 \text{ V}^{-1} \text{ s}^{-1}$ found by PR-TRMC for the D_h of hexakis-triphenylene, the previous record holder.^{75, 97} The values in the crystalline phase are in fact comparable with the room-temperature mobilities determined for single crystals of aromatic compounds⁹⁸ and approach the value of *ca.* $3 \text{ cm}^2 \text{ V}^{-1} \text{ s}^{-1}$ found for the inter-sheet mobility in graphite.⁹⁹ As well as their excellent charge mobility one compound, namely HBC-PhC₁₂, is liquid-crystalline at all temperatures studied. The compound is malleable at room temperature and can be readily compressed by hand to a density of 0.95 g cm^{-3} . This value is considerably higher than can be achieved with polycrystalline solids. In addition the high solubility of this compound in organic solvents means that it can be readily spin-coated and therefore an attractive proposition for device applications.

For opto-electronic applications the ability of planar graphenes to self-assemble by π -stacking into highly-ordered structures has attracted attention in such varied fields as field-effect transistors,¹⁰⁰ photovoltaic cells¹⁰¹ and molecular electronic devices.¹⁰² Judicious alkyl substitutions, as touched upon already have resulted in discotic liquid crystalline behaviour over a large temperature range.⁹⁶ Structural features such as these, that give rise to high charge carrier mobilities and liquid-crystalline mesophases over an extensive temperature range, are highly desirable. The former ultimately controls the switching speed and current density/light intensity obtainable and the latter the applicability of a future device. In addition the ordered soft states of discotic liquid crystals offer the molecular control of film morphology and the potential for self-healing. Some lucrative end-products based on liquid crystals are on the market e.g. in the production of optical compensating films.¹⁰³ The latter involving a photopolymerisable discotic are used to increase the angle of view on most modern LCDs. The field is progressing rapidly and many authors predict that ‘electronics

based on organic thin-film materials will soon become the mainstay of our technological existence'.¹⁰⁴

3.1.6. N-doped HBCs

In this work it was hoped that an investigation into N-doped long chain HBCs would yield compounds with a range of superior and desirable properties in terms of their versatility, solubility and photoluminescence. The number and position of the N-atoms would be under synthetic control and offer a means of tuning their electron-accepting character. Enhanced solubility would aid processibility and ultimately thin film formation and blending, and their considerable fluorescence would give an additional spectroscopic handle for the study of solvent-interaction and aggregation.

One member of the N-doped HBC family, known as nitrogen-heterosuperbenzene (N-HSB) is shown in Figure 46, and had been studied in great detail in the group.¹⁴

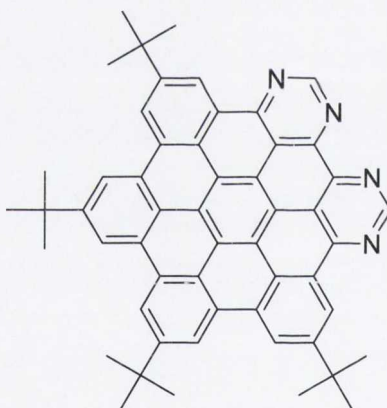


Figure 46: Structure of the first N-doped HBC, N-heterosuperbenzene(N-HSB).

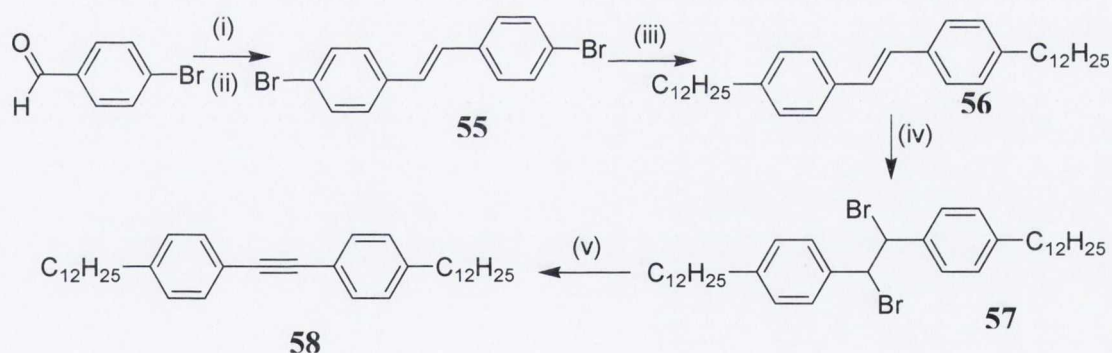
However the solubilising *tert*-butyl groups on the periphery was felt likely to hinder the formation of a discotic liquid crystalline material. Although N-HSB had been shown to stack in a columnar fashion in solution it is a micro-crystalline solid and does not undergo a phase transition from the K phase to the D_h phase. N-HSB molecules stack in a columnar fashion in solution but the inter-planar distance is too great (due to the *tert*-butyl groups) to facilitate the formation of a discotic liquid crystalline material. However in the solid phase N-HSB molecules have been shown to arrange themselves in a helical arrangement of the polar discs,¹⁶ as shown in Figure 47.

3.2. Results and Discussion

3.2.1. Synthesis of hexa(4-dodecylphenyl)benzene (**60**)

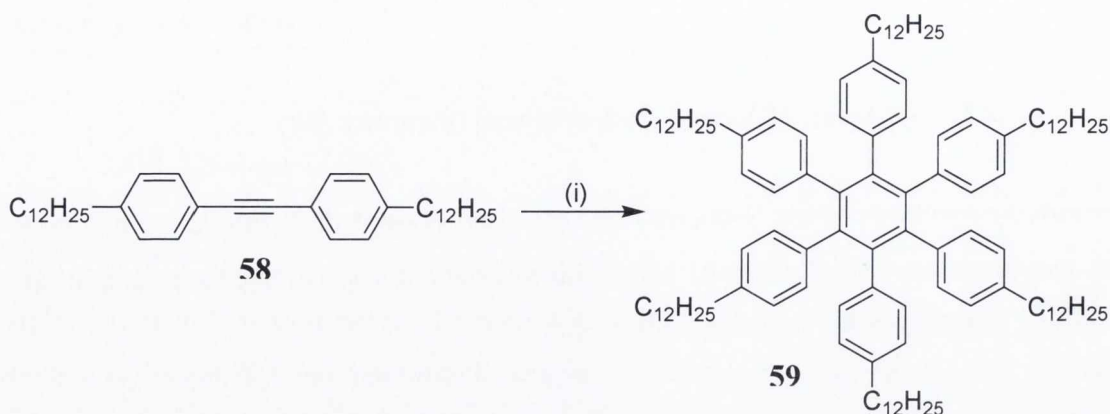
Before the synthesis of the N-doped HBC could be attempted, its all-carbon analogue **60** was prepared. This would be beneficial to establish the key synthetic conditions and as a comparator for future measurements.

The synthesis of 4,4'-didodecyldiphenylacetylene (**58**) can be seen in Scheme 40. *Trans*-4,4'-dibromostilbene (**55**) was prepared *via* the Mc.Murry synthesis, which involves the coupling of two molecules of 4-bromobenzaldehyde in the presence of zinc powder and titanium tetrachloride. The off-white solid **55** was synthesised in 82% yield. The long alkyl chains were introduced quantitatively by the Kumada coupling between **55** and the Grignard reagent, dodecylmagnesiumbromide with $\text{NiCl}_2(\text{dppp})$ as catalyst, yielding **56** as a waxy off-white solid. Bromination of the double bond using a quantitative amount of bromine in chloroform furnished **57** as a white crystalline solid, again in almost quantitative yield. The final step in the synthesis of **58** was the removal of two molecules of hydrogen bromide. This was achieved by refluxing **57** in *tert*-butanol in the presence of potassium *tert*-butanolate.



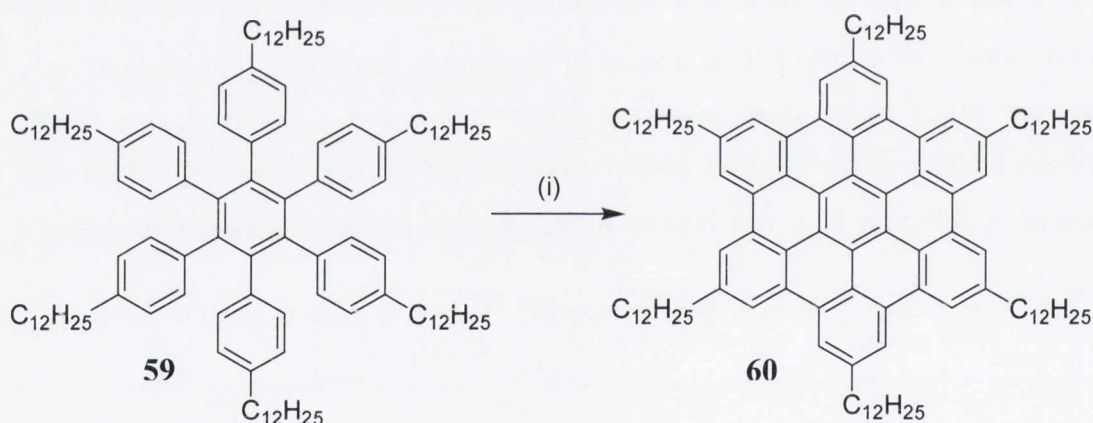
*Scheme 40: The synthetic route toward **58**. (i) Zn , TiCl_4 , THF , -10°C . (ii) 4-bromobenzaldehyde, THF , reflux, 5 h (82 %). (iii) dodecylmagnesiumbromide, $\text{NiCl}_2(\text{dppp})$, diethyl ether, RT, 18 h, (93 %). (iv) Br_2 , CHCl_3 , RT, 18 h (94 %). (v) potassium *tert*-butanolate, *t*-butanol reflux, 18 h (86 %).*

The uncyclised polyphenylene (**59**) was synthesised by the cyclotrimerisation of **58** with a catalytic amount of $\text{Co}_2(\text{CO})_8$ in refluxing dioxane yielding compound **59** in 68 % yield, as shown in Scheme 41.



*Scheme 41: The cyclotrimerisation of **58** yielding **59**. (i) $\text{Co}_2(\text{CO})_8$, dioxane, reflux, 20h (68 %).*

It was found that **59** upon cyclodehydrogenation using FeCl_3 (Scheme 42) gave **60**, in 64 % yield with no apparent destruction or damage to the long alkyl chains provided that a flow of argon is maintained through the reaction mixture during the entire reaction.



*Scheme 42: The synthesis of HBC **60**, via cyclodehydrogenation of the polyphenylene precursor **59**. (i) FeCl_3 , CH_3NO_2 , CH_2Cl_2 , RT, 2 h (64 %).¹⁵*

3.2.2. Synthesis of 1,2-dipyrimidyl-3,4,5,6-tetra(4-dodecylphenyl)benzene (**67**)

Once the conditions for cyclodehydrogenation had been optimised, attempts were then made to synthesise the N-doped analogues of **59** and **60**. This required the synthesis of a number of precursors that had to be synthesised in a systematic manner. The synthesis of the alkyl-substituted 1,2-diaryl-1,2-diketone **63** was accomplished using

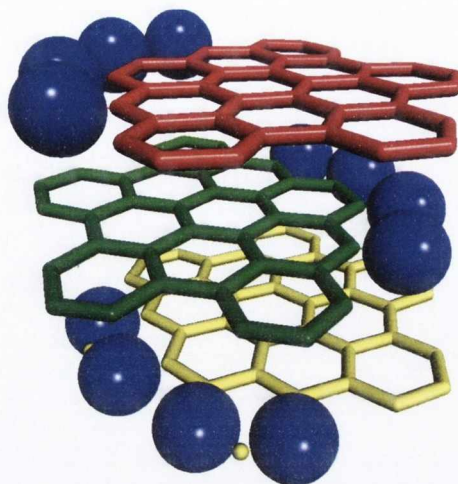


Figure 47: The synchrotron molecular structure of N-HSB showing, the helical arrangement of molecules (inter-plane distance 3.5Å).

In the following section the synthesis and investigation of a long chained analogue of N-HSB is detailed. As mentioned already coupling of bulky components into long chain alkyl units has been reported to improve mesomorphic and charge transport properties in discotic materials.¹⁰⁵ These desirable affects have been attributed to the restriction in the lateral and rotational motion of the central core and the concomitant increase in the barrier to conformational change and dynamic disorder. It is hoped that the permanent dipole induced by the asymmetric presence of N-atoms will assist in the anchoring of the aromatic rings within the columnar stacks, giving a head-to-tail or homeotropic intra-columnar arrangement with reduced rotational disorder. This might be expected to enhance electron mobility due to the shift in electron density from aromatic to pyrimidyl in the frontier orbitals.

Replacement of the *tert*-butyl groups with dodecyl alkyl chains it is hoped will result in a discotic liquid crystalline material mimicking the behaviour of HBC-PhC₁₂. The presence of the dodecyl chains is expected to yield a head-to-tail configuration (Figure 48) as opposed to the helical configuration observed for N-HSB (Figure 47).

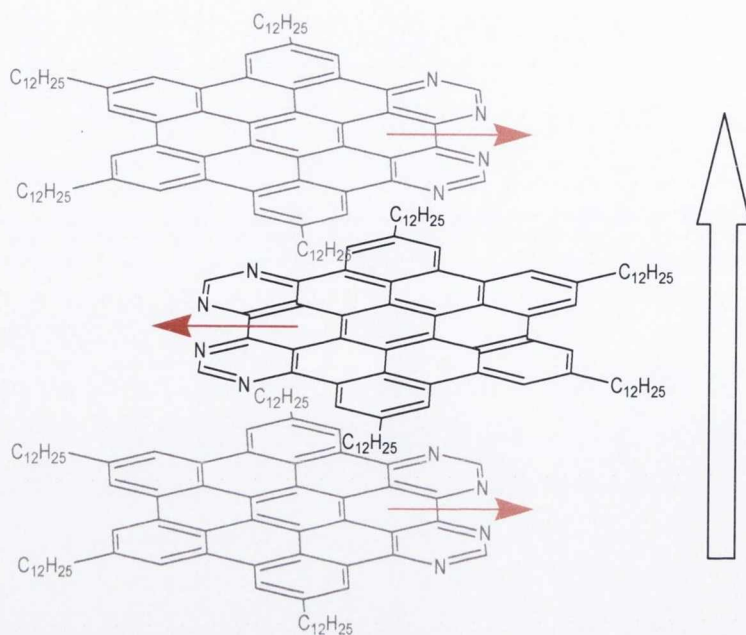


Figure 48: Dipole moment (red arrows) and a possible head-to-tail orientation within aggregates formed by self-association.

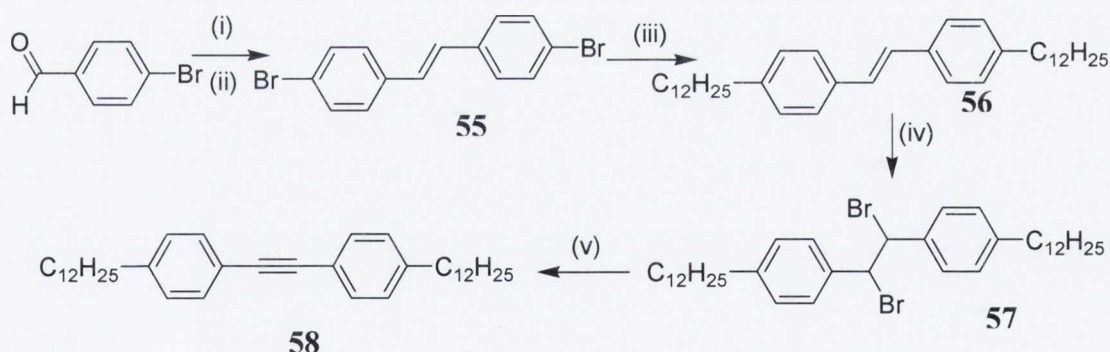
This work therefore presents the first successful synthesis of a long chain and nitrogen-containing PAH, **68**, and details its comprehensive characterisation including conductivity measurements and photophysical properties. To date **68** is the only heteroatom HBC core that has quantifiable charge carrier mobility.

3.2. Results and Discussion

3.2.1. Synthesis of hexa(4-dodecylphenyl)benzene (**60**)

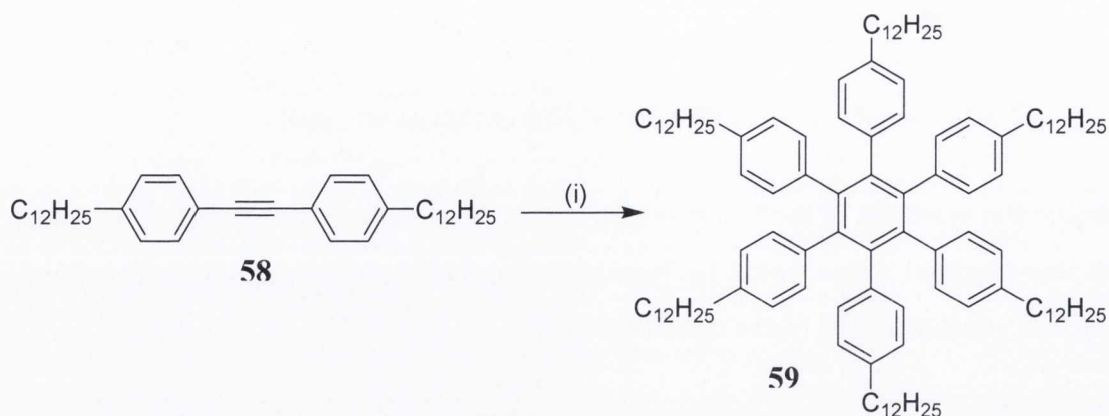
Before the synthesis of the N-doped HBC could be attempted, its all-carbon analogue **60** was prepared. This would be beneficial to establish the key synthetic conditions and as a comparator for future measurements.

The synthesis of 4,4'-didodecyldiphenylacetylene (**58**) can be seen in Scheme 40. *Trans*-4,4'-dibromostilbene (**55**) was prepared *via* the Mc.Murry synthesis, which involves the coupling of two molecules of 4-bromobenzaldehyde in the presence of zinc powder and titanium tetrachloride. The off-white solid **55** was synthesised in 82% yield. The long alkyl chains were introduced quantitatively by the Kumada coupling between **55** and the Grignard reagent, dodecylmagnesiumbromide with $\text{NiCl}_2(\text{dppp})$ as catalyst, yielding **56** as a waxy off-white solid. Bromination of the double bond using a quantitative amount of bromine in chloroform furnished **57** as a white crystalline solid, again in almost quantitative yield. The final step in the synthesis of **58** was the removal of two molecules of hydrogen bromide. This was achieved by refluxing **57** in *tert*-butanol in the presence of potassium *tert*-butanolate.



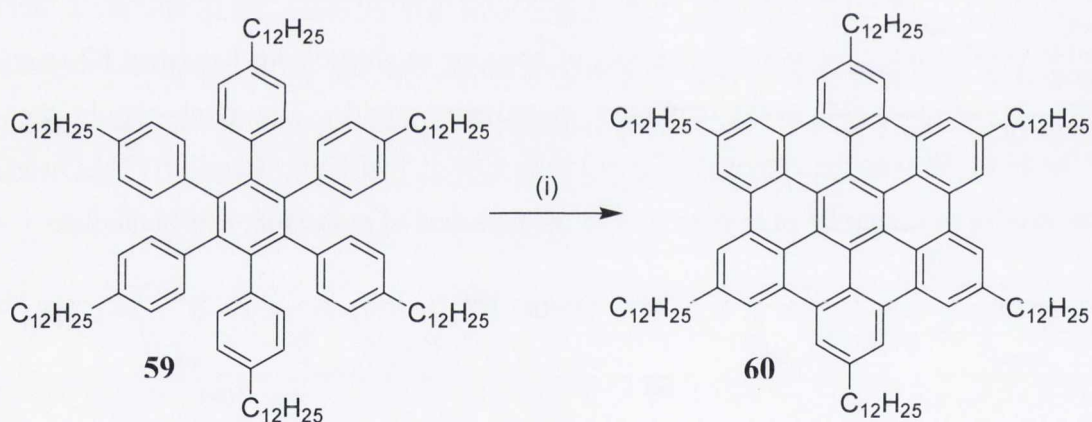
*Scheme 40: The synthetic route toward **58**. (i) Zn, TiCl_4 , THF, -10°C . (ii) 4-bromobenzaldehyde, THF, reflux, 5 h (82 %). (iii) dodecylmagnesiumbromide, $\text{NiCl}_2(\text{dppp})$, diethyl ether, RT, 18 h, (93 %). (iv) Br_2 , CHCl_3 , RT, 18 h (94 %). (v) potassium *tert*-butanolate, *t*-butanol reflux, 18 h (86 %).*

The uncyclised polyphenylene (**59**) was synthesised by the cyclotrimerisation of **58** with a catalytic amount of $\text{Co}_2(\text{CO})_8$ in refluxing dioxane yielding compound **59** in 68 % yield, as shown in Scheme 41.



*Scheme 41: The cyclotrimerisation of **58** yielding **59**. (i) $\text{Co}_2(\text{CO})_8$, dioxane, reflux, 20h (68 %).*

It was found that **59** upon cyclodehydrogenation using FeCl_3 (Scheme 42) gave **60**, in 64 % yield with no apparent destruction or damage to the long alkyl chains provided that a flow of argon is maintained through the reaction mixture during the entire reaction.

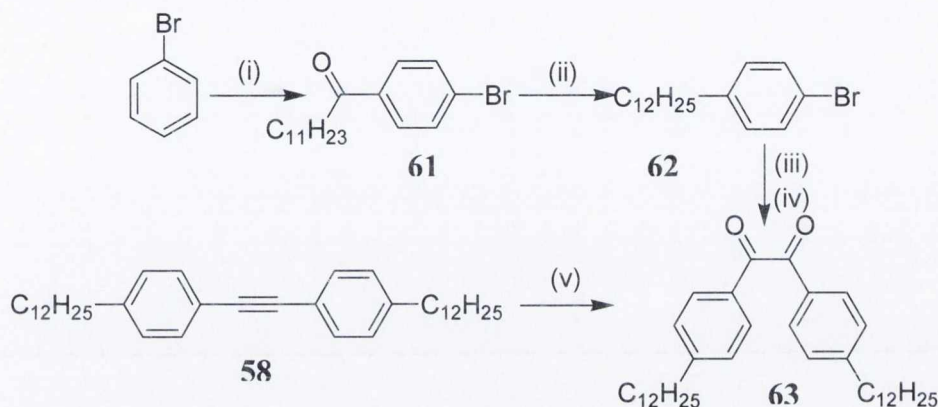


*Scheme 42: The synthesis of HBC **60**, via cyclodehydrogenation of the polyphenylene precursor **59**. (i) FeCl_3 , CH_3NO_2 , CH_2Cl_2 , RT, 2 h (64 %).¹⁵*

3.2.2. Synthesis of 1, 2-dipyrimidyl-3, 4, 5, 6-tetra(4-dodecylphenyl)benzene (**67**)

Once the conditions for cyclodehydrogenation had been optimised, attempts were then made to synthesise the N-doped analogues of **59** and **60**. This required the synthesis of a number of precursors that had to be synthesised in a systematic manner. The synthesis of the alkyl-substituted 1,2-diaryl-1,2-diketone **63** was accomplished using

two different methods. **Method A** (steps (i), (ii), (iii) and (iv) in Scheme 43) used the procedure of Muller-Westerhoff⁴² which includes lithiation of 4-bromododecylbenzene (**62**) with *n*-butyllithium in tetrahydrofuran and subsequent treatment with DMPD. **62** was readily synthesised by the Friedel-Crafts acylation of bromobenzene with dodecanoyl chloride (76%) followed by a Wolff-Kishner reduction of the resulting ketone (76 %). **Method B** (step (v) in Scheme 43) involved the oxidation of **58** with iodine in dimethylsulfoxide at 155 °C (74 %).²⁸



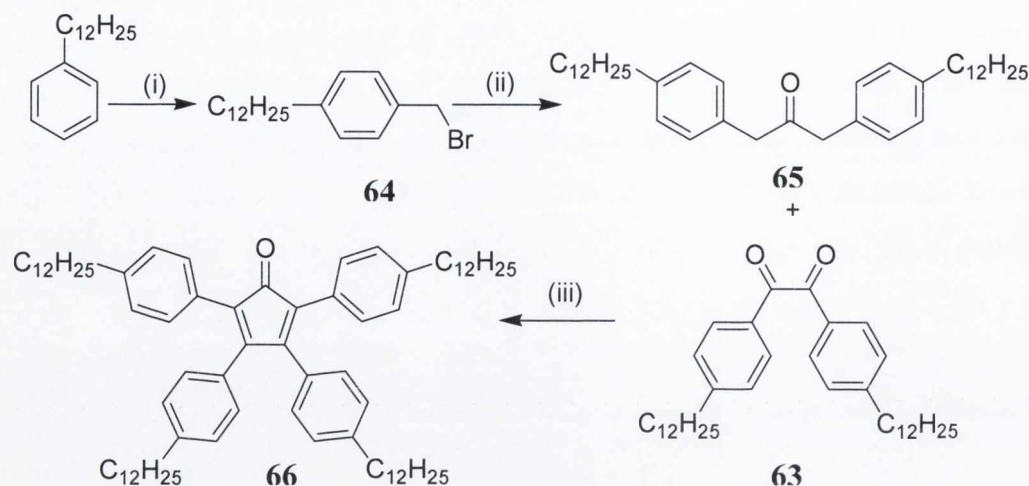
Scheme 43: The two possible routes for the synthesis of the 1,2-diaryl-1,2-diketone, **63**.

Method A: (i) dodecanoyl chloride, AlCl_3 , 50 °C, 1 h (76 %). (ii) hydrazine hydrate, KOH, triethylene glycol, reflux, 2 h (76 %). (iii) *n*-BuLi, THF, -78 °C, 90 min. (iv) DMPD, THF, -78 °C \rightarrow RT, 18 h (40 %). **Method B:** (v) I_2 , DMSO, 155 °C, 18 h (74 %).²⁸

The synthesis of the alkyl-substituted 1,3-diaryl-2-propanone **65** proved more problematic because it was dependent on the formation of dodecyl benzylbromide **64**. The latter which was synthesised by the reaction of dodecylbenzene with paraformaldehyde and hydrobromic acid in glacial acetic acid could only be formed in low yield. Even extending the reaction time to 4 days at 75 °C only yielded 14 % of **64** (extra time was shown to have no effect on the yield). To overcome the problem a large scale up was undertaken to ensure that enough **64** was synthesised for later synthetic steps. Scale up was possible since the precursors for **64** were commercially available and cheap, this avoided further optimisation of an unproductive reaction.

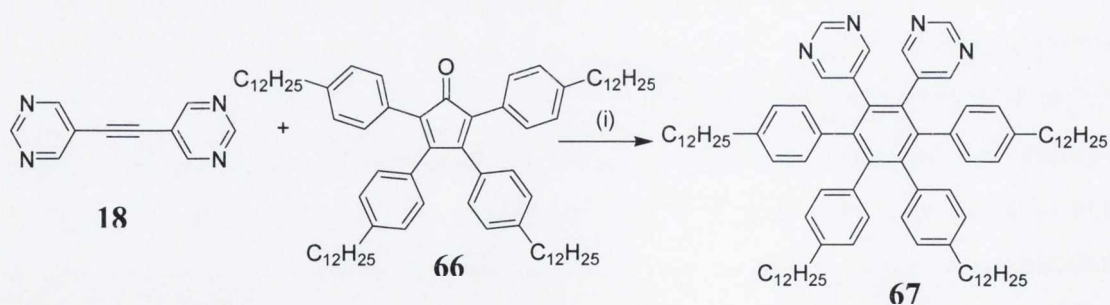
1,3-diaryl-2-propanone **65** was successfully synthesised in 54 % yield using iron pentacarbonyl in a biphasic system. Subsequent two-fold Knoevenagel condensation of **63** and **65** in an ethanolic potassium hydroxide solution yielded the

tetraphenylcyclopentadienone **66** in 53 % yield as a thick purple oil. The synthesis of **65** and **66** can be seen in Scheme 44.²⁸



*Scheme 44: Synthetic pathway for the synthesis of the cyclopentadienone, **66**. (i) paraformaldehyde, HBr, glacial acetic acid, 75 °C, 4 d (14 %). (ii) NaOH, benzyltriethylammonium chloride, Fe(CO)₅, CH₂Cl₂/H₂O, reflux, 18 h (54 %). (iii) KOH, C₂H₅OH, reflux, 5 min (53 %).²⁸*

Central to the work is the introduction of heteroatoms into a polyphenylene precursor. Polyphenylene **67**, the precursor to compound **68**, was synthesised in 48 % yield *via* the Diels-Alder [2 + 4]-cycloaddition of **18** and **66** in a benzophenone melt at 200 °C for 6 hours with the liberation of carbon monoxide (Scheme 45). The careful choice of starting materials and the established stereochemistry of the [2 + 4]-cycloaddition reaction meant that the system was chemoselective, ensuring the *ortho*-arrangement of the pyrimidine subunits on the generated benzene core of **67**.



*Scheme 45: The synthesis of N-doped, dodecyl substituted polyphenylene **67** via a Diels-Alder [2 + 4]-cycloaddition reaction. (i) benzophenone, 200 °C, 6 h (48 %).*

Polyphenylene **67** was purified by column chromatography, followed by recrystallisation from hexane and was isolated as a waxy off-white substance.

3.2.2.1. NMR Spectroscopic Characterisation of 67

The structure of **67** as drawn in Figure 49, has a C_2 axis of symmetry which simplifies its ^1H and ^{13}C NMR spectra. The two most downfield signals with an integral ratio of 2:4, respectively in the ^1H spectrum can be readily assigned due to the protons of the pyrimidine ring. The proton with the most downfield signal at δ 8.78 ppm can be assigned to H10 which is located between the two nitrogen atoms. The electron-withdrawing properties of the nitrogen atoms have shifted this signal to this downfield position. The other proton of the pyrimidine ring H7 can be seen at δ 8.24 ppm. The remaining aromatic signals, which consists of four doublets are rather complicated to assign. One doublet can be clearly seen at δ 6.74 ppm, however the other three doublets overlap in the region δ 6.70-6.68 ppm. In order to fully assign these protons an NOE experiment was carried out on H7, which showed that H7 had an interaction with H8 and H11 at δ 6.75 ppm and δ 6.70 ppm, although which was which could not be determined. Nevertheless this showed that H8 and H11 were one spin-system in the phenyl ring closest to the pyrimidine ring and that H9 and H12 at δ 6.68 ppm and δ 6.69 ppm must be another spin system in the phenyl ring furthest away from the pyrimidine ring. The interactions between H8 and H11 as well as H9 and H12 were further confirmed by a ^1H - ^1H COSY experiment.

Full assignment of the aromatic proton signals was achieved by carrying out a HMBC experiment. Although the benzylic protons of the long-alkyl chains are non-equivalent they do overlap at δ 2.37 ppm, and from the HMBC, H11 and H12 were assigned at δ 6.75 and δ 6.68 ppm respectively from their long-range CH coupling to the benzylic carbon atoms. So by elimination H8 and H9 were assigned to the signals at δ 6.70 and δ 6.69 ppm, respectively.

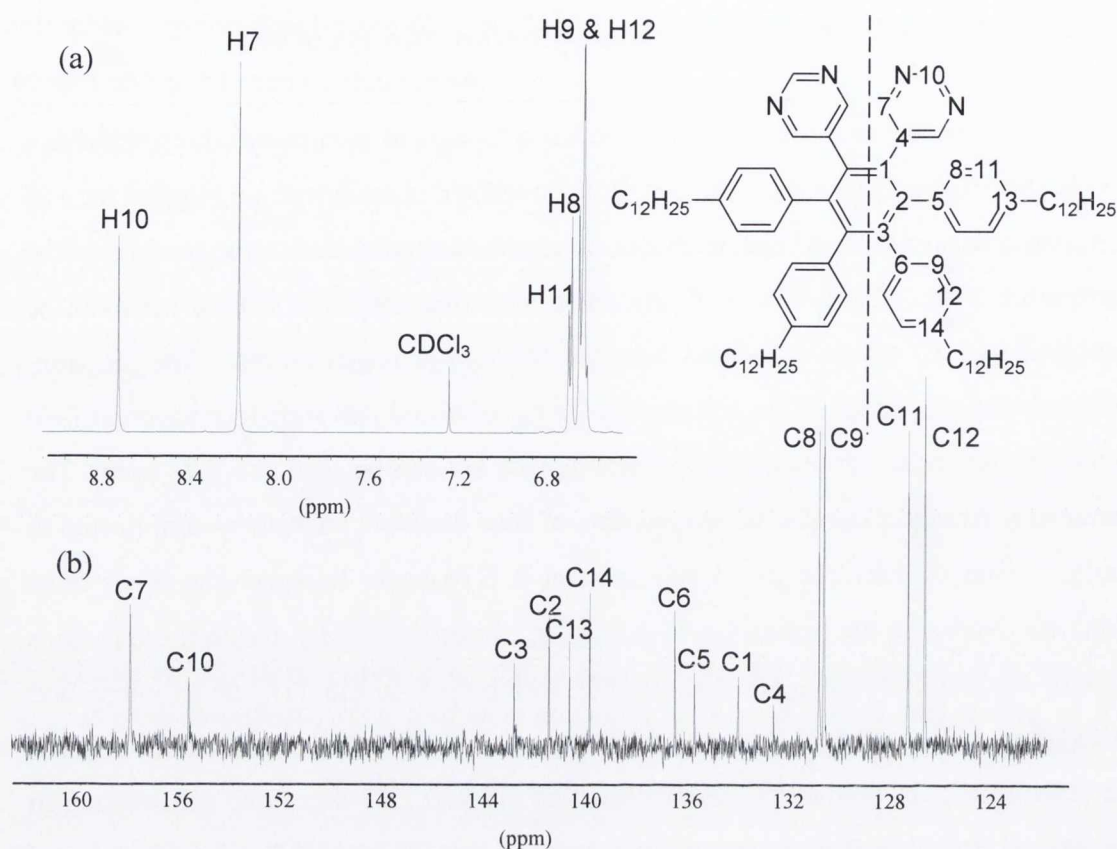


Figure 49: (a) ^1H NMR (600 MHz) and (b) ^{13}C NMR (150 MHz) spectra of the aromatic region of **67** (CDCl_3 , RT).

In the aliphatic region of the ^1H NMR spectrum the terminal methyl groups of the alkyl-chains can be seen as a triplet at δ 0.91 ppm, this implies that although the two-chains are non-equivalent they appear as one signal with a coupling constant of 6.7 Hz. As mentioned earlier the benzylic protons of the two non-equivalent chains can be seen overlapping at δ 2.37 ppm. The rest of the aliphatic protons are seen as a multiplet integrating to 80 in the region δ 1.45–1.13 ppm, as is customary with dodecyl chains in these types of systems since apart from the terminal methyl group and the benzylic protons there is little to distinguish the other protons from each other.

The aromatic region of the ^{13}C NMR spectrum of **67** is also shown in Figure 49 (b). This shows 8 quaternary carbon signals in the region δ 142–133 ppm which corresponds to the chemically distinct carbon atoms, C1–6, and C13–14. Again the two most downfield signals at δ 157.9 and 155.6 ppm were assigned to the deshielded aromatic carbon atoms of the pyrimidine ring, C7 and C10 respectively. The remaining CHs were readily assigned as shown in Table 12, by ^{13}C – ^1H COSY since

the aromatic protons were already assigned. Full assignment of the quaternary carbons can also be seen in Table 12, and were achievable by HMBC experiments. The signals due to the quaternary carbon atoms were assigned by their long range interactions with known protons.

¹³ C signal (ppm)	¹³ C environment	¹³ C assignment
157.9	CH	C7
155.6	CH	C10
142.8	q	C3
141.5	q	C2
140.7	q	C13
139.9	q	C14
136.5	q	C6
135.8	q	C5
134.0	q	C1
132.7	q	C4
130.9	CH	C8
130.7	CH	C9
127.4	CH	C11
126.7	CH	C12

Table 12: Assignment of ¹³C NMR signals from ¹³C-¹H COSY and HMBC spectroscopic experiments on **67**.

3.2.2.2. UV-vis Absorption Spectroscopy of **67**

The configuration adopted by molecules has been shown to play a major role in determining the shape and position of absorption maxima in the electronic spectra of aromatic molecules. Ogliaruso in 1965 proposed that structural rigidity and the angle between the outer rings and the central ring as important factors in the elucidation of the electronic spectra of polyphenylenes.¹⁰⁶ Non-planar molecules usually have structureless absorption spectra, whereas planar, rigid molecules with high symmetry show well resolved vibrational bands. Hexaphenylbenzene exhibits electronic characteristics typical of a non-planar molecule, with an absorption maximum at λ_{max} 247 nm, and a shoulder at λ 271 nm.¹⁰⁷ It has a slightly structured absorption spectrum, and there is no effective conjugation between the rings. Interestingly, the principal absorption of hexaphenylbenzene is exactly the same as the major absorption band for biphenyl and many other oligophenylenes.¹⁰⁸

In the case of biphenyl which is non-planar in solution,¹⁰⁹ a wide structureless absorption band is observed. Like many oligophenylenes, it exhibits a large change in conformation between the ground and the first excited states i.e. the molecule becomes more planar upon excitation. The UV-vis absorption spectrum of biphenyl contains a broad structureless p-band ($\lambda_{\text{max}} = 250$ nm) and the forbidden α and α^* bands which are partially submerged in the long-wavelength end of the p-band at 270 nm.¹⁰⁹ The vibrational freedom of the phenyl rings causes the bell-like structure of the p-band.

The normalized absorption spectrum for the N-doped polyphenylene **67**, in toluene can be seen in Figure 50.

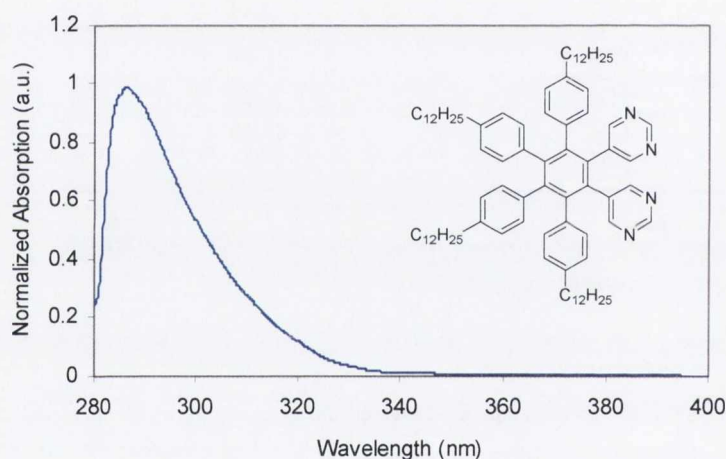
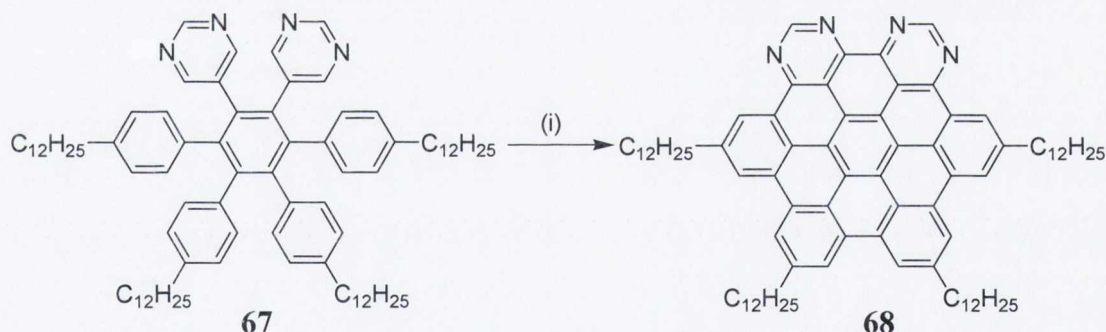


Figure 50: The normalized absorption spectrum of **67** in toluene.

As can be seen in Figure 50 the electronic spectrum for **67** is very broad and exhibits no fine-structure, so it becomes difficult to determine the 0-0 transition.¹⁰⁷ The spectrum is structureless as it is with hexaphenylbenzene and biphenyl since in the ground state steric hindrance imposes a non-planar configuration on the chromophore.¹⁰⁷ The spectrum shows an absorption band at λ_{max} 288 nm with a molar extinction coefficient of 4.9×10^3 L mol⁻¹ cm⁻¹. However when **67** is fully cyclised to planar **68** there is a dramatic change in the absorption spectrum as expected.

3.2.3. Synthesis and Characterisation of tetra *-peri*-(dodecyl-benzo)-*-peri*-(pyrimidino)-coronene (**68**)

Cyclodehydrogenation of **67** with FeCl_3 generated the first long chain containing N-functionalized heterosuperbenzene, **68** (Scheme 46). Compound **68** was purified by chromatography yielding a dark red waxy substance in 24 % yield, and was found to be soluble in most organic solvents. The low yield obtained for **68** could be explained by the possibility of competing reactions such as intermolecular aryl-aryl coupling⁶ or de-alkylation which could not be suppressed. From a purely thermodynamic point of view, incomplete cyclisation would be unfavourable because of the formation of a fully dehydrogenated system gives the largest gain in resonance energy,⁷⁰ however it is known that partially cyclised products are obtained during the synthesis of N-doped HBCs. Although most of the HCl produced during the course of the reaction is removed by bubbling argon through the reaction mixture it is predicted that some of the side products will be chlorinated thus leading to a further lowering in the yield.³ Nevertheless it was possible to isolate the non-chlorinated fully cyclised product from the reaction mixture.



Scheme 46: Synthesis of **68** via the cyclodehydrogenation of **67**. (i) FeCl_3 , CH_3NO_2 , CH_2Cl_2 , RT, 2 h (24 %).

NMR characterisation of **68**, proved to be very problematic which was to be expected. Although the presence of the long alkyl chains increases the solubility of **68** it also allows the aromatic cores to stack much closer together than in its *tert*-butyl analogue. This proposed enhanced aggregation is similarly seen in HBC- PhC_{12} which in order to get a proton NMR spectrum it required running the experiment at 85 °C in $p\text{-C}_6\text{D}_4\text{Cl}_4$ on a 500 MHz spectrometer.¹¹⁰ Even at elevated temperatures on a 600 MHz spectrometer no fine structure can be seen for **68**. It is our contention that compound

68 with its permanent dipole moment exhibits an increase in stacking and stronger association compared to HBC-PhC₁₂. The spectrum in Figure 51 of **68** although very broad, is indicative of a pure compound. Any partially cyclised impurities would appear as sharp signals.

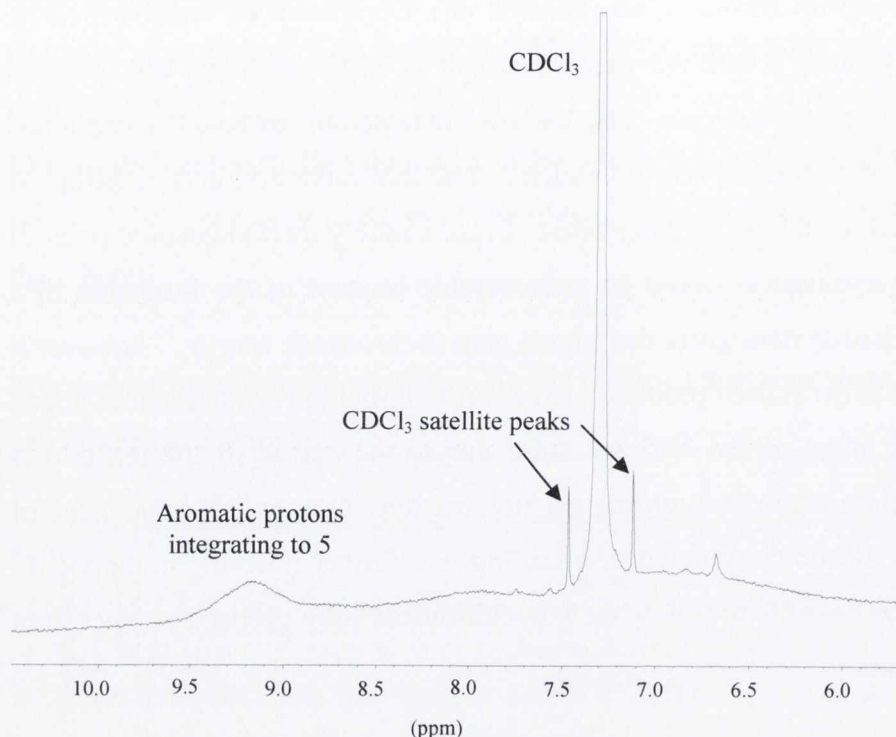


Figure 51: The ¹H NMR spectrum of **68** (CDCl₃, RT, 600 MHz).

However the accurate mass MALDI-TOF spectrum of **68** shown in Figure 52, contained a single molecular ion at m/z 1199.8804 in accord with the formation of [C₈₆H₁₁₁N₄]⁺, [MH]⁺ (calculated 1199.8809) with the expected isotope distribution.

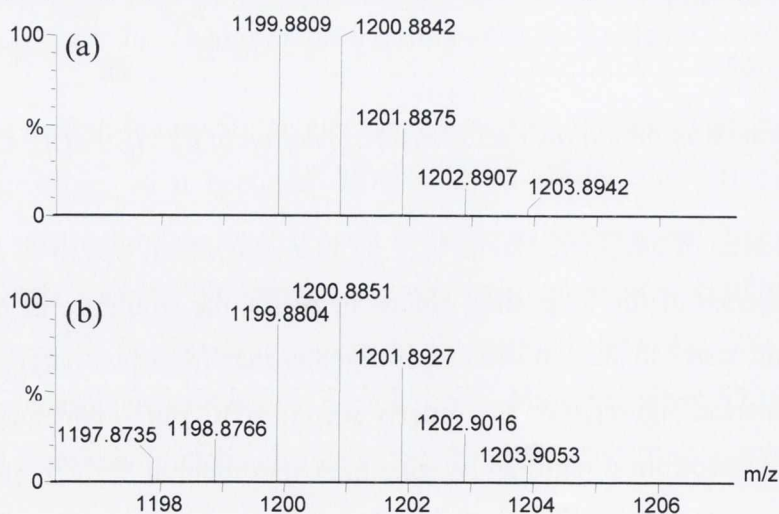


Figure 52: MALDI-TOF mass spectrum, (a) simulated isotopic distribution expected and (b) experimental mass spectrum obtained for **68**.

3.2.4. Solubility

One major drawback with HBCs is their low solubility in most solvents and the need for high boiling solvents such as dichlorobenzene or tetrachloroethane for spectral analysis. In contrast **68** with its built in dodecyl and nitrogen solubilising units, shows a dramatic increase in solubility compared with reported all-carbon analogues. It is soluble in a wide variety of common organic solvents such as benzene, toluene, chloroform, dichloromethane, tetrahydrofuran, diethylether and it is even slightly soluble in the non-polar solvent hexane. However it was noted that **68** was less soluble in these solvents than N-HSB, even though both the dodecyl groups (in **68**) and the *tert*-butyl groups (in N-HSB) help make the ligand more soluble. Both compounds have a comparable dipole moment therefore there must be other factors at work regarding the variation in their relative solubilities.

3.2.5. Thermal Stability

Thermal stability is important to extend LED applications where thermally sensitive polymer materials can fail. HBCs have been shown to be thermally stable up to and beyond 1000 °C. It was therefore important to examine the thermal stability of **68** which was examined by thermogravimetric analysis (TGA). As shown in Figure 53 there was an initial loss in mass of 5-10 % between 100-250 °C attributed to the removal of trapped solvent molecules. Decomposition around 470 °C agrees with the mass loss of the dodecyl groups.^{14,34} This suggests that the simplest heterosuperbenzenes, without substituents, are likely to be highly thermally stable. This is not surprising however as it is believed that the all-carbon PAH derivative, coronene is formed in interstellar media at many thousands °C. The extremely high thermal stability of the central unit of **68** would make them particularly suitable for many LED applications.

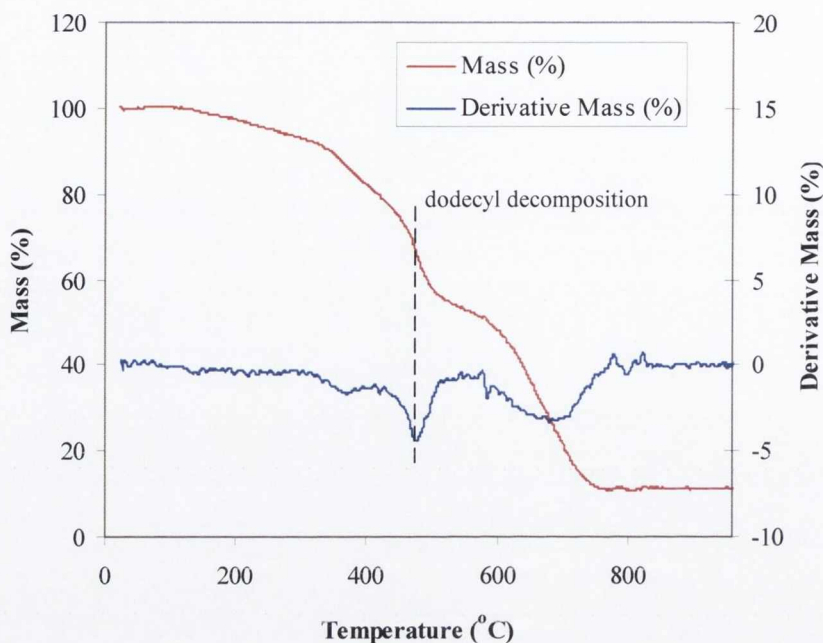


Figure 53: Thermogravimetric analysis of **68** showing 5-10 % solvent loss and dodecyl decomposition.

3.2.6. Differential Scanning Calorimetry (DSC)

The DSC trace of **68**, shown in Figure 54, shows only one phase transition (assigned to $D_1 \rightarrow D_2$) which is due to conformational changes within the mesophase i.e. **68** is liquid crystalline over all temperatures studied. DSC simply measures the heat supplied or extracted during the phase transition process. The first heating trace shows a phase transition at *ca.* 5 °C with no other phase changes detected i.e. there is no transition from the crystalline to the liquid crystalline phase nor is there a phase change from the liquid crystalline to the isotropic liquid phase. It has been shown in the literature that the change in enthalpy due to conformational changes within the mesophase are in the range 16-28 kJ mol⁻¹, which is comparable to the average change in enthalpy observed for **68**, 20 kJ mol⁻¹. Crystalline to liquid crystalline and liquid crystalline to isotropic phase transitions have much greater changes in enthalpy, in the order of 60-70 kJ mol⁻¹.⁶ These assignments will be discussed later in relation to the charge carrier mobility of **68**.

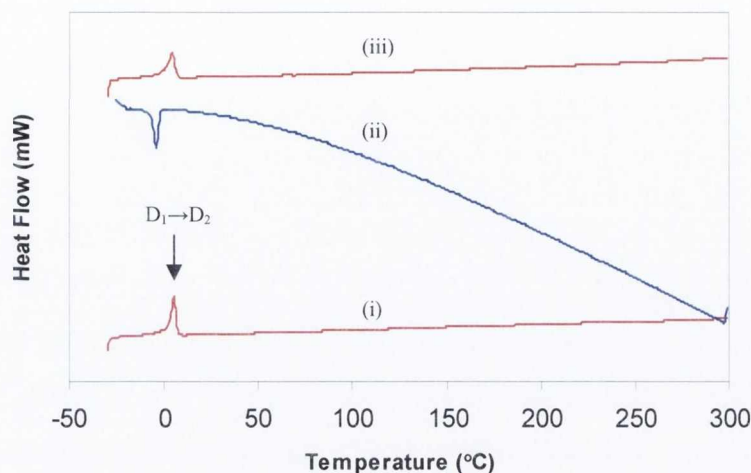


Figure 54: The differential scanning calorimetry (DSC) trace for **68**, scanning between -30 - $+300$ °C at a scan rate of 10 °C min^{-1} . (i) first heat, (ii) first cooling, (iii) second heat.

The cooling curve shows the transition at *ca.* -4.5 °C. The discrepancy in the two values can be explained by supercooling within the instrument as well as instrumental hysteresis attributed to the temperature scan rate.

HBC-PhC₁₂ is the only other HBC based liquid crystalline material known to be liquid crystalline at room temperature and over all other temperatures studied. This compound however exhibits a phase transition at 18 °C. Obviously that fact that **68** undergoes this transition at *ca.* 5 °C is a significant difference, which can be attributed to the fact that **68** has a permanent dipole which has been induced by the asymmetric presence of N-atoms whereas HBC-PhC₁₂ does not. The effect of this permanent dipole moment will assist in the anchoring of the aromatic rings within the stacks, giving head-to-tail or homotropic intra-columnar arrangement with reduced rotational disorder.

The DSC also confirms that scanning from -30 °C to 300 °C results in no significant decomposition of **68** as the DSC traces are reproducible within experimental error.

3.2.7. Photophysical Properties of 68

3.2.7.1. UV-vis Absorption Spectroscopy

UV-vis spectroscopy is invaluable when studying PAHs as it yields information on the electronic structure of the compounds. The UV-vis absorption spectra of **68**, shown in Figure 55 (b), can be compared to the uncyclised polyphenylene precursor, **67** (Figure 50) and the all-carbon analogue **60** (Figure 55 (a)). We can see from the UV-vis absorption spectra of the cyclised compound **68** that the increase in planarity and rigidity of the system has resulted in well-resolved bands compared to the uncyclised polyphenylene precursor **67**.

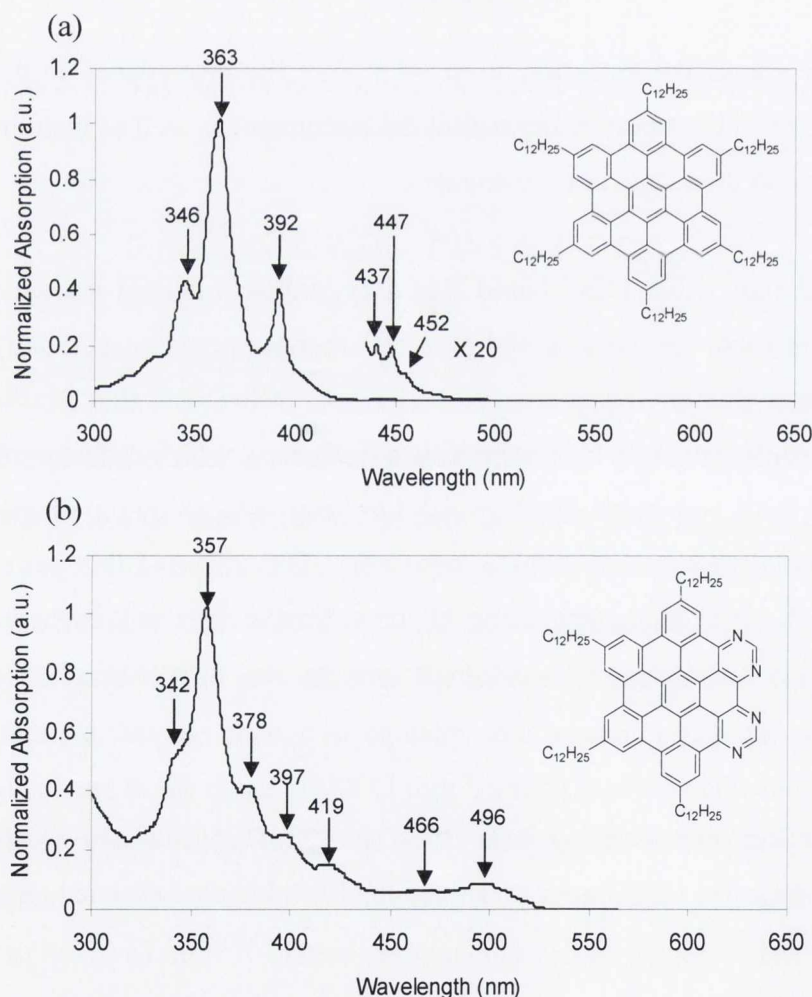


Figure 55: The normalized absorption spectra of (a) **60** and (b) **68**, both in toluene.

The highly structured electronic absorption spectrum of **68** in toluene (Figure 55 (b)) can be readily compared to the all-carbon analogue **60** in the same solvent (Figure 55 (b)). From the highly structured shape of the UV-vis spectrum in the 300-400 nm region we can say with confidence that although some modification has taken place in the synthesis of **68**, with the introduction of four nitrogens, the HBC chromophore is still intact.

In the 300-400 nm region the UV-vis spectrum of **68** has a $\lambda_{\text{max}} = 357$ nm, which is blue-shifted by 6 nm when compared to **60**. As well as this there is also an additional band at λ 378 nm, which is not present in the spectrum of **60**.

It has been shown in the literature and within the group that PAHs typically show three types of bands, namely α , β and p-bands, in agreement with Clar's result.¹¹¹ The β -bands (at λ 363 nm for **60**) correspond to the electronic interaction between the benzoid rings of the PAH, a red-shift in these bands is a consequence of increasing the electronic interaction, for example by extending the π -system.³⁴

It is very difficult to infer anything from the p-bands, since for **60** they appear at *ca.* λ 392 nm and involve the localization of the π -electrons in the excited state. Therefore since localization takes place in different positions in different PAHs direct comparisons with other PAH derivatives is not possible.³⁴

In the region 400-550 nm the extremely weak α -band at λ 452 nm ($\epsilon = 200$) for **60**, is assigned as the 0-0 transition, which is strictly forbidden in the D_{6h} symmetry and coincides with the first recognizable fluorescence band for **60** at λ 468.5 nm. However in the case of **68** there is a large increase in the molar absorptivity for the low energy bands at λ 419, 466 and 496 nm. For **68** the 0-0 transition (α -band) is much more intense due to the lifting of molecular symmetry to C_{2v} . Thus the red-shifted band at λ 496 nm is assigned to the 0-0, $^1(\pi, \pi^*)$ transition, with enhanced molar absorptivity when compared to **60**.³⁴

It has been shown in the literature that for other HBC derivatives where the 0-0 band is apparently absent, its position can be estimated at around 430-435 nm by using the approximate mirror image relationship between absorption and emission. This is

considerably red-shifted from that of benzene in cyclohexane which appears at λ 270 nm.¹¹²

The molar extinction coefficients for **60** and **68** were recorded in toluene and can be seen in Table 13. From the table it is clear that the molar extinction coefficients for **68** show a more than 40 fold increase in the intensity of the 0-0, $^1(\pi, \pi^*)$ transition compared to **60**, for reasons already discussed. In contrast there is a reduction in the intensity of λ_{max} in **68** compared to **60**. This is a direct result of the introduction of four withdrawing nitrogen atoms, which deplete the π -electron density within the core of **68** as compared with **60**. This kind of effect has been observed before, for example when comparing pyrimidine and benzene.^{34,113}

60	λ_{max}	346	363	392				
	$\epsilon \text{ (M}^{-1} \text{ cm}^{-1}\text{)}$	79,000	180,000	71,000				
68	λ_{max}	342	357	378	397	419	466	496
	$\epsilon \text{ (M}^{-1} \text{ cm}^{-1}\text{)}$	31,000	49,000	23,000	13,000	8,000	4,000	4,500

Table 13: The molar extinction coefficients for the absorption maxima at each wavelength of **60** and **68**, both in toluene.

3.2.7.2. Electronic Transitions within **68**

In general the bonding orbitals of a nitrogen containing aromatic compound have π and n character and the lowest energy unfilled orbitals (LUMOs) are π^* -orbitals.¹¹⁴⁻¹¹⁶ Promotion of an electron from the n to the π^* orbital ($n \rightarrow \pi^*$), leads to an excited state in which the electron is delocalised over the entire aromatic system, which will give rise to excited singlet $^1(n, \pi^*)$ and triplet $^3(n, \pi^*)$ states. Similarly a $\pi \rightarrow \pi^*$ transition will lead to the excited states $^1(\pi, \pi^*)$ and $^3(\pi, \pi^*)$.^{34,114}

The UV-vis spectra of **68** in various organic solvents shows two types of transition, the $\pi \rightarrow \pi^*$ and the $n \rightarrow \pi^*$. These generate an overall spectrum which is complex and shows several component bands.

There are many methods to elucidate the nature of the absorption bands, the simplest being application of Kasha's criteria and comparison of the UV-vis spectra of **68** and

60.¹¹⁴ According to Kasha an $n \rightarrow \pi^*$ transition is absent in **60**. By comparing absorption spectra **60** and **68** it has already been possible to assign the low energy bands at λ 466 and 496 nm as $\pi \rightarrow \pi^*$ transitions, with the 0-0 transition at λ 496 nm. In fact direct comparison between the two compounds would suggest that all the bands in the spectrum of **68** are of $\pi \rightarrow \pi^*$ character, except for the band at λ 378 nm, which is clearly new and which is absent in the absorption spectrum of **60** and can therefore be assigned as a $n \rightarrow \pi^*$ transition.³⁴

$\pi \rightarrow \pi^*$ and $n \rightarrow \pi^*$ transitions can also be distinguished by the effect of polar and non-polar solvents on UV-visible spectra.¹¹⁴ Polar solvents are more strongly hydrogen-bonded to the heteroatoms in the ground state than in a π^* excited state. The energy of the n ground state is therefore lowered and a shift in the absorption maxima to shorter wavelengths is observed for an $n \rightarrow \pi^*$ transition in polar solvents. In direct contrast a shift in the absorption maxima to longer wavelengths is observed in some $\pi \rightarrow \pi^*$ transitions in polar solvents: the excited state is more polar than the ground state, hence the interaction with a polar solvent reduces the energy difference between the two states.

Figure 56 shows the UV-vis spectrum of **68** in solvents of differing polarity, the most important features are the loss of fine structure in some solvents and the marked shift that can be caused by varying the polarity of the solvent.

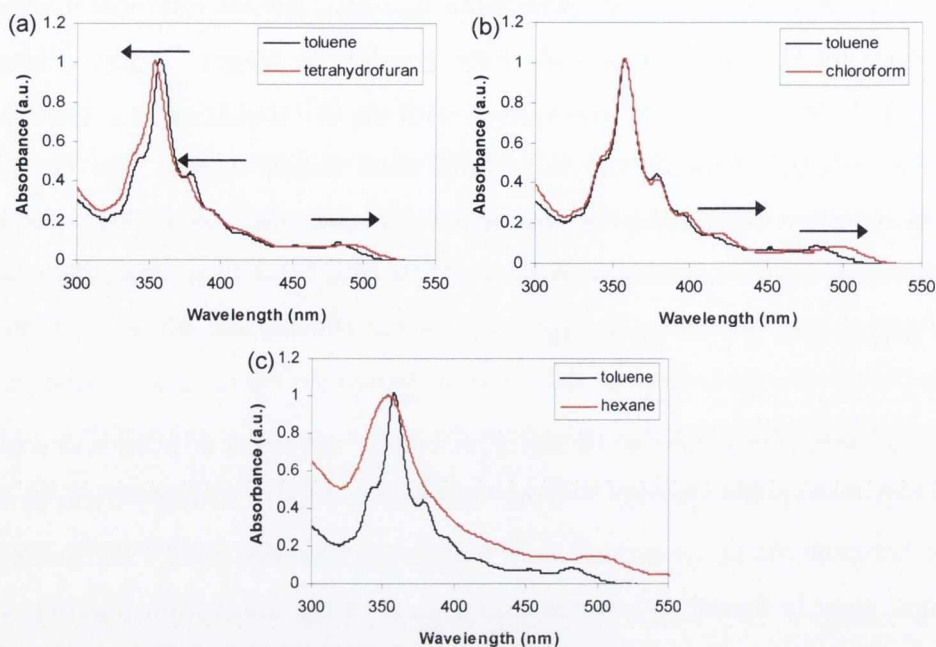


Figure 56: (a)-(c). Absorption spectra of **68** in various solvents. The arrows indicate the direction that the absorption bands have shifted on increasing solvent polarity.

Figure 56 (a) compares the UV-vis spectra of **68** in toluene and the more polar tetrahydrofuran. There is a blue-shift in the λ_{max} from 357 nm in toluene to 355 nm in tetrahydrofuran. The band at λ 378 nm in toluene has also been blue-shifted to 376 nm in tetrahydrofuran. The bands in the red region at λ 419 nm, 466 nm and 496 nm in toluene have all undergone a red-shift by 1-2 nm in tetrahydrofuran. On applying Kasha's criteria, this would indicate that the absorption bands in the red-region (400-500 nm) are in fact $\pi \rightarrow \pi^*$ transitions, and the bands at λ 357 nm and 378 nm in toluene are $n \rightarrow \pi^*$ or at least have some $n \rightarrow \pi^*$ character.

Figure 56 (b) shows very large red-shifts in the $\pi \rightarrow \pi^*$ transitions at the low energy end of the absorption spectrum of **68** when dissolved in chloroform. These shifts are larger than those expected from the magnitude of the polarity change from toluene to chloroform, which suggests that there might be some solvent-specific effects in addition to polarity ones.

Figure 56 (c) shows the effect on the UV-vis spectrum of **68** in hexane. Although hexane is less polar than toluene the expected shifts due to polarity as observed for chloroform and tetrahydrofuran were not observed. It was also noted, as can be seen

in Figure 55 (c) that there was a total loss of resolution and fine structure due to poor solubility in hexane.

3.2.7.3. Emission Spectroscopy-Comparison of 68 with 60

The combined plots of the absorption and fluorescence spectra of **60** and **68** are shown in Figure 57 (a) and (b). The fluorescence spectra for **60** is highly structured, however broadening does take place in the fluorescence spectra of **68** probably due to aggregation which occurs at extremely low concentrations.

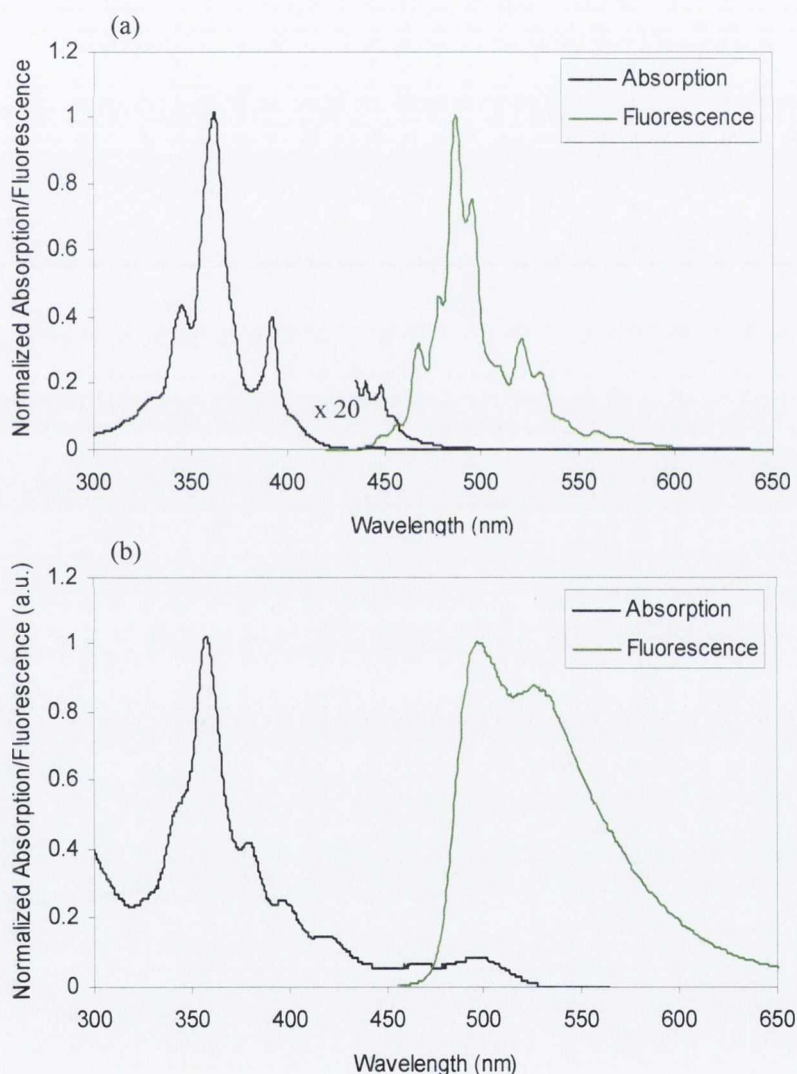


Figure 57: Absorption and fluorescence spectra for (a) **60** and (b) **68**, both in toluene, exciting at λ 363 and 357 nm, respectively.

As can be seen in Figure 57 (a) and (b) all the bands in the fluorescence spectrum of **68** are shifted slightly to the red by around 15 nm when compared to **60**. However the

main feature shown is the fluorescence from the lowest energy excited state, which was expected upon the removal of molecular symmetry from D_{6h} for **60** to C_{2v} for **68**.

As the absorption at 496 nm in toluene is the 0-0, $\pi \rightarrow \pi^*$ transition, a mirror image relationship would thus suggest that the λ_{\max} at 499 nm in the emission spectrum of **68** is from the $^1(\pi, \pi^*)$ excited state.³⁴

3.2.7.4. General Characteristics

Fluorescence of organic compounds usually originates from the lowest excited singlet level, S_1 , even though absorption may initially populate a higher energy singlet state, such as S_2, S_3, \dots, S_n .¹¹⁴ This is due to rapid internal conversion (IC) from S_n to S_1 , followed by vibrational degradation. Radiationless IC $S_1 \rightarrow S_0$ may now occur, although this process must be of the same order or slower than for $S_n \rightarrow S_1$, otherwise fluorescence from S_1 would not occur. The forbidden Intersystem Crossing (ISC) $S_1 \rightarrow T_1$ can also compete and lead to a phosphorescent emission as shown in Figure 58.

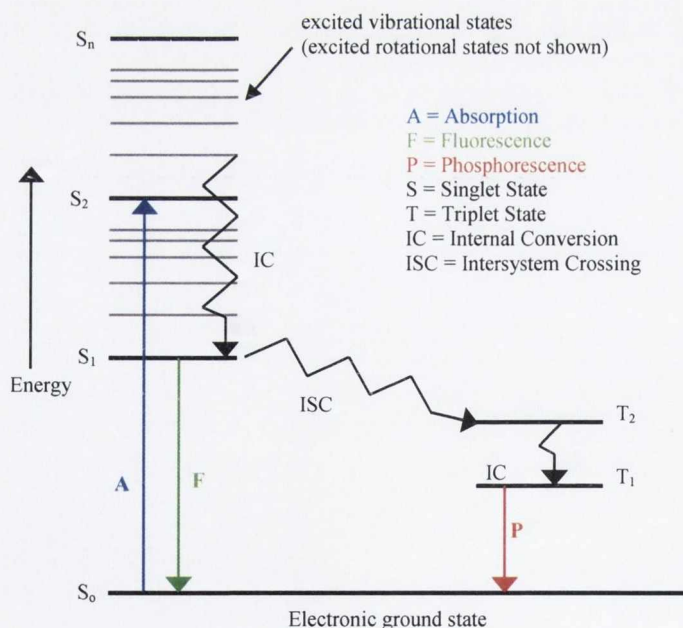


Figure 58: Jablonski energy level diagram showing the possible transitions within an excited species.

The electronic absorption spectra, and (n, π^*) and (π , π^*) nature of the excited singlet and triplet states, have been studied in detail for diazabenzenes. These molecules, for example pyrimidine, are reported to have $^1(n, \pi^*)$ states as the lowest energy singlet state and $^3(n, \pi^*)$ as the lowest energy triplet state. The diazanaphthalenes have $^1(n, \pi^*)$ as the lowest singlet excited state, and $^3(\pi, \pi^*)$ as the lowest triplet state. All the above exhibit a weak fluorescence but are found to show a strong phosphorescence.^{34,115}

Although it is generally accepted that luminescence from (n, π^*) excited states of diazabenzenes occur at lower energy than that derived from (π , π^*) states of the parent hydrocarbon,¹¹⁶ this is not the case for 1,10-phenanthroline. The fluorescence maximum for 1,10-phenanthroline is shifted towards lower energy in non-polar solvents, as is characteristic of an increased contribution from an $^1(n, \pi^*)$ state.¹¹⁶ Indeed the sensitivity of the fluorescence efficiency and lifetime to the nature of the solvent is indicative of a close proximity of $^1(n, \pi^*)$ and $^1(\pi, \pi^*)$ excited states, which are said to mix to varying degrees in 1,10-phenanthroline and hence influence its observed photophysical properties. In polar solvents, however, the first excited state for 1,10-phenanthroline is $^1(\pi, \pi^*)$. As additional aromatic rings are added to the N-containing aromatic system, additional bonding and antibonding levels are introduced with a resulting reduction of the energy of the $\pi \rightarrow \pi^*$ transition.¹¹⁷ Thus it is expected that the first excited state in **68** is a $^1(\pi, \pi^*)$ state.³⁴

As photons emitted by fluorescence have less energy than those absorbed, absorption spectra always occur at shorter wavelengths than emission spectra. This difference in wavelength, or Stokes' shift is shown in Table 14 for **68** (in toluene).

	λ_{abs} (nm)	λ_{em} (nm)	$\lambda_{\text{em}} - \lambda_{\text{abs}}$
68	496	499	4.0

Table 14: The lowest energy absorption, highest energy emission wavelength and Stokes' shift for **68** in toluene.

It has been shown that for *tert*-butyl N-HSB the Stokes' shift increases in a polar solvent such as toluene when compared to the Stokes' shift in a non-polar solvent,

such as hexane. However **68** was too insoluble in hexane to establish whether a similar effect could be prevalent.

The emission from **68** was shown to be independent of the wavelength of excitation. A solution of **68** was irradiated at all absorption band wavelengths and in each case the corrected emission could be superimposed, suggesting a single fluorescing species (see Figure 59). The highest intensity emission was generated on irradiating at $\lambda = 357$ nm, which is the λ_{max} in the absorption spectrum.

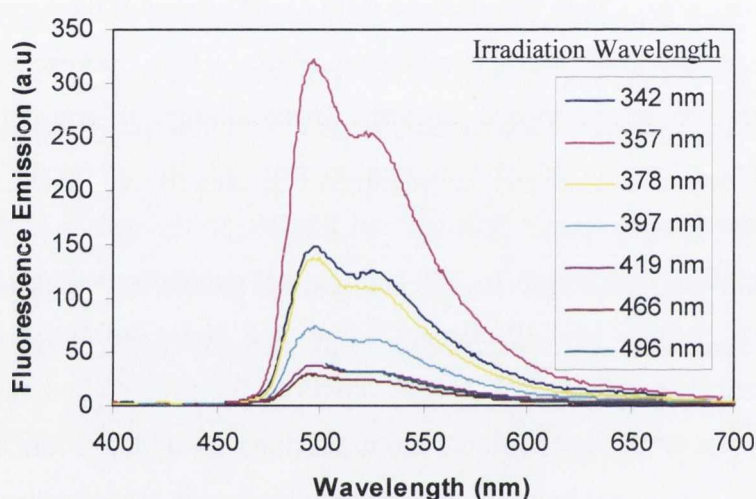


Figure 59: Overlay of the fluorescence spectra of **68** in toluene generated at different λ_{ex} .

3.2.8. Absorption and Fluorescence Properties of the Protonated form of **68**

In order to better understand the chromophoric behaviour of **68**, the effect of protonating the nitrogen atoms was studied. Compound **68** contains four nitrogen atoms each of which is capable of acting as a proton acceptor.

The absorption spectra of **68** can be seen in Figure 60 (i). Addition of the base triethylamine does not cause any spectral change, however the addition of trifluoroacetic acid causes significant changes over the entire spectrum up to 450 μL of 0.01 mol dm⁻³ whereupon no further change was observed.

Although six incremental additions of trifluoroacetic acid were added to **68**, only two are shown for clarity in Figure 60, namely, (i) 0 μL , (ii) 50 μL and (vi) 450 μL . Low concentrations were required to see any fine structure in the spectrum of **68**, however the draw back is that at these low concentration there is a loss of spectral definition.

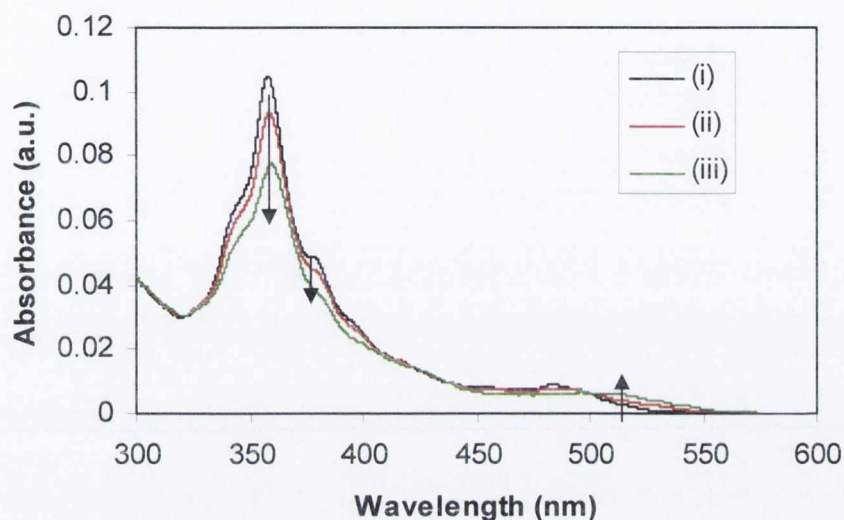


Figure 60: The absorbance spectra of **68** in toluene (2mL , $0.0013\text{ mol dm}^{-3}$) upon the addition of (i) 0 μL , (ii) 50 μL , (iii) 450 μL of trifluoroacetic acid (0.01 mol dm^{-3}).

Protonation of the peripheral nitrogen atoms on the addition of trifluoroacetic acid causes major changes in the absorption spectrum (Figure 60). But in particular a decrease in intensity of the absorption band at λ 357 nm along with the disappearance of the band absorption band at λ 378 nm. This indicates that nitrogen protonation has a profound electronic effect on the π -electron density throughout the system.³⁴

The lowest-energy band in the absorption spectrum of **68** can be assigned as a spin allowed $\pi \rightarrow \pi^*$ transition.^{116, 118} The red-shift observed for the lowest-energy absorption bands upon protonation of **68** shows that the lowest $\pi \rightarrow \pi^*$ transitions display charge-transfer character i.e. the LUMO has a higher electron density on the nitrogen atoms than the HOMO. This is similarly seen for various phenanthroline derivatives.¹¹⁸

The changes in the absorption spectrum upon addition of acid are reversible upon addition of triethylamine base, implying that an equilibrium is established in the ground state, where A denotes **68** and BH is trifluoroacetic acid.



The fluorescence spectrum is also dependent on pH. In toluene at room temperature **68** displays a structured fluorescence band (Figure 61 (i)) that is assigned to the lowest-energy $^1(\pi, \pi^*)$ level of **68** with charge transfer character. On addition of acid, the intensity of this band decreases and a new, unstructured, shorter lived luminescence band arises at longer wavelength.³⁴

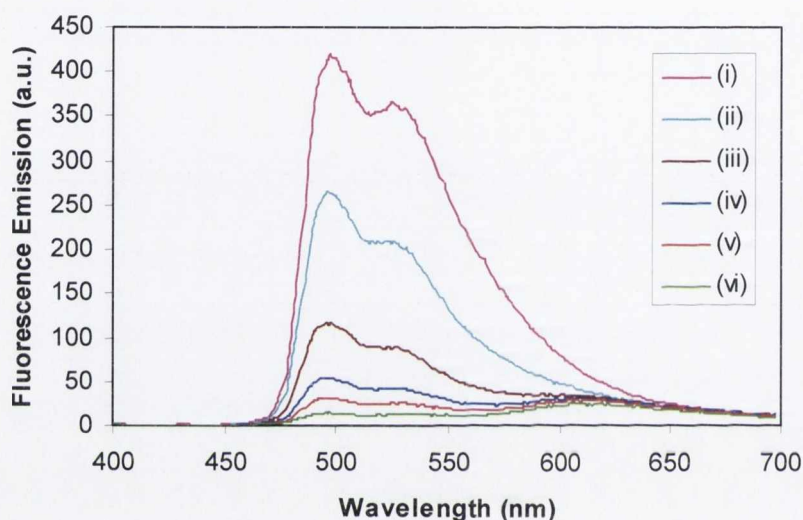


Figure 61: The fluorescence spectra of **68** in toluene (2 mL, $0.0013 \text{ mmol dm}^{-3}$) on addition of (i) 0 μL , (ii) 10 μL , (iii) 50 μL , (iv) 110 μL , (v) 200 μL , (vi) 450 μL of trifluoroacetic acid (0.01 mol dm^{-3}).

Upon addition of trifluoroacetic acid the fluorescence from the neutral compound ($\lambda_F = 499 \text{ nm}$) is quenched. The protonated species ($\lambda_F = 615 \text{ nm}$) is only slightly fluorescent and is completely quenched upon the addition of a large excess of trifluoroacetic acid. This is in direct correlation to the behaviour of various phenanthroline compounds.^{34, 116, 118}

The spectral variations are represented in Figure 62, which shows the normalized variations of two UV-vis absorption maxima of **68** and one fluorescence maximum. As can be seen in the absorption spectra, the decrease in the intensity of the absorption band at $\lambda 378 \text{ nm}$ is accompanied by a parallel increase of the intensity of the band at $\lambda 515 \text{ nm}$. The intensity decrease of the fluorescence band at $\lambda 499 \text{ nm}$ closely follows the trace for the absorption at $\lambda 378 \text{ nm}$. Unfortunately due to the

overlap of the emission band at λ 499 nm and the lower-energy emission for the protonated form of **68** at λ 615 nm, the error in this trace makes it less reliable and thus has not been included in Figure 62.

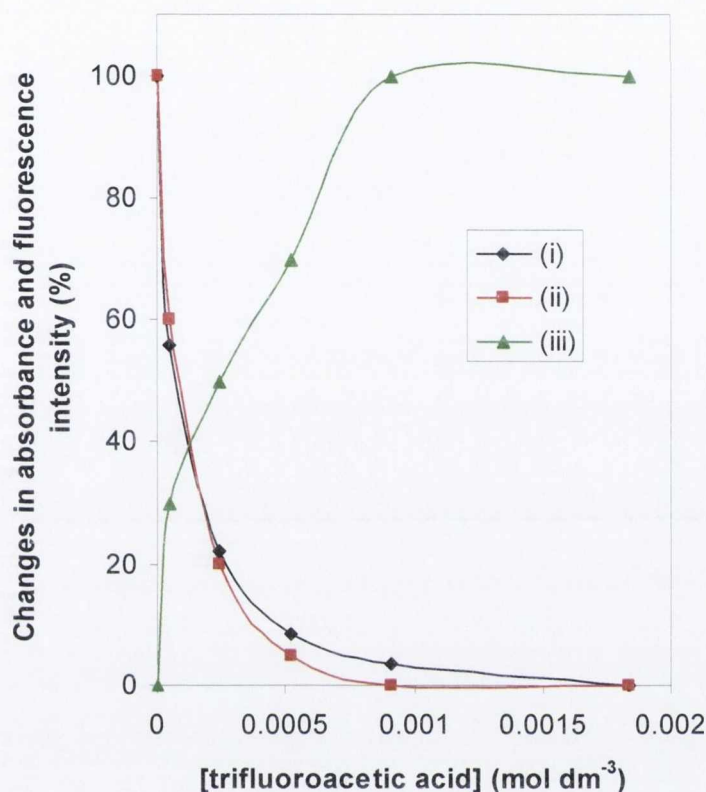


Figure 62: Normalized changes in fluorescence at (i) λ 499 nm, and absorption at (ii) λ 378 nm and (iii) λ 515 nm, upon incremental addition of trifluoroacetic acid to a toluene solution of **68** (2 mL, 0.0013 mmol dm⁻³)

The main outcome of this plot is that it confirms the assignment of the band at λ 378 nm in the absorption spectra as an $n \rightarrow \pi^*$ transition, where according to Kasha's criteria should disappear in acidic media.¹¹⁴ The decrease of the band at λ 357 nm would suggest that, although this band appears to be dominated by a $\pi \rightarrow \pi^*$ transition, it does contain some $n \rightarrow \pi^*$ character, which is removed upon protonation. Both these assignments support those made earlier.³⁴

These results also indicate that the lowest $^1(\pi, \pi^*)$ level of **68** is stabilized by protonation of the pyrimidine nitrogen because of its partial charge transfer. This was also seen for various phenanthroline derivatives.^{34, 116, 118}

3.2.9. Absorption and Fluorescence Properties of an Exciplex of **68**

It has been shown that tertiary amines quench the fluorescence of arenes in non-polar solvents and an exciplex emission with charge transfer character is observed.¹¹⁹ The emission spectra of exciplexes are assigned to a charge transfer complex $A^{\cdot-}D^+$ stabilized by an electron transfer from the donor (amine) to the acceptor (arene). Therefore, the emission frequency increases with the ionization potential (I) of the donor and decreases with the electron affinity (E) of the acceptor.

$$h\nu = I(D) - E(A) - C,$$

Where C denotes the coulomb attraction energy at equilibrium distance given by $C = qq'/r$ which is a stabilizing term so that the energetics of electron transfer is favourable for smaller distances between neutral molecules. The energy balance must contain both the electrostatic interaction given by the Coulomb term and the solvation energies.

It has been shown that different amines quench fluorescence with different solvent dependent efficiencies. In polar solvents the exciplex undergoes rapid dissociation to give solvent separated ion pairs ($A_s^{\cdot-} \dots D_s^+$), and the exciplex emission is largely quenched.¹²⁰

In non-polar solvents however the energy balance of charge separation can be equal to the electrostatic interaction energy since there is no screening by the solvent for the contact pair¹²¹ and the ions of opposite charge are held by their electrostatic interaction.¹²² Therefore, the probability of the two ions recombining with each other is higher in non-polar solvents because the distance between the ions will be smaller. The absorption spectra of **68** remained unchanged in the presence of incremental amounts of the tertiary amine, aniline. However, as can be seen in Figure 63, there are dramatic changes in the fluorescence spectra of **68** as aniline is added.³⁴

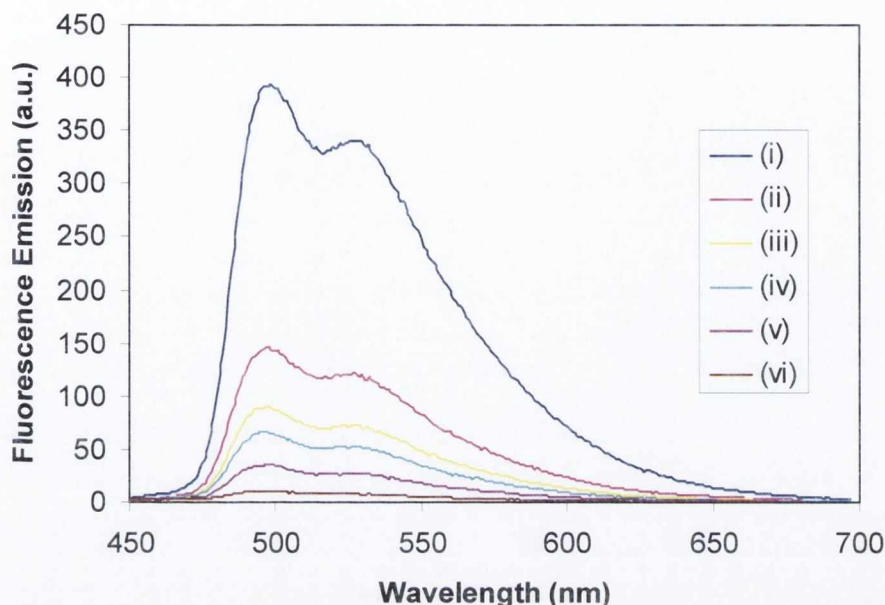


Figure 63: The fluorescence spectra of **68** in toluene (2 mL, $0.0013 \text{ mmol dm}^{-3}$) on addition of (i) 0 μL , (ii) 10 μL , (iii) 20 μL , (iv) 30 μL , (v) 60 μL , (vi) 160 μL of aniline (4.39 mol dm^{-3} in toluene).

It is generally known that photoinduced electron transfer reactions between neutral molecules results in a contact ion pair. These may recombine in the solvent cage or may form solvent separated ion pairs and free solvated ions depending on the polarity of the solvent. These species have been shown to decay non-radiatively to the ground state.¹²³ Exciplex emission is observed if the excited state is a contact ion pair.¹²⁰ The fluorescence of **68** is quenched on addition of incremental amount of aniline. It is postulated that this is due to the formation of an exciplex between the donor aniline and the acceptor **68**. That the exciplex emission is not observed could be due to the formation of non-fluorescent solvent shared ion-pairs even in the weakly polar solvent toluene,¹²⁰ which may suggest a weak electrostatic interaction energy for the contact ion pair. Figure 64 shows the normalized changes in fluorescence at λ 499nm, and the extent of fluorescence quenching by the incremental addition of aniline to **68**.³⁴

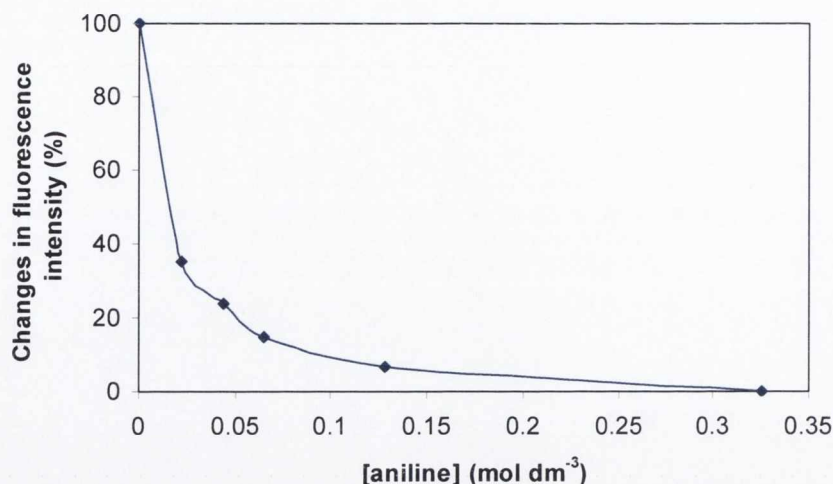


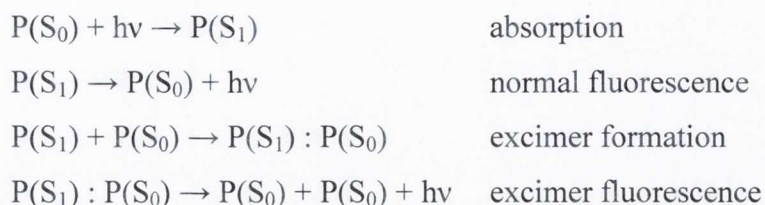
Figure 64: The normalized changes in fluorescence of **68** at λ 499 nm in toluene.

3.2.10. Quantum Yield

Many molecules that do not interact significantly in their ground state appear to form reasonably stable complexes when excited. The complexes are called *exciplexes* or *excimers*, words derived from **excited complex** and **excited dimer**. Thus, an exciplex involves the interaction of an excited molecule with a chemically different species as was discussed earlier with **68** forming an exciplex with aniline, whereas an excimer is produced by the interaction of an excited molecule with a ground-state molecule of the same chemical identity.¹¹⁴

Many PAHs and some of their derivatives exhibit excimer formation, the phenomenon is particularly pronounced in pyrene. A number of lines of evidence indicate that excimers of PAHs have well-defined structures of a “sandwich” type in which one PAH molecule sits on top of the other so as to be partially or totally overlapping.¹²⁴ Formation of such an excimer can be inhibited by incorporation of bulky substituent groups on the aromatic core. In solution, excimer formation is a diffusion-controlled process. If however molecules of a PAH are incorporated into an environment in which their mobility is severely limited (such that the rate of diffusion is small compared with the fluorescence rate constant), then only those PAH molecules that are very close to one another prior to excitation can form excimers. For example an excimer is formed between a singlet excited pyrene and a ground-

state pyrene, and the excimer then radiates. If pyrene is represented as P, the excitation scheme is thus,



The emission from the excimer is initially to a $P(S_0):P(S_0)$ pair possessing the same geometry as the excimer, but since there is no attraction between the ground-state molecules it has the same energy as the isolated $P(S_0)$ molecules, and immediately separates. The excimer, on the other hand, is stabilized with respect to an isolated $P(S_1)$ molecule, and so the emission from the excimer lies at longer wavelengths than the normal fluorescence. Excimer emission is structureless, because the lower state of the transition is essentially a continuum resulting from the repulsion of the ground state molecules.

As can be seen in Figure 65, as the concentration is increased there is a steady increase in the fluorescence of the main band at λ 499 nm which is due to the monomer of **68**. However there is also a new band forming at longer wavelength which is due to the excimer. In the concentration range $0.32 \times 10^{-3} \text{ mmol dm}^{-3}$ to $5.2 \times 10^{-3} \text{ mmol dm}^{-3}$, the fluorescence is dominated by the band at λ 499 nm, but the band due to the excimer is still present and by a concentration of $10.0 \times 10^{-3} \text{ mmol dm}^{-3}$ the bands due to the monomer and excimer are of equal intensity. Then for all concentrations after $10.0 \times 10^{-3} \text{ mmol dm}^{-3}$ the band due to the excimer becomes the dominant one.

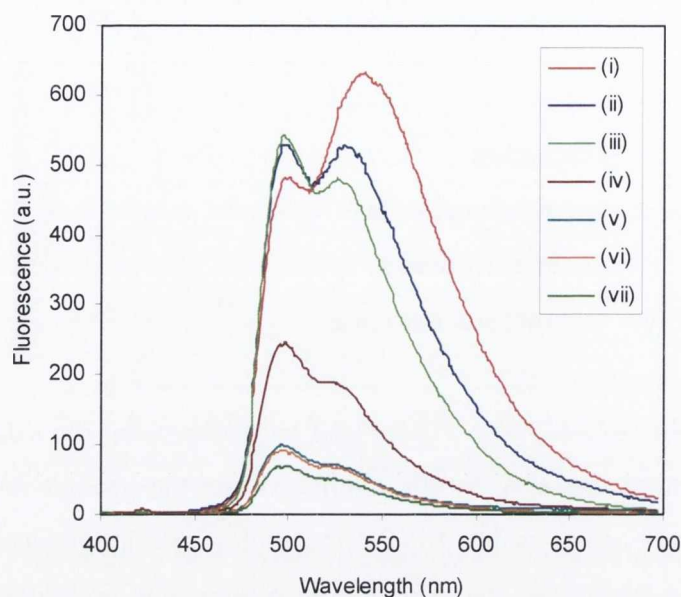


Figure 65: Fluorescence of **68** in toluene at different concentrations. Samples excited at λ 357 nm at concentrations, (i) $20 \times 10^{-3} \text{ mmol dm}^{-3}$, (ii) $10.0 \times 10^{-3} \text{ mmol dm}^{-3}$, (iii) $5.2 \times 10^{-3} \text{ mmol dm}^{-3}$, (iv) $2.6 \times 10^{-3} \text{ mmol dm}^{-3}$, (v) $1.3 \times 10^{-3} \text{ mmol dm}^{-3}$, (vi) $0.65 \times 10^{-3} \text{ mmol dm}^{-3}$, (vii) $0.32 \times 10^{-3} \text{ mmol dm}^{-3}$.

The quantum yield for **68** was calculated and compared to that for *tert*-butyl N-HSB, both were calculated relative to Coumarin 153. The quantum yield for *tert*-butyl N-HSB and **68** can be seen in Table 15.

Compound	λ_F	Φ_F
N-HSB	494	0.40
68	390	0.11

Table 15: Fluorescence data for N-HSB and **68** in toluene.

The data in Table 15 shows that there is a large difference in the values for the quantum yields for N-HSB and **68**, despite the only difference between the two molecules is that the *tert*-butyl groups in N-HSB have been changed for dodecyl chains in **68**. However it can be explained in terms of excimer formation.

The reason that the effect is so pronounced in **68** is because of the difference in the R groups on the periphery of the PAH core. It has been shown with pyrene that bulky groups such as *tert*-butyl can break-up π - π interactions between the PAH core thus preventing excimer formation. In **68** however we have substituted the *tert*-butyl

groups in N-HSB with dodecyl chains which although much longer are not as bulky and allow the PAH cores to stack much closer together, thus increasing the likelihood of excimer formation which in turn leads to a decrease in fluorescence efficiency.

3.2.11. Self-association of **68** in Solution

HBC derivatives have a high polarizability, this along with the small dipole moment of the large aromatic core, means dispersion interactions are the major contributors to the interaction energy between molecules. Compound **68** is considered to have a similarly high polarizability when compare to HBC derivatives with a similar sized aromatic core. In contrast however, it is thought that the presence of the asymmetric N-atoms in **68** provide a permanent dipole induced that will assist in the anchoring of the aromatic rings within the sacks, giving head-to-tail or homotropic intra-columnar arrangement with reduced rotational disorder. These stacking interactions can be investigated by monitoring the variation in the molar absorptivity of the main bands in the UV-vis spectra of **68** at different concentrations.³⁴

The UV-visible spectra of **68** in toluene shows two types of bands, predominantly $\pi \rightarrow \pi^*$ bands at λ 342 nm, 357 nm, 397 nm, 419 nm, 466 nm and 496 nm and $n \rightarrow \pi^*$ band at 378 nm. The band at λ 357 nm has some $n \rightarrow \pi^*$, character as determined previously. On increasing the concentration of **68** the observed bands do not show significant wavelength variation, however the molar absorptivity undergoes notable changes, implying that self-association is taking place. In solution all bands show significant hypochromic deviations from the expected Beer-Lambert relationship. Ideally the changes in molar absorptivity with respect to concentration would be established for all seven bands that appear in the UV-visible spectra of **68**, however in this case it was not possible. This is because in order to obtain sufficient definition of all seven bands very dilute solutions were required. As a results analysis was undertaken for only the three most intense bands at λ 342 nm, 357 nm and 378 nm.

In Figure 66, plots of the variation of the molar absorptivity with respect to concentration are shown for the three main bands of **68** in toluene. The hypochromic behaviour of the $\pi \rightarrow \pi^*$ bands at λ 342 nm and 357 nm, labelled (a) and (b) as well as

the $n \rightarrow \pi^*$ band at λ 378 nm, labelled (c) is clearly observable. According to the theory of hypochromism in polynucleotides,¹²⁵ if the transition moments of the interacting groups are randomly orientated with respect to each other, there is no net effect on the spectrum. For an absorbing chromophore, the direction of the transition dipole moment is the direction in which the electrons are shifted in a spectral transition. The transition dipole moment of this chromophore will interact with the induced dipoles of the neighbouring chromophores, depending on their relative orientation. If the dipoles are parallel and adjacent (vertical), a decrease in intensity of the absorption band occurs and hypochromism is observed. Conversely, if the dipoles are along the same axis and one behind the other (colinear), then the intensity of the absorption band is increased, and hyperchromism is observed.

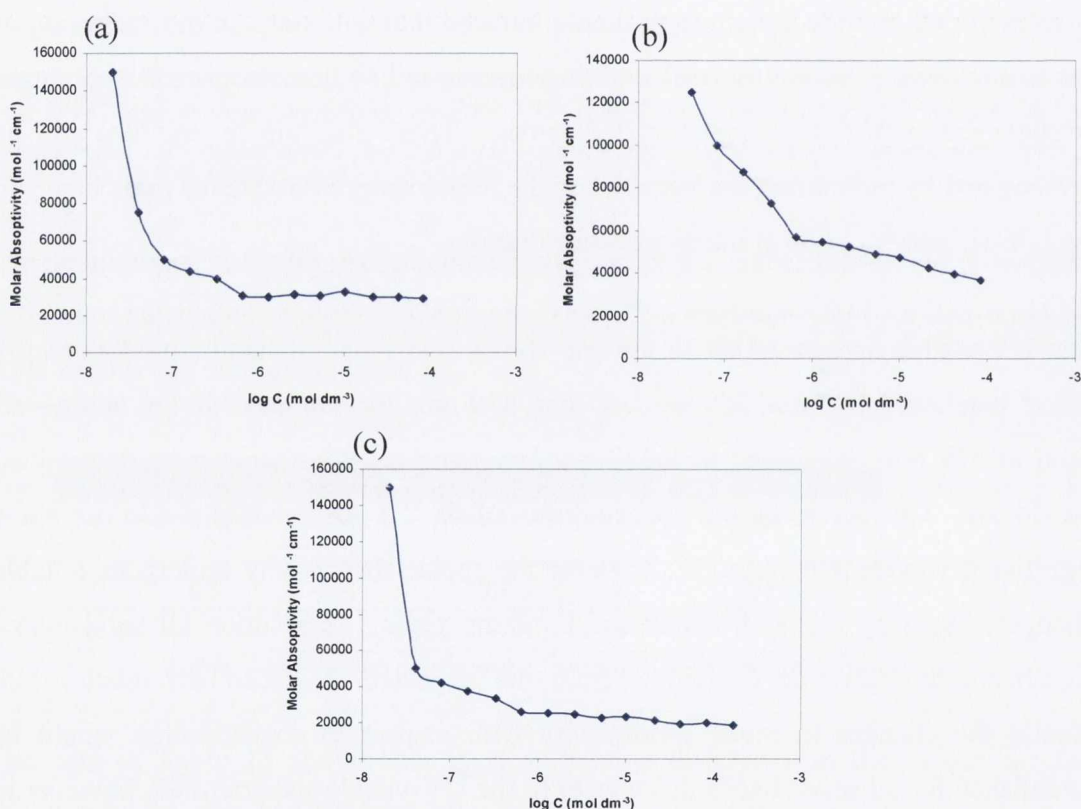


Figure 66: Hypochromic effects on the three main absorption bands of **68** in toluene, (a) λ 342 nm, (b) λ 357 nm and (c) λ 378 nm.

The plots shown in Figure 66 show clear hypochromic behaviour giving further credence to the belief that molecules **68** self-aggregate even in very dilute solutions. The mode of self-association displayed can be readily explained with regard to colinear or vertically stacked molecular interactions. The two different mechanisms of self-association can be seen in Figure 67. Colinear transition moments cause an

increase in absorption (hyperchromism), whilst parallel stacking causes a decrease in absorption (hypochromism). For molecules of **68** it would be expected that vertical stacking of **68** molecules should show hypochromism for the $\pi \rightarrow \pi^*$ bands and hyperchromism for the $n \rightarrow \pi^*$.

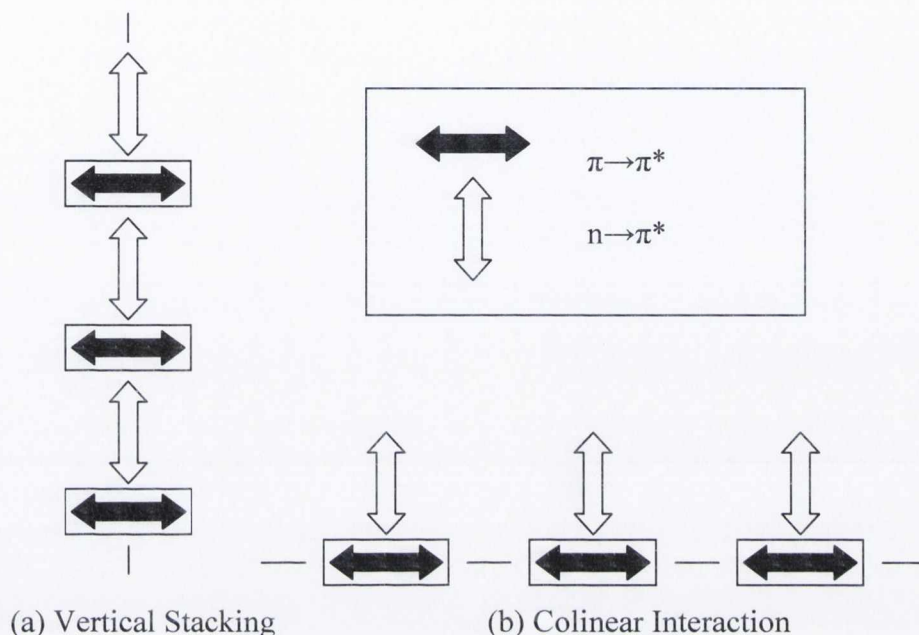
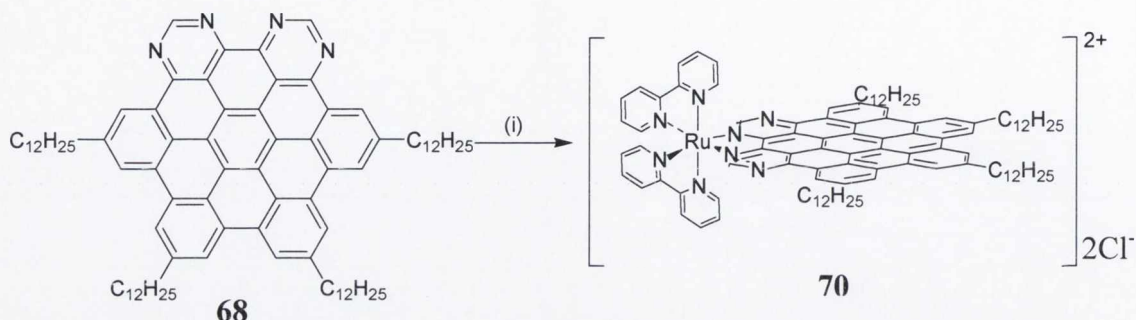


Figure 67: Models of association based on alignment of the transition dipoles of $\pi \rightarrow \pi^*$ bands (black) and $n \rightarrow \pi^*$ (unshaded).

Hypochromic behaviour in the $\pi \rightarrow \pi^*$ bands is observed for **68**, and is consistent the formation of vertical structures and the parallel stacking of the aromatic planes. This interpretation is consistent with the structure of heterosuperbenzenes, with their extensive conjugated system in which dispersion forces would be especially favoured. However, hypochromism is dominant at all three wavelengths studied, and the expected hyperchromism for the $n \rightarrow \pi^*$ band at λ 378 nm is not observed. This band is known to have some $\pi \rightarrow \pi^*$ character but the lack of observed hyperchromism could be down to the fact that the $n \rightarrow \pi^*$ band is relatively weak, or it could be involved in an interaction with the solvent molecules.³⁴

3.2.12. Ruthenium(II) Complex of **68**

tert-butyl N-HSB was produced specifically because it had ligand potential. **68** was similarly blessed with this coordinating ability and the formation of $[\text{Ru}(\text{bpy})_2(\textbf{68})]\text{Cl}_2$ (**70**) was undertaken for comparison with $[\text{Ru}(\text{bpy})_2(\text{N-HSB})]^{2+}$.³⁴



Scheme 47: The synthesis of the ruthenium(II) complex **70** from $[\text{Ru}(\text{bpy})_2\text{Cl}_2]$, (**69**).
(i) **69**, 1, 1, 2, 2-tetrachloroethane and diethylene glycol ethyl ether, 120°C , 18 h, (44 %).

Complex **70** was synthesised by heating $[\text{Ru}(\text{bpy})_2\text{Cl}_2]$ and a slight excess of **68** in a degassed mixture of 1, 1, 2, 2-tetrachloroethane and ethylene glycol ethyl ether under an argon atmosphere (Scheme 47).¹²⁶ The reaction mixture was heated to 120°C for 18 hours to form a dark green solution, which was filtered to remove any unreacted $[\text{Ru}(\text{bpy})_2\text{Cl}_2]$. Purification by column chromatography on alumina using chloroform:methanol (90:10) as the solvent system yielded the desired complex as a green-black solid in 44 % yield, which was left as the chloride salt.

The ESI-accurate mass spectrum of **70** (Figure 68) showed a single isotope envelope at m/z 806.4573 (calculated 806.4574), assigned to $[\text{M}-2\text{Cl}]^{2+}$ with peaks in the envelope at $1/2$ m.u. intervals confirming the $2+$ charge.

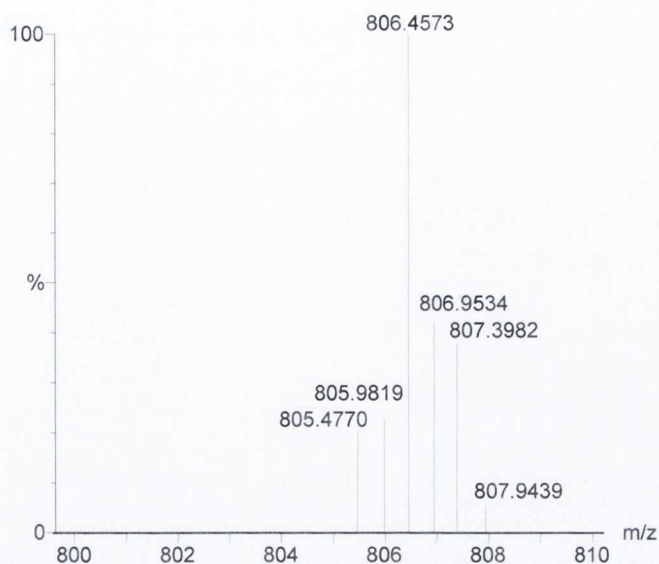


Figure 68: The ESI-mass spectrum of ruthenium complex **70** in acetonitrile.

The *tert*-butyl N-HSB analogue of **70** was known and its photophysical properties have been thoroughly investigated,¹⁷ allowing direct comparison with the UV-vis spectrum of **70**.

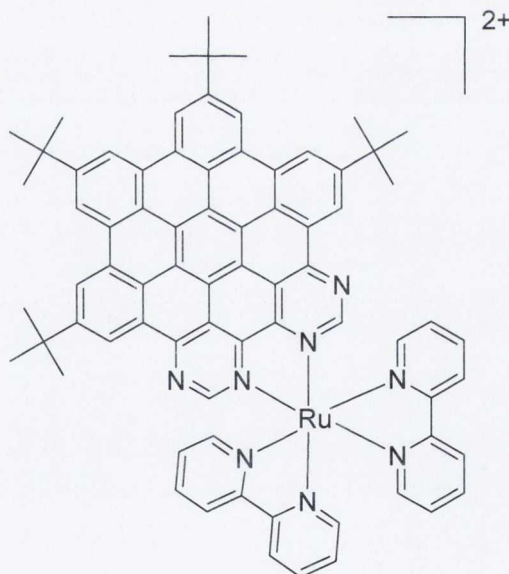


Figure 69: Representation of the *tert*-butyl analogue of **70**, $[Ru(bpy)_2(N-HSB)](PF_6)_2$. Counter ions omitted for clarity.¹⁷

The UV-vis spectra of $[Ru(bpy)_3]^{2+}$, $[Ru(bpy)_2(N-HSB)]^{2+}$ and **70** can be seen in Figure 70. The absorption spectrum of $[Ru(bpy)_3]^{2+}$, Figure 70 (i) is well known.⁸ The bands at λ 185 (not shown) and at λ 285 nm have been assigned to LC $\pi \rightarrow \pi^*$ transitions of the bpy ligands. The two remaining intense bands at λ 240 (not shown)

and 450 nm have been assigned to MLCT $d \rightarrow \pi^*$ transitions. The two shoulders between λ 300 and 350 nm are most likely due to MC $d \rightarrow d$ transitions.³⁴

Figure 70 shows that there is excellent agreement between the UV-vis spectra of $\text{Ru}(\text{bpy})_2(\text{N-HSB})]^{2+}$ and **70**. The superimposable nature of the spectra confirm beyond doubt that complete cyclodehydrogenation to **68** had occurred.

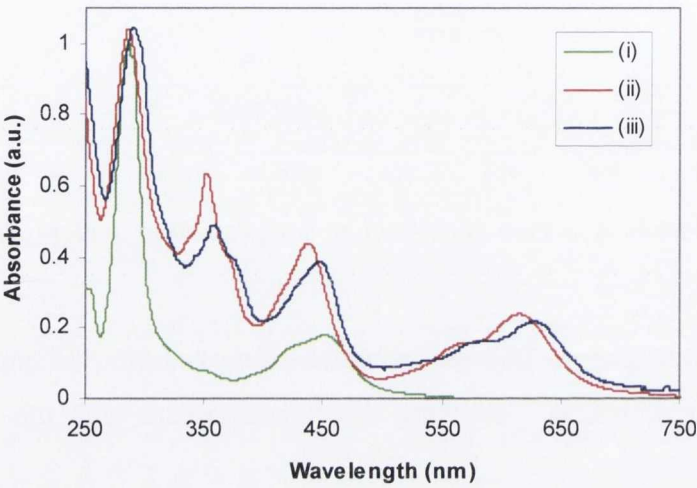


Figure 70: The absorption spectra of (i) $[\text{Ru}(\text{bpy})_3]^{2+}$, (ii) $[\text{Ru}(\text{bpy})_2(\text{N-HSB})]^{2+}$ and (iii) **70** in acetonitrile.

The principle bands shown in Figure 70 are highlighted in Table 16. As can be seen in both Figure 70 and Table 16 all the bands in **70** are red-shifted compared to those of $[\text{Ru}(\text{bpy})_2(\text{N-HSB})]^{2+}$. This could be down to the slightly increased electron donating properties of the dodecyl chains compared to the *tert*-butyl, or due to increased aggregation. An X-ray crystal structure of **70** would help in this matter as it could be compared to the already known structure of $[\text{Ru}(\text{bpy})_2(\text{N-HSB})]^{2+}$,¹²⁷ hence the distance between the aromatic cores could be calculated to see if there is increased aggregation in **70**.

70	λ_{max} (nm)	287	354	443	578	622
$[\text{Ru}(\text{bpy})_2(\text{N-HSB})]^{2+}$	λ_{max} (nm)	283	346	433	563	611

Table 16: The principle bands in the absorption spectrum of **70** and $[\text{Ru}(\text{bpy})_2(\text{N-HSB})]^{2+}$ in acetonitrile.

Analogous to other polypyridyl ruthenium complexes, the ultraviolet region of the absorption spectrum of **70** (Figure 70 (iii)) is dominated by the intra-ligand, LC $\pi \rightarrow \pi^*$ transition due to the bpy at λ 287 nm. The visible region of the spectrum is characterised by the presence of two broad $d \rightarrow \pi^*$ MLCT transitions, located at λ 443 nm (close to the corresponding transition of $[\text{Ru}(\text{bpy})_3]^{2+}$ at λ 450 nm) and at λ 622 nm, each with a less intense shoulder at shorter wavelength. The intense band at λ 443 is assigned to the MLCT due to the coordinated bpy. The red-shifted absorption band at λ 622 nm, which is not present in the free ligand is associated with promotion of a ruthenium d electron into a π^* orbital of the ligand **68**. This MLCT is considerably red-shifted compared to that of $[\text{Ru}(\text{bpy})_3]^{2+}$, because of the extended conjugation and enhanced electron affinity of ligand **68**.³⁴ Since the highly conjugated ligand, **68** is more delocalised than bpy, there are lower-lying π^* acceptor orbitals which stabilize the excited electron and lead to lower MLCT states.³⁴

These results also help to explain the unusual green colour of the Ru(II) complex **70**. Ruthenium polypyridyl complexes are usually orange due to the single MLCT absorption band in the region λ 450 nm, which absorbs blue light. Complex **70** on the other hand in an unusual strong black-green colour as a result of the spectral sum of the yellow $[\text{Ru}(\text{bpy})_3]^{2+}$ chromophore and the blue $[\text{Ru}(\text{68})]^{2+}$ chromophore.³⁴

Further photophysical characterisation of **70** was not undertaken because of the minute amounts of available complex and because this was not the focus of this work.

3.2.13. One Dimensional Charge Carrier Mobility in 68

3.2.13.1. Introduction

The direct measurement of individual electron and hole mobilities using time-of-flight (TOF) technique has proven to be possible for only a few of the many discotic materials which have been synthesised, mainly hexaalkoxy-, or hexaalkylthio-substituted derivatives of tri-phenylene.¹²⁸ A more universally applicable technique has been that of pulse-radiolysis time-resolved microwave conductivity technique (PR-TRMC), which has been applied to a large variety of discotic materials.⁹³ Over the last few years a number of HBC derivatives have been shown to exhibit excellent one dimensional charge carrier mobilities, $\Sigma\mu_{1D}$ determined *via* PR-TRMC, where $\Sigma\mu_{1D}$ are plotted as a function of the temperature. Where the same compounds have been investigated by both TOF and PR-TRMC techniques, good to reasonable agreement between the mobility values determined has been found.⁹⁷

The large HOMO-LUMO gap of >1 eV for the aromatic cores of discotics results in a extremely small concentration of intrinsic charge carriers. In order to investigate their electronic properties it is necessary to artificially introduce charge carriers. Excess charge carriers can also be produced using a short pulse of high energy (ionizing) radiation, pulse radiolysis. PR-TRMC is therefore used to study changes in materials upon irradiation, if the electron and/or holes produced are mobile, the conductivity of the material increases. This is monitored as an increase in the microwave power absorbed by the sample.

3.2.13.2. Sample Preparation and the Sample Cell

Discotic materials for PR-TRMC analysis are usually polycrystalline solids. However some materials, such as **68**, are discotic at room temperature and thus are characterised by a sticky, malleable texture. Samples are prepared for a PR-TRMC experiment by compressing the material by hand into a rectangular cell using a close-fitting PTFE rod as shown in Figure 71. The length (*ca.* 10 mm) and weight (*ca.* 200 mg) of sample are measured and used to calculate the fraction of the sample volume

actually consisting of bulk solid. When less than 200 mg of the material is available, as was the case with **68**, the sample can be compressed into a rectangular shaped cavity of dimensions 2 x 6 x 3 mm within a perspex block and a fill-factor, which is usually between 0.6 and 0.8 is used to correct the radiation-induced conductivity for the fact that the sample volume is not completely filled.

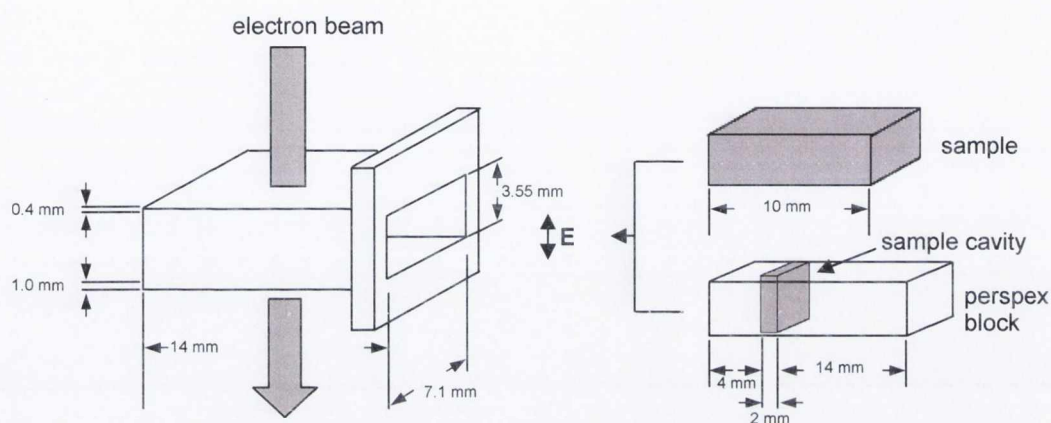


Figure 71: The PR-TRMC waveguide cell, which can be either filled completely with material or can be filled with a perspex block which has a smaller sample cavity. Also indicated is the electric field component (E) of the microwaves which is parallel to the narrow wall side of the waveguide, and determines the direction in which the conductivity is probed.

The filled cell is attached to the waveguide circuitry and is enclosed in a cryostat capable of covering a temperature range from -100 to 200 °C, which is monitored by a thermocouple which is in contact with the cell.

3.2.13.3. Formation of Mobile Charge Carriers

The cell is irradiated with a single pulse of 3 MeV from a Van de Graaff accelerator, as shown in Figure 72, which causes the formation of mobile charge carriers within the sample. Microwaves produced by a source pass to a circulator which directs the microwaves to the cell containing the sample. The microwaves penetrate the sample and are reflected at the end of the cell by a metal plate. The reflected wave is directed by the circulator to a detector which can detect rapid changes in the microwave power level. The output is monitored by a transient digitizer. When mobile charge carriers

are formed within the sample after pulse-irradiation this results in a change in the absorption of microwave power as a result of a change in the conductivity of the material.

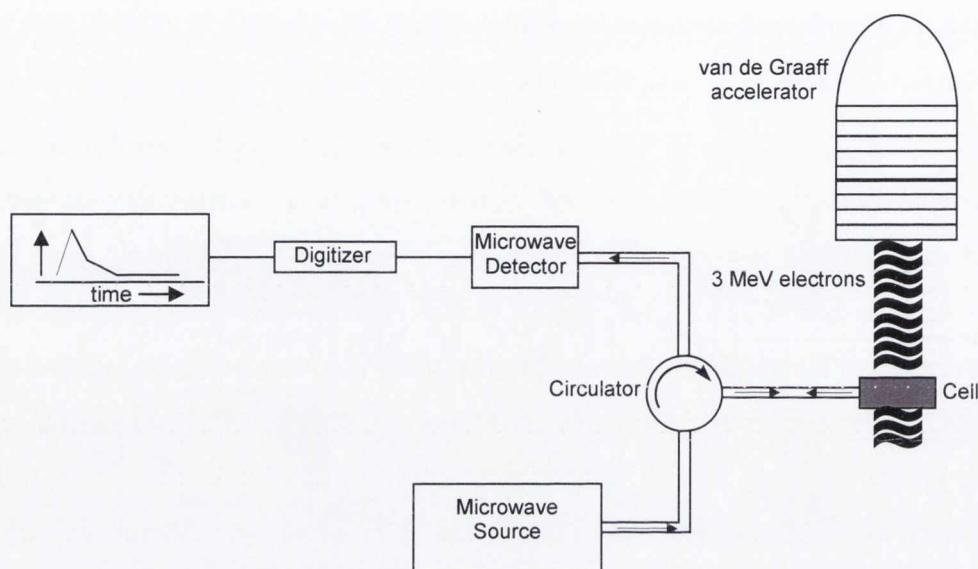


Figure 72: Schematic representation of the PR-TRMC set-up.

Therefore from a known concentration of charge carriers produced by the 3 MeV pulse (which can be calculated and related to the change in the absorption of microwave power), the mobility is determined from the end-of-pulse value of the resulting transient conductivity.¹²⁹⁻¹³⁶

3.2.13.4. Charge Carrier Mobility Results for 68

The temperature dependence of the one-dimensional charge mobility determined from the end-of pulse conductivity is shown in Figure 73 for **68**. As can be seen there is a slight rise in charge mobility as the temperature is raised but there is no dramatic phase transition at 5°C, the temperature at which there should be a phase transition according to the DSC.

When discotic materials reach the phase transition temperature, where the transition from solid to discotic takes place, there is a sudden drop in the charge mobility, the drop is usually from a maximum conductivity prior to the phase transition temperature

to a minimum just after it. This drop is then followed by a gradual increase in mobility with increasing temperature but it never reaches the value prior to the phase transition. Compound **68** however is shown to conduct, it has an average charge carrier mobility of $0.04 \text{ cm}^2 \text{ V}^{-1} \text{ s}^{-1}$ over the temperature range $-80 - 90 \text{ }^\circ\text{C}$ with a maximum charge carrier mobility of $0.05 \text{ cm}^2 \text{ V}^{-1} \text{ s}^{-1}$ at $60 \text{ }^\circ\text{C}$.

As was mentioned no evidence is found for an abrupt change in the one dimensional charge mobility of **68** at any temperature within the range studied. Even on cooling to $-80 \text{ }^\circ\text{C}$ no abrupt increase in charge mobility is observed, which is normally indicative of the formation of a crystalline phase. The charge mobilities upon heating over the temperature range can be seen in Figure 73, the cooling plot has been omitted for clarity since it overlaps exactly with the heating plot with no deviations.

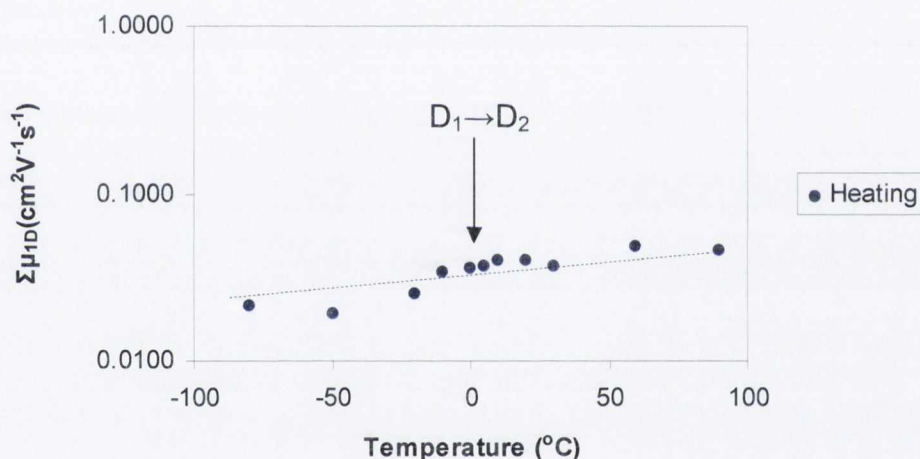


Figure 73: The temperature dependence of the intra-columnar mobility of **68**. Phase transition temperature as indicated by DSC shown as a vertical arrow.

In view of the fact that no abrupt transition was observed, it can be concluded that **68** is in fact liquid-crystalline at all temperatures studied. In support of this conclusion, the compound was found to be malleable even at room temperature. Therefore the peak at $5 \text{ }^\circ\text{C}$ in the DSC can be attributed to a conformational change within the mesophase. This makes sense and follows with other work found in the literature.

For **68** the change in enthalpy at $5 \text{ }^\circ\text{C}$ is 20 kJmol^{-1} , which is comparable to the two phase transitions seen in HBC-PhC₁₂ (28 and 16 kJmol^{-1}), which was also liquid-crystalline at all temperatures studied, and were attributed to conformational changes within the mesophase. These values are much lower than the enthalpies observed

when a transition from the crystalline to the discotic phase takes place, 78 and 99 kJ mol⁻¹, for HBC-C₁₂ and HBC-C₁₄ respectively.⁹⁶

The absence of a K phase is significant and has a direct impact on the charge carrier mobility. The all-carbon analogues HBC-C₁₂ and HBC-C₁₄ have the highest recorded charge carrier mobilities for HBCs in the K phase, however their charge carrier mobilities in the D_h phase are drastically lower. Despite this, the charge carrier mobility of discotic **68** is still lower than that measured for HBC-PhC₁₂ which is the only other HBC material that exhibits no K phase. It may be that the polarity induced by the nitrogen atoms in **68** is counterproductive and reduces the mapping or overlap of the HOMO and LUMO orbitals of adjacent molecules in the stack. Most probably the tetra-substituted **68** is less insulated than its hexa-substituted carbon counterpart. Insulation is required to reduce inter-columnar conductivity losses and to promote efficient intramolecular close-packing. Further work to promote head-to-tail molecular orientation in the stacks and to improve the insulation of the N-HSB core will be required.

3.3. Summary

By the careful modification of already known synthetic routes towards polyphenylene compounds and HBC based compounds, **68** was successfully synthesised and comprehensively characterised. To date **68** is the only reported compound that contains nitrogen atoms within the HBC core that has been shown to have quantifiable one dimensional charge carrying properties. The synthesis of molecules having unusual electronic properties has been of considerable interest in recent years. At the moment semiconductors are often extrinsically doped *via* chemical oxidation or reduction to enhance their conducting properties, however these processes have many problems associated with them. Firstly these processes are often unselective and secondly they often yield unstable materials due to the disruption caused to the structure of the material by the doping agent. However the research presented here provides the possibility for doping HBCs with nitrogen atoms in a very controlled and logical manner. The nitrogen atoms are actually an intrinsic part of the HBC core.

The synthetic route towards the synthesis of **68** allows us to produce N-doped graphite analogues, building on the known stereochemistry associated with the [2 + 4]-cycloaddition reaction as well as the cyclodehydrogenation of the polyphenylene products of the [2 + 4]-cycloaddition reaction, yielding an N-doped HBC platform. Compound **68** combines in a complementary manner the properties of superbenzene with those of bipyrimidine, yielding a molecule with enhanced π -electron mobility which is evident from the planar nature of the molecule. A factor that usually inhibits the application of HBCs is that they are generally insoluble in most common solvents, this has also been overcome in **68** by the inclusion of the four nitrogen atoms and the long aliphatic dodecyl chains.

Since the nitrogens are an intrinsic part of the HBC core there is no loss in stability as is seen when external doping agents are introduced into a material. TGA of **68** indicates that apart from mass loss due to solvents no decomposition is seen until *ca.* 470 °C at which point the flexible long-alkyl chains are lost. The DSC also confirms this excellent thermal stability since when scanning between -30 - +300 °C no decomposition is observed and the DSC traces are very reproducible.

Both the absorption and emission properties of **68** are presented. The absorption and emission spectra are in general similar to other HBC derivatives and compare well to those observed for N-HSB. When compared to HBC **60** significant solvent induced shifts can be observed, which are due to the presence of the additional excited states introduced by the nitrogen atoms. When comparing the UV-vis spectra of **68** with that of N-HSB they are virtually superimposable, photophysical properties of the chromophore are little changed on converting the *tert*-butyl groups in N-HSB to dodecyl chains in **68**. However dodecyl chains in **68** are considerably less bulky than *tert*-butyl groups and as a result stronger aggregates are formed at very low concentrations, therefore the absorption spectra of **68** are less resolved at higher concentrations than those of N-HSB as a result.

The fluorescence spectra of **68** are also discussed and compared to HBC **60**, the main difference is the enhancement of the 0-0 transition, which was expected upon the removal of molecular symmetry from D_{6h} for **60** to C_{2v} for **68**. Addition of trifluoroacetic acid to toluene solutions of **68** causes strong changes in the absorbance and fluorescence spectra. The low energy absorption bands are red-shifted, and the intensity of the structured, short lived $^1(\pi, \pi^*)$ fluorescence band decreases and a new unstructured shorter-lived fluorescence band is observed at longer wavelength.

The probable formation of exciplexes and excimers of **68** are also discussed. Aniline forms an exciplex with **68**, which upon incremental addition of aniline leads to the total quenching of the fluorescence. Compound **68** was also found to have a considerably smaller fluorescent quantum yield than its *tert*-butyl analogue, N-HSB. This was explained in terms of excimer formation which in turn decreases the fluorescence efficiency in solution.

The aggregation of **68** was investigated, and it was shown that molecules of **68** do indeed aggregate strongly in solution at extremely low concentrations. Hypochromic behaviour in all the $\pi \rightarrow \pi^*$ bands is observed, which is consistent with the formation of vertical structures and the parallel stacking of the aromatic planes.

The one dimensional charge carrier mobility of **68** was determined by pulse-radiolysis time-resolved microwave conductivity technique (PR-TRMC). It was shown to

conduct and to have an average charge carrier mobility of $0.04 \text{ cm}^2 \text{ V}^{-1} \text{ s}^{-1}$ over the temperature range $-80 - +90 \text{ }^\circ\text{C}$ with a maximum charge carrier mobility of $0.05 \text{ cm}^2 \text{ V}^{-1} \text{ s}^{-1}$ at $60 \text{ }^\circ\text{C}$. Although this is significantly lower than the charge carrier mobilities observed for all-carbon HBCs, it is the only reported compound to date that contains nitrogen atoms (or any heteroatom for that matter) within the HBC core that has been shown to have charge carrying properties. Another interesting property of **68** is that it is liquid-crystalline at all temperatures studied and was found to be malleable even at room temperature. Only one other HBC based compound in the literature has been reported to be liquid-crystalline at all temperatures studied.

The combination of the highly coordinating bipyridyl functionality and the extended conjugation, through the π -electron system, provides an exciting and unique family of tuneable fluorophores. Compound **68** as well as other N-doped HBC compounds synthesised within the group are part of an ever growing family and can be considered as models of active graphitic nanostructures with electroactive nitrogens on the periphery. The incorporation of nitrogen atoms within the HBC framework renders these materials sensitive towards external triggers and enhances their solubility.

In conclusion the synthetic methodology adopted towards the synthesis of **68** have been proven. The presence of the nitrogen atoms has rendered overall electron-accepting properties to **68** compared to its all-carbon analogue, **60**. Although the one dimensional charge carrier mobility is not as high as that for **60**, there is no doubt that the successful synthesis of **68** will be an important step towards synthesising N-doped HBCs with excellent conducting properties in the future.

3.4. Future Work

The successful synthesis of **68** opens up possibilities in the development of the N-HSB family. There remain additional techniques for consideration of the solid state and conductivity properties of **68** e.g. variable temperature powder X-ray diffraction analysis could be carried out on **68** to yield structural information and possibly to identify a low temperature crystalline phase for comparison with the single X-ray crystallographic data for N-HSB. DSC and PR-TRMC have shown that 5 °C marks the transition temperature of a conformational change within the mesophase. X-ray powder diffraction at temperatures above and below the transition temperature should provide structural information regarding this change.

N-HSB compounds such as **68** contain donor and acceptor end groups, connected by an unsaturated conjugated unit and highly delocalised molecular orbitals that are characterised by small energy separation between ground and excited states. Excitation results in the appearance of very strong absorption bands, a redistribution of electronic charge within the molecule, and a change in molecular dipole moment. This might be expected to give the systems interesting NLO properties and warrants further investigation.

All-carbon C₁₂H₂₅-HBC has different properties to **68**, therefore the chains and the heteroatom are having an effect. Therefore future efforts should focus on developing N-doped HBCs with improved charge carrier mobilities compared to **68**, and to approach the values obtained for all-carbon analogues. The use of differing ligand substitution patterns, electron-donating (which activates cyclodehydrogenation³⁵) and branched-chain ligands could be explored to investigate their influence on the nature of the aggregation in solution, solid and liquid crystalline forms of the molecules.

Table 17 shows the significant effect that altering the alkyl chains on the periphery of the all-carbon HBC core has on the one dimensional mobility.¹³⁷ Therefore a series of compounds exactly like **68** is required, but incorporating different alkyl groups on the periphery. These compounds are essential to establish if a trend exists in the charge mobilities of these N-doped systems as is observed with the all-carbon HBCs when the alkyl groups are altered.

R group	$\Sigma\mu_{1D}$ (cm ² V ⁻¹ s ⁻¹)	
	D _h phase (max)	K phase (max)
-C ₁₄ H ₂₉	0.31	1.13
-C ₁₂ H ₂₅	0.38	0.96
-C ₁₀ H ₂₁	0.26	0.55
-C _{8,2} *	0.26	0.54
-C _{8,2}	0.62	0.30
-PhC ₁₂ H ₂₅	0.46	---

C8,2* =

C8,2 =

Table 17: Maximum one dimensional mobilities, $\Sigma\mu_{1D}$, determined for the discotic (D_h) and crystalline (K) phases for a range of alkyl substituted HBCs.¹³⁷

It is known that insulation is required around HBC cores to reduce inter-columnar conductivity losses and to promote efficient intramolecular close-packing. However should the series of compounds mentioned above still have mobilities significantly lower than the all-carbon systems, the lack of insulation at the nitrogen end of the HBC core would require investigation. This could be done by again synthesising an analogue **68** but with swallow-tailed alkyl chains on the periphery, as shown in Figure 74. This could be readily done *via* a similar route as for **68** only changing the dodecyl group for the -C_{10,6} group at an early synthetic stage. Incorporation of these swallow-tailed alkyl groups should offer more insulation from adjacent cores than is the case with the dodecyl chains in **68**.

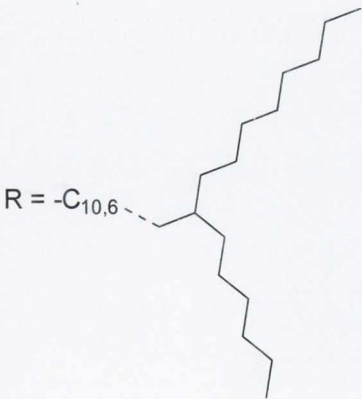
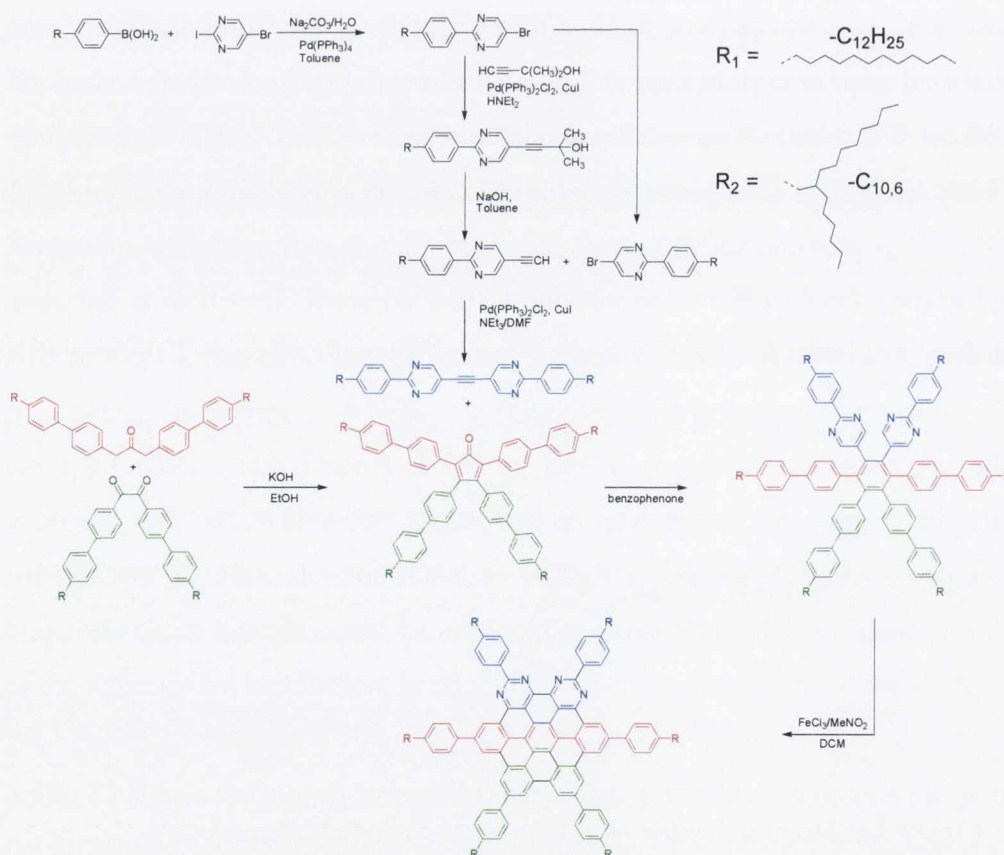


Figure 74: Structure of the -C_{10,8}, swallow-tailed alkyl group.¹³⁸

These swallow-tailed groups have already been incorporated on to the periphery of triangle-shaped discotic graphenes by Mullen *et al.*¹³⁸ and have been shown to aid

purification, allow control over the thermotropic properties and help solution fabrication into efficient photovoltaic devices. They have also been shown to produce discotic materials with extremely broad liquid crystalline ranges.

If the charge mobility of the swallow-tailed analogue of **68** is still significantly lower than the all-carbon systems shown in Table 17, this would imply that there is still insufficient insulation at the nitrogen end of the HBC core. This could only be overcome by complete insulation of the HBC core as shown in Scheme 48. The two molecules shown in Scheme 48 represent two possibilities that could be synthesised following the same general synthetic route as that undertaken in the synthesis of **68**. It is hoped that the full insulation of the N-doped cores as compared to **68** will reduce the inter-columnar conductivity losses whilst the long alky chains should still promote efficient intramolecular close packing.



*Scheme 48: Two possible N-doped systems which could be synthesised employing the route utilised in the synthesis of **68**.*

However the synthesis of these two molecules could prove to be very difficult and it is not known if these types of systems with substituents between the pyrimidyl nitrogens will allow successful cyclodehydrogenation.

It is hoped in the future that molecules based on the N-HSB motif will offer a technology platform for further research. When applied to devices it is hoped that these molecules will become new molecular materials in opto-electronic devices (e.g. Light Emitting Diodes) and as tuneable luminescent materials. It is hoped that these materials one day will help satisfy current trends in the miniaturisation of electronic devices and future demands for low-cost, flexible and energy-efficient photonic devices.

Chapter 4: Experimental

4.1. General Methods

Unless otherwise stated, all reactions were carried out under an argon atmosphere using standard schlenk techniques. All solvents were distilled under nitrogen from appropriate drying agents and degassed prior to use. Flash chromatography was performed using silica gel (Fluka 60) or activated alumina (Brockman I, Aldrich Chemical) as the stationary phase, all separations were carried out in air. Chemicals were purchased from Sigma-Aldrich Chemical Co. Ltd. and were used without further purification.

Electrospray mass spectra were recorded on a micromass LCT tof electrospray mass spectrometer. Accurate mass spectra were recorded against Lucine Enkephalin (555.6 g mol^{-1}) and reported to within 5 ppm. MALDI-TOF mass spectra were recorded on a Waters MALDI-QTOF Premier spectrometer using an α -cyano-4-hydroxy cinnamic acid matrix. Accurate mass spectra were referenced against [Glu¹]-Fibrinopeptide B ($1570.6 \text{ g mol}^{-1}$) and reported to within 5 ppm. NMR spectra were recorded in CDCl_3 , CD_2Cl_2 , $\text{C}_2\text{D}_2\text{Cl}_4$ or CD_3CN with (i) a Bruker Avance DPX-400 MHz spectrometer at the following frequencies: 400.13 MHz for ^1H and 100.6 MHz for ^{13}C , (ii) an AV-400 MHz spectrometer at 400.23 MHz for ^1H and 100.6 MHz for ^{13}C or (iii) an AV-600 MHz spectrometer at 600.13 MHz for ^1H and 150.6 MHz for ^{13}C . The signals for ^1H and ^{13}C spectra were referenced to TMS at δ 0.00, coupling constants were recorded in hertz (Hz) to one decimal place. All 1-D ^1H and ^{13}C spectra were recorded using the Bruker Avace 400 MHz spectrometer unless otherwise stated. ^{13}C signals were assigned with the aid of DEPT experiments. 2-D correlation spectra were recorded on the AV-400 MHz spectrometer or the AV-600 MHz spectrometer and were employed to assign ^1H and ^{13}C peaks. Homonuclear correlation spectroscopy was performed using TOCSY or ^1H - ^1H COSY experiments, heteronuclear correlation spectroscopy was performed using HSQC, HMQC or HMBC (long-range) experiments.

Cyclic Voltammetry was performed using a CH instruments electrochemical analyser model 600B and a conventional three-electrode cell with a Ag/AgCl (sat. KCl) reference electrode. All solutions were degassed with N_2 before measurements were taken and a blanket of N_2 was maintained over the solution for the duration of the

experiment. Tetrabutylammonium hexafluorophosphate was used as the supporting electrolyte for all the experiments.

All photophysical studies were carried out with solutions contained within $1 \times 1 \text{ cm}^2$ quartz cells in HPLC grade solvents and were degassed using N_2 bubbling. UV-visible absorption spectra were recorded on a Shimadzu UV-2450 spectrophotometer and the data analysed using UVProbe software. Fluorescence spectra were recorded on a Varian Cary Eclipse luminescence spectrometer. Emission quantum yields were measured in reference to Coumarin 153 in methanol.

Details of the instrumentation and methods employed for the determination of the charge carrier mobility *via* pulse-radiolysis time-resolved microwave conductivity (PR-TRMC) can be seen in chapter 3 (which was carried out at TU Delft in the Netherlands).

4.2. Experimental Procedures

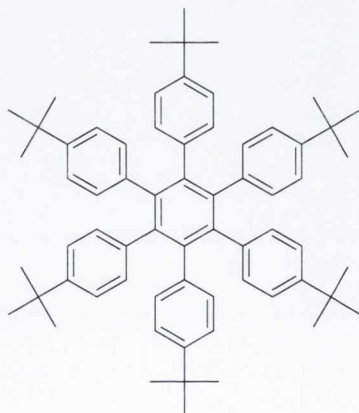
4.2.1. Synthesis of di(4-*tert*-butylphenyl)acetylene (1)



Tetrakis(triphenylphosphine)palladium (0.48 g, 0.42 mmol) and copper(I) iodide (0.16 g, 0.85 mmol) were dissolved in piperidine (250 mL). To this 4-*tert*-butyl-iodobenzene (4.4 g, 16.9 mmol) was added and allowed to stir at room temperature for 30 minutes, after which time 4-*tert*-butylphenylacetylene (2.67 g, 16.9 mmol) was added and the reaction was allowed to stir at room temperature for a further 24 hours. The mixture was diluted with dichloromethane (200 mL), washed with a saturated ammonium chloride solution (2 x 200 mL) and water (2 x 200 mL) and then dried over magnesium sulphate. The solvent was removed *in vacuo* and the residue recrystallised from methanol/ethanol (1:1) to furnish the desired product as colourless crystals.

Yield: 3.8 g, 78 %. **M.pt:** 178-179 °C. **¹H NMR** (CDCl₃) δ: 7.49 (d, 4 H, ³J_{HH} = 8.0 Hz, -CH Ar), 7.39 (d, 4 H, ³J_{HH} = 8.0 Hz, -CH Ar), 1.36 (s, 18 H, -C(CH₃)₃). **¹³C NMR** (CDCl₃) δ: 150.87 (2 C, quat Ar), 130.84 (4 C, -CH Ar), 124.87 (4 C, -CH Ar), 120.02 (2C, quat Ar), 88.41 (2 C, quat Ar), 34.33 (2 C, quat, -C(CH₃)₃), 30.76 (6 C, -CH, -C(CH₃)₃).

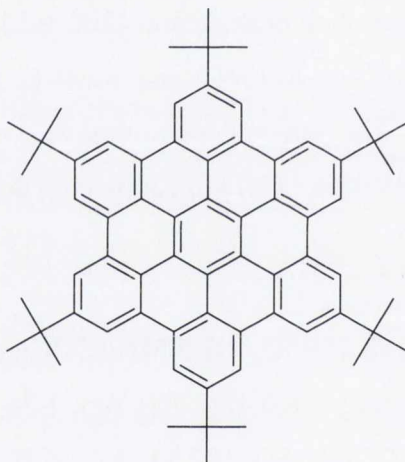
4.2.2. Synthesis of hexa(4-*tert*-butylphenyl)benzene (2)



Di(4-*tert*-butylphenyl)acetylene (0.8 g, 2.76 mmol) and cobalt octacarbonyl (0.03 g, 0.08 mmol) were placed in a round-bottomed flask, dioxane (40 mL) was injected and the mixture was refluxed for 20 hours. Once the time had elapsed the reaction mixture was allowed to cool to room temperature and the crystalline precipitate was filtered off and dissolved in CS₂. Filtration of this solution and removal of the solvent under reduced pressure afforded the desired compound as colourless crystals.

Yield: 0.14 g, 18 %. **M.pt:** >300 °C. **¹H NMR at 60°C** (C₂D₂Cl₄) δ: 6.75 (d, 12 H, ³J_{HH} = 8.0 Hz, -CH Ar), 7.65 (d, 12 H, ³J_{HH} = 8.0 Hz, -CH Ar), 1.07 (s, 54 H, -C(CH₃)₃).

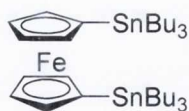
4.2.3. Synthesis of hexa-*tert*-butyl-hexa-*peri*-hexabenzocoronene (3)



A solution of iron(III) chloride (1.16 g, 7.2 mmol) in nitromethane (2 mL) was added dropwise to a stirred solution of hexa(4-*tert*-butylphenyl)benzene (0.13 g, 0.15 mmol) in dichloromethane (65 mL). The resulting green reaction mixture was stirred for 18 hours at room temperature and then quenched with methanol (10 mL). The solution was washed with 5N hydrochloric acid (5 x 150 mL), water (2 x 100 mL) and dried over MgSO₄. Filtration over silica gel with dichloromethane afforded the desired product as a yellow solid.

Yield: 0.08 g, 62 %. **M.pt:** >300 °C. **¹H NMR** (CDCl₃) δ: 9.34 (s, 12 H, -CH Ar), 1.85 (s, 54 H, -C(CH₃)₃). **¹³C NMR** (CDCl₃) δ: 148.88 (6 C, quat Ar), 130.38 (12 C, quat Ar), 123.88 (6 C, quat Ar), 120.35 (6 C, quat Ar), 118.76 (12 C, -CH Ar), 35.58 (6 C, quat, -C(CH₃)₃), 31.88 (18 C, -CH, -C(CH₃)₃).

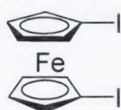
4.2.4. Synthesis of 1,1'-(tri-*n*-butylstannyl)ferrocene (4)



A schlenck was charged with ferrocene (1.71 g, 9.22 mmol) as a suspension in hexane (25 mL). This suspension was lithiated with two equivalents of *n*-BuLi (12.2 mL, 1.6 M, 19.44 mmol) which was added over the course of 10 minutes. The suspension was then treated with two equivalents of tetramethylethylenediamine and allowed to stir at room temperature overnight. The pale orange powder was then isolated *via* canular filtration and dried under vacuum. To this powder, diethylether (20 mL) was added at 0 °C. This slurry was treated with tributyltinchloride (6 g, 18.44 mmol, 5 mL) and was then allowed to warm to room temperature over a six hour period. The diethylether layer was washed with water and NaCl and dried over MgSO₄. The solvent was removed to afford a crude product, which contained varying amounts of ferrocene, mono-(tri-*n*-butylstannyl)ferrocene, and 1, 1'-(tri-*n*-butylstannyl)ferrocene. 1, 1'-(tri-*n*-butylstannyl)ferrocene was isolated by column chromatography on silica. Elution with hexane yielded the desired product as a brown oil.

Yield: 4.7 g, 67 %. **¹H NMR** (CDCl₃) δ: 4.27 (m, 4 H, -CH Fc), 4.00 (m, 4 H, -CH Fc), 1.60 (m, 12 H butyl), 1.40 (m, 12 H butyl), 1.05 (m, 12 H butyl), 0.95 (t, 18 H butyl). **¹³C NMR** (CDCl₃) δ: 73.77 (4 C, -CH Fc), 70.00 (4 C, -CH Fc), 68.27 (2 C, quat Fc), 28.79 (6 C, -CH butyl), 27.01 (6 C, -CH butyl), 13.29 (6 C, -CH butyl), 9.80 (6 C, -CH butyl). **ESI-MS** (methanol); for C₃₄H₆₂FeSn₂: [M]⁺ calculated *m/z* 766.2245, found *m/z* 766.2261.

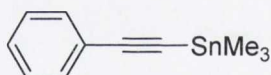
4.2.5. Synthesis of 1, 1'-iodoferrocene (5)



Iodine (2.8 g, 10.1 mmol) was added to **4** (3.83 g, 5 mmol) in dichloromethane (40mL). The solution was stirred for 18 hours at room temperature. It was then washed with aqueous sodium thiosulphate solution (10% w/v) and filtered through neutral alumina. After removal of the solvents, the crude product was taken up in methanol and potassium fluoride (1 g) was added to precipitate out any stannylated by-products, which were eliminated by filtration through neutral alumina. After evaporation of the methanol, the product was extracted with diethylether, washed with water and dried over MgSO_4 . Removal of the solvents afforded pure 1, 1'-iodoferrocene as a brown oil.

Yield: 1.66 g, 76 %. $^1\text{H NMR}$ (CDCl_3) δ : 4.40 (s, 4 H, -CH Fc), 4.20 (s, 4 H, -CH Fc). $^{13}\text{C NMR}$ (CDCl_3) δ : 77.14 (4 C, -CH Fc), 71.86 (4 C, -CH Fc), 39.94 (2 C, quat Fc). **ESI-MS** (methanol); for $\text{C}_{10}\text{H}_8\text{FeI}_2$: $[\text{M}]^+$ calculated m/z 437.8065, found m/z 437.8083.

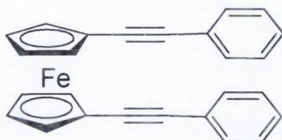
4.2.6. Synthesis of phenylalkynyltrimethylstannane (6)



Phenylacetylene (0.93 g, 9.1 mmol, 1 mL) was dissolved in tetrahydrofuran (10 mL) and cooled to -78°C . To this solution was added $n\text{-BuLi}$ (5.7 mL, 9.12 mmol, 1.6 M) and the mixture was allowed to stir for 20 minutes at 0°C , after which trimethyltinchloride (9.1 mL, 9.1 mmol) was used to quench the reaction. After stirring for an hour at 20°C the solvent was removed. The crude product was then dissolved in hexane and washed with water. Transparent crystals of phenylalkynyltrimethylstannane were obtained by slow evaporation of hexane.

Yield: 1.63 g, 68 %. $^1\text{H NMR}$ (CDCl_3) δ : 7.50-7.48 (m, 2 H, -CH Ar), 7.31 (m, 3 H, -CH Ar). $^{13}\text{C NMR}$ (CDCl_3) δ : 131.47 (2 C, -CH Ar), 127.72 (2 C, -CH Ar), 127.63 (1 C, -CH Ar), 123.11 (1 C, quat Ar), 108.47 (1 C, quat, $-\text{C}\equiv\text{C}$), 92.92 (1 C, quat, $-\text{C}\equiv\text{C}-$), -8.10 (3 C, $-\text{CH}_3$).

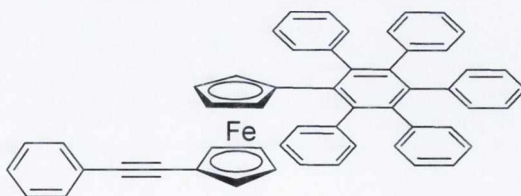
4.2.7. Synthesis of 1, 1'-bis(phenylethynyl)ferrocene (7)



To a stirred solution of **5** (0.8 g, 1.83 mmol) in tetrahydrofuran (65 mL) was added **6** (1.2 g, 4.47 mmol) followed by tetrakis(triphenylphosphine)palladium (0.0416 g, 0.036 mmol). The mixture was allowed to stir at 75 °C for 20 hours during which time the solution darkened and gave a dark red-brown suspension. It was evaporated to dryness, and then subjected to column chromatography on neutral grade II alumina. Elution with hexane gave an orange band containing unchanged starting material. Elution with hexane:dichloromethane (3:1) gave a yellow-orange band which was evaporated to dryness to leave 1, 1'-bis(phenylethynyl)ferrocene.

Yield: 0.35 g, 50 %. **¹H NMR** (CDCl₃) δ: 7.47-7.44 (m, 4 H, -CH Ar), 7.30-7.29 (m, 6 H, -CH Ar), 4.58 (s, 4 H, -CH Fc), 4.36 (s, 4 H, -CH Fc). **¹³C NMR** (CDCl₃) δ: 130.99 (4 C, -CH Ar), 127.7 (4 C, -CH Ar), 127.22 (2 C, -CH Ar), 123.34 (2 C, quat Ar), 86.79 (2 C, quat, -C≡C-), 86.16 (2 C, quat, -C≡C-), 72.56 (4 C, -CH Fc), 70.54 (4 C, -CH Fc), 66.55 (2 C, quat Fc). **ESI-MS** (methanol); for C₂₆H₁₈Fe: [M]⁺ calculated *m/z* 386.0758, found *m/z* 386.0776.

4.2.8. Synthesis of 1-(1,2,3,4,5-pentaphenyl-6-ferrocenyl-benzene)-1'-phenylacetylene (8)



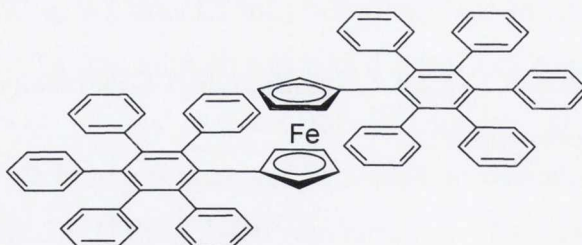
Compound **7** (128 mg, 0.332 mmol), benzophenone (0.8 g) and tetraphenylcyclopentadienone (281 mg, 0.731 mmol) were mixed in a round bottomed flask and attached to an air condenser. The mixture was heated at 175 °C for 2 days. The mixture was then subjected to flash column chromatography on silica using

hexane:dichloromethane (2:1) as eluent. The orange band was collected and evaporated to afford the desired product as a light coloured orange solid.

Yield: 0.11g, 44%. **M.pt:** 239-240 °C. **^1H NMR** (CD_2Cl_2) δ : 7.45-7.44 (m, 2 H, -CH Ar), 7.38-7.36 (m, 3 H, -CH Ar), 7.19-7.09 (m, 10 H, -CH Ar), 6.83-6.79 (m, 15 H, -CH Ar), 4.11 (t, 2 H, $^3J_{\text{HH}} = 1.8$ Hz, -CH Fc), 3.94 (t, 2H, $^3J_{\text{HH}} = 1.8$ Hz, -CH Fc), 3.78 (t, 2 H, $^3J_{\text{HH}} = 1.8$ Hz, -CH Fc), 3.68 (t, 2 H, $^3J_{\text{HH}} = 1.8$ Hz, -CH Fc). **^{13}C NMR** (600 MHz) (CDCl_3) δ : 141.67 (1 C, quat Ar), 141.47 (1 C, quat Ar), 141.39 (1 C, quat Ar), 140.64 (1 C, quat Ar), 140.46 (1 C, quat Ar), 139.62 (1 C, quat Ar), 136.73 (1 C, quat Ar), 133.08 (1 C, quat Ar), 131.94 (2 C, -CH Ar), 131.21 (2 C, -CH Ar), 131.07 (2 C, -CH Ar), 130.84 (2 C, -CH Ar), 128.11 (2 C, -CH Ar), 126.61 (2 C, -CH Ar), 126.35 (1 C, -CH Ar), 126.12 (2 C, -CH Ar), 126.09 (2 C, -CH Ar), 125.75 (1 C, -CH Ar), 124.81 (1 C, -CH Ar), 88.37 (1 C, quat, $-\text{C}\equiv\text{C}-$), 87.79 (1 C, quat Fc), 85.56 (1 C, quat, $-\text{C}\equiv\text{C}-$), 84.20 (1 C, quat Fc), 74.11 (2C, -CH Fc), 71.98 (2C, -CH Fc), 70.60 (2C, -CH Fc), 69.92 (2C, -CH Fc). **ESI-MS** (methanol); for $\text{C}_{54}\text{H}_{38}\text{Fe}$: $[\text{M}]^+$ calculated m/z 742.2323, found m/z 742.2297. **IR** ν (cm^{-1}): $\nu(\text{C-H st, aromatic})$: 3079, 3053, 3023, $\nu(\text{C}\equiv\text{C st})$: 2207, $\nu(\text{C}=\text{C st})$: 1599, 1494, 1441, $\nu(\text{C-H rock Fc})$: 1070, 1026, 1010.

4.2.9. Synthesis of 1,1'-di-(1,2,3,4,5-pentaphenyl-6-ferrocenyl-benzene)

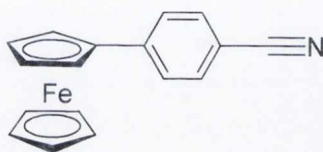
(9)



Compound **7** (128 mg, 0.332 mmol), benzophenone (1 g) and tetraphenylcyclopentadienone (281 mg, 0.731 mmol) were mixed in a round bottomed flask and attached to an air condenser. The mixture was heated at 175 °C for 3 days. The mixture was then subjected to flash column chromatography on silica using hexane:dichloromethane (2:1) as eluent. The orange band was collected and evaporated to afford the desired product as a light coloured orange solid.

Yield: 65 mg, 18 %. **M.pt:** >200 °C (decomp.). **¹H NMR** (CDCl₃) δ : 7.00 (m, 20 H, -CH Ar), 6.78 (m, 30 H, -CH Ar), 3.43 (s, 4 H, -CH Fc), 3.19 (s, 4 H, -CH Fc). **ESI-MS** (toluene); for C₈₂H₅₈Fe: [M]⁺ calculated m/z 1098.3888, found m/z 1098.3873. **IR** ν (cm⁻¹): ν (C-H st, aromatic): 33078, 3053, 3022, ν (C=C st): 1599, 1464, ν (C-H rock Fc): 1073, 1027.

4.2.10. Synthesis of 4-ferrocenylbenzonitrile (10)



Ferrocene (3.80 g, 20.4 mmol) was added to sulphuric acid (25 mL, spec. grav. 1.84) and the resulting deep blue ferrocenium solution was stirred at room temperature for 2 hours. The solution was then poured into ice/water (100 mL) and allowed to warm to room temperature.

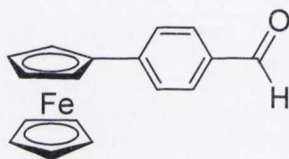
A solution of sodium nitrite (0.91 g, 13.2 mmol) in water (5 mL) at 0 °C was added dropwise to a stirred solution of 4-aminobenzonitrile (1.42 g, 12.0 mmol) in 1:1 water/hydrochloric acid (spec. grav. 1.18) (10 mL) at 0 °C and stirred at this temperature for 30 minutes to ensure full diazotization. Copper powder (1.0 g) was added to the ferrocenium solution and the diazonium solution was added dropwise with vigorous stirring.

After 24 hours stirring at room temperature, effervescence due to liberated nitrogen had ceased and ascorbic acid (5 g) was added to the dark mixture to reduce any remaining ferrocenium to ferrocene. Dichloromethane (100 mL) was added and the organic layer separated. The aqueous layer was extracted further with dichloromethane (4 x 50 mL), and the combined organic extracts were filtered through Celite before removal of the solvent *in vacuo* to give a dark solid. This was subjected to column chromatography using gradient elution. The first yellow fraction, eluted with hexane, yielded unchanged ferrocene. The second orange-red fraction,

eluted with 60/40 (dichloromethane/hexane) gave upon evaporation of solvents the desired product as an orange-red microcrystalline solid.

Yield: 1.22 g, 35 %. **M.pt:** 140-142 °C. **^1H NMR** (CDCl_3) δ : 7.58 (d, 2 H, $^3J_{\text{HH}} = 8.5$ Hz, -CH Ar), 7.54 (d, 2 H, $^3J_{\text{HH}} = 8.5$ Hz, -CH Ar), 4.72 (t, 2H, $^3J_{\text{HH}} = 2.0$ Hz, -CH Fc), 4.45 (t, 2H, $^3J_{\text{HH}} = 2.0$ Hz, -CH Fc), 4.07 (s, 5 H, -CH Fc). **^{13}C NMR** (CDCl_3) δ : 145.16 (1 C, quat Ar), 131.73 (2 C, -CH Ar), 125.75 (2 C, -CH Ar), 118.99 (1 C, quat Ar), 108.30 (1C, quat, $-\text{C}\equiv\text{N}$), 81.91 (1C quat Fc), 69.76 (2 C, -CH Fc), 69.47 (5C, -CH Fc), 66.47 (2C, -CH Fc). **ESI-MS** (toluene); for $\text{C}_{17}\text{H}_{13}\text{FeN}$: $[\text{M}]^+$ calculated m/z 287.0397, found m/z 287.0390.

4.2.11. Synthesis of 4-ferrocenylbenzaldehyde (**11**)

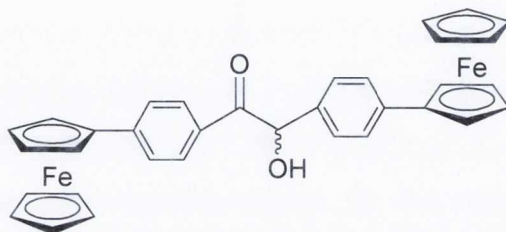


A solution of DIBAL (*diisobutylaluminiumhydride*; 1.0 M in dry dichloromethane, 10.5 mL) was added dropwise to a stirred solution of **10** (3 g, 10.45 mmol) in dry toluene (60 mL) at room temperature. Addition was complete after 15 minutes. The solution was stirred for a further 6 hours then methanol (45 mL) was added to destroy any residual DIBAL. Aqueous sulphuric acid (10 %, 60 mL) was added to hydrolyse the intermediate imine complex and the solution was extracted with dichloromethane (5 x 100 mL). The organic extracts were combined and evaporated to yield the crude product. This was purified by column chromatography with an 80/20 (dichloromethane/hexane) solution as eluent. The first fraction (red/orange) was 4-ferrocenylbenzonitrile, and the second fraction (orange) yielded the desired product.

Yield: 2.77 g, 91 %. **^1H NMR** (CDCl_3) δ : 9.99 (s, 1 H, -CHO), 7.81 (d, 2 H, $^3J_{\text{HH}} = 8.0$ Hz, -CH Ar), 7.61 (d, 2H, $^3J_{\text{HH}} = 8.0$ Hz, -CH Ar), 4.76 (t, 2 H, $^3J_{\text{HH}} = 1.8$ Hz, -CH Fc), 4.46 (t, 2H, $^3J_{\text{HH}} = 1.8$ Hz, -CH Fc), 4.07 (s, 5 H, -CH Fc). **^{13}C NMR** (CDCl_3) δ : 191.30 (1 C, -CHO), 146.90 (1 C, quat Ar), 133.54 (1 C, quat Ar), 129.54

(2 C, -CH Ar), 125.68 (2 C, -CH Ar), 82.51 (1 C, quat Fc), 69.87 (2 C, -CH Fc), 69.62 (5 C, -CH Fc), 66.73 (2 C, -CH Fc).

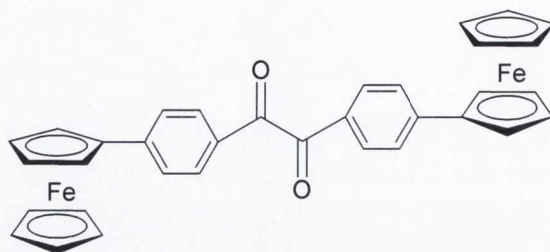
4.2.12. Synthesis of (12)



Compound **11** (2 g, 6.89 mmol) and sodium cyanide (0.6 g, 12.2 4mmol) were dissolved in water (3mL) and ethanol (10mL), and refluxed for 1 hour. The solution was cooled, resulting in the formation of a red precipitate, which was collected by suction filtration. The precipitate was dried and subjected to column chromatography on silica eluting with dichloromethane. The first orange band yielded unreacted 4-ferrocenylbenzaldehyde and the second orange-red band afforded the desired product.

Yield: 1.18 g, 59 %. **M.pt:** 117-118 °C. **¹H NMR** (CDCl₃) δ: 7.87 (d, 2 H, ³J_{HH} = 8.5 Hz, -CH Ar), 7.47,(m, 4 H, -CH Ar), 7.30 (d, 2 H, ³J_{HH} = 8.5 Hz, -CH Ar), 5.91 (d, 1 H, ³J_{HH} = 6.0 Hz, -CH(OH)), 4.68 (s, 2 H, -CH Fc), 4.63 (s, 2 H, -CH Fc), 4.55 (d, 1 H, ³J_{HH} = 6.0 Hz, -OH), 4.41 (s, 2 H, -CH Fc), 4.32 (s, 2 H, -CH Fc), 4.02 (s, 10 H, -CH Fc). **¹³C NMR** (CDCl₃) δ: 197.63 (1 C, -CO), 146.39 (1 C, quat Ar), 139.41 (1 C, quat Ar), 136.52 (1 C, quat Ar), 130.19 (1 C, quat Ar), 128.84 (2 C, -CH Ar), 127.30 (2 C, -CH Ar), 126.19 (2 C, -CH Ar), 125.31 (2 C, -CH Ar), 83.95 (1 C, quat Fc), 82.17 (1 C, quat Fc), 75.25 (1 C, -CH(OH)), 69.39 (5 C, -CH Fc), 69.14 (5 C, -CH Fc), 66.66 (2 C, -CH Fc), 66.46 (2 C, -CH Fc), 66.09 (2 C, -CH Fc), 66.06 (2 C, -CH Fc). **ESI-MS** (methanol); for C₃₄H₂₈Fe₂O₂: [M]⁺ calculated *m/z* 580.0788, found *m/z* 580.0773. **IR** ν (cm⁻¹): ν(O-H st): 3444, ν(C-H st, aromatic): 3095, 2960, ν(C=O st): 1665, ν(C=C st): 1601, 1561, 1526, ν(C-H rock Fc): 1106, 1069, 1031.

4.2.13. Synthesis of 1,2-bis(4-phenylferrocene)ethane-1,2-dione (13)

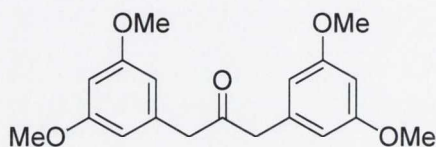


Reaction carried out in air

Compound **12** (1.2 g, 2.07 mmol) was dissolved in chloroform (30 mL) to this was added manganese dioxide (0.72 g, 8.27 mmol). The mixture was then refluxed for 24 hours. After cooling to room temperature, the solution was filtered through celite and washed until the filtrate ran clear. The solvent was removed *in vacuo* yielding the desired product.

Yield: 1.05 g, 88 %. **M.pt:** 134-135 °C. **¹H NMR** (CDCl₃) δ: 7.93 (d, 4 H, ³J_{HH} = 8.5 Hz, -CH Ar), 7.57 (d, 4 H, ³J_{HH} = 8.5 Hz, -CH Ar), 4.77 (t, 4 H, ³J_{HH} = 1.5 Hz, -CH Fc), 4.47 (t, 4 H, ³J_{HH} = 1.5 Hz, -CH Fc), 4.07 (s, 10 H, -CH Fc). **¹³C NMR** (CDCl₃) δ: 193.71 (2 C, -CO), 147.54 (2 C, quat Ar), 129.95 (2 C, quat Ar), 129.75 (4 C, -CH Ar), 125.61 (4 C, -CH Ar), 82.38 (2 C, quat Fc), 70.14 (4 C, -CH Fc) 69.78 (10 C, -CH Fc), 66.89 (4 C, -CH Fc). **ESI-MS** (methanol); for C₃₄H₂₆Fe₂O₂Na: [MNa]⁺ calculated *m/z* 601.0529, found *m/z* 601.0532. **IR** ν (cm⁻¹): ν(C-H st, aromatic): 3096, 2961, ν(C=O, st): 1670, 1658, ν(C=C st): 1604, 1560, 1523, ν(C-H rock Fc): 1218, 1173, 1103, 1082.

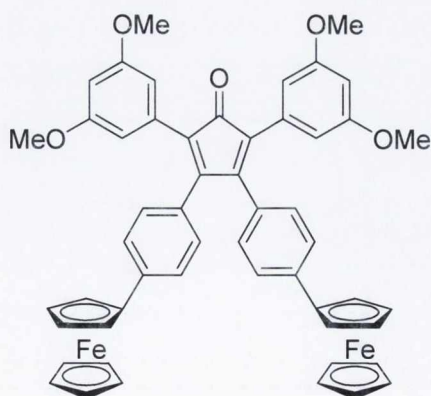
4.2.14. Synthesis of 1,3-bis-(3,5-dimethoxy)propan-2-one (14)



Calcium Hydroxide (3.2 g, 43.2 mmol) and tetrabutylammonium hydrogensulphate (1.83 g, 5.7 mmol) were dissolved in 1:1 dichloromethane:water (240 mL) and argon was bubbled through the reaction mixture for 30 minutes to degas the solution. 3, 5-dimethoxybenzyl bromide (5.0 g, 21.6 mmol) was added followed by iron pentacarbonyl (1.5 mL, 10.8 mmol) and the reaction was stirred at room temperature for five and a half hours with a constant stream of argon circulated over the reaction. The reaction mixture was then oxidised in air and acidified with 10 % HCl (120 mL). The aqueous phase was extracted with dichloromethane and the organic washings were combined and reduced to a yellow/orange oil. The oil was subjected to column chromatography on silica. Eluting with diethylether yielded the desired product as an off-white waxy solid.

Yield: 2.3 g, 65 %. **¹H NMR** (CDCl₃) δ: 6.39 (t, 2 H, ⁴J_{HH} = 2.0 Hz, -CH Ar), 6.32 (d, 4 H, ⁴J_{HH} = 2.0 Hz, -CH Ar), 3.78 (s, 12 H, -OCH₃), 3.66 (s, 4 H, -CH₂-). **¹³C NMR** (CDCl₃) δ: 205.04 (1 C, -CO), 160.51 (4 C, quat Ar), 135.64 (2 C, quat Ar), 107.07 (4 C, -CH Ar), 98.71 (2 C, -CH Ar), 54.86 (2C, -CH₂-), 48.78 (4 C, -OCH₃). **ESI-MS** (methanol); for C₁₉H₃₃ONa: [MNa]⁺ calculated *m/z* 353.1365, found *m/z* 353.1374.

4.2.15. Synthesis of 2,5-bis-(3,5-dimethoxy-phenyl)-3,4-bis-(4-phenylferrocene)-cyclopenta-2,4-dienone (15)

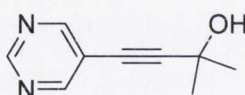


Compound **13** (1.3 g, 2.25 mmol) and potassium hydroxide (0.22 g, 3.85 mmol) were dissolved in ethanol (25 mL) and heated to reflux. A solution of **14** (0.79 g, 2.4

mmol) was dissolved in ethanol (25 mL) and added dropwise, the mixture was then refluxed for 3 hours. The solution was then cooled to room temperature, then in ice, and filtered to yield the desired product.

Yield: 0.38 g, 64 %. **M.pt:** 204-205 °C. **¹H NMR** (CDCl₃) δ: 7.32 (d, 4 H, ³J_{HH} = 8.5 Hz, -CH Ar), 6.91 (d, 4 H, ³J_{HH} = 8.5 Hz, -CH Ar), 6.51 (d, 4 H, ⁴J_{HH} = 2.0 Hz, -CH Ar), 6.39 (t, 2 H, ⁴J_{HH} = 2.0 Hz, -CH Ar), 4.64 (t, 4 H, ³J_{HH} = 1.8 Hz, -CH Fc), 4.34 (t, 4 H, ³J_{HH} = 1.8 Hz, -CH Fc), 4.01 (s, 10 H, -CH Fc), 3.66 (s, 12 H, -OCH₃). **¹³C NMR** (CDCl₃) δ: 199.36 (1C, -CO), 159.81 (4 C, quat Ar), 154.30 (2 C, quat Ar), 139.78 (2C, quat Ar), 132.17 (2 C, quat Ar), 129.98 (2 C, quat Ar), 129.16 (4 C, -CH Ar), 124.68 (4 C, -CH Ar), 124.26 (2C, quat Ar), 107.47 (4 C, -CH Ar), 100.11 (2 C, -CH Ar), 83.40 (2 C, quat Fc), 69.37 (10 C, -CH Fc), 69.04 (4 C, -CH Fc), 65.96 (4 C, -CH Fc), 54.71 (4 C, -OCH₃). **ESI-MS** (toluene); for C₅₃H₄₄Fe₂O₅: [M]⁺ calculated *m/z* 872.1888, found *m/z* 872.1897. **IR** ν (cm⁻¹): ν(C-H st, aromatic): 3086, 2997, ν(C-H st, -OCH₃): 2834, ν(C=O st): 1702, ν(C=C st): 1603, 1589, 1524, ν(C-O st, -OCH₃): 1275, ν(C-H rock Fc): 1193, 1104, 1096, 1044.

4.2.16. Synthesis of 2-methyl-4-pyrimidin-5-yl-but-3-yn-2-ol (16)

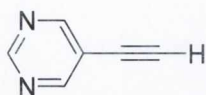


Bis(triphenylphosphine)palladium(II) dichloride (0.239 g, 0.34 mmol), copper(I) iodide (0.038 g, 0.2 mmol), 5-bromopyridine (5.35 g, 33.65 mmol) and 2-methyl-3-butyn-2-ol (3.9 mL, 40.24 mmol) were stirred in diethylamine (90 mL) at room temperature for 3 hours. The solvent was removed under reduced pressure and the solid extracted into dichloromethane. After washing with water the organic layer was dried over MgSO₄. The residue was then subjected to column chromatography on silica, elution with diethylether followed by recrystallisation from ethyl acetate and petroleum ether yielded the desired product.

Yield: 3.22 g, 59 %. **¹H NMR** (CDCl₃) δ: 9.14 (s, 1 H, -CH Ar), 8.80 (s, 2 H, -CH Ar), 3.32 (s, 1 H, -OH), 1.64 (s, 6 H, -CH₃). **¹³C NMR** (CDCl₃) δ: 158.29 (2 C, -CH

Ar), 156.13 (1 C, -CH Ar), 119.09 (1 C, quat Ar), 101.21 (1 C, quat, -C≡C-), 74.72 (1 C, quat, -C≡C-), 64.89 (1 C, quat, -C(CH₃)₂), 30.76 (2 C, -CH₃).

4.2.17. Synthesis of 5-ethynylpyrimidine (17)

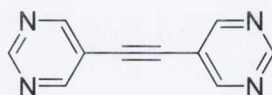


Reaction carried out in air

Compound **16** (1.8 g, 11.1 mmol) was dissolved in toluene (90 mL) along with NaOH (0.224 g, 5.6 mmol) and refluxed for 2 hours. After cooling the solution was washed with water (2 x 100 mL) and the organic phase was separated, dried over MgSO₄ and reduced *in vacuo*. The white solid was subjected to column chromatography on silica, eluting with dichloromethane:methanol (9:1) yielded the desired product.

Yield: 0.50 g, 43 %. ¹H NMR (CDCl₃) δ: 9.12 (s, 1H, -CH Ar), 8.84 (s, 2 H, -CH Ar), 3.43 (s, 1 H, -C≡CH). ¹³C NMR (CDCl₃) δ: 158.90 (2 C, -CH Ar), 156.81 (1 C, -CH Ar), 118.33 (1 C, quat Ar), 98.90 (1C, quat, -C≡C-), 84.07 (1C, quat, -C≡C-).

4.2.18. Synthesis of dipyrimidine acetylene (18)

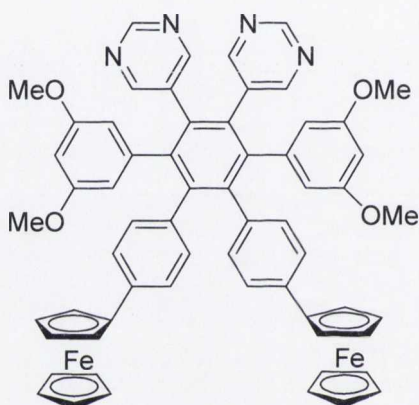


Compound **17** (0.45 g, 4.33 mmol) was dissolved in triethylamine (50 mL) and added *via* cannula to a solution of 5-bromopyrimidine (0.69 g, 4.33 mmol), bis(triphenylphosphine)palladium(II) dichloride (0.36 g, 0.52 mmol) and copper(I) iodide (0.05 g, 0.06 mmol) in dimethylformamide (100 mL). The mixture was heated to 55 °C for 90 minutes then left stirring overnight at room temperature. The solvents were removed *in vacuo*, washed with water and extracted into dichloromethane. The organic phase was dried over MgSO₄, solvents removed *in vacuo* again before being

subjected to column chromatography on silica. Elution with diethylether followed by recrystallisation from ethyl acetate and petroleum ether yielded the desired product.

Yield: 0.29 g, 37 %. **M.pt:** 172-174°C. $^1\text{H NMR}$ (CDCl_3) δ : 9.24 (s, 2 H, -CH Ar), 8.93 (s, 4 H, -CH Ar). $^{13}\text{C NMR}$ (CDCl_3) δ : 158.39 (4 C, -CH Ar), 157.13 (2 C, -CH Ar), 118.15 (2 C, quat Ar), 88.63 (2 C, quat, $-\text{C}\equiv\text{C}-$).

4.2.19. Synthesis of 1,2-dipyrimidyl-3,6-bis(3,5-dimethoxyphenyl)-4,5-bis-(4-phenylferrocene)benzene (19)

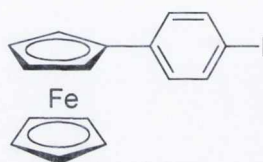


Compound **15** (0.4 g, 0.46 mmol), **18** (0.075 g, 0.41 mmol) and benzophenone (1.5 g) were mixed in a round bottomed flask and attached to an air condenser. The mixture was heated at 200 °C for 18 hours. The mixture was then subjected to flash column chromatography on silica. Eluting with dichloromethane removed all the benzophenone and any un-reacted cyclopentadienone. Elution with diethylether/methanol (9:1) yielded the desired product.

Yield: 0.24 g, 58 %. **M.pt:** >200 °C (decomp.). $^1\text{H NMR}$ (CDCl_3) δ : 8.86 (s, 2 H, -CH Ar), 8.33 (s, 4 H, -CH Ar), 7.05 (d, 4 H, $^3J_{\text{HH}} = 8.0$ Hz, -CH Ar), 6.80 (d, 4 H, $^3J_{\text{HH}} = 8.0$ Hz, -CH Ar), 6.05 (m, 6 H, -CH Ar), 4.55 (s, 4 H, -CH Fc), 4.26 (s, 4 H, -CH Fc), 3.89 (s, 10 H, -CH Fc), 3.52 (s, 12 H, $-\text{OCH}_3$). $^{13}\text{C NMR}$ (600MHz) (CDCl_3) δ : 159.87 (4 C, quat Ar), 157.68 (4 C, -CH Ar), 156.09 (2 C, quat Ar), 142.40 (2 C, quat Ar), 141.34 (2 C, quat Ar), 140.21 (2 C, quat Ar), 136.77 (2 C, quat Ar), 136.68 (2 C, quat Ar), 133.73 (2 C, quat Ar), 132.62 (2 C, -CH Ar), 130.57 (4 C,

-CH Ar), 124.15 (4 C, -CH Ar), 109.85 (4 C, -CH Ar), 98.51 (2 C, -CH Ar), 84.36 (2 C, quat Fe), 69.81 (10 C, -CH Fe), 69.12 (4 C, -CH Fe), 66.05 (4 C, -CH Fe), 55.03 (4 C, -OCH₃). **MALDI-TOF MS**; for C₆₂H₅₀Fe₂N₄O₄: [M]⁺ calculated *m/z* 1026.2531, found *m/z* 1026.2560. **IR** ν (cm⁻¹): ν (C-H st, aromatic): 3024, 2939, ν (C-H st, -OCH₃): 2837, ν (C=C st): 1607, ν (C=N st):1603, 1550, ν (C-O st, -OCH₃): 1279, ν (C-H rock Fe): 1200, 1161, 1136.

4.2.20. Synthesis of 4-iodophenylferrocene (20)



Ferrocene (7.6 g, 40.8 mmol) was added to sulphuric acid (50 mL, spec. grav. 1.84) and the resulting deep blue ferrocenium solution was stirred at room temperature for 2 hours. The solution was then poured into ice/water (200 mL) and allowed to warm to room temperature.

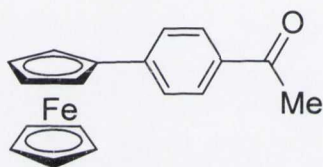
A solution of sodium nitrite (1.82 g, 26.4 mmol) in water (10 mL) at 0 °C was added dropwise to a stirred solution of 4-iodoaniline (5.26 g, 24 mmol) in 1:1 water/hydrochloric acid (spec. grav. 1.18) (20 mL) at 0 °C, and stirred at this temperature for 30 minutes to ensure full diazotization. Copper powder (2.0 g) was added to the ferrocenium solution and the diazonium solution was added dropwise with vigorous stirring.

After 24 hours stirring at room temperature, effervescence due to liberated nitrogen had ceased and ascorbic acid (10 g) was added to the dark mixture to reduce any remaining ferrocenium to ferrocene. Dichloromethane (200 mL) was added and the organic layer separated. The aqueous layer was extracted further with dichloromethane (4 x 100 mL), and the combined organic extracts were filtered through Celite before removal of the solvent *in vacuo* to give a dark solid. This was subjected to column chromatography on silica using hexane as eluent. The first

yellow fraction yielded unchanged ferrocene, and the second orange fraction, yielded the desired product as an orange crystalline solid.

Yield: 3.11 g, 33 %. **^1H NMR** (CDCl_3) δ : 7.61 (d, 2 H, $^3J_{\text{HH}} = 8.5$ Hz, -CH Ar), 7.23 (d, 2 H, $^3J_{\text{HH}} = 8.5$ Hz, -CH Ar), 4.63 (t, 2 H, $^3J_{\text{HH}} = 1.8$ Hz, -CH Fc), 4.36 (t, 2H, $^3J_{\text{HH}} = 1.8$ Hz, -CH Fc), 4.05 (s, 5 H, -CH Fc). **^{13}C NMR** (CDCl_3) δ : 138.73 (1 C, quat Ar), 136.91 (2 C, -CH Ar), 127.25 (2 C, -CH Ar), 90.11 (1 C, quat Ar), 83.61 (1 C, quat Fc), 69.27 (5 C, -CH Fc), 68.82 (2 C, -CH Fc), 65.97 (2 C, -CH Fc). **ESI-MS** (methanol); for $\text{C}_{16}\text{H}_{13}\text{IFe}$: $[\text{M}]^+$ calculated m/z 387.9411, found m/z 387.9402.

4.2.21. Synthesis of 4-acetylphenylferrocene (21)



Ferrocene (15.2 g, 81.6 mmol) was added to sulphuric acid (100mL, spec. grav. 1.84) and the resulting deep blue ferrocenium solution was stirred at room temperature for 2 hours. The solution was then poured into ice/water (400 mL) and allowed to warm to room temperature.

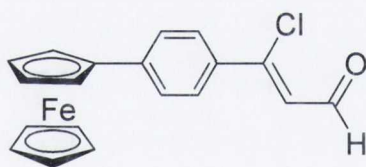
A solution of sodium nitrite (3.64 g, 52.8 mmol) in water (20 mL) at 0 °C was added dropwise to a stirred solution of 4-aminoacetphenone (6.48 g, 480 mmol) in 1:1 water/hydrochloric acid (spec. grav. 1.18) (40 mL) at 0 °C, and stirred at this temperature for 30 minutes to ensure full diazotization. Copper powder (4.0 g) was added to the ferrocenium solution and the diazonium solution was added dropwise with vigorous stirring.

After 24 hours stirring at room temperature, effervescence due to liberated nitrogen had ceased and ascorbic acid (20 g) was added to the dark mixture to reduce any remaining ferrocenium to ferrocene. Dichloromethane (400 mL) was added and the organic layer separated. The aqueous layer was extracted further with

dichloromethane (4 x 150 mL), and the combined organic extracts were filtered through Celite before removal of the solvent *in vacuo* to give a dark solid. This was subjected to column chromatography using gradient elution. The first yellow fraction, eluted with hexane, yielded unchanged ferrocene. The second orange-red fraction, eluted with 80/20 (dichloromethane/hexane) gave upon evaporation of solvents the desired product as an orange crystalline solid.

Yield: 4.9 g, 34 %. **¹H NMR** (CDCl₃) δ: 7.90 (d, 2 H, ³J_{HH} = 8.0 Hz, -CH Ar), 7.55 (d, 2 H, ³J_{HH} = 8.0 Hz, -CH Ar), 4.74 (t, 2 H, ³J_{HH} = 1.8 Hz, -CH Fc), 4.42 (t, 2 H, ³J_{HH} = 1.8 Hz, -CH Fc), 4.06 (s, 5 H, -CH Fc), 2.62 (s, 3 H, -COCH₃). **¹³C NMR** (CDCl₃) δ: 197.19 (1 C, -CO), 145.08 (1 C, quat Ar), 134.08 (1 C, quat Ar), 128.16 (2 C, -CH Ar), 125.29 (2 C, -CH Ar), 82.96 (1 C, quat Fc), 69.47 (2 C, -CH Fc), 69.42 (5 C, -CH Fc), 66.49 (2 C, -CH Fc), 26.11 (1 C, -COCH₃). **ESI-MS** (methanol); for C₁₈H₁₆FeO: [M]⁺ calculated *m/z* 304.0551, found *m/z* 304.0544.

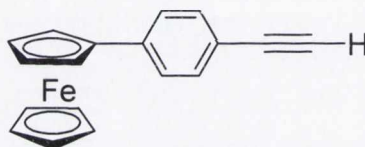
4.2.22. Synthesis of α-chloro-β-formyl-p-ferrocenylstyrene (22)



A solution of phosphorous oxychloride (1.4 mL, 14 mmol) in dimethylformamide (10 mL), prepared at 0 °C, was added dropwise to a stirred solution of **21** (1.2 g, 4 mmol) also in dimethylformamide (15 mL) at 0 °C. The reaction was allowed to proceed for 15 minutes at 0 °C and then for 4 hours at room temperature, after which it was transferred *via* cannula into a 20 % solution of sodium acetate (40 mL) and allowed to stir for 90 minutes. The solution was extracted several times with dichloromethane, and the combined organic extract was in turn washed several times with water, dried over MgSO₄ and the solvents were removed under reduced pressure. The residue was chromatographed on silica, elution with dichloromethane:hexane (2:1) yielded the desired product as a purple solid.

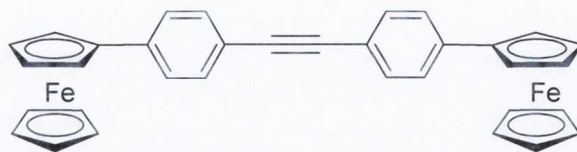
Yield: 0.7 g, 50 %. $^1\text{H NMR}$ (CDCl_3) δ : 10.25 (d, 1 H, $^3J_{\text{HH}} = 6.8$ Hz, $-\text{CHO}$), 7.70 (d, 2 H, $^3J_{\text{HH}} = 8.0$ Hz, $-\text{CH Ar}$), 7.53 (d, 2 H, $^3J_{\text{HH}} = 8.0$ Hz, $-\text{CH Ar}$), 6.72 (d, 1 H, $^3J_{\text{HH}} = 6.8$ Hz, $-\text{C}=\text{CH}$), 4.77 (s, 2H, $-\text{CH Fc}$), 4.47 (s, 2 H, $-\text{CH Fc}$), 4.11 (s, 5 H, $-\text{CH Fc}$). $^{13}\text{C NMR}$ (CDCl_3) δ : 191.22 (1 C, $-\text{CHO}$), 151.86 (1C, quat Ar), 144.20 (1 C, quat Ar), 131.89 (1 C, quat, $-\text{CCl}$), 126.87 (2 C, $-\text{CH Ar}$), 125.61 (2 C, $-\text{CH Ar}$), 122.63 (1 C, $-\text{C}=\text{CH}$), 82.58 (1 C, quat Fc), 69.64 (2 C, $-\text{CH Fc}$), 69.53 (5C, $-\text{CH Fc}$), 66.47 (2 C, $-\text{CH Fc}$).

4.2.23. Synthesis of 4-ethynylphenylferrocene (23)



Compound **22** (0.65 g, 1.85 mmol) was dissolved in dioxane (20 mL) and the solution was heated to reflux. To this solution was added rapidly NaOH (15 mL, 0.5 M). The reaction was allowed to continue for 5 minutes at reflux and the solution was then poured into deionised water (100 mL). After acidification with HCl, the solution was extracted exhaustively with diethylether and the combined ether extracts were washed to neutrality before being dried over MgSO_4 . The solvent was then removed and the residue was recrystallised from hexane to yield the desired product as an orange solid.

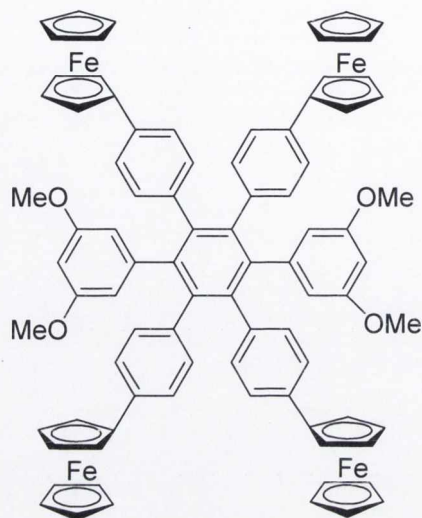
Yield: 0.49 g, 93 %. $^1\text{H NMR}$ (CD_2Cl_2) δ : 7.48 (d, 2 H, $^3J_{\text{HH}} = 8.5$ Hz), 7.43 (d, 2 H, $^3J_{\text{HH}} J = 8.5$ Hz), 4.71 (s, 2 H, $-\text{CH Fc}$), 4.40 (s, 2 H, $-\text{CH Fc}$), 4.07 (s, 5 H, $-\text{CH Fc}$), 3.19 (s, 1 H, $\text{C}\equiv\text{CH}$). $^{13}\text{C NMR}$ (CD_2Cl_2) δ : 140.20 (1 C, quat Ar), 131.58 (2 C, $-\text{CH Ar}$), 125.33 (2 C, $-\text{CH Ar}$), 118.52 (1 C, quat Ar), 83.42 (1 C, quat, $-\text{C}\equiv\text{C}-$), 83.36 (1 C, quat, $-\text{C}\equiv\text{C}-$), 76.42 (1 C, quat Fc), 69.24 (5 C, $-\text{CH Fc}$), 69.02 (2 C, $-\text{CH Fc}$), 66.10 (2 C, $-\text{CH Fc}$). **ESI-MS** (toluene); for $\text{C}_{18}\text{H}_{14}\text{Fe}$: $[\text{M}]^+$ calculated m/z 286.0445, found m/z 286.0452.

4.2.24. Synthesis of bis(4-ferrocenylphenyl)acetylene (**24**)

Compound **23** (0.6 g, 2.1 mmol), **20** (0.98 g, 2.5 mmol) and tetrakis(triphenylphosphine)palladium (0.24 g, 0.21 mmol) were dissolved in diethylamine/dimethylformamide (2/1), (45 mL). The reaction mixture was then allowed to stir at 55 °C for 48 hours. The solvents were removed *in vacuo*, washed with water and extracted into dichloromethane. The organic phase was dried over MgSO₄, solvents removed *in vacuo* again before being subjected to column chromatography on silica. Elution with dichloromethane:hexane (1:2) and then dichloromethane yielded the desired product.

Yield: 1.1 g, 94 %. **M.pt:** >300 °C. **¹H NMR (600MHz)** (CD₂Cl₂) δ: 7.52 (d, 4H, ³J_{HH} = 8.5 Hz, -CH Ar), 7.49 (d, 4H, ³J_{HH} = 8.5 Hz, -CH Ar), 4.73 (s, 4H, -CH Fc), 4.41 (s, 4H, -CH Fc), 4.08 (s, 10H, -CH Fc). **¹³C NMR (600MHz)** (CD₂Cl₂) δ: 140.64 (2 C, quat Ar), 131.27 (4 C, -CH Ar), 125.72 (4 C, -CH Ar), 120.31 (2 C, quat Ar), 89.51 (2 C, -C≡C-), 84.02 (2 C, quat Fc), 69.53 (10 C, -CH Fc), 69.26 (4 C, -CH Fc), 66.36 (4 C, -CH Fc). **ESI-MS** (toluene); for C₃₄H₂₆Fe₂: [M]⁺ calculated *m/z* 546.0733, found *m/z* 546.0713. **IR** ν (cm⁻¹): ν(C-H st, aromatic): 3089, 3051, ν(C≡H st): 1912, ν(C=C st): 1604, 1531, ν(C-H rock Fc): 1103, 1085, 1033, 1002.

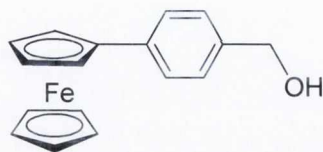
4.2.25. Synthesis of 1,2,4,5-(tetra-phenylferrocene)-3,6-(3,5-dimethoxyphenyl)benzene (25)



Compound **24** (0.15 g, 0.27 mmol), **15** (0.30 g, 0.34 mmol) and benzophenone (2 g) were mixed in a round bottomed flask and attached to an air condenser. The mixture was heated at 190 °C for 24 hours. The mixture was then subjected to flash column chromatography on silica, eluting with dichloromethane yielded the desired product.

Yield: 0.07 g, 18 %. >300 °C. **¹H NMR** (C₂D₂Cl₄) at 60°C δ: 7.06 (d, 8 H, ³J_{HH} = 8.0 Hz, -CH Ar), 6.83 (d, 8 H, ³J_{HH} = 8.0 Hz, -CH Ar), 6.14 (d, 4 H, ⁴J_{HH} = 2.0 Hz, -CH Ar), 6.02 (t, 2 H, ⁴J_{HH} = 2.0 Hz, -CH Ar), 4.54 (s, 8 H, -CH Fc), 4.23 (s, 8H, -CH Fc), 3.91 (s, 20 H, -CH Fc), 3.48 (s, 12 H, -OCH₃). **¹³C NMR (600 MHz)** (CDCl₃) δ: 159.23 (4 C, quat Ar), 142.42 (2 C, quat Ar), 140.13 (2 C, quat Ar), 139.91 (4 C, quat Ar), 138.44 (2 C, quat Ar), 136.06 (4 C, quat Ar), 130.97 (8 C, -CH Ar), 123.89(8 C, -CH Ar), 110.09 (4 C, -CH Ar), 97.57 (2 C, -CH Ar), 70.17 (8 C, -CH Fc), 69.30 (4 C, quat Fc), 66.19 (8 C, -CH Fc), 54.87 (24 C, -CH Fc & -OCH₃). **MALDI-TOF MS;** for C₈₆H₇₀Fe₄O₄: [M]⁺ calculated *m/z* 1390.2672, found *m/z* 1390.2739. **IR** ν (cm⁻¹): ν(C-H st, aromatic): 3088, 3020, ν(C-H st, -OCH₃): 2952, 2833, ν(C=C st): 1606, 1562, 1529, ν(C-O st, -OCH₃): 1274, ν(C-H rock Fc): 1158, 1104, 1062.

4.2.26. Synthesis of 1-ferrocenyl-4-benzylalcohol (26)



Ferrocene (7.6 g, 40.8 mmol) was added to sulphuric acid (50mL, spec. grav. 1.84) and the resulting deep blue ferrocenium solution was stirred at room temperature for 2 hours. The solution was then poured into ice/water (200 mL) and allowed to warm to room temperature.

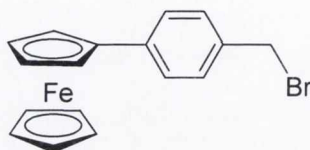
A solution of sodium nitrite (1.82 g, 13.2 mmol) in water (10 mL) at 0 °C was added dropwise to a stirred solution of 4-aminobenzylalcohol (3.0 g, 24 mmol) in 1:1 water/hydrochloric acid (spec. grav. 1.18) (20 mL) at 0 °C, and stirred at this temperature for 30 minutes to ensure full diazotization. Copper powder (2.0 g) was added to the ferrocenium solution and the diazonium solution was added dropwise with vigorous stirring.

After 24 hours stirring at room temperature, effervescence due to liberated nitrogen had ceased and ascorbic acid (10 g) was added to the dark mixture to reduce any remaining ferrocenium to ferrocene. Dichloromethane (200 mL) was added and the organic layer separated. The aqueous layer was extracted further with dichloromethane (4 x 100 mL), and the combined organic extracts were filtered through Celite before removal of the solvent *in vacuo* to give a dark solid. This was subjected to column chromatography using gradient elution. The first yellow fraction, eluted with hexane, yielded unchanged ferrocene. The second orange-red fraction, eluted with dichloromethane (with 5 % Methanol) gave desired product.

Yield: 2.2 g, 31 %. **M.pt:** 109-110 °C. **¹H NMR** (CDCl₃) δ: 7.50 (d, 2 H, ³J_{HH} = 8.3 Hz, -CH Ar), 7.31 (d, 2H, ³J_{HH} = 8.3 Hz, -CH Ar), 4.69 (s, 2 H, -CH₂-), 4.67 (t, 2 H, ³J_{HH} = 2.0 Hz, -CH Fc), 4.34 (t, 2 H, ³J_{HH} = 2.0 Hz, -CH Fc), 4.07 (s, 5 H, -CH Fc), 1.73 (br s, 1 H, -OH). **¹³C NMR** (CDCl₃) δ: 138.34 (1 C, quat Ar), 137.94 (1C, quat Ar), 126.78 (2 C, -CH Ar), 125.82 (2 C, -CH Ar), 84.60 (1 C, quat Fc), 69.17 (5 C, -

CH Fc), 68.52 (2 C, -CH Fc), 66.06 (2 C, -CH Fc), 64.83 (1 C, -CH₂). **ESI-MS** (toluene); for C₁₇H₁₆FeO: [M]⁺ calculated *m/z* 292.0551, found *m/z* 292.0552.

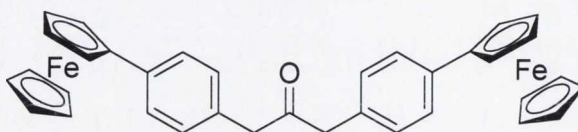
4.2.27. Synthesis of 1-ferrocenyl-4-benzylbromide (27)



Compound **26** (1 g, 3.42 mmol) was dissolved in dichloromethane (20 mL) in a 3-necked round bottomed flask. The mixture was cooled to 0 °C, and a solution of phosphorous tribromide (0.7 mL, 1.85 g, 6.85 mmol) dissolved in dichloromethane (5 mL) was added dropwise. The resulting mixture was then stirred at 0 °C for 30 minutes. The reaction mixture was poured onto 100 g of ice, neutralized with sodium hydrogen carbonate and the organic phase separated. The aqueous phase was extracted with dichloromethane, and the organic phase was collected, washed with brine, dried over MgSO₄ and dried *in vacuo*.

Yield: 1.14 g, 94 %. **¹H NMR** (CDCl₃) δ: 7.47 (d, 2 H, ³J_{HH} = 8.5 Hz, -CH Ar), 7.33 (d, 2 H, ³J_{HH} = 8.5 Hz, -CH Ar), 6.67 (t, 2 H, ³J_{HH} = 2.0 Hz, -CH Fc), 4.54 (s, 2 H, -CH₂-), 4.36 (s, 2 H, ³J_{HH} = 2.0 Hz, -CH Fc), 4.08 (s, 5 H, -CH Fc). **¹³C NMR** (CDCl₃) δ: 139.46 (1 C, quat Ar), 134.67 (1C, quat Ar), 128.69 (2 C, -CH Ar), 125.97 (2C, -CH Ar), 84.13 (1 C, quat Fc), 69.23 (5 C, -CH Fc), 68.73 (2 C, -CH Fc), 66.17 (2 C, -CH Fc), 33.52 (1 C, -CH₂).

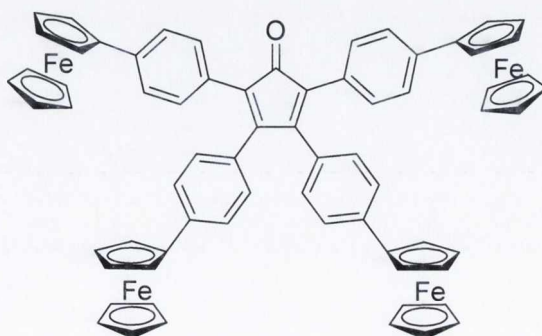
4.2.28. Synthesis of 1,3-bis-(4-ferrocenylphenyl)propan-2-one (28)



Calcium hydroxide (2.3 g, 31 mmol) and tetrabutylammonium hydrogensulphate (1.32 g, 3.88 mmol) were dissolved in 1:1 dichloromethane:water (180 mL) and argon was bubbled through the reaction mixture for 30 minutes to degas the solution. Compound **27** (5.5 g, 15.5 mmol) was added followed by iron pentacarbonyl (1.1 mL, 7.75 mmol) and the reaction was stirred at room temperature for six hours with a constant stream of argon circulated over the reaction. The reaction mixture was then oxidised in air and acidified with 10 % HCl (120 mL). The aqueous phase was extracted with dichloromethane and the organic washings were combined and reduced. This was then subjected to column chromatography on silica, eluting with dichloromethane first removed any un-reacted benzyl bromide (**27**). Further elution with dichloromethane yielded a second orange band which contained the desired product.

Yield: 2.58 g, 58 %. $^1\text{H NMR}$ (CDCl_3) δ : 7.45 (d, 4 H, $^3J_{\text{HH}} = 8.0$ Hz, -CH Ar), 7.11 (d, 4 H, $^3J_{\text{HH}} = 8.0$ Hz, -CH Ar), 4.65 (t, 4 H, $^3J_{\text{HH}} = 2.0$ Hz, -CH Fc), 4.34 (s, 4 H, $^3J_{\text{HH}} = 2.0$ Hz, -CH Fc), 4.07 (s, 10 H, -CH Fc), 3.75 (s, 4 H, -CH₂). $^{13}\text{C NMR}$ (CDCl_3) δ : 205.47 (1 C, -CO), 137.66 (2 C, quat Ar), 131.02 (2 C, quat Ar), 129.07 (4 C, -CH Ar), 125.98 (4 C, -CH Ar), 84.60 (2 C, quat Fc), 69.18 (10 C, -CH Fc), 68.49 (4 C, -CH Fc), 66.05 (4 C, -CH Fc), 48.41 (2 C, -CH₂). **ESI-MS** (toluene); for $\text{C}_{35}\text{H}_{30}\text{Fe}_2\text{ONa}$: $[\text{MNa}]^+$ calculated m/z 601.0893, found m/z 601.0919. **IR** ν (cm^{-1}): $\nu(\text{C-H st, aromatic})$: 3092, 3031, $\nu(\text{C=O st})$: 1722, $\nu(\text{C=C st})$: 1612, 1603, 1527, $\nu(\text{C-H rock Fc})$: 1103, 1083, 1056, 999.

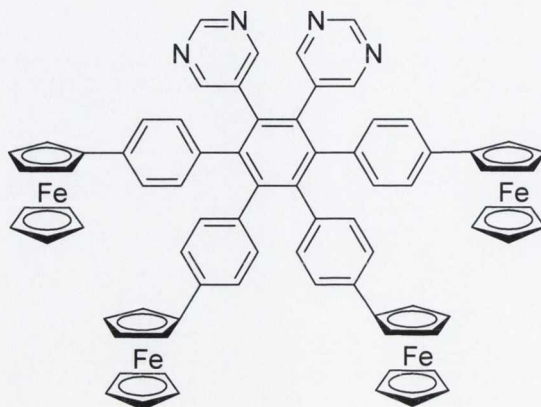
4.2.29. Synthesis of 2,3,4,5-tetra-(4-ferrocenylphenyl)cyclopenta-2,4-dienone (**29**)



Diketone **13** (0.5 g, 0.86mmol) and potassium hydroxide (0.08 g, 1.47 mmol) were dissolved in ethanol (25 mL) and heated to reflux. A solution of **28** (0.55 g, 0.95 mmol) was dissolved in ethanol:dichloromethane, 1:1 (45 mL) and added dropwise, the mixture was then refluxed for 18 hours. The solution was then cooled to room temperature, filtered and washed with ethanol followed by hexane to yield the desired product.

Yield: 0.61 g, 63 %. **¹H NMR (600 MHz)** (CDCl₃) δ : 7.39 (d, 4 H, $^3J_{\text{HH}} = 8.5$ Hz, -CH Ar), 7.34 (d, 4 H, $^3J_{\text{HH}} = 8.0$ Hz, -CH Ar), 7.30 (d, 4 H, $^3J_{\text{HH}} = 8.0$ Hz, -CH Ar), 6.94 (d, 4 H, $^3J_{\text{HH}} = 8.5$ Hz, -CH Ar), 4.67 (t, 4 H, $^3J_{\text{HH}} = 2.0$ Hz, -CH Fc), 4.64 (t, 4 H, $^3J_{\text{HH}} = 2.0$ Hz, -CH Fc), 4.35 (t, 4 H, $^3J_{\text{HH}} = 2.0$ Hz, -CH Fc), 4.33 (t, 4 H, $^3J_{\text{HH}} = 2.0$ Hz, -CH Fc), 4.05 (s, 10 H, -CH Fc), 4.04 (s, 10 H, -CH Fc). **¹³C NMR (600MHz)** (CDCl₃) δ : 200.74 (1C, -CO), 153.79 (2 C, quat Ar), 139.94 (2 C, quat Ar), 138.38 (2 C, quat Ar), 130.76 (2 C, quat Ar), 129.92 (4 C, -CH Ar), 129.51 (4 C, -CH Ar), 128.50 (2 C, quat Ar), 125.53 (4 C, -CH Ar), 124.95 (4 C, -CH Ar), 124.49 (2 C, quat Ar), 84.78 (2 C, quat Fc), 83.70 (2 C, quat Fc), 69.75 (10 C, -CH Fc), 69.51 (10 C, -CH Fc), 69.36 (4 C, -CH Fc), 68.93 (4 C, -CH Fc), 66.32 (4 C, -CH Fc), 66.25 (4 C, -CH Fc). **MALDI-TOF MS**; for C₆₉H₅₂Fe₄O: [M]⁺ calculated m/z 1120.1416, found m/z 1120.1416. **IR** ν (cm⁻¹): ν (C-H st, aromatic): 3076, ν (C=O st): 1706, ν (C=C st): 1600, 1526, 1517, ν (C-H rock Fc): 1103, 1088, 1082, 1017.

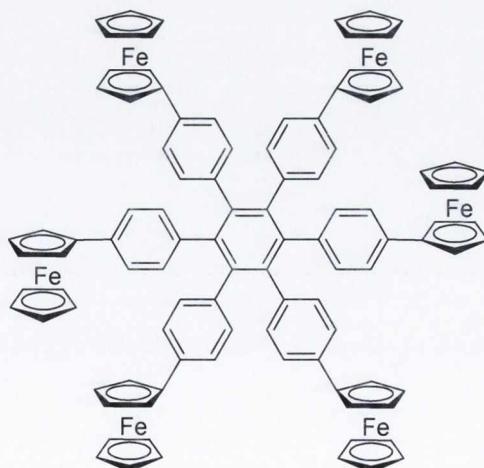
4.2.30. Synthesis of 1,2-dipyrimidyl-3,4,5,6-tetra-(4-ferrocenyl-phenyl)benzene (**30**)



Cyclopentadienone **29** (0.25 g, 0.22 mmol), **18** (0.037 g, 0.2 mmol) and benzophenone (1.0 g) were mixed in a round bottomed flask and attached to an air condenser. The mixture was heated at 200 °C for 18 hours. The mixture was then subjected to flash column chromatography on silica. Eluting with dichloromethane removed all the benzophenone and any un-reacted cyclopentadienone. Elution with diethylether/methanol (10:1) yielded the desired product.

Yield: 0.14 g, 54 %. **¹H NMR (600 MHz)** (CDCl₃) δ: 8.81 (s, 2 H, -CH Ar), 8.32 (s, 4 H, -CH Ar), 7.12 (d, 4 H, ³J_{HH} = 8.0 Hz, -CH Ar), 7.07 (d, 4 H, ³J_{HH} = 8.0 Hz, -CH Ar), 6.81 (d, 4 H, ³J_{HH} = 8.0 Hz, -CH Ar), 6.78 (d, 4 H, ³J_{HH} = 8.0 Hz, -CH Ar), 4.53 (s, 4 H, -CH Fc), 4.48 (s, 4 H, -CH Fc), 4.26 (s, 4 H, -CH Fc), 4.21 (s, 4 H, -CH Fc), 3.92 (s, 10 H, -CH Fc), 3.91 (s, 10 H, -CH Fc). **¹³C NMR (600 MHz)** (CDCl₃) δ: 157.98 (4 C, -CH Ar), 156.05 (2 C, -CH Ar), 142.42 (2 C, quat Ar), 141.48 (2 C, quat Ar), 137.48 (2 C, quat Ar), 136.85 (2C, quat Ar), 136.68 (2 C, quat Ar), 136.04 (2 C, quat Ar), 133.90 (2 C, quat Ar), 133.06 (2 C, quat Ar), 131.18 (4 C, -CH Ar), 131.08 (4 C, -CH Ar), 124.68 (4 C, -CH Ar), 124.21 (4 C, -CH Ar), 84.23 (2 C, quat Fc), 83.61 (2 C, quat Fc), 69.74 (10C, -CH Fc), 69.69 (10 C, -CH Fc), 60.05 (4 C, -CH Fc), 69.00 (4 C, -CH Fc), 66.12 (4 C, -CH Fc), 66.02 (4 C, -CH Fc). **MALDI-TOF MS;** for C₇₈H₅₈Fe₄N₄: [M]⁺ calculated *m/z* 1274.2059, found *m/z* 1274.2003. **IR** ν (cm⁻¹): ν(C-H st, aromatic): 3093, 3024, ν(C=C st): 1608, ν(C=N st):1548, 1529, ν(C-H rock Fc): 1104, 1082, 1049, 1019.

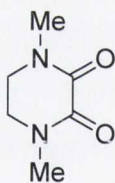
4.2.31. Synthesis of hexa(4-ferrocenylphenyl)benzene (31)



Compound **24** (0.45 g, 0.83 mmol) and cobalt octacarbonyl (0.1 g, 0.29 mmol) were placed in a round-bottomed flask, dioxane (15 mL) was injected and the mixture was refluxed for 3 hours. After evaporation of the solvent, the crude mixture was subjected to column chromatography. Elution with hexane removed the cobalt octacarbonyl and by gradually increasing the amount of dichloromethane to 50 % the product was obtained as a pale orange solid.

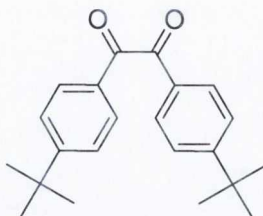
Yield: 0.11 g, 25 %. **M.pt:** >300 °C. **¹H NMR** (CDCl₃) δ: 7.07 (d, 12 H, ³J_{HH} = 8.0 Hz, -CH Ar), 6.84 (d, 12H, ³J_{HH} = 8.0 Hz, -CH Ar), 4.51 (s, 12 H, -CH Fc), 4.20 (s, 12 H, -CH Fc), 3.94 (s, 30 H, -CH Fc). **¹³C NMR** (CDCl₃) δ: 139.79 (6 C, quat Ar), 138.10 (6 C, quat Ar), 135.27 (6 C, quat Ar), 131.38 (12 C, -CH Ar), 123.53 (12 C, -CH Ar), 84.03 (6 C, quat Fc), 69.36 (30 C, -CH Fc), 68.45 (12 C, -CH Fc), 65.61 (12 C, -CH Fc). **IR** ν (cm⁻¹): ν(C-H st, aromatic): 3089, 3026, ν(C=C st): 1608, 1527, ν(C-H rock Fc), 1105, 1081, 1054, 1029.

4.2.32. Synthesis of 1, 4-dimethylpiperazine-2, 3-dione (DMPD; **32**)



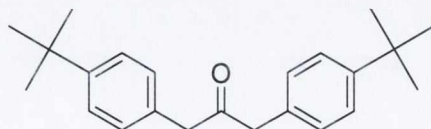
To a stirred solution of N, N'-dimethylethylenediamine (10.0 mL, 8.3 g, 94 mmol) in diethylether (200 mL) was added diethyl oxalate (12.7 mL, 13.7 g, 94 mmol) in one portion. After a few minutes white crystals began to precipitate. The mixture was stirred overnight. The product was filtered and washed with dry diethylether and recrystallised from toluene.

Yield: 11.3 g, 85 %. **¹H NMR** (CDCl₃) δ: 3.50 (s, 4 H, -CH Ar), 2.98 (s, 6 H, -CH₃). **¹³C NMR** (CDCl₃) δ: 157.03 (2 C, -CO), 45.56 (2 C, -CH Ar), 34.41 (2C, -CH₃). **ESI-MS** (methanol); for C₆H₁₀N₂O₂Na: [MNa]⁺ calculated *m/z* 165.0640, found *m/z* 165.0538.

4.2.33. Synthesis of 1, 2-bis-(4-*tert*-butyl-phenyl)ethane-1, 2-dione (33)

1-bromo-4-*tert*-butylbenzene (8 mL, 46.1 mmol) was dissolved in tetrahydrofuran (90 mL) and the solution was cooled down to -78°C . To this solution *n*-BuLi (23 mL, 2.5 M in hexane, 57.5 mmol) was added dropwise. The solution was stirred for 90 minutes at -78°C , then added *via* cannula to a solution of 1,4-dimethyl-piperazine-2,3-dione (DMPD) (4 g, 28.3 mmol) in tetrahydrofuran (120 mL) at -78°C . The reaction mixture was stirred and allowed to warm to room temperature over 1 hour, then stirred for a further 3 hours. The reaction was quenched with 5 % HCl (240 mL) and the product was extracted with dichloromethane. The organic phase was washed with water, dried over MgSO_4 , filtered and the solvents were removed under reduced pressure. Recrystallisation from hexane of the yellow oil yielded the desired product.

Yield: 3.3 g, 45 %. **M.pt:** $101\text{--}103^{\circ}\text{C}$. **^1H NMR** (CDCl_3) δ : 7.93 (d, 4 H, $^3J_{\text{HH}} = 8.5$ Hz, -CH Ar), 7.54 (d, 4 H, $^3J_{\text{HH}} = 8.5$ Hz, -CH Ar), 1.37 (s, 18 H, $-\text{C}(\text{CH}_3)_3$). **^{13}C NMR** (CDCl_3) δ : 194.11 (2 C, -CO), 158.45 (2 C, quat Ar), 130.12 (2 C, quat Ar), 129.45 (4 C, -CH Ar), 125.56 (4 C, -CH Ar), 34.95 (2 C, quat, $-\text{C}(\text{CH}_3)_3$), 30.55 (18 C, -CH, $-\text{C}(\text{CH}_3)_3$).

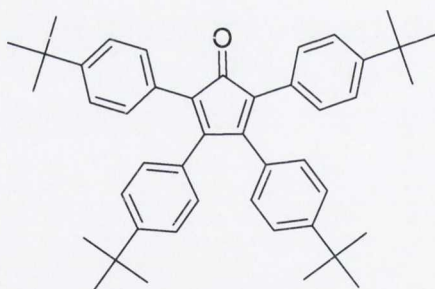
4.2.34. Synthesis of 1, 3-bis-(4-*tert*-butyl-phenyl)propan-2-one (34)

Calcium Hydroxide (2.6 g, 35.2 mmol) and tetrabutylammonium hydrogensulphate (1.5 g, 4.4 mmol) were dissolved in 1:1 dichloromethane:water (180 mL) and argon was bubbled through the reaction mixture for 30 minutes to degas the solution. 4-*tert*-

butyl-benzylbromide (4 g, 3.24 mL, 17.6 mmol) was added followed by iron pentacarbonyl (1.16 mL, 8.8 mmol) and the reaction was stirred at room temperature for five hours with a constant stream of argon circulated over the reaction. The reaction mixture was then oxidised in air and acidified with 10 % HCl (60 mL). The aqueous phase was extracted with dichloromethane and the organic washings were combined and reduced to a yellow oil. The oil was subjected to column chromatography on silica using hexane:dichloromethane (1:1) as eluent which afforded white crystals of 1, 3-bis-(4-*tert*-butyl-phenyl)propan-2-one, which were further purified by recrystallisation from hexane.

Yield: 1.91 g, 67 %. **M.pt :** 84-85°C. **¹H NMR** (CDCl₃) δ: 7.35 (d, 4 H, ³J_{HH} = 8.0 Hz, -CH Ar), 7.11 (d, 4 H, ³J_{HH} = 8.0 Hz, -CH Ar), 3.72 (s, 4H, -CH₂), 1.34 (s, 18H, -C(CH₃)₃). **¹³C NMR** (CDCl₃) δ: 205.80 (1 C, -CO), 149.44 (2 C, quat Ar), 130.59 (2 C, quat Ar), 128.75 (4 C, -CH Ar), 125.22 (4 C, -CH Ar), 48.17 (2 C, -CH₂), 34.05 (2 C, quat, -C(CH₃)₃), 30.95 (6 C, -CH, -C(CH₃)₃).

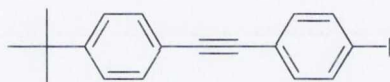
4.2.35. Synthesis of 2, 3, 4, 5-tetra-(4-*tert*-butyl-phenyl)cyclopenta-2, 4-dienone (35)



Diketone **33** (1.0 g, 3.10 mmol) and **34** (1.0 g, 3.10 mmol) were dissolved in ethanol (10 mL) and heated to reflux. Once refluxing potassium hydroxide (0.09 g, 1.55 mmol) was added in two portions over 10 minutes, after the addition the mixture was allowed to reflux for a further 15 minutes. The solution was cooled to room temperature and the red/brown solution was reduced and subjected to column chromatography on silica. Elution with hexane:dichloromethane (1:1) yielded the desired product.

Yield: 1.18 g, 62 %. **M.pt:** 237-239 °C. $^1\text{H NMR}$ (CDCl_3) δ : 7.24 (m, 8 H, , -CH Ar), 7.17 (d, 4 H, $^3J_{\text{HH}} = 8.5$ Hz, -CH Ar), 6.85 (d, 4 H, $^3J_{\text{HH}} = 8.5$ Hz, -CH Ar), 1.31 (s, 18 H, -C(CH₃)₃), 1.30 (s, 18 H, -C(CH₃)₃). $^{13}\text{C NMR}$ (CDCl_3) δ : 201.00 (1 C, -CO), 153.79 (2 C, quat Ar), 150.89 (2 C, quat Ar), 149.60 (2C, quat Ar), 130.01 (2 C, quat Ar), 129.18 (4 C, -CH Ar), 128.62 (4 C, -CH Ar), 127.66 (2 C, quat Ar), 124.46 (4 C, -CH Ar), 124.11 (4 C, -CH Ar), 123.81 (2 C, quat Ar), 34.20 (2 C, quat, -C(CH₃)₃), 34.11 (2 C, quat, -C(CH₃)₃), 30.81 (6 C, -CH, -C(CH₃)₃), 30.79 (6 C, -CH, -C(CH₃)₃).

4.2.36. Synthesis of 4-iodo-4'-*tert*-butylphenylacetylene (36)

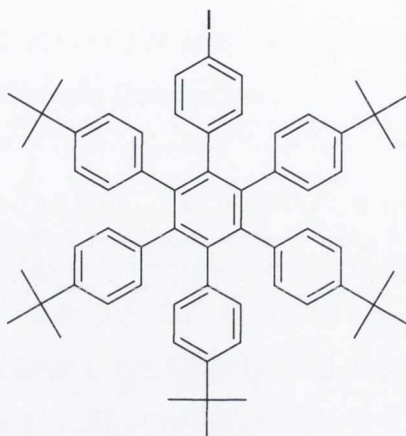


4-*tert*-butylphenylacetylene (1.37 mL, 7.58 mmol) was dissolved in tetrahydrofuran (20 mL). This was added *via* cannula to a solution of p-diiodobenzene (6.25 g, 18.96 mmol), bis(triphenylphosphine)palladium(II) dichloride (0.027 g, 0.38 mmol) and copper(I) iodide (0.007 g, 0.38 mmol) in diisopropylamine (15 mL) and tetrahydrofuran (60 mL). The mixture was stirred at room temperature for 18 hours. After the time had elapsed water (40 mL) and dichloromethane (100 mL) was added to the reaction mixture and the organic layer was separated. The aqueous layer was extracted with dichloromethane (2 x 40 mL) and the combined organic fraction was dried over MgSO₄ and reduced in volume under reduced pressure. The oily residue was subjected to column chromatography on silica, elution with hexane yielded the desired product as a yellow-white crystalline solid.

Yield: 1.77 g 65 %. $^1\text{H NMR}$ (CDCl_3) δ : 7.70 (d, 2 H, $^3J_{\text{HH}} = 8.1$ Hz, -CH Ar), 7.48 (d, 2 H, $^3J_{\text{HH}} = 8.5$ Hz, -CH Ar), 7.40 (d, 2 H, $^3J_{\text{HH}} = 8.5$ Hz, -CH Ar), 7.27 (d, 2 H, $^3J_{\text{HH}} = 8.1$ Hz, -CH Ar), 1.36 (s, 9 H, -C(CH₃)₃). $^{13}\text{C NMR}$ (CDCl_3) δ : 151.72 (1 C, quat Ar), 137.33 (2 C, -CH Ar), 132.93 (2 C, -CH Ar), 131.19 (2 C, -CH Ar), 125.26 (2 C, -CH Ar), 122.94 (1 C, quat Ar), 119.74 (1 C, quat Ar), 93.65 (1 C, quat Ar),

90.85 (1 C, quat, $-\text{C}\equiv\text{C}-$), 87.67 (1 C, quat, $-\text{C}\equiv\text{C}-$), 34.68 (1 C, quat, $-\text{C}(\text{CH}_3)_3$), 31.02 (3 C, $-\text{CH}$, $-\text{C}(\text{CH}_3)_3$).

4.2.37. Synthesis of 1-(4-iodophenyl)-2,3,4,5,6-penta(4-*tert*-butylphenyl)benzene (37)

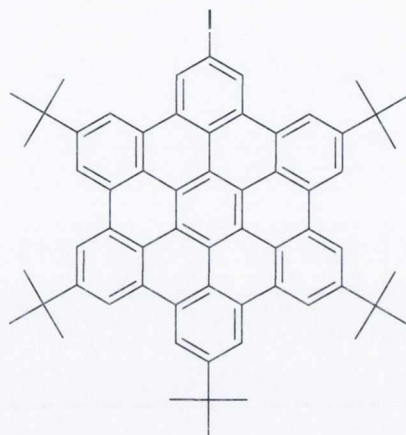


Acetylene **36** (0.27 g, 0.74 mmol), **35** (0.5 g, 0.82 mmol) and diphenylether (2.5 g) were mixed in a round bottomed flask and attached to an air condenser. The mixture was heated at 280 °C for 18 hours. After cooling to room temperature ethanol (20 mL) was added to the reaction mixture. The solvent was decanted and the remaining solid was then subjected to flash column chromatography on silica eluting with hexane:dichloromethane (10:1) furnished the desired product.

Yield: 0.44 g, 63 %. **^1H NMR** (CDCl_3) δ : 7.18 (d, 2 H, $^3J_{\text{HH}} = 8.0$ Hz, $-\text{CH}$ Ar), 6.9-6.8 (m, 10 H, $-\text{CH}$ Ar), 6.7-6.6 (m, 10 H, $-\text{CH}$ Ar), 6.60 (d, 2 H, $^3J_{\text{HH}} = 8.0$ Hz, $-\text{CH}$ Ar), 1.15 (s, 18 H, $-\text{C}(\text{CH}_3)_3$), 1.12 (s, 27 H, $-\text{C}(\text{CH}_3)_3$). **^{13}C NMR** (CDCl_3) δ : 147.72 (quat Ar), 147.36 (quat Ar), 147.32 (quat Ar), 140.70 (quat Ar), 140.67 (quat Ar), 140.56 (quat Ar), 139.86 (quat Ar), 138.42 (quat Ar), 137.6 (quat Ar), 137.57 (quat Ar), 137.38 (quat Ar), 135.32 (2 C, $-\text{CH}$ Ar), 133.44 (2 C, $-\text{CH}$ Ar), 130.89 (4 C, $-\text{CH}$ Ar), 130.83 (6 C, $-\text{CH}$ Ar), 123.22 (4 C, $-\text{CH}$ Ar), 122.91 (2 C, $-\text{CH}$ Ar), 122.89 (4 C, $-\text{CH}$ Ar), 90.43 (quat Ar), 33.98 (2 C, quat, $-\text{C}(\text{CH}_3)_3$), 33.88 (3 C, quat, $-\text{C}(\text{CH}_3)_3$), 31.05 (6 C, $-\text{CH}$, $-\text{C}(\text{CH}_3)_3$), 31.02 (9 C, $-\text{CH}$, $-\text{C}(\text{CH}_3)_3$). **MALDI-TOF MS;**

calculated for $C_{62}H_{69}I$: $[M]^+$ calculated m/z 940.4444, found m/z 940.4480.
IR ν (cm^{-1}): $\nu(C-H$ st, aromatic): 3036, $\nu(C-H$ st, $-CH_3$): 2961, 2902, 2865.

4.2.38. Synthesis of 2-iodo-5,8,11,14,17-penta-*tert*-butylhexa-*peri*-hexabenzocoronene (Iodo-HBC; **38**)

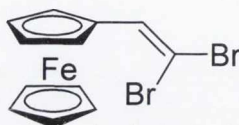


A solution of iron(III) chloride (1.8 g, 14.0 mmol) in nitromethane (3 mL) was added dropwise to a stirred solution of **37** (0.35 g, 0.47 mmol) in dichloromethane (40 mL). An argon stream was bubbled through the reaction mixture throughout the entire reaction. After stirring for 45 minutes the reaction was quenched with methanol (40 mL). The precipitate was filtered, washed with methanol (100 mL) and dried under reduced pressure. The crude product was purified by column chromatography on silica, elution hexane:dichloromethane (4:1) yielded the desired product.

Yield: 0.30 g, 85 %. **M.pt:** > 300 °C. **1H NMR** ($CDCl_3$) δ : 9.20 (s, 2 H, $-CH$ Ar), 9.15 (s, 2 H, $-CH$ Ar), 9.07 (s, 2 H, $-CH$ Ar), 8.96 (s, 2 H, $-CH$ Ar), 8.86 (s, 2 H, $-CH$ Ar), 8.69 (s, 2 H, $-CH$ Ar), 1.95 (s, 9 H, $-C(CH_3)_3$), 1.91 (s, 18 H, $-C(CH_3)_3$), 1.82 (s, 18 H, $-C(CH_3)_3$). **^{13}C NMR** ($CDCl_3$) δ : 148.56 (quat Ar), 148.40 (quat Ar), 148.37 (quat Ar), 131.97 (quat Ar), 130.17 (quat Ar), 129.92 (quat Ar), 129.84 (quat Ar), 129.68 (quat Ar), 129.61 (2 C, $-CH$ Ar), 128.23 (quat Ar), 124.06 (quat Ar), 123.25 (quat Ar), 123.21 (quat Ar), 123.09 (quat Ar), 120.22 (quat Ar), 119.83 (quat Ar), 119.72 (quat Ar), 118.95 (quat Ar), 118.88 (2 C, $-CH$ Ar), 118.85 (2 C, $-CH$ Ar), 118.58 (2 C, $-CH$ Ar), 118.54 (2 C, $-CH$ Ar), 118.48 (2 C, $-CH$ Ar), 35.65 (1 C, quat $-C(CH_3)_3$), 35.59 (2 C, quat $-C(CH_3)_3$), 35.52 (2 C, quat $-C(CH_3)_3$), 32.01 (3 C, $-CH$, -

$\text{C}(\text{CH}_3)_3$, 31.98 (6 C, -CH, - $\text{C}(\text{CH}_3)_3$), 31.93 (6 C, -CH, - $\text{C}(\text{CH}_3)_3$). **MALDI-TOF MS**; calculated for $\text{C}_{62}\text{H}_{57}\text{I}$: $[\text{M}]^+$ calculated m/z 928.3505, found m/z 928.3549. **IR** ν (cm^{-1}): $\nu(\text{C-H st, aromatic})$: 3099, $\nu(\text{C-H st, -CH}_3)$: 2953, 2902, 2866.

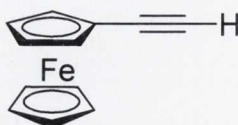
4.2.39. Synthesis of 2,2-dibromo-1-ferrocenyl ethylene (39)



To a solution of triphenylphosphine (6.8 g, 26 mmol) and carbontetrabromide (4.3 g, 13 mmol) in dichloromethane (12 mL) was added a solution of ferrocenecarboxaldehyde (1.4 g, 6.5 mmol) in dichloromethane (5 mL) at 0 °C. The mixture was stirred for 15 minutes and filtered through a celite pad. The filtrate was evaporated and passed through a short silica column (hexane:ethyl acetate 5:1) which yielded 2,2-dibromo-1-ferrocenyl ethylene quantitatively.

Yield: 2.4 g, 93 %. **M.pt:** 53-54°C. **^1H NMR** (CDCl_3) δ : 7.15 (s, 1 H, -C=CH), 4.73 (m, 2 H, -CH Fc), 4.36 (m, 2 H, -CH Fc), 4.26 (s, 5 H, -CH Fc). **^{13}C NMR** (CDCl_3) δ : 135.19 (1 C, -C=CH), 83.15 (1 C, quat, -C=CBr₂), 79.41 (quat Fc), 69.20 (5 C, -CH Fc), 69.14 (2 C, -CH Fc), 68.84 (2 C, -CH Fc). **ESI-MS** (methanol); for $\text{C}_{12}\text{H}_{10}\text{FeBr}_2$: $[\text{M}]^+$ calculated m/z 369.8478, found m/z 369.8469.

4.2.40. Synthesis of ethynylferrocene (40)

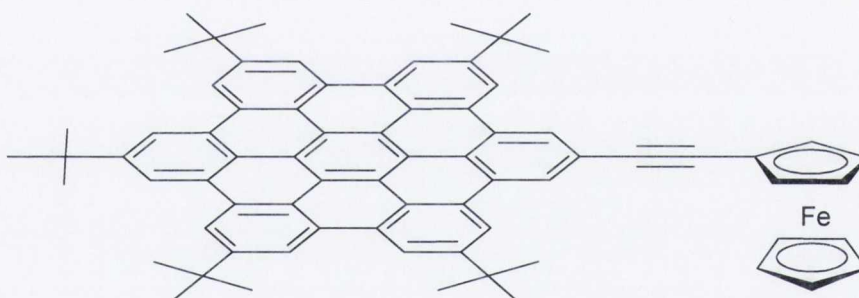


To a solution of **39** (5 g, 13.52 mmol) in tetrahydrofuran (40mL) was added *n*-BuLi (16.9mL, 1.6M in hexane, 27mmol) at -78°C. The mixture was stirred for 1 hour at -78 °C and then for a further 1 hour at room temperature. The reaction was quenched by the addition of water and the product was extracted with diethylether. The

combined organic layer was washed with brine and dried over MgSO_4 , then the solvents were removed *in vacuo*. The residue was passed through a short silica column, elution with hexane yielded the desired product which was purified further by recrystallisation from hexane.

Yield: 2.37 g, 83 %. **M.pt:** 53-54 °C. ^1H NMR (CDCl_3) δ : 4.50 (t, 2 H, $^3J_{\text{HH}} = 1.8$ Hz, -CH Fc), 4.25 (s, 5 H, -CH Fc), 4.23 (t, 2H, $^3J_{\text{HH}} = 1.8$ Hz, -CH Fc), 2.76 (s, 1 H, -C \equiv CH). ^{13}C NMR (CDCl_3) δ : 82.18 (1 C, -C \equiv C-), 73.16 (1 C, -C \equiv C-), 71.32 (2 C, -CH Fc), 69.63 (5C, -CH Fc), 68.31 (2 C, -CH Fc), 63.40 (1 C, quat Fc). **ESI-MS** (acetonitrile); for $\text{C}_{12}\text{H}_{10}\text{Fe}$: $[\text{M}]^+$ calculated m/z 210.0132, found m/z 210.0130.

4.2.41. Synthesis of 2-ethynylferrocenyl-5,8,11,14,17-penta-*tert*-butylhexa-*peri*-hexabenzocoronene (Ferrocenyl-HBC; 41)

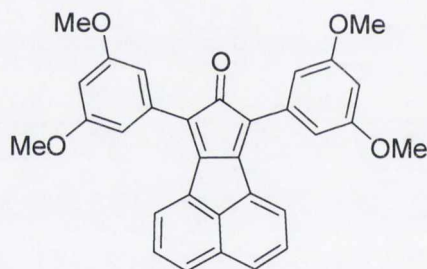


Compound **40** (0.027 g, 0.13 mmol) was dissolved in triethylamine (3 mL) and added *via* cannula to a solution of **38** (0.1 g, 0.11 mmol) and tetrakis(triphenylphosphine)palladium (0.006 g, 0.006 mmol) in toluene (8 mL). The mixture was heated at 70 °C for 18 hours. The solvents were removed *in vacuo*, washed with water and extracted into dichloromethane. The organic phase was dried over MgSO_4 , solvents removed *in vacuo* again before being subjected to column chromatography on silica. Elution with hexane:dichloromethane (1:1) followed by recrystallisation from methanol yielded the desired product.

Yield: 0.08 g, 77 %. **M.pt:** >200 °C (decomp.). ^1H NMR (600 MHz) (CDCl_3) δ : 9.24 (s, 2 H, -CH Ar), 9.18 (s, 2 H, -CH Ar), 9.13 (s, 2 H, -CH Ar), 9.04 (s, 2 H, -CH Ar), 8.91 (s, 2 H, -CH Ar), 8.81 (s, 2 H, -CH Ar), 4.85 (s, 2 H, -CH Fc), 4.50 (s, 5 H, -

CH Fc), 4.46 (s, 2 H, -CH Fc), 1.98 (s, 9 H, -C(CH₃)₃), 1.95 (s, 18 H, -C(CH₃)₃), 1.89 (s, 18 H, -C(CH₃)₃). **¹³C NMR (600 MHz)** (CDCl₃) δ : 148.72 (quat Ar), 148.69 (quat Ar), 148.61 (quat Ar), 130.49 (quat Ar), 130.31 (quat Ar), 130.14 (quat Ar), 130.10 (quat Ar), 129.98 (quat Ar), 129.28 (quat Ar), 124.80 (quat Ar), 124.21 (2 C, -CH Ar), 123.52 (quat Ar), 123.49 (quat Ar), 123.47 (quat Ar), 121.46 (quat Ar), 120.47 (quat Ar), 120.30 (quat Ar), 120.12 (quat Ar), 119.59 (quat Ar), 119.32 (2 C, -CH Ar), 118.99 (2 C, -CH Ar), 118.83 (2 C, -CH Ar), 118.80 (2 C, -CH Ar), 118.78 (2 C, -CH Ar), 91.50 (1 C, quat Fc), 89.21 (1 C, -C \equiv C-), 87.39 (1 C, -C \equiv C-), 71.51 (2 C, -CH Fc), 69.98 (5 C, -CH Fc), 68.93 (2 C, -CH Fc), 35.62 (3 C, quat, -C(CH₃)₃), 35.59 (2 C, quat, -C(CH₃)₃), 31.98 (6 C, -CH, -C(CH₃)₃), 31.94 (9 C, -CH, -C(CH₃)₃). **MALDI-TOF MS**; for C₇₄H₆₆Fe: [M]⁺ calculated m/z 1010.4514, found m/z 1010.4509. **IR** ν (cm⁻¹): ν (C-H st, aromatic): 3099, ν (C-H st, -CH₃): 2954, 2904, 2666, ν (C \equiv C st): 2200 ν (C=C st): 1606, 1578, ν (C-H rock Fc): 1090, 1055.

4.2.42. Synthesis of (42)



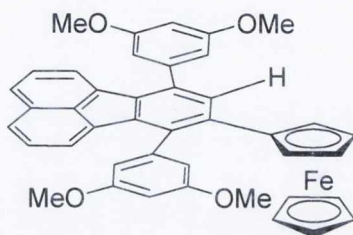
Reaction carried out in air

Acenaphthenequinone (0.55 g, 3.03 mmol) and **14** (1.0 g, 3.03 mmol) were dissolved in methanol (180 mL) then sodium hydroxide (0.18 g, 4.5 mmol) was added. The mixture was then left stirring overnight. It was then kept at 0 °C for 1 hour, after which the green precipitate was filtered and washed with methanol.

Yield: 1.11 g, 77 %. **¹H NMR** (CDCl₃) δ : 8.14 (d, 2 H, ³J_{HH} = 8.0 Hz, -CH Ar), 7.90 (d, 2 H, ³J_{HH} = 8.0 Hz, -CH Ar), 7.63 (t, 2 H, ³J_{HH} = 8.0 Hz, -CH Ar), 7.01 (d, 4 H, ⁴J_{HH} = 2.0 Hz, -CH Ar), 6.56 (t, 2 H, ⁴J_{HH} = 2.0 Hz, -CH Ar), 3.90 (s, 12 H, -OCH₃). **¹³C NMR** (CDCl₃) δ : 186.57 (1 C, -CO), 160.37 (4 C, quat Ar), 153.93 (4 C, quat Ar), 144.42 (4 C, quat Ar), 132.61 (4 C, quat Ar), 131.66 (4 C, quat Ar), 130.93 (4 C, quat Ar), 128.02 (2 C, -CH Ar), 127.37 (2 C, -CH Ar), 121.20 (2 C, quat Ar), 120.88

(2 C, -CH Ar), 106.56 (4 C, -CH Ar), 100.57 (2 C, -CH Ar), 55.06 (4 C, -OCH₃). **ESI-MS** (toluene); for C₃₁H₂₄O₅Na: [MNa]⁺ calculated *m/z* 499.1521, found *m/z* 499.1521.

4.2.43. Synthesis of (43)

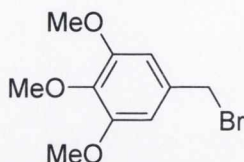


Compound **40** (0.066 g, 0.32 mmol), benzophenone (0.8 g) and **42** (0.15g, 0.32 mmol) were mixed in a round bottomed flask and attached to an air condenser. The mixture was heated at 200°C for 18 hours. The mixture was then subjected to flash column chromatography on silica using diethylether:hexane (1:2) as eluent. The orange/red band was collected and evaporated to afford the desired product.

Yield: 0.2 g, 94 %. **M.pt:** 253-254 °C. **¹H NMR** (CD₂Cl₂) δ: 7.81 (s, 1 H, -CH Ar), 7.78-7.76 (m, 2 H, -CH Ar), 7.45-7.32 (m, 2 H, -CH Ar), 7.38 (dd, 1H, ³J_{HH} = 7.8 Hz, -CH Ar), 6.90 (d, 2 H, ⁴J_{HH} = 2.0 Hz, -CH Ar), 6.73 (d, 1H, ³J_{HH} = 7.0 Hz, -CH Ar), 6.69 (t, 1 H, ⁴J_{HH} = 2.0 Hz, -CH Ar), 6.66 (t, 1H, ⁴J_{HH} = 2.0 Hz, -CH Ar), 6.59 (d, 2 H, ³J_{HH} = 2.0 Hz, -CH Ar), 4.28 (t, 2 H, ³J_{HH} = 2.0 Hz, -CH Fc), 4.19 (t, 2H, ³J_{HH} = 2.0 Hz, -CH Fc), 4.12 (s, 5 H, -CH Fc), 3.91 (s, 6 H, -OCH₃), 3.83 (s, 6 H, -OCH₃). **¹³C NMR** (CD₂Cl₂) δ: 160.91 (1 C, quat Ar), 160.64 (1 C, quat Ar), 142.48 (1 C, quat Ar), 141.67 (1 C, quat Ar), 137.43 (1 C, quat Ar), 137.09 (1 C, quat Ar), 136.61 (1 C, quat Ar), 135.91 (1 C, quat Ar), 135.31 (1 C, quat Ar), 135.26 (1 C, quat Ar), 133.35 (1 C, quat Ar), 132.34 (1 C, quat Ar), 129.95 (1 C, -CH Ar), 129.19 (1 C, quat Ar), 127.26 (1 C, -CH Ar), 127.14 (1 C, -CH Ar), 126.10 (1 C, -CH Ar), 125.92 (1 C, -CH Ar), 123.21 (1 C, -CH Ar), 122.34 (1 C, -CH Ar), 107.25 (1 C, -CH Ar), 106.45 (1 C, -CH Ar), 99.38 (1 C, -CH Ar), 99.21 (1 C, -CH Ar), 84.45 (1 C, quat Fc), 69.38 (2 C, -CH Fc), 69.16 (5 C, -CH Fc), 67.85 (2 C, -CH Fc), 55.02 (2 C, -OCH₃), 54.99 (2C, -OCH₃). **ESI-MS** (methanol); for C₄₂H₃₄FeO₄: [M]⁺ calculated *m/z* 658.1806, found

m/z 658.1816. **IR** ν (cm^{-1}): $\nu(\text{C-H st, aromatic})$: 3087, 3012, $\nu(\text{C-H st, -OCH}_3)$: 2937, 2837, $\nu(\text{C=C st})$: 1587, $\nu(\text{C-O st, -OCH}_3)$: 1201, $\nu(\text{C-H rock Fc})$: 1150, 1104, 1056.

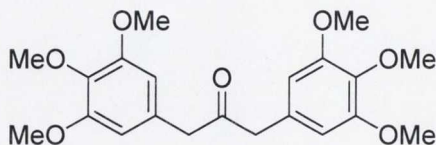
4.2.44. Synthesis of 3, 4, 5-trimethoxybenzylbromide (44)



3, 4, 5-trimethoxybenzyl alcohol (6.09 g, 30.5 mmol) was dissolved in dichloromethane (75 mL) in a 3 necked round bottomed flask. The mixture was cooled to $-5\text{ }^{\circ}\text{C}$, and a solution of phosphorous tribromide (2.1 mL, 6.1 g, 22.2 mmol), dissolved in dichloromethane (5 mL) was added dropwise. The resulting mixture was poured onto ice (100 g), neutralized with sodium hydrogencarbonate, and the organic phase was separated. The aqueous phase was extracted with dichloromethane (3 x 20 mL), and the combined organic phase was washed with brine (30 mL), dried over MgSO_4 and the solvents were removed *in vacuo*. This yielded the desired product as a yellow/white solid.

Yield: 7.0 g, 88 %. $^1\text{H NMR}$ (CDCl_3) δ : 6.63 (s, 2 H, -CH Ar), 4.47 (s, 2 H, - CH_2), 3.88 (s, 6 H, - OCH_3), 3.85 (s, 3 H, - OCH_3).

4.2.45. Synthesis of 1,3-bis-(3,4,5-trimethoxy)propan-2-one (45)

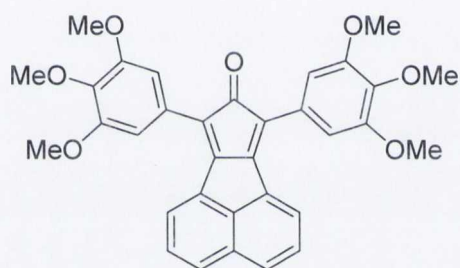


Calcium hydroxide (2.96 g, 40 mmol) and tetrabutylammonium hydrogensulphate (1.7 g, 5.0 mmol) were dissolved in 1:1 dichloromethane:water (200 mL) and argon was bubbled through the reaction mixture for 30 minutes to degas the solution. Compound **44** (5.22 g, 20.0 mmol) was added followed by iron pentacarbonyl (1.96

mL, 10.0 mmol) and the reaction was stirred at room temperature for eight hours with a constant stream of argon circulated over the reaction. The reaction mixture was then oxidised in air and acidified with 10 % HCl (35 mL). The aqueous phase was extracted with dichloromethane (3 x 50 mL) and the organic washings were combined and reduced to yellow/brown oil. The desired product was obtained by flash chromatography using silica and eluting with ethyl acetate:hexane (2:1) yielding the desired product as a off-white solid.

Yield: 2.28 g, 58 %. $^1\text{H NMR}$ (CDCl_3) δ : 6.33 (s, 4 H, -CH Ar), 3.82 (s, 6 H, -OCH₃), 3.81 (s, 12 H, -OCH₃), 3.67 (s, 4 H, -CH₂).

Synthesis of (46)



Reaction carried out in air

Acenaphthenequinone (0.54 g, 2.94 mmol) and **45** (1.15 g, 2.94 mmol) were dissolved in methanol (150 mL) then sodium hydroxide (0.30 g, 5.38 mmol) was added. The mixture was then left stirring overnight. It was then kept at 0 °C for 1 hour, after which the green precipitate was filtered and washed with methanol. The green crude product was purified by flash chromatography on silica eluting with dichloromethane:methanol (20:1), yielding a green solid.

Yield: 1.03 g, 65 %. $^1\text{H NMR}$ (CDCl_3) δ : 8.14 (d, 2 H, $^3J_{\text{HH}} = 7.0$ Hz, -CH Ar), 7.91 (d, 2 H, $^3J_{\text{HH}} = 8.5$ Hz, -CH Ar), 7.64 (dd, 2 H, $^3J_{\text{HH}} = 7.5$ Hz, -CH Ar), 7.10 (s, 4 H, -CH Ar), 3.97 (s, 12 H, -OCH₃), 3.96 (s, 6 H, -OCH₃). $^{13}\text{C NMR}$ (CDCl_3) δ : 171.47 (1C, quat -CO), 153.21 (2C, quat Ar), 152.92 (4C, quat Ar), 144.42 (1C, quat Ar), 138.03 (1C, quat Ar), 131.82, (2C, quat Ar), 131.12 (2C, quat Ar), 128.02 (2C, -CH

Ar), 127.33 (2C, -CH Ar), 126.31 (2C, quat Ar), 121.03 (2C, quat Ar), 120.43 (2C, -CH Ar), 105.83 (4C, -CH Ar), 60.60 (2C, -OCH₃), 55.85 (4C, -OCH₃).

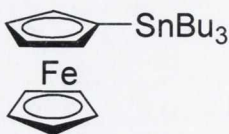
4.2.46. Synthesis of lithioferrocene (47)



Ferrocene (10 g, 53.75 mmol) was dissolved in tetrahydrofuran (65 mL) and cooled to 0 °C. Under efficient stirring *t*-BuLi (34.8 mL, 1.7 M in pentane, 59.16 mmol) was added over a 15 minute period. Immediately after the addition was completed, hexane (75 mL) was added and the mixture was cooled to -78 °C to precipitate the crude product, consisting of a mixture of lithioferrocene and unreacted ferrocene. The precipitate was isolated by schlenk filtration and washed with hexane (3 x 80 mL) until the filtrate was almost colourless, indicating complete removal of unreacted ferrocene. The schlenk filter was evacuated and the product was thoroughly dried *in vacuo*, affording pyrophoric yellowish powder, which was transferred under proper precautions with protection to a storage schlenk.

Yield: 5.61 g, 54 %. Due to the extreme air-sensitivity of lithioferrocene no analytical or spectroscopic data could be obtained.

4.2.47. Synthesis of tri-*n*-butylstannyl-ferrocene (48)

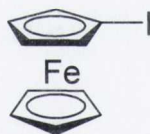


Compound **47** (5.61 g, 29.2 2mmol) was taken up in tetrahydrofuran (15 mL) and hexane (15 mL) and stirred at 0 °C for 30 minutes. Once the time had elapsed tributyltinchloride (14.27 g, 11.89 mL 43.84 mmol,) was added over 20 minutes. The

mixture was allowed to stir for a 90 minutes after which the reaction mixture was hydrolysed with aqueous sodium hydroxide solution. The product was extracted with diethylether, and then the organic layer was washed with brine and water and dried over MgSO_4 . The solvent was then removed *in vacuo* and the crude product was subjected to column chromatography on silica. Elution with hexane yielded the desired product as a brown-black oil.

Yield: 6.14 g, 44 %. $^1\text{H NMR}$ (CDCl_3) δ : 4.41 (s, 2 H, -CH Fc), 4.17 (s, 5 H, -CH Fc), 4.09 (s, 2 H, -CH Fc), 1.66 (m, 6 H, -CH butyl), 1.45 (m, 6 H, -CH butyl), 1.12 (m, 6 H, -CH butyl), 1.08 (m, 9 H, -CH butyl). $^{13}\text{C NMR}$ (CDCl_3) δ : 73.78 (2 C, -CH Fc), 69.85 (2 C, -CH Fc), 68.24 (1 C, quat Fc), 67.50 (5 C, -CH Fc), 28.84 (3 C, -CH butyl), 27.06 (3 C, -CH butyl), 13.35 (3 C, -CH butyl), 9.85 (3 C, -CH butyl). **ESI-MS** (methanol); for $\text{C}_{22}\text{H}_{36}\text{FeSn}$: $[\text{M}]^+$ calculated m/z 476.1188, found m/z 476.1198.

4.2.48. Synthesis of iodoferrocene (49)



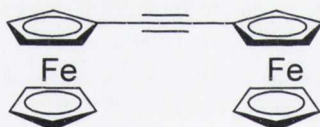
Iodine (3.61 g, 14.2 mmol) was added to **48** (6.14 g, 12.9 mmol) in dichloromethane (55 mL). The solution was stirred for 18 hours at room temperature. It was then washed with aqueous sodium thiosulphate solution (10 % w/v), extracted into dichloromethane, washed with water and dried over MgSO_4 . The solvent was then removed *in vacuo* and the crude product was subjected to column chromatography on silica:KF (90:10). Recrystallisation from pentane afforded pure iodoferrocene.

Yield: 3.25 g, 81 %. $^1\text{H NMR}$ (CDCl_3) δ : 4.44 (t, 2 H, $^3J_{\text{HH}} = 2.0$ Hz, -CH Fc), 4.22 (s, 5 H, -CH Fc), 4.18 (t, 2 H, $^3J_{\text{HH}} = 2.0$ Hz, -CH Fc). $^{13}\text{C NMR}$ (CDCl_3) δ : (2 C, -CH Fc), (5 C, -CH Fc), (2 C, -CH Fc), (1 C, quat Fc). **ESI-MS** (methanol); for $\text{C}_{10}\text{H}_9\text{FeI}$: $[\text{M}]^+$ calculated m/z 311.9098, found m/z 311.9098.

4.2.49. Synthesis of cuprous ferrocenylacetylide (**50**)

A solution of copper(I) iodide (2.04 g, 10.71 mmol) in 30% aqueous ammonia (30 mL) was added to a solution of **40** (1.5 g, 7.14 mmol) in absolute ethanol (40 mL). After stirring for 15 minutes at room temperature the yellow salt was filtered off and quickly washed with small portions of water, then ethanol and finally diethylether. The salt was dried in an oven at 80 °C for 2 hours.

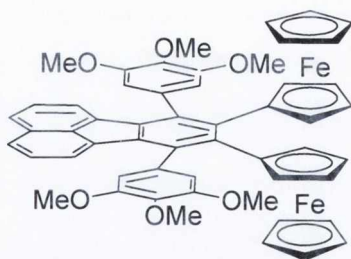
Yield: 1.01 g, 52 %. $^1\text{H NMR}$ (CDCl_3) δ : 4.24 (s, 5 H, -CH Fc), 4.18 (s, 4 H, -CH Fc).

4.2.50. Synthesis of diferrocenylacetylene (**51**)

A solution of **50** (1g, 3.67mmol) and **49** (1.45g, 4.65mmol) in pyridine (40mL) was heated at reflux for 8 hours. The reaction mixture was cooled to room temperature, diluted with water and extracted with diethylether. The ether portion was washed with water, 5% hydrochloric acid, 5% sodium hydroxide solution and finally with water then dried over MgSO_4 . After the removal of the solvents *in vacuo* the residue was subjected to column chromatography on alumina. Elution with hexane:benzene (2:1) yielded the desired product as an orange powder.

Yield: 0.27 g, 19 %. Due to poor solubility only mass spectrometry was possible for characterisation. **ESI-MS** (toluene); for $\text{C}_{22}\text{H}_{18}\text{Fe}_2$: $[\text{M}]^+$ calculated m/z 394.0107, found m/z 394.0120.

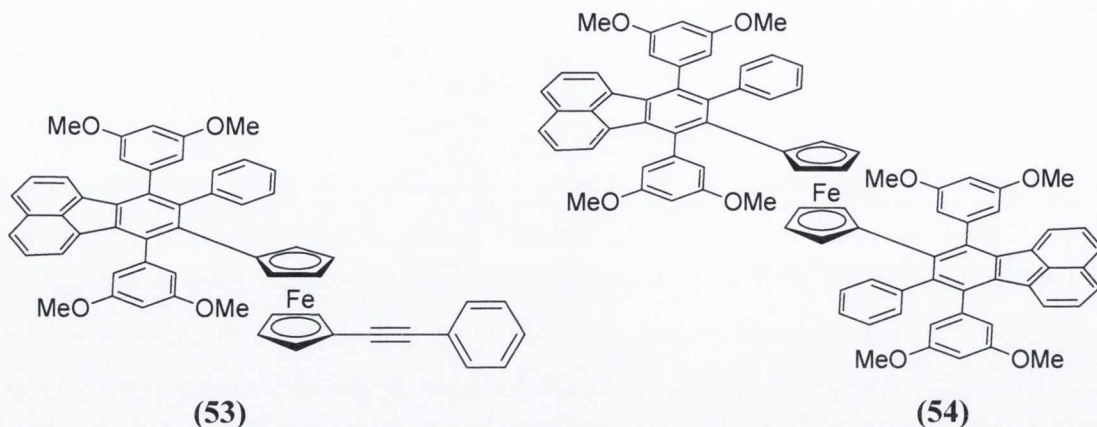
4.2.51. Synthesis of (52)



Acetylene **51** (0.15 g, 0.37 mmol), benzophenone (1.5 g) and **46** (0.20 g, 0.37 mmol) were mixed in a round bottomed flask and attached to an air condenser. The mixture was heated at 200 °C. The mixture was then subjected to flash column chromatography on silica using dichloromethane as eluent. The orange/red band was collected and evaporated to afford the desired product.

Yield: 0.3g, 38 %. **M.pt:** >200 °C (decomp.). **¹H NMR** (CDCl₃) δ: 7.73 (d, 2 H, ³J_{HH}=8.5 Hz, -CH Ar), 7.33 (dd, 2 H, ³J_{HH}=7.8 Hz, -CH Ar), 6.95 (s, 4 H, -CH Ar), 6.40 (d, 2 H, ³J_{HH}=7.0 Hz, -CH Ar), 4.13 (s, 6 H, -OCH₃), 4.07 (s, 4 H, -CH Fc), 3.95 (s, 16 H, -CH Fc and -OCH₃), 3.81 (s, 10 H, -CH Fc). **¹³C NMR** (CDCl₃) δ: 152.74 (2 C, quat Ar), 137.91 (2 C, quat Ar), 137.50 (2 C, quat Ar), 137.47 (2 C, quat Ar), 135.90 (2 C, quat Ar), 135.76 (2 C, quat Ar), 134.86 (2 C, quat Ar), 132.99 (2 C, quat Ar), 129.10 (2 C, quat Ar), 127.14 (2 C, -CH Ar), 125.84 (2 C, -CH Ar), 122.92 (2 C, -CH Ar), 108.37 (4 C, -CH Ar), 89.60 (2 C, quat Fc), 72.78 (4 C, -CH Fc), 68.81 (10 C, -CH Fc), 66.59 (4 C, -CH Fc), 60.96 (2 C, -OCH₃), 55.82 (4 C, -OCH₃). **ESI-MS** (methanol); for C₅₄H₄₆Fe₂O₆: [M]⁺ calculated *m/z* 902.1993, found *m/z* 902.1957. **IR** ν (cm⁻¹): ν(C-H st, aromatic): 3091, ν(C-H st, -OCH₃): 2954, 2033, ν(C=C st): 1577, ν(C-O st, -OCH₃): 1232, ν(C-H rock Fc): 1121, 1107, 1004.

4.2.52. Synthesis of (53) and (54)



Di-acetylene **7** (0.1 g, 0.26 mmol), **42** (0.26 g, 0.54 mmol) and benzophenone (1.5 g) were mixed in a round bottomed flask and attached to an air condenser. The mixture was heated at 200 °C for 24 hours. The mixture was then subjected to flash column chromatography on silica using first hexane:dichloromethane (2:1) and dichloromethane as eluent. The first orange-red band was the mono- Diels-Alder product (**53**) whereas the second band which was red was the di- Diels-Alder product (**54**).

4.2.52.1. Characterisation of (53)

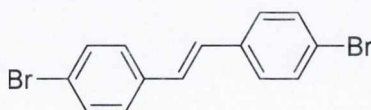
Yield: 0.0 g, 29 %. **M.pt:** 210-211 °C. **¹H NMR (600 MHz)** (CD₂Cl₂) δ: 7.76 (d, 1 H, ³J_{HH} = 8.6 Hz, -CH Ar), 7.74 (d, 1 H, ³J_{HH} = 9.0 Hz, -CH Ar), 7.37 (dd, 1 H, ³J_{HH} = 7.8 Hz, -CH Ar), 7.31 (dd, 1 H, ³J_{HH} = 7.8 Hz, -CH Ar), 7.23-7.21 (m, 5 H, -CH Ar), 7.14 (d, 2H, ³J_{HH} = 7.0 Hz, -CH Ar), 6.93 (t, 1 H, ³J_{HH} = 7.3 Hz, -CH Ar), 6.91 (d, 2 H, ⁴J_{HH} = 2.3 Hz, -CH Ar), 6.81 (t, 2 H, ³J_{HH} = 8.0 Hz, -CH Ar), 6.77 (t, 1 H, ⁴J_{HH} = 2.0 Hz, -CH Ar), 6.51 (d, 1 H, ³J_{HH} = 7.0 Hz, -CH Ar), 6.35-6.34 (m, 2 H, -CH Ar), 6.23 (d, 2 H, ⁴J_{HH} = 2.0 Hz, -CH Ar), 4.32 (s, 2 H, -CH Fc), 4.05 (s, 2 H, -CH Fc), 3.98 (s, 2 H, -CH Fc), 3.93 (s, 6 H, -OCH₃), 3.88 (s, 2 H, -CH Fc), 3.68 (s, 6 H, -OCH₃). **¹³C NMR (600 MHz)** (CD₂Cl₂) δ: 161.09 (quat Ar), 160.77 (quat Ar), 144.10 (quat Ar), 142.43 (quat Ar), 142.36 (quat Ar), 141.51 (quat Ar), 138.38 (quat Ar), 138.33 (quat Ar), 137.93 (quat Ar), 137.04 (quat Ar), 136.31 (quat Ar), 135.03 (quat Ar), 133.55 (quat Ar), 132.57 (quat Ar), 131.88 (-CH Ar), 131.11 (-CH Ar), 129.83 (quat Ar), 128.04 (-CH Ar), 127.85 (-CH Ar), 127.46 (-CH Ar), 126.59 (-CH

Ar), 126.54 (-CH Ar), 124.06 (-CH Ar), 123.68 (quat Ar), 123.14 (-CH Ar), 108.95 (-CH Ar), 108.35 (-CH Ar), 100.15 (-CH Ar), 99.43 (-CH Ar), 87.76 (1C, -C≡C-), 86.84 (1C, -C≡C-), 73.33 (2 C, -CH Fc), 72.76 (2 C, -CH Fc), 70.49 (2 C, -CH Fc), 70.12 (2 C, -CH Fc), 55.89 (2 C, -OCH₃), 55.61 (2 C, -OCH₃). **ESI-MS** (toluene); calculated for C₅₆H₄₂FeO₄: [M]⁺ calculated *m/z* 834.2433, found *m/z* 834.2421. **IR** *v* (cm⁻¹): *v*(C-H st, aromatic): 3147, 3060, *v*(C-H st, -OCH₃): 2960, 2933, *v*(C≡C st): 2206, *v*(C=C st): 1589, *v*(C-O st, -OCH₃): 1201, *v*(C-H rock Fc): 1056, 1044, 1025.

4.2.52.2. Characterisation of (54)

Yield: 0.0538g, 16%. **M.pt:** 284-285 °C. **¹H NMR (600 MHz)** (CDCl₃) δ: 7.76 (d, 2 H, ³J_{HH} = 8.0 Hz, -CH Ar), 7.74 (d, 2 H, ³J_{HH} = 8.0 Hz, -CH Ar), 7.34 (dt, 4 H, ³J_{HH} = 8.0 Hz, -CH Ar), 7.08 (d, 2 H, ³J_{HH} = 7.1 Hz, -CH Ar), 7.05 (t, 4 H, ³J_{HH} = 7.5 Hz, -CH Ar), 6.96 (d, 4 H, ³J_{HH} = 7.2 Hz, -CH Ar), 6.65 (t, 2 H, ⁴J_{HH} = 2.0 Hz, -CH Ar), 6.60 (d, 2 H, ³J_{HH} = 7.2 Hz, -CH Ar), 6.55 (d, 4 H, ⁴J_{HH} = 2.2 Hz, -CH Ar), 6.34 (d, 2 H, ³J_{HH} = 7.2 Hz, -CH Ar), 6.32 (t, 2 H, ⁴J_{HH} = 2.0 Hz, -CH Ar), 6.30 (d, 4 H, ⁴J_{HH} = 2.0 Hz, -CH Ar), 3.70 (s, 8 H, -CH Fc and -OCH₃), 3.59 (s, 8 H, -CH Fc and -OCH₃). **¹³C NMR (600 MHz)** (CD₂Cl₂) δ: 161.72 (quat Ar), 160.76 (quat Ar), 143.96 (quat Ar), 142.42 (quat Ar), 142.09 (quat Ar), 141.16 (quat Ar), 138.50 (quat Ar), 138.29 (quat Ar), 138.04 (quat Ar), 137.08 (quat Ar), 136.36 (quat Ar), 134.96 (quat Ar), 134.59 (quat Ar), 133.55 (quat Ar), 131.89 (-CH Ar), 129.85 (quat Ar), 128.06 (-CH Ar), 127.93 (-CH Ar), 127.43 (-CH Ar), 126.64 (-CH Ar), 126.57 (-CH Ar), 126.27 (-CH Ar), 124.04 (-CH Ar), 123.13 (-CH Ar), 108.71 (-CH Ar), 108.34 (-CH Ar), 99.96 (-CH Ar), 99.45 (-CH Ar), 55.74 (-OCH₃ and -CH Fc), 55.50 (-OCH₃ and -CH Fc). **MALDI-TOF MS**; for C₈₆H₆₆FeO₈: [M]⁺ calculated *m/z* 1282.4107, found *m/z* 1282.4147. **IR** *v* (cm⁻¹): *v*(C-H st, aromatic): 3054, *v*(C-H st, -OCH₃): 2835, *v*(C=C st): 1587, *v*(C-O st, -OCH₃): 1202, *v*(C-H rock Fc): 1059, 1049, 1028.

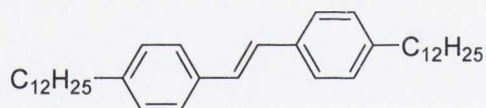
4.2.53. Synthesis of *trans*-4, 4'-dibromostilbene (55)



To a stirred suspension of zinc powder (19.9 g, 30 mmol) in dry tetrahydrofuran (300 mL), titanium tetrachloride (16.5 mL, 151 mmol) was added slowly at $-10\text{ }^{\circ}\text{C}$. Then, a solution of 4-bromobenzaldehyde (10.0 g, 54 mmol) in dry tetrahydrofuran (250 mL) was added dropwise at reflux temperature and the mixture was stirred further under reflux for 5 hours. The solution was quenched with saturated NaHCO_3 solution and extracted with ethyl acetate. The extract was washed with brine, then water, dried over MgSO_4 , concentrated and washed with hexane to yield the desired product as a white solid.

Yield: 7.5 g, 82 %. **M.pt:** $184\text{--}185^{\circ}\text{C}$. $^1\text{H NMR}$ (CDCl_3) δ : 7.50 (d, 4 H, $^3J_{\text{HH}} = 8.3$ Hz, -CH Ar), 7.38 (d, 4 H, $^3J_{\text{HH}} = 8.3$ Hz, -CH Ar), 7.04 (s, 2 H, -C=CH). $^{13}\text{C NMR}$ (CDCl_3) δ : 135.45 (2 C, quat Ar), 131.41 (4 C, -CH Ar), 127.67 (2 C, -C=CH), 127.57 (4 C, -CH Ar), 121.19 (2 C, quat Ar).

4.2.54. Synthesis of 4, 4'-didodecyl-*trans*-stilbene (56)

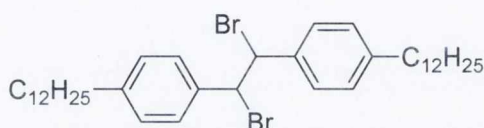


Dodecylmagnesiumbromide (50 mL, 1 M in diethylether, 0.5 mol) was added to a solution of **55** (7.45 g, 22 mmol) and $\text{NiCl}_2(\text{dppp})$ (0.48 g, 0.89 mmol) in diethylether (60 mL). After stirring overnight, 2 M aqueous HCl was added to the reaction mixture. The organic phase, together with some precipitate was separated from the aqueous phase and the solvent was removed under reduced pressure. The residue was dissolved in dichloromethane and filtered over silica to afford the desired product as a white solid.

Yield: 10.6 g, 93 %. **M.pt:** $80\text{--}82^{\circ}\text{C}$. $^1\text{H NMR}$ (CDCl_3) δ : 7.44 (d, 4 H, $^3J_{\text{HH}} = 8.0$ Hz, -CH Ar), 7.18 (d, 4 H, $^3J_{\text{HH}} = 8.0$ Hz, -CH Ar), 7.07 (s, 2 H, -C=CH), 2.63 (t, 4 H, $^3J_{\text{HH}} = 7.5$ Hz, -CH dodecyl), 1.1-1.5 (m, 40 H, -CH dodecyl), 0.91 (t, 6 H, $^3J_{\text{HH}} = 7.0$ Hz, -CH dodecyl). $^{13}\text{C NMR}$ (CDCl_3) δ : 141.97 (2 C, quat Ar), 134.50 (2 C, quat

Ar), 128.27 (4 C, -CH Ar), 127.24 (2 C, -C=CH), 125.85 (4 C, -CH Ar), 35.28 (-CH dodecyl Ar), 31.49 (-CH dodecyl), 31.03 (-CH dodecyl), 29.23 (-CH dodecyl), 29.21 (-CH dodecyl), 29.16 (-CH dodecyl), 29.09 (-CH dodecyl), 28.92 (-CH dodecyl), 28.88 (-CH dodecyl), 22.26 (-CH dodecyl), 13.70 (-CH dodecyl).

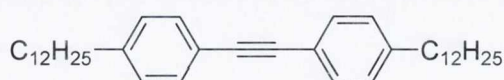
4.2.55. Synthesis of 1, 2 –dibromo-1, 2-bis(4-dodecylphenyl)ethane (57)



Bromine (1 mL, 19.6 mmol) was added to a solution of **56** (10 g, 19.4 mmol) in chloroform (120 mL). After stirring overnight at room temperature the solution was washed with aqueous sodium sulfite and water and dried over MgSO_4 . The solvent was removed to yield the desired product.

Yield: 12.3 g, 94 %. **M.pt:** 115-117°C. $^1\text{H NMR}$ (CDCl_3) δ : 7.43 (d, 4 H, $^3J_{\text{HH}} = 8.0$ Hz, -CH Ar), 7.24 (d, 4 H, $^3J_{\text{HH}} = 8.0$ Hz, -CH Ar), 7.09 (d, 4 H, $^3J_{\text{HH}} = 8.0$ Hz, -CH Ar), 6.98 (d, 4 H, $^3J_{\text{HH}} = 8.0$ Hz, -CH Ar), 5.51 (s, 2 H, -CHBr), 5.48 (s, 2 H, -CHBr), 2.65 (t, 4 H, $^3J_{\text{HH}} = 7.5$ Hz, -CH dodecyl), 2.52 (t, 4 H, $^3J_{\text{HH}} = 7.5$ Hz, -CH dodecyl), 1.1-1.9 (m, 40 H, -CH dodecyl), 0.90 (t, 6 H, $^3J_{\text{HH}} = 7.0$ Hz, -CH dodecyl). $^{13}\text{C NMR}$ (CDCl_3) δ : 143.55 (2 C, quat Ar), 142.98 (2 C, quat Ar), 136.89 (2 C, quat Ar), 134.62 (2 C, quat Ar), 128.31 (4 C, -CH Ar), 127.98 (4 C, -CH Ar), 127.65 (4 C, -CH Ar), 127.26 (4 C, -CH Ar), 59.10 (2 C, -CHBr), 56.06 (2 C, -CHBr), 35.33 (-CH dodecyl), 35.10 (-CH dodecyl), 31.49 (-CH dodecyl), 30.79 (-CH dodecyl), 30.71 (-CH dodecyl), 29.24 (-CH dodecyl), 29.16 (-CH dodecyl), 29.07 (-CH dodecyl), 28.95 (-CH dodecyl), 28.93 (-CH dodecyl), 22.27 (-CH dodecyl), 13.70 (-CH dodecyl).

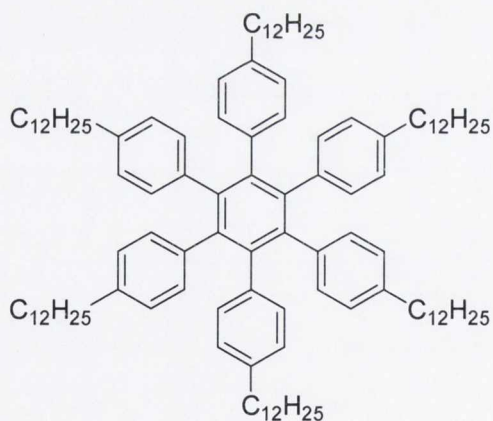
4.2.56. Synthesis of 4,4'-didodecyldiphenylacetylene (58)



A solution of **57** (12.0 g, 17.7 mmol) and potassium-*tert*-butoxide (25 g, 223 mmol) in *tert*-butanol (180 mL) was heated at reflux for 18 hours. The reaction mixture was then cooled to room temperature and extracted with methyl-*tert*-butyl ether. The organic phase was washed with 2 N hydrochloric acid and a saturated sodium bicarbonate solution and dried over MgSO₄. After evaporation of the solvent the crude product was recrystallised from toluene to afford the desired product.

Yield: 7.9 g, 86 %. **M.pt:** 57-58 °C. **¹H NMR** (CDCl₃) δ: 7.45 (d, 4 H, ³J_{HH} = 8.0 Hz, -CH Ar), 7.17 (d, 4 H, ³J_{HH} = 8.0 Hz, -CH Ar), 2.63 (t, 4 H, ³J_{HH} = 7.8 Hz, -CH dodecyl), 1.6-1.2 (m, 40 H, -CH dodecyl), 0.91 (t, 6H, ³J_{HH} = 6.8 Hz, -CH dodecyl). **¹³C NMR** (CDCl₃) δ: 142.78 (2 C, quat Ar), 131.00 (4 C, -CH Ar), 127.98 (4 C, -CH Ar), 120.13 (2 C quat Ar), 88.46 (2 C, -C≡C-), 35.46 (-CH dodecyl), 31.48 (-CH dodecyl), 30.84 (-CH dodecyl), 29.23 (-CH dodecyl), 29.20 (-CH dodecyl), 29.15 (-CH dodecyl), 29.05 (-CH dodecyl), 28.92 (-CH dodecyl), 28.82 (-CH dodecyl), 22.26 (-CH dodecyl), 13.70 (-CH dodecyl).

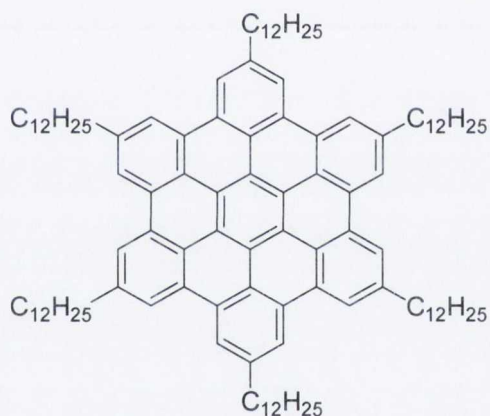
4.2.57. Synthesis of hexa(4-dodecylphenyl)benzene (**59**)



Acetylene **58** (0.5g, 0.97mmol) and cobalt octacarbonyl (0.01g, 0.05mmol) were placed in a round-bottomed flask, dioxane (20mL) was injected and the mixture was refluxed for 20 hours. Once the time had elapsed the reaction mixture was allowed to cool to room temperature and the crystalline precipitate was filtered off and dissolved in CS₂. Filtration of this solution and removal of the solvent under reduced pressure afforded the desired compound as colourless crystals.

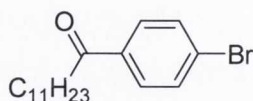
Yield: 0.34 g, 68 %. **M.pt:** >300 °C. **¹H NMR** (CDCl₃) δ: 6.69 (d, 12 H, ³J_{HH} = 8.0 Hz, -CH Ar), 6.63 (d, 12 H, ³J_{HH} = 8.0 Hz, -CH Ar), 2.36 (t, 12 H, ³J_{HH} = 7.0 Hz, -CH dodecyl), 1.43-1.12 (m, 120 H, -CH dodecyl), 0.90 (t, 18 H, ³J_{HH} = 7.0 Hz, -CH dodecyl). **¹³C NMR (600 MHz)** (CDCl₃) δ: 140.28 (6 C, quat Ar), 139.03 (6 C, quat Ar), 138.29, (6 C, quat Ar), 131.40 (12 C, -CH Ar), 126.44 (12 C, -CH Ar), 35.37 (-CH dodecyl), 31.94 (-CH dodecyl), 31.25 (-CH dodecyl), 29.78 (-CH dodecyl), 29.75 (-CH dodecyl), 29.71 (-CH dodecyl), 29.70 (-CH dodecyl), 29.56 (-CH dodecyl), 29.39 (-CH dodecyl), 28.88 (-CH dodecyl), 22.70 (-CH dodecyl), 14.10 (-CH dodecyl).

4.2.58. Synthesis of hexa-dodecyl-hexa-*peri*-hexabenzocoronene (60)



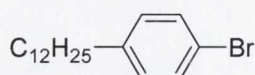
A solution of iron(III) chloride (0.32 g, 3.1.95 mmol) in nitromethane (3mL) was added dropwise to a stirred solution of **59** (0.1 g, 0.07 mmol) in dichloromethane (40mL). The resulting green reaction mixture was stirred for 30 minutes at room temperature and then quenched with methanol (10mL). Water (10mL) and dilute ammonia (20mL) was added and the mixture allowed to stir for 2 hours. Once the time had elapsed it was extracted into chloroform, washed with water and dried over MgSO₄. The residual oil was purified by column chromatography on silica. Elution with toluene yielded the desired product as a yellow solid.

Yield: 0.06 g, 64 %. **M.pt:** >300 °C. **¹H NMR (600 MHz)** (CDCl₃) δ: 8.44 (s, 12 H, -CH Ar), 2.03 (m, 12 H, -CH dodecyl), 1.46-1.31 (m, 120 H, -CH dodecyl), 0.90 (m, 18 H, -CH dodecyl).

4.2.59. Synthesis of 4-bromododecanoylbenzene (**61**)

Dodecanoyl chloride (21.9 g, 23.4 mL, 0.1 mol) was added dropwise to a mixture of bromobenzene (31.3 g, 21 mL, 0.2 mol) and aluminium chloride (16 g, 0.12 mol). The reaction mixture was then stirred at 50 °C for 1 hour, poured into ice water, and extracted with dichloromethane. The organic phase was washed with 2 N hydrochloric acid and brine and dried over MgSO₄. After removal of the solvents *in vacuo*, the residue was purified by recrystallisation from ethanol which yielded the desired product.

Yield: 25.9 g, 76%. **M.pt:** 64-65 °C. **¹H NMR** (CDCl₃) δ: 7.83 (d, 2 H, ³J_{HH} = 8.5 Hz, -CH Ar), 7.61 (d, 2 H, ³J_{HH} = 8.5 Hz, -CH Ar), 2.94 (t, 2 H, ³J_{HH} = 7.5 Hz, -CH dodecyl), 1.74 (q, 2 H, ³J_{HH} = 7.5 Hz, -CH dodecyl), 1.1-1.3 (m, 18 H, -CH dodecyl), 0.90 (t, 3 H, ³J_{HH} = 7.0 Hz, -CH dodecyl). **¹³C NMR** (CDCl₃) δ: 199.08 (1 C, -CO), 135.31 (1 C, quat Ar), 131.40 (2C, -CH Ar), 129.16 (2 C, -CH Ar), 127.54 (1 C, quat Ar), 38.15 (-CH dodecyl), 31.46 (-CH dodecyl), 29.17 (-CH dodecyl), 29.05 (-CH dodecyl), 29.02 (-CH dodecyl), 28.89 (-CH dodecyl), 28.87 (-CH dodecyl), 23.82 (-CH dodecyl), 22.25 (-CH dodecyl), 13.69 (-CH dodecyl).

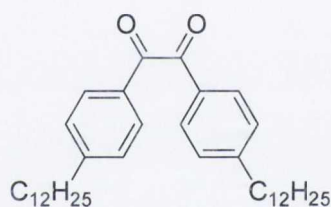
4.2.60. Synthesis of 4-bromododecylbenzene (**62**)

A mixture of **61** (25 g, 73.68 mmol), hydrazine hydrate (10.73 mL, 220 mmol) and potassium hydroxide (16.5 g, 294 mmol) in triethylene glycol (125 mL) was heated at reflux for 2 hours. The mixture was distilled at atmospheric pressure until the temperature of the reaction mixture reached 210 °C. After cooling to room temperature, the resulting mixture was poured into water, acidified with concentrated hydrochloric acid (25 mL), and extracted with dichloromethane. The organic phase

was washed with water, dried over MgSO_4 and concentrated under reduced pressure. The residue was purified by column chromatography on silica, elution with petroleum ether yielded the desired product as a colourless oil.

Yield: 18.3 g, 76 %. $^1\text{H NMR}$ (CDCl_3) δ : 7.41 (d, 2 H, $^3J_{\text{HH}} = 8.5$ Hz, -CH Ar), 7.08 (d, 2 H, $^3J_{\text{HH}} = 8.5$ Hz, -CH Ar), 2.58 (t, 2 H, $^3J_{\text{HH}} = 7.5$ Hz, -CH dodecyl), 1.1-1.6 (m, 20 H, -CH dodecyl), 0.92 (t, 3H, $^3J_{\text{HH}} = 7.0$ Hz, -CH dodecyl). $^{13}\text{C NMR}$ (CDCl_3) δ : 141.41 (1 C, quat Ar), 130.80 (2 C, -CH Ar), 129.73 (2 C, -CH Ar), 118.79 (1 C, quat Ar), 34.92 (-CH dodecyl), 31.50 (-CH dodecyl), 30.91 (-CH dodecyl), 29.24 (-CH dodecyl), 29.22 (-CH dodecyl), 29.14 (-CH dodecyl), 29.04 (-CH dodecyl), 28.93 (-CH dodecyl), 28.76 (-CH dodecyl), 22.28 (-CH dodecyl), 13.71 (-CH dodecyl).

4.2.61. Synthesis of 4,4'-didodecylbenzil (63)



4.2.61.1. Method A

n-BuLi (14.82 mL, 2.24 M, 33.2 mmol) was added to **62** (9 g, 27.66 mmol) in tetrahydrofuran (60 mL) at -78°C and allowed to stir at this temperature for 90 minutes. Once the time had elapsed it was added *via* cannula to a suspension of DMPD (**32**) (1.8 g, 12.57 mmol) in tetrahydrofuran (80 mL) also at -78°C and allowed to warm to room temperature and stirred for a further 18 hours. The reaction was quenched with HCl (2 M) and dichloromethane was added, the organic phase was removed and washed with HCl (2 M) and deionised water, and dried over MgSO_4 . After evaporation of the solvent the resulting solid was purified by column chromatography on silica, eluting with a mixture of dichloromethane : petroleum ether (3:1) yielded the desired product.

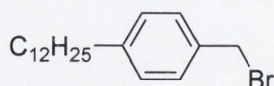
Yield: 2.77 g, 40 %.

4.2.61.2. Method B

A mixture of **58** (2.0 g, 3.88 mmol) and iodine (0.49 g, 1.92 mmol) in dimethyl sulfoxide (10 mL) was stirred at 155 °C for 18 hours. After cooling to room temperature the reaction mixture was poured into an aqueous sodium thiosulphate solution (50 mL) and extracted with dichloromethane. The organic phase was washed with water and dried over MgSO₄. After evaporation of the solvent the residue was purified by column chromatography on silica, elution with petroleum ether/dichloromethane (3:1) yielded the desired product as yellow crystals.

Yield: 1.57 g, 74 %.

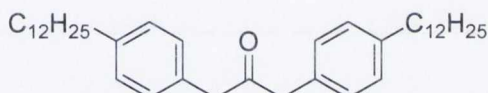
M.pt: 47-48 °C. **¹H NMR** (CDCl₃) δ: 7.90 (d, 4 H, ³J_{HH} = 8.5 Hz, -CH Ar), 7.32 (d, 4 H, ³J_{HH} = 8.5 Hz, -CH Ar), 2.70 (t, 4 H, ³J_{HH} = 7.7 Hz, -CH dodecyl), 1.7-1.2 (m, 40 H, -CH dodecyl), 0.90 (t, 6 H, ³J_{HH} = 7.0 Hz, -CH dodecyl). **¹³C NMR** (CDCl₃) δ: 194.11 (2 C, -CO), 150.57 (2 C, quat Ar), 130.39, (2 C, quat Ar), 129.63 (4 C, -CH Ar), 128.62 (4 C, -CH Ar), 35.79 (-CH dodecyl), 31.47 (-CH dodecyl), 30.58 (-CH dodecyl), 29.21 (-CH dodecyl), 29.18 (-CH dodecyl), 29.10 (-CH dodecyl), 28.99(-CH dodecyl), 28.90 (-CH dodecyl), 28.80 (-CH dodecyl), 22.25 (-CH dodecyl), 13.69 (-CH dodecyl).

4.2.62. Synthesis of 4-bromomethyldodecylbenzene (64)

Phenyldodecane (20 g, 81mmol) and paraformaldehyde (2.5 g, 83 mmol) were dissolved in glacial acetic acid (120 mL). Then hydrobromic acid (40 mL, 33 % in acetic acid) was added at once. The solution was then heated to 75 °C for 4 days after which it was poured into water and extracted with dichloromethane. The organic phase was dried over MgSO₄, filtered over celite and evaporated to dryness. The oily residue was subjected to column chromatography on silica, elution with petroleum ether yielded the desired product.

Yield: 9.6 g, 14 %. **M.pt:** 45-46 °C. $^1\text{H NMR}$ (CDCl_3) δ : 7.32 (d, 2 H, $^3J_{\text{HH}} = 8.0$ Hz, -CH Ar), 7.17 (d, 2 H, $^3J_{\text{HH}} = 8.0$ Hz, -CH Ar), 4.52 (s, 2 H, $-\text{CH}_2$), 2.61 (t, 2 H, $^3J_{\text{HH}} = 7.5$ Hz, -CH dodecyl), 1.1-1.5 (m, 20 H, -CH dodecyl), 0.91 (t, 3 H, $^3J_{\text{HH}} = 7.0$ Hz, -CH dodecyl). $^{13}\text{C NMR}$ (CDCl_3) δ : 143.02 (1 C, quat Ar), 134.52 (1 C, quat Ar), 128.52 (2 C, -CH Ar), 128.41 (2 C, -CH Ar), 35.26 (1 C, $-\text{CH}_2$), 33.40 (-CH dodecyl), 31.49 (-CH dodecyl), 30.93 (-CH dodecyl), 29.23 (-CH dodecyl), 29.15 (-CH dodecyl), 29.07 (-CH dodecyl), 28.92 (-CH dodecyl), 28.88 (-CH dodecyl), 22.27 (-CH dodecyl), 13.71 (-CH dodecyl).

4.2.63. Synthesis of 1,3-bis(4-dodecylphenyl)-propan-2-one (65)

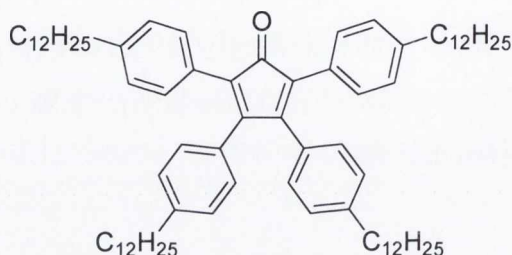


Iron pentacarbonyl (2.4 g, 1.64 mL, 12.25 mmol) was added to a refluxing mixture of **64** (8 g, 23.57 mmol), sodium hydroxide (4.1 g, 102.5 mmol), benzyltriethylammonium chloride (0.18 g, 0.79 mmol), deionised water (5 mL) and dichloromethane (60 mL). The reaction mixture was then refluxed with rigorous stirring for 18 hours. After cooling to room temperature the reaction mixture was neutralized with hydrochloric acid (2 M). The organic phase was separated, washed with hydrochloric acid (2 M) and deionised water, dried over MgSO_4 and the solvent evaporated under reduced pressure. The resulting solid was purified by chromatography on silica. Elution with petroleum ether/dichloromethane (3:1) yielded the desired product.

Yield: 3.5 g, 54 %. **M.pt:** 73-74 °C. $^1\text{H NMR}$ (CDCl_3) δ : 7.14 (d, 4 H, $^3J_{\text{HH}} = 8.0$ Hz, -CH Ar), 7.07 (d, 4 H, $^3J_{\text{HH}} = 8.0$ Hz, -CH Ar), 3.70 (s, 4 H, $-\text{CH}_2$), 2.60 (t, 4 H, $^3J_{\text{HH}} = 7.5$ Hz, -CH dodecyl), 1.1-1.6 (m, 40 H, -CH dodecyl), 0.91 (t, 6 H, $^3J_{\text{HH}} = 7.0$ Hz, -CH dodecyl). $^{13}\text{C NMR}$ (CDCl_3) δ : 205.85 (1 C, $-\text{CO}$), 141.29 (2 C, quat Ar), 130.73 (2 C, quat Ar), 128.90 (4 C, -CH Ar), 128.29 (4 C, -CH Ar), 48.22 (2 C, $-\text{CH}_2$), 35.15 (-CH dodecyl), 31.49 (-CH dodecyl), 31.05 (-CH dodecyl), 29.24 (-CH dodecyl),

29.21 (-CH dodecyl), 29.17 (-CH dodecyl), 29.09 (-CH dodecyl), 28.92 (-CH dodecyl), 22.26 (-CH dodecyl), 13.70 (-CH dodecyl).

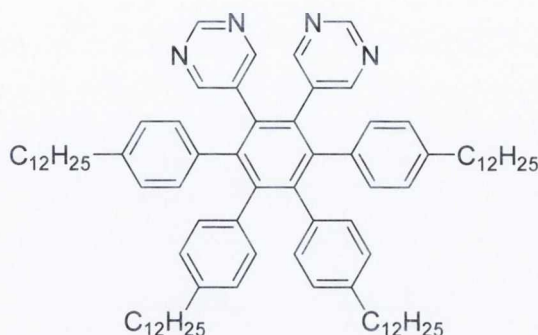
4.2.64. Synthesis of tetra(4-dodecyl-phen-1-yl)cyclopentadienone (**66**)



A solution of potassium hydroxide (0.15 g, 2.67 mmol) in ethanol (2 mL) was added to a refluxing solution of **63** (0.15 g, 2.74 mmol) and **65** (1.35 g, 247 mmol) in ethanol (15 mL). After 5 minutes the reaction mixture was cooled to 0 °C, and the resulting purple oil was separated from the solvent. The viscous oil was subjected to column chromatography. Elution with hexane/dichloromethane (4:1) yielded the desired product as a purple solid.

Yield: 1.4 g, 53 %. **M.pt:** 53-54 °C. **¹H NMR (600 MHz)** (CDCl₃) δ: 7.18 (d, 4H, ³J_{HH} = 8.3 Hz, -CH Ar), 7.06 (d, 4H, ³J_{HH} = 8.3 Hz, -CH Ar), 6.97 (d, 4 H, ³J_{HH} = 8.0 Hz, -CH Ar), 6.83 (d, 4 H, ³J_{HH} = 8.0 Hz, -CH Ar), 2.57 (m, 8 H, -CH dodecyl), 1.1-1.6 (m, 80 H, -CH dodecyl), 0.91 (t, 12 H, ³J_{HH} = 6.7 Hz, -CH dodecyl). **¹³C NMR (600 MHz)** (CDCl₃) δ: 200.94 (1 C, -CO), 153.95 (2 C, quat Ar), 143.01 (2 C, quat Ar), 141.87 (2 C, quat Ar), 130.52 (2 C, quat Ar), 129.78 (4C, -CH Ar), 129.19 (4C, -CH Ar), 128.21 (2 C, quat Ar), 127.85 (4C, -CH Ar), 127.68 (4C, -CH Ar), 124.49 (2 C, quat Ar), 35.65 (-CH dodecyl), 35.59 (-CH dodecyl), 31.77 (-CH dodecyl), 31.06 (-CH dodecyl), 30.89 (-CH dodecyl), 29.56 (-CH dodecyl), 29.54 (-CH dodecyl), 29.49 (-CH dodecyl), 29.45 (-CH dodecyl), 29.36 (-CH dodecyl), 29.25 (-CH dodecyl), 29.22 (-CH dodecyl), 29.21 (-CH dodecyl), 29.03 (-CH dodecyl), 22.53 (-CH dodecyl), 13.95 (-CH dodecyl).

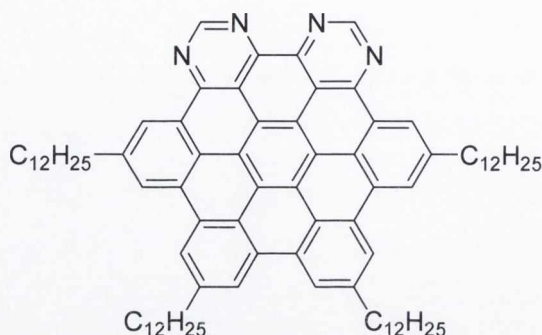
4.2.65. Synthesis of 1, 2-dipyrimidyl-3, 4, 5, 6-tetra(4-dodecyl-phenyl)benzene (67)



A mixture of **66** (1.37 g, 1.30 mmol), **18** (0.21 g, 1.17 mmol) and benzophenone (3.5 g) were heated to 200 °C for 6 hours. After cooling to room temperature the product was purified by chromatography on silica. Elution with diethylether followed by recrystallisation from hexane yielded the desired product as an off white waxy solid.

Yield: 0.66 g, 48 %. **¹H NMR (600 MHz)** (CDCl₃) δ: 8.78 (s, 2 H, -CH Ar), 8.24 (s, 4 H, -CH Ar), 6.74 (d, 4 H, ³J_{HH} = 8.0 Hz, -CH Ar), 6.70-6.67 (m, 12 H, -CH Ar), 2.37 (m, 8 H, -CH dodecyl), 1.45-1.13 (m, 80 H, -CH dodecyl), 0.91 (t, 12H, ³J_{HH} = 6.70 Hz, -CH dodecyl). **¹³C NMR (600 MHz)** (CDCl₃) δ: 157.90 (4 C, -CH Ar), 155.59 (2 C, -CH Ar), 142.83 (quat Ar), 141.48 (quat Ar), 140.67 (quat Ar), 139.88 (quat Ar), 136.53 (quat Ar), 135.77 (quat Ar), 134.04 (quat Ar), 132.64 (quat Ar), 130.85 (4 C, -CH Ar), 130.66 (4 C, -CH Ar), 127.35 (4 C, -CH Ar), 126.67 (4 C, -CH Ar), 35.18 (-CH dodecyl), 35.16 (-CH dodecyl), 31.78 (-CH dodecyl), 31.00 (-CH dodecyl), 30.86 (-CH dodecyl), 29.60 (-CH dodecyl), 29.58 (-CH dodecyl), 29.56 (-CH dodecyl), 29.54 (-CH dodecyl), 29.51 (-CH dodecyl), 29.49 (-CH dodecyl), 29.35 (-CH dodecyl), 29.32 (-CH dodecyl), 29.23 (-CH dodecyl), 28.78 (-CH dodecyl), 28.70 (-CH dodecyl), 22.53 (-CH dodecyl), 13.94 (-CH dodecyl). **IR** ν (cm⁻¹): ν(C-H st, aromatic): 3023, ν(C-H st, -C₁₂H₂₅): 2956, 2021, 851, ν(C=N st): 1548, 1515.

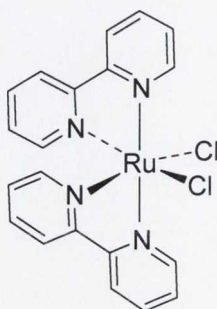
4.2.66. Synthesis of tetra-*peri*-(dodecyl-benzo)-di-*peri*-(pyrimidino)-coronene ($C_{12}H_{25}$ -N-HSB; **68)**



A solution of iron(III) chloride (0.55 g, 3.4 mmol) in nitromethane (3 mL) was added dropwise to a stirred solution of **67** (0.15 g, 0.14 mmol) in dichloromethane (30 mL). The resulting green reaction mixture was stirred for 4 hours at room temperature and then quenched with methanol (10 mL). Water (10 mL) and dilute ammonia (20 mL) was added and the mixture allowed to stir for 2 hours. Once the time had elapsed it was extracted into chloroform, washed with water and dried over $MgSO_4$. The residual red oil was purified by column chromatography on silica with toluene/methanol (98/2) to afford the desired product as a red waxy solid.

Yield: 0.023 g, 24 %. **1H NMR (600 MHz)** ($CDCl_3$) δ : 9.16 (s, 10 H, -CH Ar), 1.66-1.46 (m, 88 H, -CH dodecyl), 0.99 (m, 12 H, -CH dodecyl). **MALDI-TOF MS;** for $C_{86}H_{111}N_4$: $[MH]^+$ calculated m/z 1199.8809, found m/z 1199.8809.

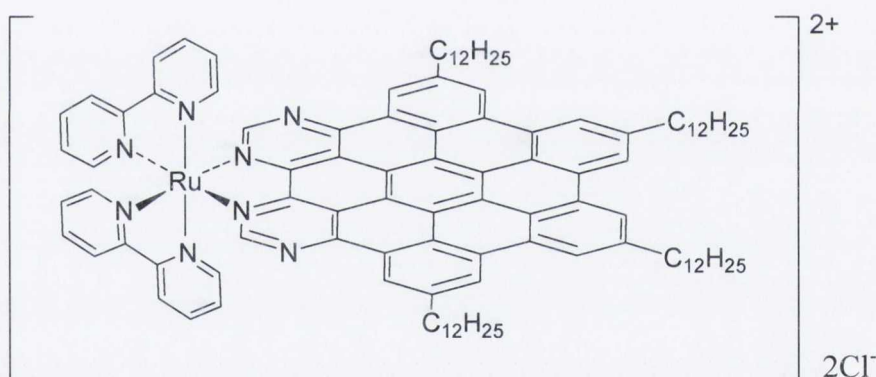
4.2.67. Synthesis of $[Ru(bpy)_2Cl_2] \cdot 2H_2O$ (69**)**



$\text{RuCl}_3 \cdot 3\text{H}_2\text{O}$ (1 g, 3.82 mmol), bipyridine (1.2 g, 7.69 mmol) and lithium chloride (1.09 g, 25.6 mmol) were heated at reflux in dimethylformamide (15 mL) for 8 hours. Once the time had elapsed the reaction mixture was cooled to room temperature and acetone (30 mL) was added. The resulting solution was left at 0 °C overnight. Filtering yielded the desired product as a green-black microcrystalline solid, which was washed with water then diethylether.

Yield: 1.5 g, 72 %. ^1H NMR (600 MHz) (CD_3CN) δ : 10.08 (d, 1 H, $^3J_{\text{HH}} = 5.0$ Hz, -CH Ar), 8.41 (d, 1 H, $^3J_{\text{HH}} = 8.0$ Hz, -CH Ar), 8.24 (d, 1 H, $^3J_{\text{HH}} = 8.0$ Hz, -CH Ar), 8.00 (t, 1 H, $^3J_{\text{HH}} = 8.0$ Hz, -CH Ar), 7.69 (t, 1 H, $^3J_{\text{HH}} = 6.4$ Hz, -CH Ar), 7.60 (m, 2 H, -CH Ar), 7.01 (t, 1 H, $^3J_{\text{HH}} = 6.0$ Hz, -CH Ar).

4.2.68. Synthesis of $[\text{Ru}(\text{bpy})_2(\text{68})]\text{Cl}_2$ - (70)



Compound **68** (8.4 mg, 0.007 mmol) and **69** (6.0 mg, 0.01 mmol) were sonicated in a mixture of 1, 1, 2, 2-tetrachloroethane (1 mL) and diethylene glycol ethyl ether (2 mL) for 10 minutes. The solution was degassed by passing a stream of argon through the solution for 30 minutes. After heating the solution for 18 hours at 120 °C, it was allowed to cool to room temperature and filtered. The solvent were removed and the green oily product was subjected to column chromatography on alumina. Elution with chloroform:methanol (90: 10) yielded the product as a black-green solid.

Yield: 5.1 mg, 44 %. **ESI-MS** (acetonitrile); calculated for $\text{C}_{106}\text{H}_{126}\text{N}_8\text{Ru}$: $[\text{M}-2\text{Cl}]^{2+}$ calculated m/z 1612.9149, found m/z 1612.9146

References

1. M. Muller, C. Kubel and K. Mullen, *Chemistry-a European Journal*, 1998, **4**, 2099-2109.
2. A. F. Thuneman, D. Ruppelt, S. Ito and K. Mullen, *Journal of Materials Chemistry*, 1999, **9**, 1055-1057.
3. V. S. Iyer, M. Wehmeier, J. D. Brand, M. A. Keegstra and K. Mullen, *Angewandte Chemie-International Edition in English*, 1997, **36**, 1604-1607.
4. V. S. Iyer, K. Yoshimura, V. Enkelmann, R. Epsch, J. P. Rabe and K. Mullen, *Angewandte Chemie-International Edition*, 1998, **37**, 2696-2699.
5. P. Kovacic and A. Kyriakis, *Journal of the American Chemical Society*, 1963, **85**, 454-+.
6. P. Kovacic and M. B. Jones, *Chemical Reviews*, 1987, **87**, 357-379.
7. M. Wehmeier, M. Wagner and K. Mullen, *Chemistry-a European Journal*, 2001, **7**, 2197-2205.
8. F. Barigelletti, L. Decola, V. Balzani, P. Belser, A. Vonzelewsky, F. Vogtle, F. Ebmeyer and S. Grammenudi, *Journal of the American Chemical Society*, 1989, **111**, 4662-4668.
9. M. D. Watson, A. Fechtenkotter and K. Mullen, *Chemical Reviews*, 2001, **101**, 1267-1300.
10. P. Rempala, J. Kroulik and B. T. King, *Journal of the American Chemical Society*, 2004, **126**, 15002-15003.
11. R. Rathore and C. L. Burns, *Journal of Organic Chemistry*, 2003, **68**, 4071-4074.
12. P. Rempala, J. Kroulik and B. T. King, *Journal of Organic Chemistry*, 2006, **71**, 5067-5081.
13. F. Murphy, *Ph.D Thesis*, Trinity College Dublin, 2008.
14. S. M. Draper, D. J. Gregg and R. Madathil, *Journal of the American Chemical Society*, 2002, **124**, 3486-3487.
15. P. Herwig, C. W. Kayser, K. Mullen and H. W. Spiess, *Advanced Materials*, 1996, **8**, 510-&.
16. S. M. Draper, D. J. Roberts and B. Lankage, 2008.
17. S. M. Draper, D. J. Gregg, E. R. Schofield, W. R. Browne, M. Duati, J. G. Vos and P. Passaniti, *Journal of the American Chemical Society*, 2004, **126**, 8694-8701.
18. D. J. Gregg, E. Bothe, P. Hofer, P. Passaniti and S. M. Draper, *Inorganic Chemistry*, 2005, **44**, 5654-5660.
19. I. Manners, *Angewandte Chemie-International Edition in English*, 1996, **35**, 1603-1621.
20. A. C. Ribou, J. P. Launay, M. L. Sachtleben, H. Li and C. W. Spangler, *Inorganic Chemistry*, 1996, **35**, 3735-3740.
21. I. R. Butler, S. Mussig and M. Plath, *Inorganic Chemistry Communications*, 1999, **2**, 424-427.
22. N. J. Long, *Angewandte Chemie-International Edition in English*, 1995, **34**, 21-38.
23. J. D. McKinney, P. A. Anderson, T. A. Hamor, C. J. Jones, K. Paxton and A. Porch, *Journal of Organometallic Chemistry*, 1998, **558**, 147-153.
24. L. J. Li, A. Decken, B. G. Sayer, M. J. McGlinchey, P. Bregaint, J. Y. Thepot, L. Toupet, J. R. Hamon and C. Lapinte, *Organometallics*, 1994, **13**, 682-689.

25. B. Mailvaganam, B. G. Sayer and M. J. McGlinchey, *Journal of Organometallic Chemistry*, 1990, **395**, 177-185.
26. H. K. Gupta, S. Brydges and M. J. McGlinchey, *Organometallics*, 1999, **18**, 115-122.
27. L. E. Harrington, J. F. Britten and M. J. McGlinchey, *Canadian Journal of Chemistry-Revue Canadienne De Chimie*, 2003, **81**, 1180-1186.
28. S. Ito, M. Wehmeier, J. D. Brand, C. Kubel, R. Epsch, J. P. Rabe and K. Mullen, *Chemistry-a European Journal*, 2000, **6**, 4327-4342.
29. X. Don, W. Pisula, J. Wu, G. J. Bodwell and K. Mullen, *Chemistry-a European Journal*, 2008, **14**, 240-249.
30. M. Laskoski, W. Steffen, M. D. Smith and U. H. F. Bunz, *Chemical Communications*, 2001, 691-692.
31. M. Laskoski, G. Roidl, M. D. Smith and U. H. F. Bunz, *Angewandte Chemie-International Edition*, 2001, **40**, 1460-+.
32. M. Laskoski, J. G. M. Morton, M. D. Smith and U. H. F. Bunz, *Journal of Organometallic Chemistry*, 2002, **652**, 21-30.
33. P. T. Herwig, V. Enkelmann, O. Schmelz and K. Mullen, *Chemistry-a European Journal*, 2000, **6**, 1834-1839.
34. D. J. Gregg, *Ph.D Thesis*, Trinity College Dublin, 2002.
35. X. Dou, X. Y. Yang, G. J. Bodwell, M. Wagner, V. Enkelmann and K. Mullen, *Organic Letters*, 2007, **9**, 2485-2488.
36. X. L. Feng, W. Pisula, M. Takase, X. Dou, V. Enkelmann, M. Wagner, N. Ding and K. Mullen, *Chemistry of Materials*, 2008, **20**, 2872-2874.
37. B. J. Coe, C. J. Jones, J. A. McCleverty, D. Bloor and G. Cross, *Journal of Organometallic Chemistry*, 1994, **464**, 225-232.
38. V. J. Chebny, D. Dhar, S. V. Lindeman and R. Rathore, *Organic Letters*, 2006, **8**, 5041-5044.
39. Rosenblu.M, N. Brawn, Papenmei.J and Applebau.M, *Journal of Organometallic Chemistry*, 1966, **6**, 173-&.
40. K. M. Roth, A. A. Yasseri, Z. M. Liu, R. B. Dabke, V. Malinovskii, K. H. Schweikart, L. H. Yu, H. Tiznado, F. Zaera, J. S. Lindsey, W. G. Kuhr and D. F. Bocian, *Journal of the American Chemical Society*, 2003, **125**, 505-517.
41. A. Balakumar, A. B. Lysenko, C. Carcel, V. L. Malinovskii, D. T. Gryko, K. H. Schweikart, R. S. Loewe, A. A. Yasseri, Z. M. Liu, D. F. Bocian and J. S. Lindsey, *Journal of Organic Chemistry*, 2004, **69**, 1435-1443.
42. U. T. Muellerwesterhoff and M. Zhou, *Journal of Organic Chemistry*, 1994, **59**, 4988-4992.
43. B. Weinberger, G. Tanguy and H. D. Abbayes, *Journal of Organometallic Chemistry*, 1985, **280**, C31-C33.
44. H. Desabbayes, J. C. Clement, P. Laurent, G. Tanguy and N. Thilmont, *Organometallics*, 1988, **7**, 2293-2299.
45. H. D. Abbayes, J. C. Clement, P. Laurent, J. J. Yaouanc, G. Tanguy and B. Weinberger, *Journal of Organometallic Chemistry*, 1989, **359**, 205-214.
46. R. G. Potter and T. S. Hughes, *Organic Letters*, 2007, **9**, 1187-1190.
47. P. Stepnicka, L. Trojan, J. Kubista and J. Ludvik, *Journal of Organometallic Chemistry*, 2001, **637**, 291-299.
48. A. J. Moore, A. Chesney, M. R. Bryce, A. S. Batsanov, J. F. Kelly, J. A. K. Howard, I. F. Perepichka, D. F. Perepichka, G. Meshulam, G. Berkovic, Z. Kotler, R. Mazor and V. Khodorkovsky, *European Journal of Organic Chemistry*, 2001, 2671-2687.

49. J. Polin and H. Schottenberger, *Organic Synthesis*, Vol 73, 1996, **73**, 262-269.
50. N. Tsuboya, R. Hamasaki, M. Ito, M. Mitsuishi, T. Miyashita and Y. Yamamoto, *Journal of Materials Chemistry*, 2003, **13**, 511-513.
51. S. K. Burley and G. A. Petsko, *Advances in Protein Chemistry*, 1988, **39**, 125-189.
52. G. R. Desiraju and A. Gavezzotti, *Journal of the Chemical Society-Chemical Communications*, 1989, 621-623.
53. G. R. Desiraju and A. Gavezzotti, *Acta Crystallographica Section B-Structural Science*, 1989, **45**, 473-482.
54. C. A. Hunter and J. K. M. Sanders, *Journal of the American Chemical Society*, 1990, **112**, 5525-5534.
55. R. Foster, *Organic Charge-Transfer Complexes*, Academic Press: London, 1969.
56. A. V. Muehldorf, D. Vanengen, J. C. Warner and A. D. Hamilton, *Journal of the American Chemical Society*, 1988, **110**, 6561-6562.
57. P. Hobza, H. L. Selzle and E. W. Schlag, *Journal of the American Chemical Society*, 1994, **116**, 3500-3506.
58. A. S. Shetty, J. S. Zhang and J. S. Moore, *Journal of the American Chemical Society*, 1996, **118**, 1019-1027.
59. J. C. Calabrese, L. T. Cheng, J. C. Green, S. R. Marder and W. Tam, *Journal of the American Chemical Society*, 1991, **113**, 7227-7232.
60. K. N. Jayaprakash, P. C. Ray, I. Matsuoka, M. M. Bhadbhade, V. G. Puranik, P. K. Das, H. Nishihara and A. Sarkar, *Organometallics*, 1999, **18**, 3851-3858.
61. K. R. J. Thomas and J. T. Lin, *Journal of Organometallic Chemistry*, 2001, **637**, 139-144.
62. Y. Okada, T. Nakagawa and T. Hayashi, *Inorganica Chimica Acta*, 2001, **312**, 197-200.
63. H. Fink, N. J. Long, A. J. Martin, G. Opromolla, A. J. P. White, D. J. Williams and P. Zanello, *Organometallics*, 1997, **16**, 2646-2650.
64. W. Y. Wong, G. L. Lu, K. F. Ng, C. K. Wong and K. H. Choi, *Journal of Organometallic Chemistry*, 2001, **637**, 159-166.
65. N. J. Long, A. J. Martin, R. Vilar, A. J. P. White, D. J. Williams and M. Younus, *Organometallics*, 1999, **18**, 4261-4269.
66. L. T. Scott, M. M. Hashemi, D. T. Meyer and H. B. Warren, *Journal of the American Chemical Society*, 1991, **113**, 7082-7084.
67. R. Faust, *Angewandte Chemie-International Edition in English*, 1995, **34**, 1429-1432.
68. R. D. Broene and F. Diederich, *Tetrahedron Letters*, 1991, **32**, 5227-5230.
69. J. C. Fetzer and W. R. Biggs, *Polycyclic Aromatic Compounds*, 1994, **5**, 193-199.
70. F. Dotz, J. D. Brand, S. Ito, L. Gherghel and K. Mullen, *Journal of the American Chemical Society*, 2000, **122**, 7707-7717.
71. L. T. Scott, M. M. Hashemi and M. S. Bratcher, *Journal of the American Chemical Society*, 1992, **114**, 1920-1921.
72. P. W. Rabideau and A. Sygula, *Accounts of Chemical Research*, 1996, **29**, 235-242.
73. R. B. M. Ansems and L. T. Scott, *Journal of the American Chemical Society*, 2000, **122**, 2719-2724.
74. L. T. Scott, M. S. Bratcher and S. Hagen, *Journal of the American Chemical Society*, 1996, **118**, 8743-8744.

75. D. Adam, P. Schuhmacher, J. Simmerer, L. Haussling, K. Siemensmeyer, K. H. Etzbach, H. Ringsdorf and D. Haarer, *Nature*, 1994, **371**, 141-143.
76. R. Gvishi, R. Reisfeld and Z. Burshtein, *Chemical Physics Letters*, 1993, **213**, 338-344.
77. D. Schlettwein, D. Wohrle, E. Karmann and U. Melville, *Chemistry of Materials*, 1994, **6**, 3-6.
78. M. P. Oneil, M. P. Niemczyk, W. A. Svec, D. Gosztola, G. L. Gaines and M. R. Wasielewski, *Science*, 1992, **257**, 63-65.
79. B. Bildstein, M. Malaun, H. Kopacka, K. Wurst, M. Mitterbock, K. H. Ongania, G. Opromolla and P. Zanello, *Organometallics*, 1999, **18**, 4325-4336.
80. F. S. Kamounah and J. B. Christensen, *Journal of Chemical Research-S*, 1997, 150-150.
81. D. C. Harrowven and I. L. Guy, *Chemical Communications*, 2004, 1968-1969.
82. P. Duperrouzel and E. Leeruff, *Canadian Journal of Chemistry-Revue Canadienne De Chimie*, 1980, **58**, 51-54.
83. H. P. Diogo and M. E. M. da Piedade, *Journal of Chemical Thermodynamics*, 2002, **34**, 173-184.
84. H. Gusten and G. Heinrich, *Journal of Photochemistry*, 1982, **18**, 9-17.
85. K. Gustav and C. Seydenschwanz, *Chemical Physics Letters*, 1986, **123**, 261-263.
86. L. Sassu, L. Perezani, W. A. Ivancic, R. H. Barnes and B. W. Wabuyele, *Applied Spectroscopy*, 2001, **55**, 307-310.
87. A. A. Ruth and M. T. Wick, *Chemical Physics Letters*, 1997, **266**, 206-216.
88. J. Kolc, Thulstru.Ew and J. Michl, *Journal of the American Chemical Society*, 1974, **96**, 7188-7202.
89. M. J. Mio, L. C. Kopel, J. B. Braun, T. L. Gadzikwa, K. L. Hull, R. G. Brisbois, C. J. Markworth and P. A. Grieco, *Organic Letters*, 2002, **4**, 3199-3202.
90. F. Reinitzer, *Liquid Crystals*, 1989, **5**, 7-18.
91. C. V. Yelamaggad, V. Prasad, M. Manickam and S. Kumar, *Molecular Crystals & Liquid Crystals*, 1998, **325**, 33.
92. G. Heppke, D. Kruerke, C. Lohning, D. Lotzsch, D. Moro, M. Muller and H. Sawade, *Journal of Materials Chemistry*, 2000, **10**, 2657-2661.
93. A. M. van de Craats and J. M. Warman, *Advanced Materials*, 2001, **13**, 130-133.
94. N. Boden, R. J. Bushby, J. Cammidge, J. Clements and R. Luo, *Molecular Crystals & Liquid Crystals* 1995, **261**, 251.
95. V. S. K. Balagurusamy, S. K. Prasad, S. Chandrasekhar, S. Kumar, M. Manickam and C. V. Yelamaggad, *Pramana* 1999, **53**, 3.
96. A. M. van de Craats, J. M. Warman, A. Fechtenkotter, J. D. Brand, M. A. Harbison and K. Mullen, *Advanced Materials*, 1999, **11**, 1469-1472.
97. A. M. vandeCraats, J. M. Warman, M. P. deHaas, D. Adam, J. Simmerer, D. Haarer and P. Schuhmacher, *Advanced Materials*, 1996, **8**, 823-&.
98. M. Pope and C. E. Swenberg, *Electronic Processes in Organic Crystals*, 1982.
99. M. S. Dresselhaus and G. Dresselhaus, *Advances in Physics*, 1981, **30**, 139-326.

100. A. M. van de Craats, N. Stutzmann, O. Bunk, M. M. Nielsen, M. Watson, K. Mullen, H. D. Chanzy, H. Sirringhaus and R. H. Friend, *Advanced Materials*, 2003, **15**, 495-499.
101. S. X. Xiao, J. Y. Tang, T. Beetz, X. F. Guo, N. Tremblay, T. Siegrist, Y. M. Zhu, M. Steigerwald and C. Nuckolls, *Journal of the American Chemical Society*, 2006, **128**, 10700-10701.
102. F. Jackel, M. D. Watson, K. Mullen and J. P. Rabe, *Physical Review Letters*, 2004, **92**.
103. M. Okazaki, K. Kawata, H. Nishikawa and M. Negoro, *Polymers for Advanced Technologies*, 2000, **11**, 398-403.
104. S. R. Forrest, *Nature*, 2004, **428**, 911-918.
105. A. M. van de Craats and J. M. Warman, *Synthetic Metals*, 2001, **121**, 1287-1288.
106. Ogliarus.Ma and E. I. Becker, *Journal of Organic Chemistry*, 1965, **30**, 3354-&.
107. I. B. Berlman, H. O. Wirth and Steingra.Oj, *Journal of Physical Chemistry*, 1971, **75**, 318-&.
108. A. E. Gillam and D. H. Hey, *Journal of the Chemical Society*, 1939, 1170-1177.
109. N. I. Nijegorodov and W. S. Downey, *Journal of Physical Chemistry*, 1994, **98**, 5639-5643.
110. A. Fechtenkotter, K. Saalwachter, M. A. Harbison, K. Mullen and H. W. Spiess, *Angewandte Chemie-International Edition*, 1999, **38**, 3039-3042.
111. E. Clar, C. T. Ironside and M. Zander, *Journal of the Chemical Society*, 1959, 142-147.
112. S. Ito, P. T. Herwig, T. Bohme, J. P. Rabe, W. Rettig and K. Mullen, *Journal of the American Chemical Society*, 2000, **122**, 7698-7706.
113. F. Peral and E. Gallego, *Journal of Molecular Structure*, 1995, **372**, 101-112.
114. R. P. Wayne, *Principles and Applications of Photochemistry*, Oxford Press, 1980.
115. D. V. Bent, E. Hayon and P. N. Moorthy, *Journal of the American Chemical Society*, 1975, **97**, 5065-5071.
116. B. N. Bandyopadhyay and A. Harriman, *Journal of the Chemical Society-Faraday Transactions I*, 1977, **73**, 663-674.
117. S. K. Lee, Y. B. Zu, A. Herrmann, Y. Geerts, K. Mullen and A. J. Bard, *Journal of the American Chemical Society*, 1999, **121**, 3513-3520.
118. N. Armaroli, L. Decola, V. Balzani, J. P. Sauvage, C. O. Dietrichbuecker and J. M. Kern, *Journal of the Chemical Society-Faraday Transactions*, 1992, **88**, 553-556.
119. N. C. Yang and J. Libman, *Journal of the American Chemical Society*, 1973, **95**, 5783-5784.
120. N. Ghoneim, *Spectrochimica Acta Part a-Molecular and Biomolecular Spectroscopy*, 2001, **57**, 483-489.
121. U. Werner and H. Staerk, *Journal of Physical Chemistry*, 1995, **99**, 248-254.
122. P. Suppan, *Chimia*, 1988, **42**, 320-330.
123. T. Forster, M. Gordon and W. R. Ware, *The Exciplex*, Academic Press, New York, 1975, 1975.
124. S. D. Lidofsky, T. Imasaka and R. N. Zare, *Analytical Chemistry*, 1979, **51**, 1602-1605.

125. F. Peral and E. Gallego, *Spectrochimica Acta Part a-Molecular and Biomolecular Spectroscopy*, 2000, **56**, 2149-2155.
126. E. Baranoff, J. P. Collin, Y. Furusho, A. C. Laemmel and J. P. Sauvage, *Chemical Communications*, 2000, 1935-1936.
127. D. J. Gregg, C. M. A. Ollagnier, C. M. Fitchett and S. M. Draper, *Chemistry-a European Journal*, 2006, **12**, 3043-3052.
128. J. M. Warman, J. Piris, W. Pisula, M. Kastler, D. Wasserfallen and K. Mullen, *Journal of the American Chemical Society*, 2005, **127**, 14257-14262.
129. A. Hummel, *The Chemistry of Alkanes and Cyclohexanes*, Patai, S., Rappoport, A., Eds.; John Wiley & Sons: New York, 1992.
130. J. M. Warman and M. P. de Haas, *Pulse Radiolysis*, Tabata, Y., Ed.; CRC Press: Boston, 1991.
131. M. P. De Haas, University of Leiden: Leiden, 1977.
132. P. G. Schouten, J. M. Warman, G. H. Gelinck and M. J. Copyn, *Journal of Physical Chemistry*, 1995, **99**, 11780-11793.
133. J. M. Warman, M. P. Dehaas, K. J. Smit, M. N. Paddonrow and J. F. Vanderpol, *Molecular Crystals and Liquid Crystals*, 1990, **183**, 375-385.
134. J. M. Warman, M. P. Dehaas, J. F. Vanderpol and W. Drenth, *Chemical Physics Letters*, 1989, **164**, 581-586.
135. Y. Tabata, S. Ito and S. Tagawa, *Handbook of Radiation Chemistry*, CRC Press: Boca Raton, 1991.
136. J. M. Warman, K. D. Asmus and R. H. Schuler, *Journal of Physical Chemistry*, 1969, **73**, 931-&.
137. J. Piris, M. G. Debije, M. D. Watson, K. Mullen and J. M. Warman, *Advanced Functional Materials*, 2004, **14**, 1047-1052.
138. X. L. Feng, M. Y. Liu, W. Pisula, M. Takase, J. L. Li and K. Mullen, *Advanced Materials*, 2008, **20**, 2684-+.

Annex

Table 18: Crystal data and structure refinement for **43**.

Compound	43
Empirical formula	C ₄₂ H ₃₄ Fe O ₄
Formula weight	658.54
Temperature (K)	153(2)
Crystal system	Monoclinic
Space group	P2(1)/c
a (Å)	12.0117(6)
b (Å)	11.3475(6)
c (Å)	24.3958(13)
α (deg)	90
β (deg)	101.6820(10)
γ (deg)	90
V (Å³)	3256.3(3)
Z	4
D_{calc} (Mg/m³)	1.343
Absorption coefficient (mm⁻¹)	0.507
F(000)	1376
Crystal size (mm³)	0.41 x 0.21 x 0.15
Theta range for data collection	1.70 to 26.00°
Reflections collected	27215
Independent reflections	6401 [R(int) = 0.0657]
Completeness to theta = 26.00°	100.0 %
Data / restraints / parameters	6401 / 0 / 416
Goodness-of-fit on F²	2.294
Final R indices [I>2σ(I)]	R1 = 0.1454, wR2 = 0.3612

Table 19: Bond lengths (\AA) for **43**

Fe(1)-C(4E)	1.921(10)	C(12)-C(15)	1.410(9)
Fe(1)-C(5E)	1.982(9)	C(12)-C(1B)	1.468(9)
Fe(1)-C(3E)	1.948(10)	C(13)-C(18)	1.358(9)
Fe(1)-C(5B)	2.013(7)	C(13)-C(35)	1.391(10)
Fe(1)-C(4B)	2.019(7)	C(14)-C(25)	1.427(9)
Fe(1)-C(2B)	2.009(9)	C(16)-C(23)	1.390(9)
Fe(1)-C(3B)	2.031(9)	C(18)-C(22)	1.434(9)
Fe(1)-C(1E)	2.044(8)	O(2)-C(22)	1.338(9)
Fe(1)-C(2E)	2.024(9)	O(2)-C(31)	1.415(10)
Fe(1)-C(1B)	2.071(7)	C(20)-C(25)	1.368(10)
C(1)-C(7)	1.380(9)	C(21)-O(1)	1.349(10)
C(1)-O(3)	1.370(8)	C(21)-C(27)	1.348(12)
C(1)-C(20)	1.392(10)	C(21)-C(35)	1.456(11)
C(2)-C(26)	1.373(9)	C(22)-C(27)	1.363(11)
C(2)-C(16)	1.407(9)	C(23)-C(29)	1.407(10)
C(2)-C(4)	1.480(9)	C(23)-C(33)	1.423(10)
C(3)-C(10)	1.383(9)	C(24)-C(30)	1.415(10)
C(3)-C(4)	1.425(8)	C(26)-C(28)	1.441(10)
C(3)-C(8)	1.478(9)	C(28)-C(29)	1.357(11)
C(4)-C(5)	1.400(9)	C(30)-C(33)	1.382(11)
C(5)-C(15)	1.370(9)	O(1)-C(3A)	1.350(12)
C(5)-C(13)	1.495(9)	C(1B)-C(2B)	1.412(11)
O(3)-C(37)	1.402(9)	C(1B)-C(5B)	1.415(10)
C(7)-C(11)	1.410(10)	C(2B)-C(3B)	1.427(12)
C(8)-C(24)	1.370(9)	C(3B)-C(4B)	1.402(13)
C(8)-C(16)	1.417(9)	C(4B)-C(5B)	1.391(11)
O(4)-C(25)	1.350(8)	C(1E)-C(5E)	1.4200
O(4)-C(40)	1.427(9)	C(1E)-C(2E)	1.4200
C(10)-C(12)	1.402(9)	C(2E)-C(3E)	1.4200
C(10)-C(11)	1.490(8)	C(3E)-C(4E)	1.4200
C(11)-C(14)	1.377(9)	C(4E)-C(5E)	1.4200

Table 20: Angles ($^\circ$) for **43**

C(4E)-Fe(1)-C(5E)	42.63(19)	C(15)-C(5)-C(4)	117.4(6)
C(4E)-Fe(1)-C(3E)	43.1(2)	C(15)-C(5)-C(13)	122.8(6)
C(5E)-Fe(1)-C(3E)	71.5(2)	C(4)-C(5)-C(13)	119.9(6)
C(4E)-Fe(1)-C(5B)	151.7(4)	C(1)-O(3)-C(37)	117.8(5)
C(5E)-Fe(1)-C(5B)	165.4(4)	C(1)-C(7)-C(11)	118.8(6)
C(3E)-Fe(1)-C(5B)	120.8(4)	C(24)-C(8)-C(16)	118.7(6)
C(4E)-Fe(1)-C(4B)	162.2(5)	C(24)-C(8)-C(3)	135.6(6)
C(5E)-Fe(1)-C(4B)	125.3(4)	C(16)-C(8)-C(3)	105.7(5)
C(3E)-Fe(1)-C(4B)	154.5(5)	C(25)-O(4)-C(40)	117.2(6)
C(5B)-Fe(1)-C(4B)	40.4(3)	C(3)-C(10)-C(12)	118.4(6)
C(4E)-Fe(1)-C(2B)	102.1(4)	C(3)-C(10)-C(11)	117.9(5)
C(5E)-Fe(1)-C(2B)	112.3(5)	C(12)-C(10)-C(11)	123.6(6)
C(3E)-Fe(1)-C(2B)	126.6(4)	C(14)-C(11)-C(7)	120.5(6)
C(5B)-Fe(1)-C(2B)	67.9(3)	C(14)-C(11)-C(10)	119.4(6)
C(4B)-Fe(1)-C(2B)	68.5(3)	C(7)-C(11)-C(10)	120.0(6)
C(4E)-Fe(1)-C(3B)	122.7(4)	C(10)-C(12)-C(15)	119.7(6)
C(5E)-Fe(1)-C(3B)	102.0(4)	C(10)-C(12)-C(1B)	123.0(6)
C(3E)-Fe(1)-C(3B)	164.2(5)	C(15)-C(12)-C(1B)	117.3(6)
C(5B)-Fe(1)-C(3B)	68.0(4)	C(18)-C(13)-C(35)	122.2(6)
C(4B)-Fe(1)-C(3B)	40.5(4)	C(18)-C(13)-C(5)	120.9(6)
C(2B)-Fe(1)-C(3B)	41.4(3)	C(35)-C(13)-C(5)	116.9(6)

C(4E)-Fe(1)-C(1E)	70.74(19)	C(11)-C(14)-C(25)	119.1(6)
C(5E)-Fe(1)-C(1E)	41.27(14)	C(5)-C(15)-C(12)	122.9(6)
C(3E)-Fe(1)-C(1E)	70.22(19)	C(23)-C(16)-C(8)	124.5(6)
C(5B)-Fe(1)-C(1E)	131.8(4)	C(23)-C(16)-C(2)	123.2(6)
C(4B)-Fe(1)-C(1E)	108.5(3)	C(8)-C(16)-C(2)	112.3(5)
C(2B)-Fe(1)-C(1E)	147.6(5)	C(13)-C(18)-C(22)	119.7(6)
C(3B)-Fe(1)-C(1E)	114.9(5)	C(22)-O(2)-C(31)	119.0(6)
C(4E)-Fe(1)-C(2E)	71.2(2)	C(25)-C(20)-C(1)	119.4(6)
C(5E)-Fe(1)-C(2E)	69.98(17)	O(1)-C(21)-C(27)	116.2(7)
C(3E)-Fe(1)-C(2E)	41.83(17)	O(1)-C(21)-C(35)	122.8(8)
C(5B)-Fe(1)-C(2E)	113.1(4)	C(27)-C(21)-C(35)	121.0(7)
C(4B)-Fe(1)-C(2E)	120.6(4)	O(2)-C(22)-C(27)	116.3(6)
C(2B)-Fe(1)-C(2E)	168.0(5)	O(2)-C(22)-C(18)	124.6(7)
C(3B)-Fe(1)-C(2E)	150.7(5)	C(27)-C(22)-C(18)	119.1(7)
C(1E)-Fe(1)-C(2E)	40.85(14)	C(16)-C(23)-C(29)	117.3(7)
C(4E)-Fe(1)-C(1B)	114.9(3)	C(16)-C(23)-C(33)	115.8(7)
C(5E)-Fe(1)-C(1B)	147.6(5)	C(29)-C(23)-C(33)	126.9(7)
C(3E)-Fe(1)-C(1B)	108.5(3)	C(8)-C(24)-C(30)	118.2(6)
C(5B)-Fe(1)-C(1B)	40.5(3)	C(5B)-C(1B)-C(12)	128.3(7)
C(4B)-Fe(1)-C(1B)	68.5(3)	C(2B)-C(1B)-Fe(1)	67.4(5)
C(2B)-Fe(1)-C(1B)	40.5(3)	C(5B)-C(1B)-Fe(1)	67.5(4)
C(3B)-Fe(1)-C(1B)	68.9(3)	C(12)-C(1B)-Fe(1)	126.6(5)
C(1E)-Fe(1)-C(1B)	170.9(5)	C(1B)-C(2B)-C(3B)	109.6(7)
C(2E)-Fe(1)-C(1B)	132.4(5)	C(1B)-C(2B)-Fe(1)	72.1(5)
C(7)-C(1)-O(3)	124.2(6)	C(3B)-C(2B)-Fe(1)	70.2(5)
C(7)-C(1)-C(20)	121.6(6)	C(4B)-C(3B)-C(2B)	106.6(7)
O(3)-C(1)-C(20)	114.1(6)	C(4B)-C(3B)-Fe(1)	69.3(5)
C(26)-C(2)-C(16)	118.7(6)	C(2B)-C(3B)-Fe(1)	68.5(5)
C(26)-C(2)-C(4)	135.5(6)	C(5B)-C(4B)-C(3B)	108.2(7)
C(16)-C(2)-C(4)	105.8(5)	C(5B)-C(4B)-Fe(1)	69.6(4)
C(10)-C(3)-C(4)	120.7(5)	C(3B)-C(4B)-Fe(1)	70.2(5)
C(10)-C(3)-C(8)	131.3(5)	C(4B)-C(5B)-C(1B)	110.3(7)
C(4)-C(3)-C(8)	108.0(5)	C(4B)-C(5B)-Fe(1)	70.1(4)
C(5)-C(4)-C(3)	120.8(6)	C(1B)-C(5B)-Fe(1)	71.9(4)
C(5)-C(4)-C(2)	131.0(6)	C(5E)-C(1E)-C(2E)	108.0
C(3)-C(4)-C(2)	108.2(5)	C(5E)-C(1E)-Fe(1)	67.0(4)
O(4)-C(25)-C(20)	125.1(6)	C(2E)-C(1E)-Fe(1)	68.8(4)
O(4)-C(25)-C(14)	114.5(6)	C(1E)-C(2E)-C(3E)	108.0
C(20)-C(25)-C(14)	120.4(6)	C(1E)-C(2E)-Fe(1)	70.3(3)
C(2)-C(26)-C(28)	118.6(6)	C(3E)-C(2E)-Fe(1)	66.2(4)
C(21)-C(27)-C(22)	121.5(7)	C(4E)-C(3E)-C(2E)	108.0
C(29)-C(28)-C(26)	121.5(7)	C(4E)-C(3E)-Fe(1)	67.5(4)
C(28)-C(29)-C(23)	120.7(7)	C(2E)-C(3E)-Fe(1)	72.0(4)
C(33)-C(30)-C(24)	122.9(7)	C(3E)-C(4E)-C(5E)	108.0
C(30)-C(33)-C(23)	120.0(7)	C(3E)-C(4E)-Fe(1)	69.5(4)
C(21)-O(1)-C(3A)	118.2(8)	C(5E)-C(4E)-Fe(1)	71.0(3)
C(13)-C(35)-C(21)	116.4(7)	C(1E)-C(5E)-C(4E)	108.0
C(2B)-C(1B)-C(5B)	105.2(7)	C(1E)-C(5E)-Fe(1)	71.7(4)
C(2B)-C(1B)-C(12)	126.5(6)	C(4E)-C(5E)-Fe(1)	66.4(4)

Table 21: Crystal data and structure refinement for **52**

Compound	52
Empirical formula	C ₅₆ H ₄₈ Cl ₆ Fe ₂ O ₆
Formula weight	1141.34
Temperature (K)	153(2)
Crystal system	Triclinic
Space group	P-1
a (Å)	10.8315(8)
b (Å)	15.1082(12)
c (Å)	15.6427(12)
α (deg)	72.575(2)
β (deg)	87.682(2)
γ (deg)	83.667(2)
V (Å³)	2427.4(3)
Z	2
D_{calc} (Mg/m³)	1.562
Absorption coefficient (mm⁻¹)	0.982
F(000)	1172
Crystal size (mm³)	0.31 x 0.02 x 0.02
Theta range for data collection	1.65 to 26.00°
Reflections collected	18487
Independent reflections	9528 [R(int) = 0.0801]
Completeness to theta = 26.00°	99.8 %
Data / restraints / parameters	9528 / 0 / 631
Goodness-of-fit on F²	0.968
Final R indices [I>2sigma(I)]	R1 = 0.0742, wR2 = 0.1237

Table 22: Bond lengths (\AA) for 52

Fe(1)-C(55)	2.018(5)	C(31)-C(32)	1.392(7)
Fe(1)-C(40)	2.019(5)	C(32)-H(32A)	0.9500
Fe(1)-C(54)	2.021(5)	C(33)-C(55)	1.398(7)
Fe(1)-C(33)	2.026(5)	C(33)-C(34)	1.435(7)
Fe(1)-C(24)	2.027(5)	C(33)-H(33A)	1.0000
Fe(1)-C(52)	2.040(6)	C(34)-C(38)	1.495(7)
Fe(1)-C(50)	2.047(5)	C(35)-C(49)	1.408(7)
Fe(1)-C(42)	2.054(6)	C(35)-C(36)	1.411(8)
Fe(1)-C(16)	2.062(5)	C(36)-C(46)	1.367(7)
Fe(1)-C(34)	2.099(5)	C(36)-H(36A)	0.9500
Fe(2)-C(53)	2.008(5)	C(37)-C(41)	1.404(8)
Fe(2)-C(57)	2.008(5)	C(39)-C(60)	1.404(8)
Fe(2)-C(65)	2.027(6)	C(39)-C(47)	1.429(8)
Fe(2)-C(60)	2.029(6)	C(39)-H(39A)	1.0000
Fe(2)-C(64)	2.031(6)	C(40)-C(52)	1.422(8)
Fe(2)-C(63)	2.037(6)	C(40)-H(40A)	1.0000
Fe(2)-C(51)	2.042(7)	C(42)-C(50)	1.409(8)
Fe(2)-C(66)	2.048(6)	C(42)-C(52)	1.409(8)
Fe(2)-C(39)	2.048(6)	C(42)-H(42A)	1.0000
Fe(2)-C(47)	2.110(5)	C(44)-C(49)	1.371(8)
O(1)-C(31)	1.371(6)	C(44)-H(44A)	0.9500
O(1)-C(45)	1.430(6)	C(45)-H(45A)	0.9800
C(7)-C(22)	1.387(7)	C(45)-H(45B)	0.9800
C(7)-C(21)	1.400(7)	C(45)-H(45C)	0.9800
C(7)-C(19)	1.504(6)	C(46)-H(46A)	0.9500
O(5)-C(37)	1.368(6)	C(47)-C(57)	1.451(7)
O(5)-C(67)	1.423(6)	C(48)-H(48A)	0.9800
O(3)-C(12)	1.366(6)	C(48)-H(48B)	0.9800
O(3)-C(62)	1.415(6)	C(48)-H(48C)	0.9800
O(2)-C(11)	1.371(6)	C(49)-H(49A)	0.9500
O(2)-C(61)	1.437(6)	C(50)-H(50A)	1.0000
C(11)-C(31)	1.398(7)	C(51)-C(65)	1.399(9)
C(11)-C(12)	1.408(7)	C(51)-C(66)	1.431(8)
C(12)-C(20)	1.377(7)	C(51)-H(51A)	1.0000
O(6)-C(26)	1.364(6)	C(52)-H(52A)	1.0000
O(6)-C(48)	1.420(6)	C(53)-C(57)	1.395(8)
O(4)-C(41)	1.354(6)	C(53)-C(60)	1.402(8)
O(4)-C(59)	1.431(7)	C(53)-H(53A)	1.0000
C(15)-C(19)	1.429(6)	C(54)-C(55)	1.422(8)
C(15)-C(38)	1.441(7)	C(54)-H(54A)	1.0000
C(15)-C(47)	1.470(7)	C(55)-H(55A)	1.0000
C(16)-C(54)	1.411(7)	C(57)-H(57A)	1.0000
C(16)-C(34)	1.433(7)	C(59)-H(59A)	0.9800
C(16)-H(16A)	1.0000	C(59)-H(59B)	0.9800
C(17)-C(19)	1.377(7)	C(59)-H(59C)	0.9800
C(17)-C(18)	1.418(7)	C(60)-H(60A)	1.0000
C(17)-C(43)	1.483(7)	C(61)-H(61A)	0.9800
C(18)-C(25)	1.398(7)	C(61)-H(61B)	0.9800
C(18)-C(27)	1.464(7)	C(61)-H(61C)	0.9800
C(20)-C(23)	1.390(7)	C(62)-H(62A)	0.9800
C(20)-H(20A)	0.9500	C(62)-H(62B)	0.9800
C(21)-C(26)	1.396(7)	C(62)-H(62C)	0.9800
C(21)-H(21A)	0.9500	C(63)-C(66)	1.401(9)
C(22)-C(41)	1.395(7)	C(63)-C(64)	1.417(9)
C(22)-H(22A)	0.9500	C(63)-H(63A)	1.0000
C(23)-C(32)	1.388(7)	C(64)-C(65)	1.433(9)
C(23)-C(25)	1.501(7)	C(64)-H(64A)	1.0000

C(24)-C(50)	1.396(8)	C(65)-H(65A)	1.0000
C(24)-C(40)	1.401(8)	C(66)-H(66A)	1.0000
C(24)-H(24A)	1.0000	C(67)-H(67A)	0.9800
C(25)-C(38)	1.416(7)	C(67)-H(67B)	0.9800
C(26)-C(37)	1.392(7)	C(67)-H(67C)	0.9800
C(27)-C(29)	1.375(7)	Cl(3B)-C(1B)	1.768(6)
C(27)-C(28)	1.417(7)	Cl(3A)-C(1A)	1.753(7)
C(28)-C(35)	1.392(7)	Cl(2B)-C(1B)	1.744(6)
C(28)-C(43)	1.399(7)	Cl(2A)-C(1A)	1.757(6)
C(29)-C(46)	1.413(7)	Cl(1A)-C(1A)	1.745(6)
C(29)-H(29A)	0.9500	Cl(1B)-C(1B)	1.753(6)
C(30)-C(43)	1.380(7)	C(1B)-H(1BA)	1.0000
C(30)-C(44)	1.422(7)	C(1A)-H(1AA)	1.0000
C(30)-H(30A)	0.9500		

Table 23: Angles (°) for 52

C(55)-Fe(1)-C(40)	117.4(2)	C(16)-C(34)-Fe(1)	68.5(3)
C(55)-Fe(1)-C(54)	41.2(2)	C(33)-C(34)-Fe(1)	66.9(3)
C(40)-Fe(1)-C(54)	103.9(2)	C(38)-C(34)-Fe(1)	136.9(4)
C(55)-Fe(1)-C(33)	40.45(19)	C(28)-C(35)-C(49)	116.5(6)
C(40)-Fe(1)-C(33)	153.6(2)	C(28)-C(35)-C(36)	116.4(5)
C(54)-Fe(1)-C(33)	68.7(2)	C(49)-C(35)-C(36)	127.1(5)
C(55)-Fe(1)-C(24)	101.6(2)	C(46)-C(36)-C(35)	120.0(5)
C(40)-Fe(1)-C(24)	40.5(2)	C(46)-C(36)-H(36A)	120.0
C(54)-Fe(1)-C(24)	117.9(2)	C(35)-C(36)-H(36A)	120.0
C(33)-Fe(1)-C(24)	118.9(2)	O(5)-C(37)-C(26)	119.7(5)
C(55)-Fe(1)-C(52)	155.8(2)	O(5)-C(37)-C(41)	120.5(5)
C(40)-Fe(1)-C(52)	41.0(2)	C(26)-C(37)-C(41)	119.8(5)
C(54)-Fe(1)-C(52)	122.5(2)	C(25)-C(38)-C(15)	119.8(5)
C(33)-Fe(1)-C(52)	163.6(2)	C(25)-C(38)-C(34)	123.3(5)
C(24)-Fe(1)-C(52)	68.5(2)	C(15)-C(38)-C(34)	116.9(5)
C(55)-Fe(1)-C(50)	119.2(3)	C(60)-C(39)-C(47)	110.2(5)
C(40)-Fe(1)-C(50)	67.8(2)	C(60)-C(39)-Fe(2)	69.1(3)
C(54)-Fe(1)-C(50)	154.2(2)	C(47)-C(39)-Fe(2)	72.2(3)
C(33)-Fe(1)-C(50)	107.4(2)	C(60)-C(39)-H(39A)	124.9
C(24)-Fe(1)-C(50)	40.1(2)	C(47)-C(39)-H(39A)	124.9
C(52)-Fe(1)-C(50)	68.2(2)	Fe(2)-C(39)-H(39A)	124.9
C(55)-Fe(1)-C(42)	157.6(2)	C(24)-C(40)-C(52)	108.4(5)
C(40)-Fe(1)-C(42)	67.7(2)	C(24)-C(40)-Fe(1)	70.1(3)
C(54)-Fe(1)-C(42)	161.1(2)	C(52)-C(40)-Fe(1)	70.3(3)
C(33)-Fe(1)-C(42)	126.3(2)	C(24)-C(40)-H(40A)	125.8
C(24)-Fe(1)-C(42)	67.5(2)	C(52)-C(40)-H(40A)	125.8
C(52)-Fe(1)-C(42)	40.3(2)	Fe(1)-C(40)-H(40A)	125.8
C(50)-Fe(1)-C(42)	40.2(2)	O(4)-C(41)-C(22)	125.0(5)
C(55)-Fe(1)-C(16)	68.5(2)	O(4)-C(41)-C(37)	115.1(5)
C(40)-Fe(1)-C(16)	123.1(2)	C(22)-C(41)-C(37)	119.9(5)
C(54)-Fe(1)-C(16)	40.4(2)	C(50)-C(42)-C(52)	108.7(5)
C(33)-Fe(1)-C(16)	68.4(2)	C(50)-C(42)-Fe(1)	69.6(3)
C(24)-Fe(1)-C(16)	155.9(2)	C(52)-C(42)-Fe(1)	69.3(3)
C(52)-Fe(1)-C(16)	111.2(2)	C(50)-C(42)-H(42A)	125.6
C(50)-Fe(1)-C(16)	163.9(2)	C(52)-C(42)-H(42A)	125.6
C(42)-Fe(1)-C(16)	129.0(2)	Fe(1)-C(42)-H(42A)	125.6
C(55)-Fe(1)-C(34)	68.0(2)	C(30)-C(43)-C(28)	118.4(5)
C(40)-Fe(1)-C(34)	161.6(2)	C(30)-C(43)-C(17)	135.5(5)
C(54)-Fe(1)-C(34)	67.9(2)	C(28)-C(43)-C(17)	106.1(4)
C(33)-Fe(1)-C(34)	40.7(2)	C(49)-C(44)-C(30)	122.0(5)
C(24)-Fe(1)-C(34)	157.8(2)	C(49)-C(44)-H(44A)	119.0

C(52)-Fe(1)-C(34)	128.5(2)	C(30)-C(44)-H(44A)	119.0
C(50)-Fe(1)-C(34)	126.6(2)	O(1)-C(45)-H(45A)	109.5
C(42)-Fe(1)-C(34)	114.6(2)	O(1)-C(45)-H(45B)	109.5
C(16)-Fe(1)-C(34)	40.27(19)	H(45A)-C(45)-H(45B)	109.5
C(53)-Fe(2)-C(57)	40.7(2)	O(1)-C(45)-H(45C)	109.5
C(53)-Fe(2)-C(65)	100.6(2)	H(45A)-C(45)-H(45C)	109.5
C(57)-Fe(2)-C(65)	120.5(2)	H(45B)-C(45)-H(45C)	109.5
C(53)-Fe(2)-C(60)	40.6(2)	C(36)-C(46)-C(29)	122.8(6)
C(57)-Fe(2)-C(60)	68.3(3)	C(36)-C(46)-H(46A)	118.6
C(65)-Fe(2)-C(60)	114.8(3)	C(29)-C(46)-H(46A)	118.6
C(53)-Fe(2)-C(64)	119.6(3)	C(39)-C(47)-C(57)	104.0(5)
C(57)-Fe(2)-C(64)	157.0(2)	C(39)-C(47)-C(15)	131.0(5)
C(65)-Fe(2)-C(64)	41.3(2)	C(57)-C(47)-C(15)	124.3(5)
C(60)-Fe(2)-C(64)	104.0(3)	C(39)-C(47)-Fe(2)	67.6(3)
C(53)-Fe(2)-C(63)	159.2(3)	C(57)-C(47)-Fe(2)	65.6(3)
C(57)-Fe(2)-C(63)	160.1(3)	C(15)-C(47)-Fe(2)	137.4(4)
C(65)-Fe(2)-C(63)	68.6(2)	O(6)-C(48)-H(48A)	109.5
C(60)-Fe(2)-C(63)	126.3(3)	O(6)-C(48)-H(48B)	109.5
C(64)-Fe(2)-C(63)	40.8(2)	H(48A)-C(48)-H(48B)	109.5
C(53)-Fe(2)-C(51)	115.3(2)	O(6)-C(48)-H(48C)	109.5
C(57)-Fe(2)-C(51)	106.1(2)	H(48A)-C(48)-H(48C)	109.5
C(65)-Fe(2)-C(51)	40.2(3)	H(48B)-C(48)-H(48C)	109.5
C(60)-Fe(2)-C(51)	149.3(3)	C(44)-C(49)-C(35)	120.4(5)
C(64)-Fe(2)-C(51)	68.8(3)	C(44)-C(49)-H(49A)	119.8
C(63)-Fe(2)-C(51)	68.5(3)	C(35)-C(49)-H(49A)	119.8
C(53)-Fe(2)-C(66)	153.7(3)	C(24)-C(50)-C(42)	107.9(5)
C(57)-Fe(2)-C(66)	123.5(3)	C(24)-C(50)-Fe(1)	69.2(3)
C(65)-Fe(2)-C(66)	68.1(3)	C(42)-C(50)-Fe(1)	70.2(3)
C(60)-Fe(2)-C(66)	165.6(3)	C(24)-C(50)-H(50A)	126.0
C(64)-Fe(2)-C(66)	68.3(3)	C(42)-C(50)-H(50A)	126.0
C(63)-Fe(2)-C(66)	40.1(2)	Fe(1)-C(50)-H(50A)	126.0
C(51)-Fe(2)-C(66)	41.0(2)	C(65)-C(51)-C(66)	107.5(6)
C(53)-Fe(2)-C(39)	67.9(2)	C(65)-C(51)-Fe(2)	69.3(4)
C(57)-Fe(2)-C(39)	68.0(2)	C(66)-C(51)-Fe(2)	69.7(4)
C(65)-Fe(2)-C(39)	152.2(3)	C(65)-C(51)-H(51A)	126.3
C(60)-Fe(2)-C(39)	40.3(2)	C(66)-C(51)-H(51A)	126.3
C(64)-Fe(2)-C(39)	120.9(3)	Fe(2)-C(51)-H(51A)	126.3
C(63)-Fe(2)-C(39)	113.1(3)	C(42)-C(52)-C(40)	106.6(6)
C(51)-Fe(2)-C(39)	167.6(3)	C(42)-C(52)-Fe(1)	70.4(3)
C(66)-Fe(2)-C(39)	132.3(2)	C(40)-C(52)-Fe(1)	68.7(3)
C(53)-Fe(2)-C(47)	68.7(2)	C(42)-C(52)-H(52A)	126.7
C(57)-Fe(2)-C(47)	41.16(19)	C(40)-C(52)-H(52A)	126.7
C(65)-Fe(2)-C(47)	160.6(2)	Fe(1)-C(52)-H(52A)	126.7
C(60)-Fe(2)-C(47)	68.3(2)	C(57)-C(53)-C(60)	108.3(5)
C(64)-Fe(2)-C(47)	158.0(2)	C(57)-C(53)-Fe(2)	69.7(3)
C(63)-Fe(2)-C(47)	126.4(2)	C(60)-C(53)-Fe(2)	70.5(3)
C(51)-Fe(2)-C(47)	128.4(3)	C(57)-C(53)-H(53A)	125.9
C(66)-Fe(2)-C(47)	114.1(2)	C(60)-C(53)-H(53A)	125.9
C(39)-Fe(2)-C(47)	40.2(2)	Fe(2)-C(53)-H(53A)	125.9
C(31)-O(1)-C(45)	116.5(4)	C(16)-C(54)-C(55)	108.3(5)
C(22)-C(7)-C(21)	120.0(5)	C(16)-C(54)-Fe(1)	71.3(3)
C(22)-C(7)-C(19)	120.2(5)	C(55)-C(54)-Fe(1)	69.3(3)
C(21)-C(7)-C(19)	119.2(4)	C(16)-C(54)-H(54A)	125.9
C(37)-O(5)-C(67)	112.9(4)	C(55)-C(54)-H(54A)	125.9
C(12)-O(3)-C(62)	119.5(4)	Fe(1)-C(54)-H(54A)	125.9
C(11)-O(2)-C(61)	116.5(4)	C(33)-C(55)-C(54)	108.1(5)
O(2)-C(11)-C(31)	118.6(5)	C(33)-C(55)-Fe(1)	70.1(3)
O(2)-C(11)-C(12)	122.9(5)	C(54)-C(55)-Fe(1)	69.5(3)
C(31)-C(11)-C(12)	118.3(5)	C(33)-C(55)-H(55A)	125.9
O(3)-C(12)-C(20)	125.6(5)	C(54)-C(55)-H(55A)	125.9

O(3)-C(12)-C(11)	113.9(5)	Fe(1)-C(55)-H(55A)	125.9
C(20)-C(12)-C(11)	120.5(5)	C(53)-C(57)-C(47)	109.6(5)
C(26)-O(6)-C(48)	117.3(4)	C(53)-C(57)-Fe(2)	69.7(3)
C(41)-O(4)-C(59)	118.2(4)	C(47)-C(57)-Fe(2)	73.2(3)
C(19)-C(15)-C(38)	118.4(5)	C(53)-C(57)-H(57A)	125.2
C(19)-C(15)-C(47)	122.4(5)	C(47)-C(57)-H(57A)	125.2
C(38)-C(15)-C(47)	119.2(4)	Fe(2)-C(57)-H(57A)	125.2
C(54)-C(16)-C(34)	108.2(5)	O(4)-C(59)-H(59A)	109.5
C(54)-C(16)-Fe(1)	68.2(3)	O(4)-C(59)-H(59B)	109.5
C(34)-C(16)-Fe(1)	71.2(3)	H(59A)-C(59)-H(59B)	109.5
C(54)-C(16)-H(16A)	125.9	O(4)-C(59)-H(59C)	109.5
C(34)-C(16)-H(16A)	125.9	H(59A)-C(59)-H(59C)	109.5
Fe(1)-C(16)-H(16A)	125.9	H(59B)-C(59)-H(59C)	109.5
C(19)-C(17)-C(18)	121.5(5)	C(53)-C(60)-C(39)	107.8(6)
C(19)-C(17)-C(43)	130.9(5)	C(53)-C(60)-Fe(2)	68.9(4)
C(18)-C(17)-C(43)	107.5(5)	C(39)-C(60)-Fe(2)	70.6(4)
C(25)-C(18)-C(17)	119.8(5)	C(53)-C(60)-H(60A)	126.1
C(25)-C(18)-C(27)	131.7(5)	C(39)-C(60)-H(60A)	126.1
C(17)-C(18)-C(27)	108.5(4)	Fe(2)-C(60)-H(60A)	126.1
C(17)-C(19)-C(15)	119.4(5)	O(2)-C(61)-H(61A)	109.5
C(17)-C(19)-C(7)	116.9(4)	O(2)-C(61)-H(61B)	109.5
C(15)-C(19)-C(7)	123.7(5)	H(61A)-C(61)-H(61B)	109.5
C(12)-C(20)-C(23)	120.9(5)	O(2)-C(61)-H(61C)	109.5
C(12)-C(20)-H(20A)	119.5	H(61A)-C(61)-H(61C)	109.5
C(23)-C(20)-H(20A)	119.5	H(61B)-C(61)-H(61C)	109.5
C(26)-C(21)-C(7)	120.0(5)	O(3)-C(62)-H(62A)	109.5
C(26)-C(21)-H(21A)	120.0	O(3)-C(62)-H(62B)	109.5
C(7)-C(21)-H(21A)	120.0	H(62A)-C(62)-H(62B)	109.5
C(7)-C(22)-C(41)	120.2(5)	O(3)-C(62)-H(62C)	109.5
C(7)-C(22)-H(22A)	119.9	H(62A)-C(62)-H(62C)	109.5
C(41)-C(22)-H(22A)	119.9	H(62B)-C(62)-H(62C)	109.5
C(32)-C(23)-C(20)	119.0(5)	C(66)-C(63)-C(64)	108.6(6)
C(32)-C(23)-C(25)	118.9(5)	C(66)-C(63)-Fe(2)	70.3(3)
C(20)-C(23)-C(25)	121.8(5)	C(64)-C(63)-Fe(2)	69.4(4)
C(50)-C(24)-C(40)	108.3(6)	C(66)-C(63)-H(63A)	125.7
C(50)-C(24)-Fe(1)	70.7(3)	C(64)-C(63)-H(63A)	125.7
C(40)-C(24)-Fe(1)	69.4(3)	Fe(2)-C(63)-H(63A)	125.7
C(50)-C(24)-H(24A)	125.8	C(63)-C(64)-C(65)	107.0(7)
C(40)-C(24)-H(24A)	125.8	C(63)-C(64)-Fe(2)	69.9(3)
Fe(1)-C(24)-H(24A)	125.8	C(65)-C(64)-Fe(2)	69.2(4)
C(18)-C(25)-C(38)	119.3(5)	C(63)-C(64)-H(64A)	126.5
C(18)-C(25)-C(23)	117.8(5)	C(65)-C(64)-H(64A)	126.5
C(38)-C(25)-C(23)	122.9(4)	Fe(2)-C(64)-H(64A)	126.5
O(6)-C(26)-C(37)	115.0(5)	C(51)-C(65)-C(64)	108.7(6)
O(6)-C(26)-C(21)	124.9(5)	C(51)-C(65)-Fe(2)	70.4(4)
C(37)-C(26)-C(21)	120.0(5)	C(64)-C(65)-Fe(2)	69.5(4)
C(29)-C(27)-C(28)	117.8(5)	C(51)-C(65)-H(65A)	125.6
C(29)-C(27)-C(18)	136.2(5)	C(64)-C(65)-H(65A)	125.6
C(28)-C(27)-C(18)	105.9(5)	Fe(2)-C(65)-H(65A)	125.6
C(35)-C(28)-C(43)	124.2(5)	C(63)-C(66)-C(51)	108.3(6)
C(35)-C(28)-C(27)	124.1(5)	C(63)-C(66)-Fe(2)	69.5(4)
C(43)-C(28)-C(27)	111.8(5)	C(51)-C(66)-Fe(2)	69.3(4)
C(27)-C(29)-C(46)	118.7(5)	C(63)-C(66)-H(66A)	125.8
C(27)-C(29)-H(29A)	120.7	C(51)-C(66)-H(66A)	125.8
C(46)-C(29)-H(29A)	120.7	Fe(2)-C(66)-H(66A)	125.8
C(43)-C(30)-C(44)	118.5(5)	O(5)-C(67)-H(67A)	109.5
C(43)-C(30)-H(30A)	120.8	O(5)-C(67)-H(67B)	109.5
C(44)-C(30)-H(30A)	120.8	H(67A)-C(67)-H(67B)	109.5
O(1)-C(31)-C(32)	124.2(5)	O(5)-C(67)-H(67C)	109.5
O(1)-C(31)-C(11)	115.4(5)	H(67A)-C(67)-H(67C)	109.5

C(32)-C(31)-C(11)	120.4(5)	H(67B)-C(67)-H(67C)	109.5
C(23)-C(32)-C(31)	120.6(5)	Cl(2B)-C(1B)-Cl(1B)	111.3(4)
C(23)-C(32)-H(32A)	119.7	Cl(2B)-C(1B)-Cl(3B)	110.1(3)
C(31)-C(32)-H(32A)	119.7	Cl(1B)-C(1B)-Cl(3B)	108.3(3)
C(55)-C(33)-C(34)	108.7(5)	Cl(2B)-C(1B)-H(1BA)	109.0
C(55)-C(33)-Fe(1)	69.5(3)	Cl(1B)-C(1B)-H(1BA)	109.0
C(34)-C(33)-Fe(1)	72.4(3)	Cl(3B)-C(1B)-H(1BA)	109.0
C(55)-C(33)-H(33A)	125.6	Cl(1A)-C(1A)-Cl(3A)	111.1(4)
C(34)-C(33)-H(33A)	125.6	Cl(1A)-C(1A)-Cl(2A)	111.1(3)
Fe(1)-C(33)-H(33A)	125.6	Cl(3A)-C(1A)-Cl(2A)	109.7(4)
C(16)-C(34)-C(33)	106.6(4)	Cl(1A)-C(1A)-H(1AA)	108.3
C(16)-C(34)-C(38)	128.7(5)	Cl(3A)-C(1A)-H(1AA)	108.3
C(33)-C(34)-C(38)	123.9(5)	Cl(2A)-C(1A)-H(1AA)	108.3

Table 24: Crystal data and structure refinement for **53**

Compound	53
Empirical formula	C ₅₆ H ₄₂ Fe O ₄
Formula weight	834.75
Temperature (K)	153(2)
Crystal system	Monoclinic
Space group	P2(1)/c
a (Å)	17.8491(7)
b (Å)	10.2307(4)
c (Å)	22.8487(9)
α (deg)	90
β (deg)	103.8000(10)
γ (deg)	90
V (Å³)	4051.9(3)
Z	4
D_{calc} (Mg/m³)	1.368
Absorption coefficient (mm⁻¹)	0.424
F(000)	1744
Crystal size (mm³)	0.47 x 0.34 x 0.06
Theta range for data collection	1.84 to 27.50°
Reflections collected	38389
Independent reflections	9307 [R(int) = 0.0255]
Completeness to theta = 27.50°	100.0 %
Data / restraints / parameters	9307 / 0 / 554
Goodness-of-fit on F²	1.035
Final R indices [I>2sigma(I)]	R1 = 0.0462, wR2 = 0.1234

Table 25: Bond lengths (\AA) for **53**

C(38)-O(3)	1.365(3)	C(26)-H(26A)	0.9500
C(38)-C(37)	1.388(3)	C(27)-C(49)	1.432(3)
C(38)-C(5)	1.405(3)	C(27)-C(43)	1.433(3)
Fe(1)-C(33)	2.0312(19)	C(27)-C(40)	1.437(3)
Fe(1)-C(34)	2.032(2)	C(28)-H(28A)	0.9500
Fe(1)-C(43)	2.042(2)	O(3)-C(60)	1.428(3)
Fe(1)-C(48)	2.042(2)	C(30)-C(52)	1.385(3)
Fe(1)-C(27)	2.043(2)	C(30)-C(57)	1.392(3)
Fe(1)-C(44)	2.043(2)	C(30)-C(39)	1.454(3)
Fe(1)-C(31)	2.043(2)	C(31)-C(34)	1.415(3)
Fe(1)-C(49)	2.044(2)	C(31)-H(31A)	1.0000
Fe(1)-C(18)	2.0461(19)	C(32)-C(58)	1.385(3)
Fe(1)-C(15)	2.0886(18)	C(32)-H(32A)	0.9500
O(1)-C(23)	1.364(2)	C(33)-C(34)	1.422(3)
O(1)-C(53)	1.429(3)	C(33)-H(33A)	1.0000
C(2)-C(4)	1.421(2)	C(34)-H(34A)	1.0000
C(2)-C(11)	1.429(2)	C(35)-H(35A)	0.9500
C(2)-C(15)	1.497(2)	C(36)-C(37)	1.390(3)
C(3)-C(9)	1.382(3)	C(37)-H(37A)	0.9500
C(3)-C(8)	1.416(2)	C(39)-C(40)	1.173(3)
C(3)-C(10)	1.476(2)	C(41)-C(61)	1.391(4)
C(4)-C(9)	1.410(2)	C(41)-H(41A)	0.9500
C(4)-C(16)	1.496(2)	C(42)-C(46)	1.425(3)
C(5)-C(6)	1.378(3)	C(42)-H(42A)	0.9500
C(5)-H(5A)	0.9500	C(43)-C(44)	1.418(3)
C(6)-C(13)	1.402(3)	C(43)-H(43A)	1.0000
C(6)-C(11)	1.494(2)	C(44)-C(48)	1.417(4)
O(2)-C(14)	1.365(2)	C(44)-H(44A)	1.0000
O(2)-C(47)	1.424(3)	C(45)-C(51)	1.355(4)
C(8)-C(11)	1.393(2)	C(45)-C(52)	1.398(3)
C(8)-C(21)	1.486(2)	C(45)-H(45A)	0.9500
C(9)-C(25)	1.502(2)	C(46)-C(50)	1.370(3)
C(10)-C(28)	1.380(3)	C(46)-H(46A)	0.9500
C(10)-C(22)	1.411(3)	C(47)-H(47A)	0.9800
C(12)-C(25)	1.390(3)	C(47)-H(47B)	0.9800
C(12)-C(14)	1.397(3)	C(47)-H(47C)	0.9800
C(12)-H(12A)	0.9500	C(48)-C(49)	1.429(3)
C(13)-C(36)	1.394(3)	C(48)-H(48A)	1.0000
C(13)-H(13A)	0.9500	C(49)-H(49A)	1.0000
C(14)-C(20)	1.386(3)	C(50)-H(50A)	0.9500
C(15)-C(18)	1.443(3)	C(51)-C(56)	1.368(4)
C(15)-C(33)	1.445(3)	C(51)-H(51A)	0.9500
C(16)-C(41)	1.385(3)	C(52)-H(52A)	0.9500
C(16)-C(32)	1.388(3)	C(53)-H(53A)	0.9800
C(17)-C(25)	1.388(3)	C(53)-H(53B)	0.9800
C(17)-C(23)	1.392(3)	C(53)-H(53C)	0.9800
C(17)-H(17A)	0.9500	C(54)-H(54A)	0.9800
C(18)-C(31)	1.420(3)	C(54)-H(54B)	0.9800
C(18)-H(18A)	1.0000	C(54)-H(54C)	0.9800
O(4)-C(36)	1.369(3)	C(56)-C(57)	1.402(4)
O(4)-C(54)	1.402(4)	C(56)-H(56A)	0.9500
C(20)-C(23)	1.389(3)	C(57)-H(57A)	0.9500
C(20)-H(20A)	0.9500	C(58)-C(59)	1.340(5)
C(21)-C(42)	1.379(3)	C(58)-H(58A)	0.9500
C(21)-C(22)	1.416(3)	C(59)-C(61)	1.393(5)
C(22)-C(24)	1.403(3)	C(59)-H(59A)	0.9500

C(24)-C(50)	1.412(3)	C(60)-H(60A)	0.9800
C(24)-C(35)	1.420(3)	C(60)-H(60B)	0.9800
C(26)-C(35)	1.369(3)	C(60)-H(60C)	0.9800
C(26)-C(28)	1.417(3)	C(61)-H(61A)	0.9500

Table 26: Angles (°) for 53

O(3)-C(38)-C(37)	125.0(2)	C(43)-C(27)-C(40)	124.9(2)
O(3)-C(38)-C(5)	114.6(2)	C(49)-C(27)-Fe(1)	69.55(12)
C(37)-C(38)-C(5)	120.4(2)	C(43)-C(27)-Fe(1)	69.41(12)
C(33)-Fe(1)-C(34)	40.97(8)	C(40)-C(27)-Fe(1)	125.91(14)
C(33)-Fe(1)-C(43)	106.11(9)	C(10)-C(28)-C(26)	118.5(2)
C(34)-Fe(1)-C(43)	116.71(9)	C(10)-C(28)-H(28A)	120.8
C(33)-Fe(1)-C(48)	160.21(9)	C(26)-C(28)-H(28A)	120.8
C(34)-Fe(1)-C(48)	122.92(9)	C(38)-O(3)-C(60)	118.2(2)
C(43)-Fe(1)-C(48)	68.54(10)	C(52)-C(30)-C(57)	119.3(2)
C(33)-Fe(1)-C(27)	120.50(8)	C(52)-C(30)-C(39)	120.8(2)
C(34)-Fe(1)-C(27)	153.34(9)	C(57)-C(30)-C(39)	119.9(2)
C(43)-Fe(1)-C(27)	41.08(9)	C(34)-C(31)-C(18)	107.83(17)
C(48)-Fe(1)-C(27)	68.81(9)	C(34)-C(31)-Fe(1)	69.25(11)
C(33)-Fe(1)-C(44)	123.14(9)	C(18)-C(31)-Fe(1)	69.78(11)
C(34)-Fe(1)-C(44)	103.76(9)	C(34)-C(31)-H(31A)	126.1
C(43)-Fe(1)-C(44)	40.63(9)	C(18)-C(31)-H(31A)	126.1
C(48)-Fe(1)-C(44)	40.59(10)	Fe(1)-C(31)-H(31A)	126.1
C(27)-Fe(1)-C(44)	68.74(9)	C(58)-C(32)-C(16)	120.3(3)
C(33)-Fe(1)-C(31)	68.61(8)	C(58)-C(32)-H(32A)	119.9
C(34)-Fe(1)-C(31)	40.64(8)	C(16)-C(32)-H(32A)	119.9
C(43)-Fe(1)-C(31)	151.20(9)	C(34)-C(33)-C(15)	109.38(17)
C(48)-Fe(1)-C(31)	106.39(9)	C(34)-C(33)-Fe(1)	69.55(11)
C(27)-Fe(1)-C(31)	165.71(9)	C(15)-C(33)-Fe(1)	71.62(10)
C(44)-Fe(1)-C(31)	117.00(9)	C(34)-C(33)-H(33A)	125.3
C(33)-Fe(1)-C(49)	156.82(8)	C(15)-C(33)-H(33A)	125.3
C(34)-Fe(1)-C(49)	161.91(8)	Fe(1)-C(33)-H(33A)	125.3
C(43)-Fe(1)-C(49)	68.99(9)	C(31)-C(34)-C(33)	108.07(17)
C(48)-Fe(1)-C(49)	40.95(9)	C(31)-C(34)-Fe(1)	70.11(12)
C(27)-Fe(1)-C(49)	41.01(9)	C(33)-C(34)-Fe(1)	69.49(11)
C(44)-Fe(1)-C(49)	68.73(10)	C(31)-C(34)-H(34A)	126.0
C(31)-Fe(1)-C(49)	126.75(9)	C(33)-C(34)-H(34A)	126.0
C(33)-Fe(1)-C(18)	68.38(8)	Fe(1)-C(34)-H(34A)	126.0
C(34)-Fe(1)-C(18)	68.37(8)	C(26)-C(35)-C(24)	120.38(18)
C(43)-Fe(1)-C(18)	165.76(8)	C(26)-C(35)-H(35A)	119.8
C(48)-Fe(1)-C(18)	121.11(9)	C(24)-C(35)-H(35A)	119.8
C(27)-Fe(1)-C(18)	129.32(8)	O(4)-C(36)-C(37)	115.38(19)
C(44)-Fe(1)-C(18)	153.43(9)	O(4)-C(36)-C(13)	123.0(2)
C(31)-Fe(1)-C(18)	40.64(8)	C(37)-C(36)-C(13)	121.6(2)
C(49)-Fe(1)-C(18)	110.58(9)	C(38)-C(37)-C(36)	118.92(19)
C(33)-Fe(1)-C(15)	41.03(7)	C(38)-C(37)-H(37A)	120.5
C(34)-Fe(1)-C(15)	69.16(8)	C(36)-C(37)-H(37A)	120.5
C(43)-Fe(1)-C(15)	126.56(8)	C(40)-C(39)-C(30)	179.7(3)
C(48)-Fe(1)-C(15)	156.92(9)	C(39)-C(40)-C(27)	177.9(2)
C(27)-Fe(1)-C(15)	109.82(8)	C(16)-C(41)-C(61)	120.2(3)
C(44)-Fe(1)-C(15)	162.09(9)	C(16)-C(41)-H(41A)	119.9
C(31)-Fe(1)-C(15)	68.99(7)	C(61)-C(41)-H(41A)	119.9
C(49)-Fe(1)-C(15)	122.71(8)	C(21)-C(42)-C(46)	118.8(2)
C(18)-Fe(1)-C(15)	40.83(7)	C(21)-C(42)-H(42A)	120.6
C(23)-O(1)-C(53)	117.27(16)	C(46)-C(42)-H(42A)	120.6
C(4)-C(2)-C(11)	117.71(16)	C(44)-C(43)-C(27)	108.0(2)
C(4)-C(2)-C(15)	121.09(16)	C(44)-C(43)-Fe(1)	69.74(12)

C(11)-C(2)-C(15)	121.10(15)	C(27)-C(43)-Fe(1)	69.51(12)
C(9)-C(3)-C(8)	119.91(16)	C(44)-C(43)-H(43A)	126.0
C(9)-C(3)-C(10)	131.18(17)	C(27)-C(43)-H(43A)	126.0
C(8)-C(3)-C(10)	108.79(16)	Fe(1)-C(43)-H(43A)	126.0
C(9)-C(4)-C(2)	121.41(16)	C(48)-C(44)-C(43)	108.4(2)
C(9)-C(4)-C(16)	114.32(15)	C(48)-C(44)-Fe(1)	69.67(12)
C(2)-C(4)-C(16)	124.27(16)	C(43)-C(44)-Fe(1)	69.63(12)
C(6)-C(5)-C(38)	119.7(2)	C(48)-C(44)-H(44A)	125.8
C(6)-C(5)-H(5A)	120.1	C(43)-C(44)-H(44A)	125.8
C(38)-C(5)-H(5A)	120.1	Fe(1)-C(44)-H(44A)	125.8
C(5)-C(6)-C(13)	120.78(18)	C(51)-C(45)-C(52)	121.1(2)
C(5)-C(6)-C(11)	119.01(17)	C(51)-C(45)-H(45A)	119.5
C(13)-C(6)-C(11)	119.85(17)	C(52)-C(45)-H(45A)	119.5
C(14)-O(2)-C(47)	117.18(16)	C(50)-C(46)-C(42)	122.7(2)
C(11)-C(8)-C(3)	120.99(17)	C(50)-C(46)-H(46A)	118.7
C(11)-C(8)-C(21)	131.24(17)	C(42)-C(46)-H(46A)	118.7
C(3)-C(8)-C(21)	107.72(16)	O(2)-C(47)-H(47A)	109.5
C(3)-C(9)-C(4)	119.81(16)	O(2)-C(47)-H(47B)	109.5
C(3)-C(9)-C(25)	118.85(16)	H(47A)-C(47)-H(47B)	109.5
C(4)-C(9)-C(25)	121.35(16)	O(2)-C(47)-H(47C)	109.5
C(28)-C(10)-C(22)	118.59(18)	H(47A)-C(47)-H(47C)	109.5
C(28)-C(10)-C(3)	135.63(18)	H(47B)-C(47)-H(47C)	109.5
C(22)-C(10)-C(3)	105.72(16)	C(44)-C(48)-C(49)	108.3(2)
C(8)-C(11)-C(2)	120.02(16)	C(44)-C(48)-Fe(1)	69.74(12)
C(8)-C(11)-C(6)	114.67(16)	C(49)-C(48)-Fe(1)	69.61(12)
C(2)-C(11)-C(6)	125.24(16)	C(44)-C(48)-H(48A)	125.8
C(25)-C(12)-C(14)	118.92(17)	C(49)-C(48)-H(48A)	125.8
C(25)-C(12)-H(12A)	120.5	Fe(1)-C(48)-H(48A)	125.8
C(14)-C(12)-H(12A)	120.5	C(48)-C(49)-C(27)	107.6(2)
C(36)-C(13)-C(6)	118.5(2)	C(48)-C(49)-Fe(1)	69.45(13)
C(36)-C(13)-H(13A)	120.8	C(27)-C(49)-Fe(1)	69.44(12)
C(6)-C(13)-H(13A)	120.8	C(48)-C(49)-H(49A)	126.2
O(2)-C(14)-C(20)	115.37(17)	C(27)-C(49)-H(49A)	126.2
O(2)-C(14)-C(12)	123.97(17)	Fe(1)-C(49)-H(49A)	126.2
C(20)-C(14)-C(12)	120.65(17)	C(46)-C(50)-C(24)	120.10(19)
C(18)-C(15)-C(33)	105.02(16)	C(46)-C(50)-H(50A)	119.9
C(18)-C(15)-C(2)	126.67(16)	C(24)-C(50)-H(50A)	119.9
C(33)-C(15)-C(2)	128.06(16)	C(45)-C(51)-C(56)	119.6(2)
C(18)-C(15)-Fe(1)	68.00(10)	C(45)-C(51)-H(51A)	120.2
C(33)-C(15)-Fe(1)	67.35(10)	C(56)-C(51)-H(51A)	120.2
C(2)-C(15)-Fe(1)	132.90(13)	C(30)-C(52)-C(45)	119.8(2)
C(41)-C(16)-C(32)	118.7(2)	C(30)-C(52)-H(52A)	120.1
C(41)-C(16)-C(4)	121.70(19)	C(45)-C(52)-H(52A)	120.1
C(32)-C(16)-C(4)	119.40(19)	O(1)-C(53)-H(53A)	109.5
C(25)-C(17)-C(23)	119.46(17)	O(1)-C(53)-H(53B)	109.5
C(25)-C(17)-H(17A)	120.3	H(53A)-C(53)-H(53B)	109.5
C(23)-C(17)-H(17A)	120.3	O(1)-C(53)-H(53C)	109.5
C(31)-C(18)-C(15)	109.67(17)	H(53A)-C(53)-H(53C)	109.5
C(31)-C(18)-Fe(1)	69.58(11)	H(53B)-C(53)-H(53C)	109.5
C(15)-C(18)-Fe(1)	71.17(10)	O(4)-C(54)-H(54A)	109.5
C(31)-C(18)-H(18A)	125.2	O(4)-C(54)-H(54B)	109.5
C(15)-C(18)-H(18A)	125.2	H(54A)-C(54)-H(54B)	109.5
Fe(1)-C(18)-H(18A)	125.2	O(4)-C(54)-H(54C)	109.5
C(36)-O(4)-C(54)	117.08(18)	H(54A)-C(54)-H(54C)	109.5
C(14)-C(20)-C(23)	119.70(17)	H(54B)-C(54)-H(54C)	109.5
C(14)-C(20)-H(20A)	120.1	C(51)-C(56)-C(57)	121.1(3)
C(23)-C(20)-H(20A)	120.1	C(51)-C(56)-H(56A)	119.4
C(42)-C(21)-C(22)	117.76(17)	C(57)-C(56)-H(56A)	119.4
C(42)-C(21)-C(8)	136.45(18)	C(30)-C(57)-C(56)	119.1(3)
C(22)-C(21)-C(8)	105.76(16)	C(30)-C(57)-H(57A)	120.5

C(24)-C(22)-C(10)	123.75(18)	C(56)-C(57)-H(57A)	120.5
C(24)-C(22)-C(21)	124.22(18)	C(59)-C(58)-C(32)	121.2(3)
C(10)-C(22)-C(21)	111.99(16)	C(59)-C(58)-H(58A)	119.4
O(1)-C(23)-C(20)	115.60(17)	C(32)-C(58)-H(58A)	119.4
O(1)-C(23)-C(17)	124.04(18)	C(58)-C(59)-C(61)	119.9(2)
C(20)-C(23)-C(17)	120.35(18)	C(58)-C(59)-H(59A)	120.1
C(22)-C(24)-C(50)	116.42(19)	C(61)-C(59)-H(59A)	120.1
C(22)-C(24)-C(35)	116.15(19)	O(3)-C(60)-H(60A)	109.5
C(50)-C(24)-C(35)	127.41(19)	O(3)-C(60)-H(60B)	109.5
C(17)-C(25)-C(12)	120.89(17)	H(60A)-C(60)-H(60B)	109.5
C(17)-C(25)-C(9)	119.22(16)	O(3)-C(60)-H(60C)	109.5
C(12)-C(25)-C(9)	119.85(16)	H(60A)-C(60)-H(60C)	109.5
C(35)-C(26)-C(28)	122.63(19)	H(60B)-C(60)-H(60C)	109.5
C(35)-C(26)-H(26A)	118.7	C(41)-C(61)-C(59)	119.7(3)
C(28)-C(26)-H(26A)	118.7	C(41)-C(61)-H(61A)	120.1
C(49)-C(27)-C(43)	107.74(19)	C(59)-C(61)-H(61A)	120.1
C(49)-C(27)-C(40)	127.3(2)		

Table 27: Crystal data and structure refinement for **54**

Compound	54
Empirical formula	C ₈₀ H ₈₀ C ₁₂ Fe O ₈
Formula weight	1296.19
Temperature (K)	153(2)
Crystal system	Monoclinic
Space group	P2(1)/n
a (Å)	16.0610(9)
b (Å)	18.9164(10)
c (Å)	24.4574(13)
α (deg)	90
β (deg)	105.1660(10)
γ (deg)	90
V (Å³)	7171.8(7)
Z	4
D_{calc} (Mg/m³)	1.200
Absorption coefficient (mm⁻¹)	0.339
F(000)	2736
Crystal size (mm³)	0.24 x 0.17 x 0.02
Theta range for data collection	1.38 to 24.00°
Reflections collected	59804
Independent reflections	11265 [R(int) = 0.1115]
Completeness to theta = 24.00°	100.0 %
Data / restraints / parameters	11265 / 0 / 913
Goodness-of-fit on F²	1.686
Final R indices [I>2σ(I)]	R1 = 0.1167, wR2 = 0.2847

Table 28: Bond lengths (Å) for 54

Fe(1)-C(77)	2.031(8)	C(29)-C(65)	1.382(11)
Fe(1)-C(74)	2.041(8)	C(29)-C(68)	1.380(11)
Fe(1)-C(71)	2.029(7)	C(30)-C(39)	1.418(11)
Fe(1)-C(62)	2.036(7)	C(31)-C(42)	1.393(10)
Fe(1)-C(82)	2.036(8)	C(31)-C(43)	1.410(10)
Fe(1)-C(61)	2.032(7)	C(32)-C(40)	1.368(10)
Fe(1)-C(58)	2.052(8)	C(33)-C(75)	1.362(12)
Fe(1)-C(70)	2.066(8)	C(33)-C(54)	1.403(11)
Fe(1)-C(51)	2.071(7)	C(33)-C(39)	1.490(11)
Fe(1)-C(46)	2.085(7)	O(11)-C(68)	1.338(10)
Cl(1)-C(10A)	1.746(17)	O(11)-C(89)	1.426(12)
O(3)-C(25)	1.379(8)	C(35)-C(78)	1.384(11)
O(3)-C(86)	1.440(9)	C(35)-C(63)	1.381(11)
Cl(2)-C(10A)	1.726(15)	C(36)-C(44)	1.375(11)
O(5)-C(56)	1.384(9)	C(36)-C(38)	1.420(10)
O(5)-C(94)	1.433(10)	C(38)-C(59)	1.387(11)
O(6)-C(22)	1.369(9)	C(38)-C(55)	1.426(11)
O(6)-C(87)	1.433(9)	C(39)-C(64)	1.399(10)
O(7)-C(50)	1.381(10)	C(40)-C(56)	1.388(10)
O(7)-C(95)	1.443(11)	C(41)-C(64)	1.414(10)
C(8)-C(84)	1.362(14)	C(41)-C(46)	1.487(10)
C(8)-C(78)	1.374(12)	C(44)-C(88)	1.410(11)
O(9)-C(31)	1.365(9)	C(45)-C(50)	1.372(11)
O(9)-C(96)	1.355(13)	C(46)-C(62)	1.445(10)
C(10)-C(16)	1.422(10)	C(46)-C(74)	1.450(10)
C(10)-C(24)	1.450(10)	C(47)-C(80)	1.436(11)
C(10)-C(51)	1.486(10)	C(48)-C(79)	1.353(11)
C(11)-C(41)	1.418(10)	C(49)-C(69)	1.366(11)
C(11)-C(18)	1.415(10)	C(50)-C(72)	1.393(11)
C(11)-C(26)	1.489(11)	C(51)-C(77)	1.439(10)
C(12)-C(47)	1.356(11)	C(51)-C(71)	1.442(10)
C(12)-C(54)	1.409(11)	C(52)-C(73)	1.372(12)
C(12)-C(30)	1.501(10)	C(52)-C(65)	1.404(11)
C(13)-C(49)	1.367(10)	C(53)-C(92)	1.364(12)
C(13)-C(45)	1.393(10)	C(54)-C(66)	1.384(11)
C(13)-C(18)	1.521(11)	C(55)-C(60)	1.392(11)
C(14)-C(19)	1.392(10)	C(56)-C(57)	1.408(11)
C(14)-C(24)	1.404(10)	C(58)-C(61)	1.391(11)
C(14)-C(32)	1.518(9)	C(58)-C(74)	1.433(10)
C(15)-C(32)	1.372(10)	C(59)-C(83)	1.407(12)
C(15)-C(22)	1.394(10)	C(59)-C(90)	1.425(12)
C(16)-C(20)	1.388(10)	C(60)-C(76)	1.407(12)
C(16)-C(28)	1.526(10)	C(61)-C(62)	1.426(10)
C(17)-C(28)	1.382(10)	C(63)-C(93)	1.400(12)
C(17)-C(25)	1.387(10)	C(64)-C(65)	1.514(11)
C(18)-C(30)	1.391(10)	C(66)-C(81)	1.409(12)
C(19)-C(20)	1.424(10)	C(67)-C(68)	1.381(13)
C(19)-C(36)	1.475(11)	C(67)-C(73)	1.409(13)
C(20)-C(55)	1.488(10)	C(69)-C(72)	1.360(11)
O(12)-C(73)	1.382(11)	C(70)-C(77)	1.408(11)
O(12)-C(98)	1.423(14)	C(70)-C(82)	1.425(11)
C(22)-C(57)	1.360(11)	C(71)-C(82)	1.407(11)
C(23)-C(91)	1.367(14)	C(75)-C(91)	1.428(13)
C(23)-C(66)	1.408(13)	C(76)-C(83)	1.404(13)
C(24)-C(35)	1.500(10)	C(79)-C(85)	1.396(13)

C(25)-C(43)	1.360(10)	C(80)-C(81)	1.340(12)
C(26)-C(48)	1.393(11)	C(84)-C(93)	1.399(15)
C(26)-C(53)	1.396(11)	C(85)-C(92)	1.385(13)
O(10)-C(97)	1.367(14)	C(88)-C(90)	1.371(12)
O(10)-C(69)	1.383(10)	C(10A)-Cl(3)	1.760(15)
C(28)-C(42)	1.398(11)	O(200)-C(200)	1.38(3)

Table 29: Angles (°) for **54**

C(77)-Fe(1)-C(74)	128.8(3)	O(9)-C(31)-C(43)	115.9(7)
C(77)-Fe(1)-C(71)	68.4(3)	C(42)-C(31)-C(43)	119.8(7)
C(74)-Fe(1)-C(71)	119.4(3)	C(40)-C(32)-C(15)	120.7(7)
C(77)-Fe(1)-C(62)	120.0(3)	C(40)-C(32)-C(14)	121.2(6)
C(74)-Fe(1)-C(62)	68.6(3)	C(15)-C(32)-C(14)	118.0(7)
C(71)-Fe(1)-C(62)	163.0(3)	C(75)-C(33)-C(54)	118.2(8)
C(77)-Fe(1)-C(82)	67.8(3)	C(75)-C(33)-C(39)	135.1(8)
C(74)-Fe(1)-C(82)	152.8(3)	C(54)-C(33)-C(39)	106.6(7)
C(71)-Fe(1)-C(82)	40.5(3)	C(68)-O(11)-C(89)	117.6(8)
C(62)-Fe(1)-C(82)	125.8(3)	C(78)-C(35)-C(63)	119.0(8)
C(77)-Fe(1)-C(61)	153.7(3)	C(78)-C(35)-C(24)	120.4(8)
C(74)-Fe(1)-C(61)	68.0(3)	C(63)-C(35)-C(24)	120.5(8)
C(71)-Fe(1)-C(61)	125.1(3)	C(44)-C(36)-C(38)	117.7(7)
C(62)-Fe(1)-C(61)	41.0(3)	C(44)-C(36)-C(19)	135.7(7)
C(82)-Fe(1)-C(61)	106.6(3)	C(38)-C(36)-C(19)	106.5(7)
C(77)-Fe(1)-C(58)	166.0(3)	C(59)-C(38)-C(36)	124.6(8)
C(74)-Fe(1)-C(58)	41.0(3)	C(59)-C(38)-C(55)	124.6(8)
C(71)-Fe(1)-C(58)	106.8(3)	C(36)-C(38)-C(55)	110.7(7)
C(62)-Fe(1)-C(58)	68.5(3)	C(64)-C(39)-C(30)	120.7(7)
C(82)-Fe(1)-C(58)	117.7(3)	C(64)-C(39)-C(33)	132.1(8)
C(61)-Fe(1)-C(58)	39.8(3)	C(30)-C(39)-C(33)	107.2(7)
C(77)-Fe(1)-C(70)	40.2(3)	C(32)-C(40)-C(56)	119.5(7)
C(74)-Fe(1)-C(70)	165.6(3)	C(11)-C(41)-C(64)	118.3(7)
C(71)-Fe(1)-C(70)	68.6(3)	C(11)-C(41)-C(46)	120.4(7)
C(62)-Fe(1)-C(70)	107.4(3)	C(64)-C(41)-C(46)	121.3(7)
C(82)-Fe(1)-C(70)	40.6(3)	C(31)-C(42)-C(28)	118.9(7)
C(61)-Fe(1)-C(70)	118.7(3)	C(25)-C(43)-C(31)	119.2(7)
C(58)-Fe(1)-C(70)	151.8(3)	C(36)-C(44)-C(88)	119.2(8)
C(77)-Fe(1)-C(51)	41.1(3)	C(50)-C(45)-C(13)	118.8(8)
C(74)-Fe(1)-C(51)	108.3(3)	C(62)-C(46)-C(74)	105.1(6)
C(71)-Fe(1)-C(51)	41.2(3)	C(62)-C(46)-C(41)	128.8(7)
C(62)-Fe(1)-C(51)	154.5(3)	C(74)-C(46)-C(41)	126.1(7)
C(82)-Fe(1)-C(51)	68.8(3)	C(62)-C(46)-Fe(1)	67.7(4)
C(61)-Fe(1)-C(51)	163.2(3)	C(74)-C(46)-Fe(1)	67.8(4)
C(58)-Fe(1)-C(51)	126.8(3)	C(41)-C(46)-Fe(1)	128.4(5)
C(70)-Fe(1)-C(51)	69.0(3)	C(12)-C(47)-C(80)	117.0(8)
C(77)-Fe(1)-C(46)	109.0(3)	C(79)-C(48)-C(26)	122.1(8)
C(74)-Fe(1)-C(46)	41.1(3)	C(13)-C(49)-C(69)	120.4(8)
C(71)-Fe(1)-C(46)	154.4(3)	C(45)-C(50)-O(7)	124.0(8)
C(62)-Fe(1)-C(46)	41.0(3)	C(45)-C(50)-C(72)	120.3(8)
C(82)-Fe(1)-C(46)	164.1(3)	O(7)-C(50)-C(72)	115.7(8)
C(61)-Fe(1)-C(46)	69.0(3)	C(60)-C(55)-C(38)	117.9(7)
C(58)-Fe(1)-C(46)	69.3(3)	C(60)-C(55)-C(20)	135.3(8)
C(70)-Fe(1)-C(46)	126.9(3)	C(38)-C(55)-C(20)	106.7(7)
C(51)-Fe(1)-C(46)	119.8(3)	O(5)-C(56)-C(40)	124.8(7)
C(25)-O(3)-C(86)	117.8(6)	O(5)-C(56)-C(57)	115.0(7)
C(56)-O(5)-C(94)	117.4(6)	C(40)-C(56)-C(57)	120.2(7)
C(22)-O(6)-C(87)	117.8(6)	C(22)-C(57)-C(56)	119.2(7)
C(50)-O(7)-C(95)	116.2(7)	C(61)-C(58)-C(74)	107.4(7)

C(84)-C(8)-C(78)	118.0(10)	C(61)-C(58)-Fe(1)	69.3(4)
C(31)-O(9)-C(96)	119.5(8)	C(74)-C(58)-Fe(1)	69.1(4)
C(16)-C(10)-C(24)	116.0(6)	C(38)-C(59)-C(83)	116.4(8)
C(16)-C(10)-C(51)	122.7(6)	C(38)-C(59)-C(90)	115.6(7)
C(24)-C(10)-C(51)	121.3(6)	C(83)-C(59)-C(90)	127.9(8)
C(41)-C(11)-C(18)	121.2(7)	C(55)-C(60)-C(76)	118.4(8)
C(41)-C(11)-C(26)	124.2(6)	C(58)-C(61)-C(62)	109.6(7)
C(18)-C(11)-C(26)	114.3(7)	C(58)-C(61)-Fe(1)	70.9(4)
C(47)-C(12)-C(54)	119.9(8)	C(62)-C(61)-Fe(1)	69.6(4)
C(47)-C(12)-C(30)	135.0(8)	C(61)-C(62)-C(46)	108.6(7)
C(54)-C(12)-C(30)	105.1(7)	C(61)-C(62)-Fe(1)	69.3(4)
C(49)-C(13)-C(45)	120.3(8)	C(46)-C(62)-Fe(1)	71.3(4)
C(49)-C(13)-C(18)	123.9(7)	C(35)-C(63)-C(93)	118.9(9)
C(45)-C(13)-C(18)	115.8(7)	C(39)-C(64)-C(41)	120.3(7)
C(19)-C(14)-C(24)	120.1(7)	C(39)-C(64)-C(65)	114.1(7)
C(19)-C(14)-C(32)	117.7(6)	C(41)-C(64)-C(65)	125.2(7)
C(24)-C(14)-C(32)	121.9(7)	C(29)-C(65)-C(52)	120.6(8)
C(32)-C(15)-C(22)	120.0(7)	C(29)-C(65)-C(64)	121.7(7)
C(20)-C(16)-C(10)	121.6(7)	C(52)-C(65)-C(64)	117.5(7)
C(20)-C(16)-C(28)	114.7(7)	C(54)-C(66)-C(23)	115.2(9)
C(10)-C(16)-C(28)	123.7(7)	C(54)-C(66)-C(81)	117.7(9)
C(28)-C(17)-C(25)	118.1(7)	C(23)-C(66)-C(81)	127.1(9)
C(30)-C(18)-C(11)	119.4(7)	C(68)-C(67)-C(73)	119.8(8)
C(30)-C(18)-C(13)	119.7(7)	O(11)-C(68)-C(67)	113.9(8)
C(11)-C(18)-C(13)	120.8(7)	O(11)-C(68)-C(29)	126.3(9)
C(14)-C(19)-C(20)	119.1(7)	C(67)-C(68)-C(29)	119.8(8)
C(14)-C(19)-C(36)	132.0(7)	C(49)-C(69)-C(72)	120.4(8)
C(20)-C(19)-C(36)	108.8(6)	C(49)-C(69)-O(10)	116.8(8)
C(16)-C(20)-C(19)	120.9(7)	C(72)-C(69)-O(10)	122.7(8)
C(16)-C(20)-C(55)	131.9(7)	C(77)-C(70)-C(82)	106.3(7)
C(19)-C(20)-C(55)	107.2(6)	C(77)-C(70)-Fe(1)	68.6(4)
C(73)-O(12)-C(98)	116.3(8)	C(82)-C(70)-Fe(1)	68.6(4)
C(57)-C(22)-O(6)	124.6(7)	C(82)-C(71)-C(51)	109.0(7)
C(57)-C(22)-C(15)	120.4(7)	C(82)-C(71)-Fe(1)	70.0(4)
O(6)-C(22)-C(15)	115.0(7)	C(51)-C(71)-Fe(1)	71.0(4)
C(91)-C(23)-C(66)	121.2(9)	C(69)-C(72)-C(50)	119.8(8)
C(14)-C(24)-C(10)	121.7(7)	O(12)-C(73)-C(52)	124.4(9)
C(14)-C(24)-C(35)	115.5(6)	O(12)-C(73)-C(67)	115.1(8)
C(10)-C(24)-C(35)	122.8(7)	C(52)-C(73)-C(67)	120.5(9)
C(43)-C(25)-O(3)	124.2(7)	C(58)-C(74)-C(46)	109.4(7)
C(43)-C(25)-C(17)	122.5(7)	C(58)-C(74)-Fe(1)	69.9(4)
O(3)-C(25)-C(17)	113.3(6)	C(46)-C(74)-Fe(1)	71.0(4)
C(48)-C(26)-C(53)	117.4(7)	C(33)-C(75)-C(91)	118.5(9)
C(48)-C(26)-C(11)	121.6(7)	C(83)-C(76)-C(60)	122.5(8)
C(53)-C(26)-C(11)	121.0(7)	C(70)-C(77)-C(51)	110.8(7)
C(97)-O(10)-C(69)	120.7(9)	C(70)-C(77)-Fe(1)	71.2(4)
C(17)-C(28)-C(42)	121.5(7)	C(51)-C(77)-Fe(1)	71.0(4)
C(17)-C(28)-C(16)	119.6(7)	C(8)-C(78)-C(35)	123.0(9)
C(42)-C(28)-C(16)	118.9(6)	C(48)-C(79)-C(85)	119.3(8)
C(65)-C(29)-C(68)	120.3(8)	C(81)-C(80)-C(47)	123.5(8)
C(18)-C(30)-C(39)	119.7(7)	C(80)-C(81)-C(66)	119.5(8)
C(18)-C(30)-C(12)	131.4(7)	C(71)-C(82)-C(70)	109.1(7)
C(39)-C(30)-C(12)	108.6(7)	C(71)-C(82)-Fe(1)	69.5(4)
O(9)-C(31)-C(42)	124.3(7)	C(70)-C(82)-Fe(1)	70.8(4)
C(77)-C(51)-C(71)	104.7(6)	C(76)-C(83)-C(59)	120.1(8)
C(77)-C(51)-C(10)	126.7(7)	C(8)-C(84)-C(93)	121.1(10)
C(71)-C(51)-C(10)	128.5(7)	C(92)-C(85)-C(79)	120.0(9)
C(77)-C(51)-Fe(1)	68.0(4)	C(90)-C(88)-C(44)	122.3(8)
C(71)-C(51)-Fe(1)	67.9(4)	C(88)-C(90)-C(59)	120.5(8)
C(10)-C(51)-Fe(1)	129.2(5)	C(23)-C(91)-C(75)	121.6(10)

C(73)-C(52)-C(65)	118.8(8)	C(53)-C(92)-C(85)	119.5(9)
C(92)-C(53)-C(26)	121.6(8)	C(63)-C(93)-C(84)	119.9(10)
C(66)-C(54)-C(12)	122.4(8)	Cl(1)-C(10A)-Cl(2)	110.7(11)
C(66)-C(54)-C(33)	125.1(8)	Cl(1)-C(10A)-Cl(3)	108.7(8)
C(12)-C(54)-C(33)	112.5(7)	Cl(2)-C(10A)-Cl(3)	111.3(8)